DEVELOPMENT OF NOVEL CERAMIC SUBSTRATES FOR HIGH T_C SUPERCONDUCTORS AND THE PREPARATION OF SUPERCONDUCTING FILMS ON THESE NEW SUBSTRATES

THESIS SUBMITTED TO THE UNIVERSITY OF KERALA

FOR THE DEGREE OF

DOCTOR OF PHILOSOPHY

IN

PHYSICS

BY

JOSE KURIAN

REGIONAL RESEARCH LABORATORY

(COUNCIL OF SCIENTIFIC AND INDUSTRIAL RESEARCH)

TRIVANDRUM - 695 019

JULY 1997

Dedicated to My Sister

DECLARATION

I Jose Kurian hereby declare that, this thesis entitled "DEVELOPMENT OF NOVEL CERAMIC SUBSTRATES FOR HIGH T_c SUPERCONDUCTORS AND THE PREPARATION OF SUPERCONDUCTING FILMS ON THESE NEW SUBSTRATES." is a bonafide record of the research work done by me and that no part of this thesis has been presented earlier for any degree , diploma of any other University.

(Jose Kurian)

Prof. J. KOSHY, Ph D., C. Phys., F. Inst. P (Lond)

वैज्ञानिक एवं औद्योगिक अनुसन्धान परिषद्
COUNCIL OF SCIENTIFIC & INDUSTRIAL RESEARCH
क्षेत्रीय अनुसंधान प्रयोगशाला, तिरुवनन्तपुरम्
REGIONAL RESEARCH LABORATORY
THIRUVANANTHAPURAM,
तिरुवनन्तपुरम-695 019
THIRUVANANTHAPURAM-695 019, INDIA

CERTIFICATE

This is to certify that the thesis entitled " DEVELOPMENT OF NOVEL CERAMIC SUBSTRATES FOR HIGH T_c SUPERCONDUCTORS AND THE PREPARATION OF SUPERCONDUCTING FILMS ON THESE NEW SUBSTRATES. " is an authentic record of the research work carried out by Mr. Jose Kurian, MSc. under my supervision in partial fulfilment of the requirement for the Degree of Doctor of Philosophy of University of Kerala,and further that no part of this thesis have been presented before for any other degree.

(Jacob Koshy)

Grams : "CONSEARCH" Telex : 0435-232 Fax : (0471) 490186 Phones : 490674 (O) 433 495 (R)
e-mail : jacob@csrritrd.ren.nic.in (International) ren! csrritrd ! jacob (domestic)

ACKNOWLEDGEMENT

With great pleasure I express my deep sense of gratitude and respect to Prof. Jacob Koshy, Head, Electronic Ceramics Division, Regional research laboratory, Trivandrum, for his valuable guidance, constant encouragement and continued support given to me throughout the work.

I am grateful to Dr. G. Vijay Nair, Director, Regional Research Laboratory, Trivandrum, and Dr. A.D. Damodaran, former Director, Regional Research Laboratory, Trivandrum, for providing all the facilities to carry out this work and for their encouragement and valuable suggestions throughout this work.

My sincere thanks are due to Dr. K.G.K. Warrier, Dr. J. James, Dr. U. Syamaprasad, Dr. V. John, Mr. S.K. Gosh, Dr. Y.P Yadava and Mr. S. Ananthakumar for their encouragement and help at various stages of this study.

My heart felt thanks are due to Mr. K.V. Oonnikrishnan Nair, Mrs. J.D. Sudha, Mr. V.S. Prasad, Mr. K.S.G. Kurup, Mr. S.G.K. Pillai, Mr. P. Mukundan, Mr. P. Guruswamy Mr.K.P.Sadasivan Mr. P. Vijayakumar and Mr.N.Srinivasalu for their help with different instrumental facilities.

I extend my sincere thanks to Prof. R. Pinto, Prof. R . Vijayaraghavan, Dr. P.R. Apte, and Mr. S.P. Pai of TIFR Bombay for their valuable suggestions and encouragement. I am also extremely thankful to Prof. K.G. Nair, Dean, Faculty of technology, CUSAT and Prof. C.P. Girija Vallabhan, Prof. V.P.N. Nampoori and Mr. S.S. Harilal of International School of Photonics, CUSAT, for their help at various stages of the work. I take this opportunity to thank Dr. H.K. Varma, Mr. P. Sreekumar and Mr. R. Rajesh of Sree

Chithirathirunal Institute of Medical Science and Technology for their valuable discussions. I also extend my thanks to Dr. K. Krishnan and Mr. C. Gopalakrishnan of Analytical Spectroscopy Division, VSSC, Trivandrum for their help in some of the experimental measurements. I am thankful to Dr. S.N. Kalkura, CGC, Anna University, Madras for his timely help and useful discussions

It is with great pleasure I thank my colleagues, Mr. P.K. Sajith, Miss. Asha. M. John, Mr. R. Jose, Mr. Jiji Thomas,Dr. K.S. Kumar, Dr. P.R.S. Warrier, Mr. M.S. Sarma, Mr. G. Sreekumar, Dr. T.G. Babu, Dr. K.V. Paulose, Dr. M.K. Jayaraj, Dr. H. Sreemoolanathan, Dr. R. Ratheesh, Dr. N. Santha, Dr. S. Suma, Dr. Nanthakumar. Dr. J. Issac, Mr. Joseph Job, Mr. K. Satheeshkumar, Mr. U. Harish, Dr. Sivakumar, Mr. C.R. Chenthamarakshan, Mr. J. Somarajan and Mr. J. Eldo for their continuous support and friendly advice. Also I thank my friends and well-wishers for their help and inspiration.

I express my deep sense of gratitude to the Council of Scientific and Industrial Research, New Delhi, for the award of Junior/Senior Research Fellowship during the last five years.

I express my deep sense of gratitude to my parents and sister for their constant encouragement and support.

Above all, I thank The Almighty God for His Grace and Blessings.

Jose Kurian

PREFACE

The recent discovery of superconductivity above liquid nitrogen temperature in certain ceramic perovskite oxides has generated enormous amount of research activities in the field of superconductivity. It was realised that the immediate applications of these new class of superconductors are in the form of thick and thin films in microelectronic devices. In the preparation of superconductor films, substrates play a vital role. The high chemical reactivity of these high T_C superconductors (HTSC) at the processing temperature with most of the known substrate materials imposes severe restrictions on the materials available as substrates for HTSC films. Therefore, the search for new substrate materials which satisfy the substrate requirements such as chemical non-reactivity, thermal and lattice matching, favourable dielectric properties, free from any phase transition, etc. is undertaken on a global level.

A study on the development and characterisation of novel ceramic substrates for high T_C superconductors, and the preparation and characterisation of high T_C superconductor films with excellent superconducting characteristics on the newly developed substrates is described in detail in this thesis. A group of perovskite ceramic materials Ba_2RENbO_6 (RE = Pr, Nd, Sm, Eu and Gd) {BRENO} were prepared and sintered as single phase materials by solid state reaction method for their use as substrates for HTSC materials. These materials are found to be isostructural and have complex cubic perovskite structure and are chemically non-reacting with HTSC materials even at the extreme processing conditions. The dielectric constants and loss factor values of these materials are in a range suitable for their use as substrates for microwave applications. These materials do not possess any phase transition in the temperature range of 30 to 1300°C and are mechanically strong and stable in atmospheric conditions. Also they offer

reasonable thermal expansion match with the HTSC films. High thermal conductivity value of BRENO (~80 $Wm^{-1}K^{-1}$) as compared to Al_2O_3 and MgO, is an added advantage for substrate applications. BRENO also offers a reasonable number of coincidence sites with $YBa_2Cu_3O_{7-\delta}$ (YBCO) superconductor for promoting better epitaxial growth of YBCO films.

These new materials are found to form good superconductor-insulator composites, making a percolation study possible in the composites. The results of the percolation study agreed well with the theoretically predicted values. Percolation studies also confirms the suitability of BRENO as substrates for HTSC materials from chemical reactivity point of view. The suitability of BRENO as substrates for HTSC were further confirmed by developing superconducting films with excellent superconducting properties on BRENO substrates. The superconducting YBCO thick films developed on polycrystalline BRENO materials by screen printing/dip-coating techniques gave $T_C(0)$ of 92 K and J_C of ~$3x10^4 A/cm^2$ at 77 K and zero magnetic field. *In situ* grown YBCO thin films {$T_C(0)$ = 90 K} on polycrystalline BRENO substrates gave J_C of ~10^5 A/cm^2. Bi(2223) thick films developed on BRENO (RE = Gd and Eu) by dip-coating gave $T_C(0)$ of 109 K and J_C of ~$4x10^3$ A/cm^2.

LIST OF PUBLICATIONS
(Journals only)

1. J. Koshy, J.K. Thomas, **J. Kurian**, Y.P. Yadava and A.D. Damodaran. $YBa_2HfO_{5.5}$: a new perovskite suitable as a substrate for YBCO films. *Materials Letters*, **15** (1992) 298.

2. J. Koshy, J.K. Thomas, **J. Kurian**, Y.P. Yadava and A.D. Damodaran. Superconducting $YBa_2Cu_3O_{7-\delta}$ thick film (Tc(0)=92 K) on $SmBa_2NbO_6$: a newly developed perovskite ceramic substrate. *Physica C*, **215** (1993) 209.

3. J. Koshy, J.K. Thomas, **J. Kurian**, Y.P. Yadava and A.D. Damodaran. Development and characterisation of $GdBa_2NbO_6$, a new ceramic substrate for YBCO thick films. *Materials Letters*, **17** (1993) 393.

4. J. Koshy, **J. Kurian**, J.K. Thomas, Y.P. Yadava and A.D. Damodaran., Rare-Earth Barium Niobates: A New Class of Potential Substrates for $YBa_2Cu_3O_{7-\delta}$ Superconductor. *Jpn. J. Appl. Phys.*, 33 (1994) 117.

5. J. Koshy, **J. Kurian**, Y.P. Yadava, P.K. Sajith, A.D. Damodaran, S.P. Pai, Dhananjayakumar, R. Pinto and R. Vijayaraghavan. Growth of YBCO thin films (Tc(0)=90 K) by pulsed laser ablation on polycrystalline $GdBa_2NbO_6$, a new perovskite ceramic substrate. *Physica C*, **225** (1994) 101.

6. J. Koshy, K.S. Kumar, **J. Kurian**, Y.P. Yadava and A.D. Damodaran. Superconducting Bi-cuprate thick film Tc(0)=110 K on $DyBa_2SnO_{5.5}$: A newly developed perovskite substrate. *Appl. Phys. Lett.*, **65** (1994) 2857.

7. J. Koshy, K.S. Kumar, **J. Kurian**, Y.P. Yadava and A.D. Damodaran.
$DyBa_2SnO_{5.5}$: a new ceramic substrate for superconducting YBCO (Tc(0)=92 K) and Bi(2223) (Tc(0)=110 K) thick films.
***Physica C*, 234** (1994) 211.

8. J. Koshy, K.S. Kumar, **J. Kurian**, Y.P. Yadava and A.D. Damodaran.
Rare-Earth Barium Stannates: Synthesis, Characterizaton and Potential Use as Substrates for $YBa_2Cu_3O_{7-\delta}$ Superconductor.
***J. Am. Ceram. Soc.*, 78** (1995) 3088.

9. **J. Kurian**, J. Koshy, P.R.S. Wariar, Y.P. Yadava and A.D. Damodaran.
Synthesis and Characterisation of Rare-Earth Barium Antimonates, a New Group of Complex Perovskites Suitable as Substrates for $YBa_2Cu_3O_{7-\delta}$ Films.
***J. Solid State Chem.*, 116** (1995) 193.

10. J. Koshy, K.S. Kumar, **J. Kurian**, Y.P. Yadava and A.D. Damodaran.
Normal state transport and superconductivity in $YBa_2Cu_3O_{7-\delta}$-$PrBa_2SnO_{5.5}$ system.
***Jpn. J. Appl. Phys.*, 34** (1995) 5644.

11. J. Koshy, K.S. Kumar, **J. Kurian**, Y.P. Yadava and A.D. Damodaran.
Transport properties of the superconducting $Bi_2Sr_2Ca_2Cu_3O_{10}$-$DyBa_2SnO_{5.5}$ percolation system.
***Phys. Rev. B*, 51** (1995) 9096.

12. J.K. Thomas, **J. Kurian**, M.A. Ittyachen and J. Koshy.
Superconducting $YBa_2Cu_3O_{7-\delta}$ and $YBa_2Cu_3O_{7-\delta}$ -Ag thick films by dip-coating on $YBa_2HfO_{5.5}$ ceramic substrate.
***Materials Letters*, 25** (1995) 301.

13. J. Koshy, P.K. Sajith, **J. Kurian**, Y.P. Yadava, K.S. Kumar and A.D. Damodaran.
Barium rare-earth zirconates: synthesis, characterisation and their possible application as substrate for $YBa_2Cu_3O_{7-\delta}$ superconductor.
Mater. Res. Bull., **30** (1995) 1447.

14. K.S. Kumar, **J. Kurian**, P.K. Sajith and J. Koshy.
Superconducting YBCO-Ag (Tc(0)=92 K) and Bi(2223)-Ag (Tc(0)=110 K) composite thick films by dip-coating on $DyBa_2SnO_{5.5}$, a new ceramic substrate.
Physica C, **256** (1996) 312.

15 K.S. Kumar, **J. Kurian** and J. Koshy.
Transport Properties of the $YBa_2Cu_3O_{7-\delta}$-$DyBa_2SnO_{5.5}$ Percolation System.
J. Supercond., **9** (1996) 333.

16. P.R.S Wariar, **J. Kurian**, A.D. Damodaran and J. Koshy.
Development of superconducting $YBa_2Cu_3O_{7-\delta}$ and $YBa_2Cu_3O_{7-\delta}$-Ag thick films by dip-coating on $SmBa_2SbO_6$, a new ceramic substrate material.
Appl. Supercond., **4** (1996) 111.

17. **J. Kurian**, H.K. Varma, J. Koshy, S.P. Pai and R. Pinto.
Growth of YBCO-Ag thin films (Tc(0)=89 K) by pulsed laser ablation on polycrystalline Ba_2LaNbO_6, a new perovskite ceramic substrate.
Appl. Phys. Lett., **69** (1996) 2909.

18. S.P. Pai, J. Jasudasn, P.R. Apte, R. Pinto, **J. Kurian**, P.K. Sajith, J. James and J. Koshy.
$YBa_2Cu_3O_{7-\delta}$ films with high critical current density on epitaxial films of Ba2LaNbO6, a new perovskite substrate substrate for $YBa_2Cu_3O_{7-\delta}$ superconductor.
Europhysics Letters (accepted for publication)

LIST OF PATENTS

International Patents

1. A novel ceramic substrate useful for the preparation of superconducting films and a process for preparing the films
   J. Koshy, J.K.Thomas, **J. Kurian**, Y.P.Yadava and A.D. Damodaran
   U.S. Patent 08/221, 154 dated 31.3.1994

2. Ceramic substrates for superconducting films
   J. Koshy, J.K. Thomas, **J. Kurian**, Y.P.Yadava and A.D. Damodaran
   European Patent 9930 2354.9 dated 31.3.1994

3. A novel ceramic substrate for Bi-cuparate superconductors and a process for the same
   J. Koshy, **J. Kurian**, P.K. Sajith, K.S. Kumar, R. Jose, M.J. Asha and A.D. Damodaran
   European Patent 96308464.5-2208 dated 22.11.1996

Indian Patents

4. A process for the preparation of new ceramic substrate $REBa_2MO_6$ (where RE = rare earth metals, M = metal like Nb, Sb, Hf, Sn,Zr) usefulfor the preparation of superconducting $YBa_2Cu_3O_{7-\delta}$ filsm which are usefulfor microwave application
   J. Koshy, J.K. Thomas, **J. Kurian**, Y.P. Yadava and A.D. Damodaran
   Indian Patent 1274/DEL/92 dated 31.12.1992

5. A process for the preparation of superconducting $YBa_2Cu_3O_{7-\delta}$ thick films on new ceramic substrate $REBa_2MO_6$ (where RE = rare earth metals and M = metals like Nb, Sb, Sn, Hf, Zr)
   J. Koshy, J.K. Thomas, **J. Kurian**, Y.P. Yadava and A.D. Damodaran
   Indian patent 660/DEL/93 dated 29.6.1993

6. Process for preparation of novel ceramic substrates $Ba_2DyMO_{5.5}$ (M = Zr, Sn and Hf) for Bi-cuprate superconductors and a process for the preparation of phase pure superconducting Bi(2223) and Bi(2223)-Ag thick film on this newly developed substrate
   J. Koshy, **J. Kurian**, P.K.Sajith, K.S. Kumar, R. Jose, A M. John and A.D. Damodaran
   Indian Patent 1028/Del/96 dated 16.05.1996

CONTENTS

CHAPTER 1

GENERAL INTRODUCTION

1.1. Superconductivity

One of the most exciting developments in science during the twentieth century was the discovery of superconductivity in 1911 by H. Kamerlingh Onnes, at the university of Leiden in Holland. He observed that the resistance of a rod of frozen mercury suddenly dropped to an immeasurable value when cooled to 4 K. This state was characterised by remarkable electrical and magnetic properties and was designated by as the superconducting state. Later many other elements, alloys and intermetallic compounds were found become superconducting at sufficiently low temperatures.

Superconductors have four important characteristics, namely, zero resistivity, Meissner effect, Josephson effect and Quantisation of magnetic field. Zero resistivity means, a material in its superconducting stage offers no resistance to the flow of direct electric current or in other words, superconductor is a perfect electric conductor. Meissner effect: a superconductor will expel magnetic flux from its interior by an internally induced electric field. Thus a superconductor in a weak magnetic field will act as a perfect diamagnet with zero magnetic induction in its interior. Josephson effect is a remarkable electrical property associated with the tunnelling of superconducting electron pairs from a superconductor through a thin layer of insulator into another

superconductor. This effect can be utilized for high frequency switching systems. Quantization of magnetic field: the total magnetic flux that passes through a superconducting ring may assume only quantized values, integral multiples of the flux quantum hc/q, where q = -2e, the charge of an electron pair. The first two properties (zero resistivity and Meissner effect) are related to electric power applications whereas the last two properties (Josephson effect and Quantization of magnetic field) are related to microelectronic applications. In addition, superconductors have three critical parameters; critical temperature (T_c), critical magnetic field (H_c) and critical current density (J_c). The critical temperature is defined as that temperature at which a specimen undergoes a transition from a state of normal electrical resistivity to the superconducting state. The critical value of the applied magnetic field for the destruction of superconductivity is called the critical magnetic field and is a function of temperature. Similarly, the critical current density is defined as the critical value of current which the superconductor can support without destroying the superconductivity and is a function of temperature and applied magnetic field.

1.2. Ceramics

The High Temperature Superconductors (HTSC) belong to a group of materials called ceramics. The term 'Ceramics' has evolved from the Greek word 'Keramos', means objects made of fired clay. An appropriate general definition of ceramics can be given as the manufacture of shaped inorganic, non-metallic, high temperature materials traditionally done by

three general processes, i.e. preparation of cementatious powder, shaping of the same to an object and heating it to form a permanent object. Some of the important characteristics of ceramic materials are high strength at elevated temperatures, low electrical and thermal conductivity, strong resistance to deformation, brittleness, low toughness and high corrosion resistance to environment. Over the ages, man has developed a number of products based on natural materials like clay and silicates. During the last century quite a large number of technologically important, non-conventional ceramic materials have emerged and they were properly termed as new ceramics or fine ceramics or more recently as advanced ceramics. More clearly, fine ceramics are ceramics synthesised using highly refined raw materials, rigorously controlled composition and strictly regulated forming and sintering. Newly designed devices incorporate ceramic materials because of their useful chemical, electrical, mechanical, thermal and structural properties.

Ceramic materials are brittle and fracture with little or no deformation, in contrast to metals, which yield and deform. As a result, ceramics cannot be formed into shape by the normal deformation process used for metals. Two basic processes have been developed for shaping ceramics. One is to use fine ceramic particles mixed with a liquid or binder or lubricant or pore spaces, to make a combination that has rheological properties which permits shaping. Then by heat treatment the fine particles in the shaped body are agglomerated into a cohesive, useful product. The essentials of this procedure are first to find or prepare fine

particles, shape them and then consolidate them by heating. The second basic process is to melt the material to form a liquid and then shape it during cooling and solidification. Ceramics have inorganic structures and almost all ceramics have a crystal structure.

1.3. Perovskites

Perovskites, which derive that name from the specific mineral known as perovskite, are ceramic materials that have a particular atomic arrangement. The compounds of the perovskite family are probably the most numerous, the most widely studied and the most important. The structure family is named after the rare mineral perovskite, $CaTiO_3$. The ideal perovskite structure described by the general formula ABX_3, consists of cubes made up of three distinct chemical elements that are present in the ratio 1:1:3. Of the three distinct chemical elements, A and B are metallic cations and the X atoms are non-metallic anions. The larger one of the cations, A, lies at the centre of the cube and the other, B, occupy all the eight corners. The X anions lie at the midpoints of the cubes twelve edges, giving corner-shared strings of BX_6 octahedra, which extends infinitely in three dimensions. Fig.1.1 shows the crystal structure diagram of ABX_3 perovskite unit cell. The BX_6 octahedra are perfect with 90° angles and six equal B-X bonds. Each atom is surrounded by equidistant X anions. The ideal perovskite structure can also be regarded as a close packed structure in which the X atoms and the A atoms are stacked in cubic close packed layers along the cubic (111) direction. Some of the resulting octahedral holes are occupied by B atoms.

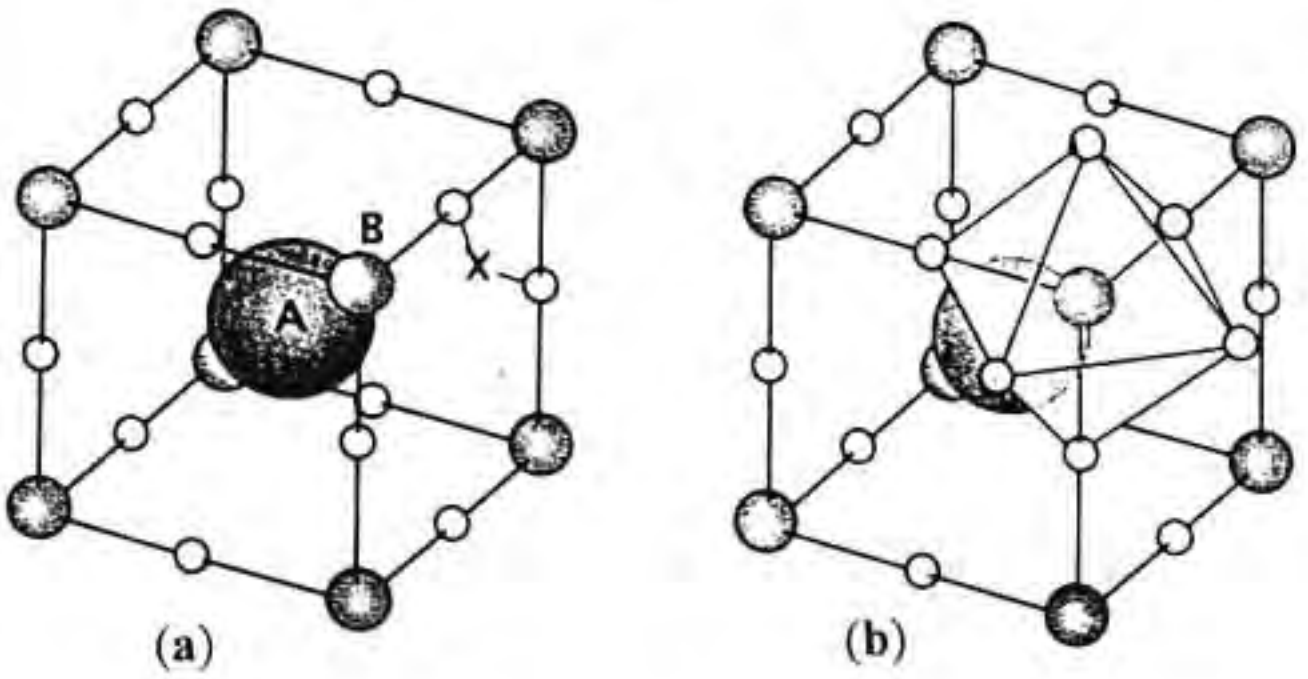

Fig. 1.1 Crystal structure diagram of (a) ABX_3 perovskite unit cell and (b) shows the six anions surrounding the B cation forming an octahedron.

Both natural and synthetic perovskites exhibit an array of electrical properties and are of technical importance. Whereas a given crystal structure is usually associated with a specific electrical property, perovskites run the whole range from insulators to semiconductors, superionic conductors, metal-like conductors and now high temperature superconductors. Most of the new high temperature superconductors belong to the family of perovskites. Slight modifications of the ideal perovskite architecture often result in new features. There is no one to one correlation; a given modification does not automatically produce a particular degree of electrical conductivity. Yet when the ideal perovskite structure is altered, the possibility of new electrical or other properties arises [8]. Like other ceramics ideal perovskites are electrical insulators. Moreover, the bonds along the three axes of the cube are alike leads to isotropic properties of the bulk material. Many of the perovskites are some

what distorted. The simple modification or alteration of the ideal perovskite unit cell which leads to slight distortion or deviation from the ideal shape or composition leads to a new array of optical, elastic, electrical and other physical properties.

In the perovskite structure, A or B sites can be filled with two or more types of cations. There are a good number of complex compounds with the ideal perovskite structure. Here two or more cations randomly occupy either the twelve fold site (A site) or the octahedral site (B site). There are many complex perovskites which contain two or more octahedral cations. In some cases the different cations occupy the octahedral sites at random and in other cases an ordering takes place on the octahedral sites, with two different cations occupying distinct crystallographic site. In the case of two different cations, B and B′, occupying the octahedral sites, the ordering of the two cations (B and B′) at the octahedral sites leads to the formation of a superstructure or in other words the doubling of the basic unit cell, which results in cubic phase of $A_2BB'O_6$. The ordering of the B and B' cations at the octahedral sites means; B and B' cations strictly fill alternate octahedral positions throughout the structure. The octahedral sites can be filled not only by two different elements but also by differently charged ions of the same element. Similarly the ordering of the A sites can also lead to the formation of superstructures. The ordering of the B site at $A_2BB'O_6$ compounds and the A site of $AA'B_2O_6$ compounds have been investigated by different groups [11-15].

1.4. High T_C Ceramic Superconductors

1.4.1. Evolution of High Temperature Superconductivity

After the discovery of superconductivity in 1911 by Kamerlingh Onnes in mercury, the superconducting transition temperature (T_C) had been gradually increased from 4 K and over the years many other materials were found to be superconducting. The next major discovery in the field of superconductivity occurred in 1933 in Waltter Meissner's Superconductivity Laboratory in Berlin where Meissner and Ochsenfield found that a magnet placed near a superconductor will be repelled by the superconductor. Later in 1952 John Hulm and George Hardy discovered that V_3Si having a transition temperature of 17 K and at Bell Laboratory Matthias made Nb_3Sn with $T_C = 18$ K. The discovery of niobium compound, which could carry a large current and also withstand the high magnetic field produced, was a major breakthrough in this area and this has greatly enhanced the capability of using superconductors in electromagnets. Another major event in the field of superconductivity occured in 1957 when John Bardeen, Leon Cooper and Robert Shrieffer at the University of Illinois proposed their famous BCS theory to explain the mechanism of low temperature superconductivity which remained mysterious until that time. This theory was very successful not only in explaining what was known about superconductivity but in predicting new phenomena that later were confirmed by laboratory experiments. The theory is based on a coherent pairing of electrons such that all pairs have

identically the same momenta. The pairing results from a long range attraction between electrons [3]. For the next few years there was no major advances in superconductivity. In 1973, John R. Gavaler found that Nb_3Ge had a T_C of 23 K. This remained a record for quite a long time until 1986 when Bednorz and Muller at IBM's Zurich Laboratory found indications of superconductivity in a class of metal oxide ceramics called perovskites. In the years from 1960 to 1986 several hundred materials were found to be superconducting at sufficiently low temperatures. However, the highest T_C achieved in this period was 23K, which still require either liquid helium or liquid hydrogen.

In 1986, J. George Bednorz and K. Alex Muller found indications of superconductivity at ~30 K in a mixed oxide compound of lanthanum, barium and copper [16]. This was confirmed by Takagi et al and others as due to $La_{2-x}Ba_xCuO_4$ phase with layered perovskite K_2NiF_4 type structure [17,18]. Subsequently there was a world wide search for high T_C oxide superconductors. Soon after, many research groups around the world confirmed the findings of Bednorz and Muller. Later in December 1986 Paul Chu's group at the University of Houston found T_C onset of 52.5 K for La-Ba-Cu-O compound under pressure [19,20]. During this same period, Bell Laboratories in USA reported that replacement of barium by the smaller strontium atom had resulted in a higher T_C and this was later confirmed by different groups [21,22]. In 1987, Paul Chu and M.K. Wu found that a new compound Yttrium-Barium-Copper-Oxide with a T_C

of ~92 K [23]. For the first time in history, superconductivity above the boiling point of liquid nitrogen (77 K) was discovered, representing one of the greatest triumphs of scientific endeavour. This discovery was confirmed by different groups [24-29] and the phase responsible for high temperature superconductivity was identified as $YBa_2Cu_3O_{7-\delta}$ and established its crystal structure [30-33]. Since then researchers around the world have substituted ten other rare-earth elements for Y to produce compounds that superconduct at ~90 K [34-44]. Now it has been established that the substitution of yttrium by any rare-earth ion (except Ce, Pr and Tb) in $YBa_2Cu_3O_{7-\delta}$ would produce compounds that are superconducting with T_C of about 90 K. The maximum superconducting transition temperature has been further raised when superconductivity in Bismuth-Strontium-Calcium-Copper-Oxide system was reported by Meda *et al.* in 1988 [45]. Of the three phases in the Bi-Sr-Ca-Cu-O system, the maximum T_C value of ~110 K was reported for $Bi_2Sr_2Ca_2Cu_3O_{10+\delta}$ [46]. This was soon followed by the discovery of superconductivity in Thallium-Barium-calcium-Copper-Oxide system [47]. Later different superconducting phases have been reported in the Tl-Ba-Ca-Cu-O system and $Tl_2Ba_2Ca_2Cu_3O_{10}$ gave a maxium T_C value of ~125 K [48]. This remained as a record value of T_C until the discovery of superconductivity at 130 K in Mercury-Barium-Calcium-Copper-Oxide system by Schilling *et al* in 1993 [49]. The phase responsible for this high value of T_C was identified as $HgBa_2Ca_2Cu_3O_{8+\delta}$ and this when synthesised as a single phase compound

gave a T_C of 135 K [50]. A higher T_C of about 150 K was reported in $HgBa_2Ca_2Cu_3O_{8+\delta}$ which was synthesised by the application of pressure (150 kbar) [51].

By this time many superconducting compounds were reported and among them $Ag_{1-x}Cu_xBa_2Ca_{n-1}Cu_nO_{2n+3-\delta}$ (x = 0.75) and $Cu_{1-x}Ba_2Ca_{n-1}Cu_nO_{2n+4-\delta}$ have T_C of about 117 K and 116 K respectively [52,53]. The advantage highlighted for Ag and Cu-based superconductors is their nontoxicity, compared to Tl and Hg-based superconductors. T_C values of some of the high T_C superconductors are given in table 1.1. In contrast to these high T_C superconductor compounds where copper is an essential element, copper less superconductor $Ba_{0.6}K_{0.4}BiO_3$ was also reported by cava *et al* [54]. Figure 1.2 summarizes the historical evolution of superconductivity since its discovery by H.K. Onnes to the recent developments in oxide superconductors.

1.4.2. Yttrium Barium Copper Oxide Superconductor

Superconductivity above liquid nitrogen temperature in a mixed oxide of yttrium, barium and copper was confirmed by several other groups after its discovery by Wu *et al* [23] and the phase responsible for such high value of T_C was identified as $YBa_2Cu_3O_{7-\delta}$ (YBCO). YBCO has an oxygen deficient perovskite structure with an orthorhombic symmetry. The crystal structure of YBCO superconductor have been elucidated from x-ray diffraction data [24,30,56] and neutron diffraction studies [33,57-61].

Table 1.1 T_C and Crystal structure of high T_C cuparate superconductors

Material.	T_C (K)	Structure
$La_{2-x}Ba_xCuO_{4+\delta}$	30	Tetragonal
$La_{2-x}Sr_xCuO_{4+\delta}$	40	"
$YBa_2Cu_3O_{7-\delta}$	92	Orthorhombic
$YBa_2Cu_4O_{10}$	80	Tetragonal
$REBa_2Cu_3O_{7-\delta}$	~92	Orthorhombic
(Re = rare-earth		
except Ce, Pr & Tb)		
Bi_2Sr_2CuO	~17	"
$Bi_2Sr_2CaCu_2O$	80	"
$Bi_2Sr_2Ca_2Cu_3O$	110	"
$TlBa_2CuO_{5+\delta}$	20	Tetragonal
$TlBa_2CaCu_2O_{7+\delta}$	80	"
$TlBa_2Ca_2Cu_3O_{9+\delta}$	110	"
$TlBa_2Ca_3Cu_4O_{12+\delta}$	122	"
$Tl_2Ba_2Ca_1Cu_2O_{8+\delta}$	110	"
$Tl_2Ba_2Ca_2Cu_3O_{10+\delta}$	125	"
$Tl_2Ba_2Ca_3Cu_4O_{12+\delta}$	105	"
$HgBa_2CuO_{5+\delta}$	94	"
$HgBa_2Ca_1Cu_2O_{7+\delta}$	104	"
$HgBa_2Ca_2Cu_3O_{9+\delta}$	135	"
$HgBa_2Ca_3Cu_4O_{12+\delta}$	105	"
$HgBa_2Ca_4Cu_5O_{8+\delta}$	105	"
$HgBa_2Ca_5Cu_6O_x$	95	"

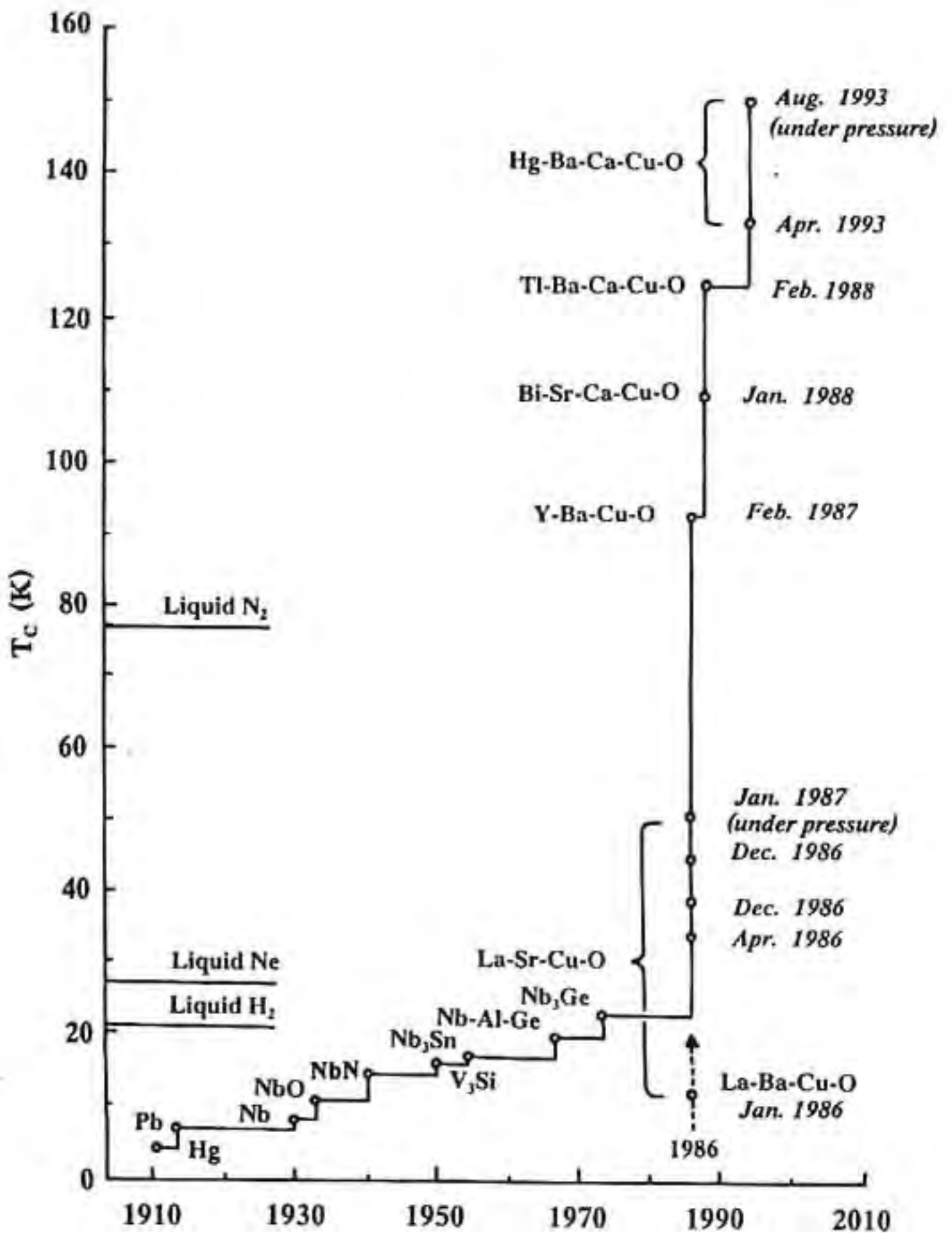

Fig. 1.2 Evolution of superconductive transition temperature subsequent to the discovery of the phenomenon (ref. 55).

Later more detailed studies on structure have been reported using single crystals [62-67]. The structure of $YBa_2Cu_3O_{7-\delta}$ is related to cubic perovskite structure with one of the cube axes tripled. In $YBa_2Cu_3O_{7-\delta}$ structure the c-axis of the unit cell is tripled with two inequivalent Cu planes, labelled Cu1 and Cu2, sandwiched between Ba planes for Cu1 and Ba and Y planes for Cu2 [1]. Also, in addition to the two dimensional CuO_2 layers, there exist O-Cu-O linear chains along the b-axis in the basal plane, leaving behind two types of Cu sites, namely Cu1 and Cu2 in the crystalline cell. The Cu1 atom co-ordination in square planer for the CuO_2 chains, and for Cu2 it corresponds with that of square pyramidal in the CuO_2 layers [4].

A very important point in $YBa_2Cu_3O_{7-\delta}$ is the role played by the orthorhombic and tetragonal phases. The tetragonal phase ($\delta > 0.7$) is semiconducting and T_c is maximized by reducing δ to < 0.1 and obtain a fully orthorhombic phase. In both the orthorhombic and tetragonal phases oxygen sites in the Y plane are vacant, leaving Cu2 five fold co-ordinated. In the case of ideal orthorhombic phase, the O4 and O5 sites in the Cu1 plane are occupied differently. As $\delta \to 0$ the O4 sites are occupied along the b-axis and similar O5 sites are vacant along the a-axis, giving b-axis Cu1-O4 chains. In the tetragonal phase ($\delta = 1$) both O4 and O5 sites are vacant. The structure of the orthorhombic and tetragonal phases of $YBa_2Cu_3O_{7-\delta}$ are shown in Fig.1.3.

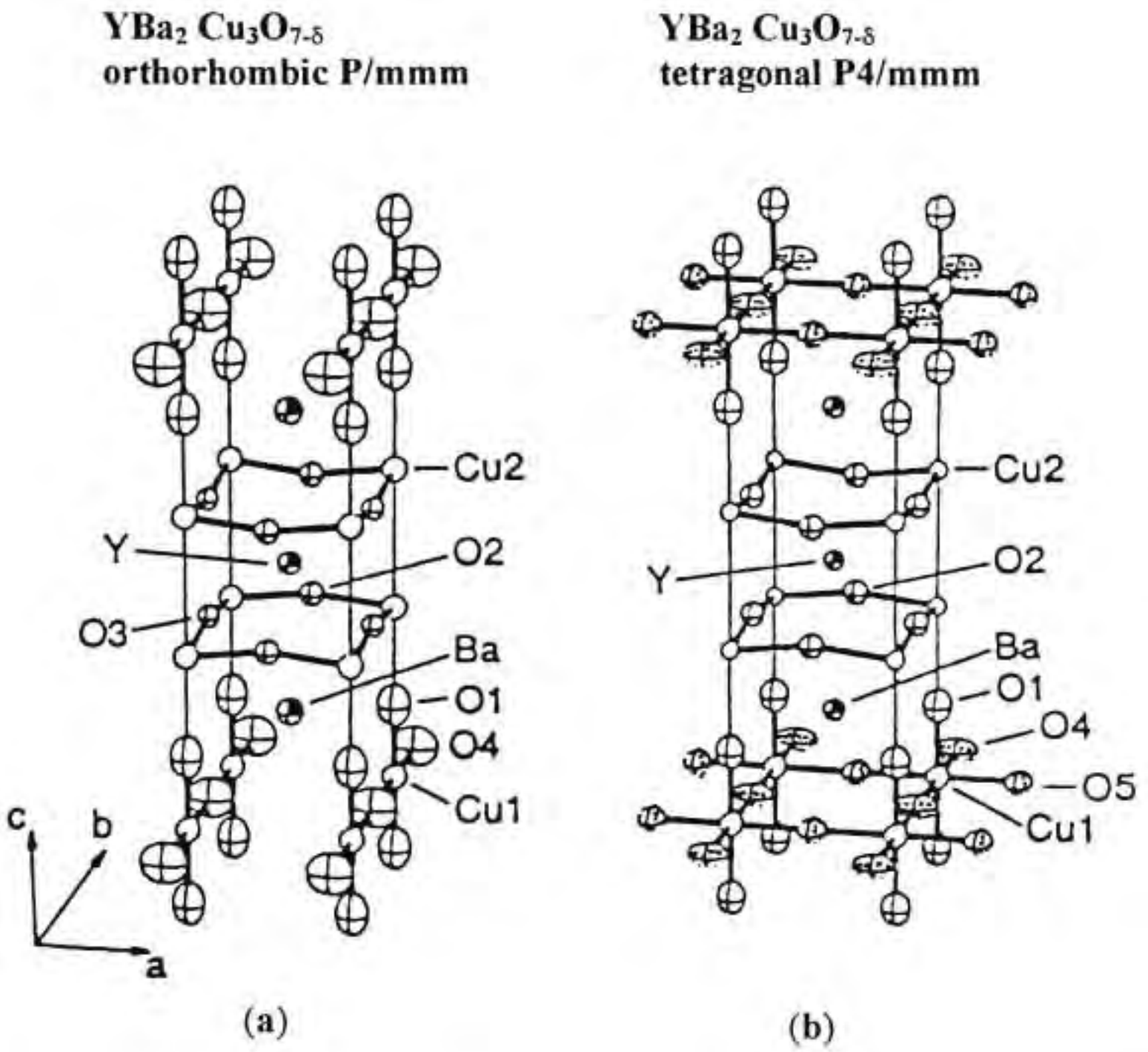

Fig. 1.3 The structure of (a) orthorhombic and (b) tetragonal phases of $YBa_2Cu_3O_{7-\delta}$ compound.

The $YBa_2Cu_3O_{7-\delta}$ compound undergoes phase transition from superconducting orthorhombic structure to non-superconducting tetragonal structure as the oxygen content changes from 7 to 6. At high temperatures (>700°C) the structure is tetragonal and the slow cooling of the high temperature tetragonal phase to lower temperature (<700°C) enables the

absorption of oxygen from the atmosphere which results in a phase change into the orthorhombic structure which exhibits high temperature superconductivity. These transformations, i.e. orthorhombic to tetragonal and vice versa, are reversible. On the other hand, rapidly cooled YBCO samples remain in the tetragonal form and are not superconducting at 90 K, but at a much lower temperature. When the oxygen content in the YBCO sample is in the range 6 to 6.5, the compound is tetragonal and if it is in the range 6.5 to 7.0, it is orthorhombic [68]. In the orthorhombic form all the O4 sites are occupied and in the tetragonal form they are vacant. Quenching of YBCO from high temperature results in oxygen deficiency and the quenched samples remain in the tetragonal phase. On the other hand if the compound is cooled slowly in oxygen from high temperature, oxygen is absorbed [69] and the tetragonal to orthorhombic transformation occurs. The structural transformations and the associated superconducting properties depending on the oxygen content of YBCO have been reported by several groups [70-75]. A typical curve for the variation of T_C with the oxygen content is shown in Fig.1.4.

The superconducting phase $YBa_2Cu_3O_{7-\delta}$ has an orthorhombic structure with lattice parameters a = 3.8231 Å, b = 3.8864 Å and c = 11.6807 Å [76]. The powder X-ray diffraction data (diffraction angle; 2θ and the corresponding d spacing with indices) of $YBa_2Cu_3O_{7-\delta}$ are given in table 1.2. The d-spacings for the X-ray pattern were calculated for Cu Kα radiation (λ = 1.54050 Å). YBCO belong to type II superconductors. The

studies of YBCO single crystals showed marked anisotropic behaviour in resistivity [77], magnetic susceptibility [78], critical magnetic field [78,79] and critical current density [80,81]. Some of the important properties of YBCO are summarised in table 1.3. Superconductivity of YBCO samples is greatly degraded by the interaction with water and humid air [85,86].

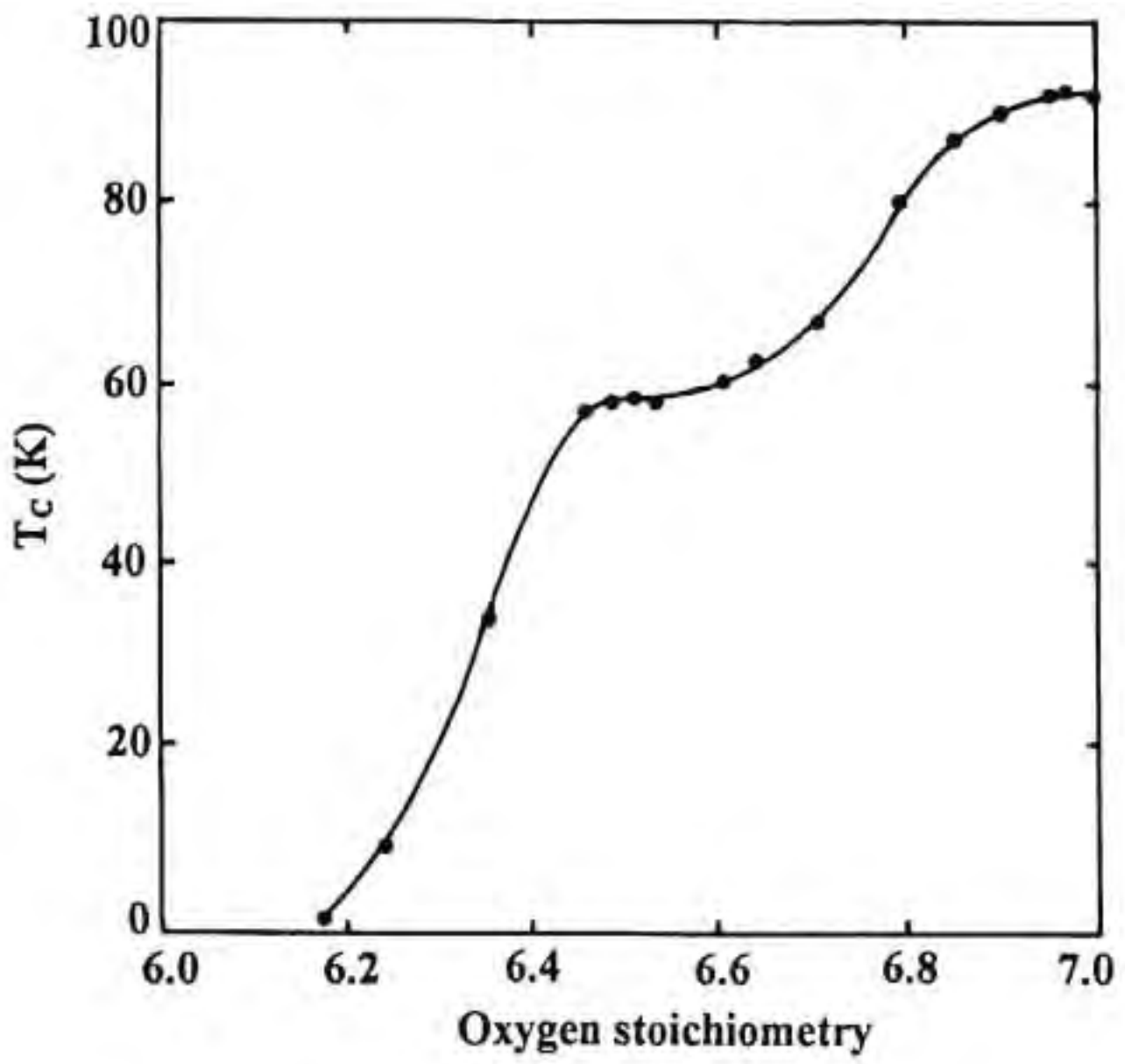

Fig. 1.4 The variation of T_C with oxygen stoichiometry for $YBa_2Cu_3O_{7-\delta}$ compound.

A survey of the literature shows that good amount of work has been carried out in the substitution of different ions in YBCO superconductor. As mentioned earlier the substitution of Y by any rare-earth other than

Table 1.2 Powder X-ray diffraction data of $YBa_2Cu_3O_7$ (ref. 76)

				Calculated			Observed		
No.	h	k	l	2θ(deg.)	'd' (Å)	I/I_o	2θ(deg.)	'd' (Å)	I/I_o
1.	0	0	1	7.562	11.6807	1.48	7.557	11.6883	1.00
2.	0	0	2	15.157	5.8404	2.74	15.169	5.8357	4.00
3.	0	0	3	22.820	3.8936	6.57	22.835	3.8910	10.00
4.	0	1	0	22.862	3.8864	8.00	Absent		
5.	1	0	0	23.246	3.8231	3.97	23.274	3.8186	4.00
6.	0	1	2	27.544	3.2355	5.20	27.554	3.2344	3.00
7.	1	0	2	27.868	3.1987	9.30	27.893	3.1959	5.00
8.	0	1	3	32.524	2.7506	90.10	32.538	2.7494	55.00
9.	1	0	3	32.802	2.7279	100.00	32.842	2.7274	100.00
10.	1	1	0	32.833	2.7254	98.43	Absent		
11.	1	1	1	33.741	2.6542	1.73	33.757	2.6529	2.00
12.	1	1	2	36.344	2.4698	4.11	36.37	2.4681	3.00
13.	0	0	5	38.502	2.3361	11.38	38.512	2.3356	13.00
14.	0	1	4	38.529	2.3346	5.77	Absent		
15.	1	0	4	38.770	2.3207	3.91	38.799	2.3190	5.00
16.	1	1	3	40.360	2.2328	22.72	40.384	2.2315	14.00
17.	0	0	6	46.613	1.9468	16.62	46.633	1.9460	22.00
18.	0	2	0	46.704	1.9432	29.74	46.725	1.9424	21.00
19.	2	0	0	47.525	1.9115	28.14	47.580	1.9095	12.00
20.	1	1	5	51.476	1.7737	7.17	51.495	1.7731	4.00
21.	0	1	6	52.529	1.7406	1.48	52.526	1.7407	3.00
22.	0	2	3	52.592	1.7387	1.55	Absent		
23.	1	2	0	52.801	1.7323	1.12	52.733	1.7344	4.00
24.	2	0	3	53.345	1.7159	1.49	53.400	1.7143	2.00
25.	2	1	0	53.365	1.7153	1.75	Ab sent		
26.	0	0	7	54.980	1.6687	2.00	54.997	1.6682	2.00
27.	1	2	2	55.264	1.6608	2.71	55.313	1.6594	1.00
28.	1	1	6	58.185	1.5842	31.14	58.207	1.5836	26.00
29.	1	2	3	58.244	1.5827	36.74	Absent		
30	2	1	3	58.772	1.5697	32.25	58.826	1.5684	13.00
31.	0	2	5	62.073	1.4939	4.93	62.080	1.4938	2.00
32.	1	2	4	62.262	1.4899	1.74	62.262	1.4899	2.00
33.	2	0	5	62.751	1.4794	4.75	62.809	1.4782	3.00
34.	2	1	4	62.770	1.4790	2.32	Absent		
35.	1	1	7	65.536	1.4231	3.20	65.571	1.4225	2.00
36.	0	2	6	68.119	1.3753	9.90	68.134	1.3750	5.00
37.	0	1	8	68.602	1.3668	3.76	68.618	1.3665	5.00
38.	1	0	8	68.763	1.3640	4.38	68.797	1.3634	13.00
39.	2	0	6	68.765	1.3640	9.61	Absent		
40.	2	2	0	68.836	1.3627	16.77	68.888	1.3618	12.00

Table 1.3 Properties of $YBa_2Cu_3O_{7-\delta}$ superconductor

Structure	Orthorhombic Perovskite
Lattice parameters (Å)	a = 3.8231, b = 3.8864 & c = 11.6807
Theoretical density (gm/cm^3)	6.374
Thermal expansivity (K^{-1})	11.5 x 10^{-6}
Specific heat (J kg^{-1} K^{-1})	431
Thermal conductivity (W m^{-1} K^{-1})	2.4 x 10^{-2}
Hall carrier density (cm^{-3})	4 x 10^{21} (for a material of resistivity 400 μ.Ω.cm. just above T_c)
BCS coherence length (nm)	1.4
London penetration depth (nm)	200
Mean free path (nm)	1.2
$T_c(0)$ (K)	92
$H_c(0)$ (T)	1
$H_{c2}(0)$ (T)	120
Absolute thermoelectric power (μV/K)	3
J_c at 77 K and zero field (A/cm^2)	10^3-10^4 (bulk) 10^6-10^7 (epitaxial thin films)

those of Ce, Pr and Tb show no substantial variation in T_c and the value of T_c is around 90 K [34-36]. The partial substitution of barium by strontium or calcium shows a depression in T_c [87]. There are enormous

number of reports of the partial substitution of Cu by Pd, Co, Fe, Ni, Zr, etc. [88-95]. In all these cases it was observed that the T_C showed a decreasing trend. The partial substitution of oxygen by sulphur showed no change in T_C and it is reported that this has resulted in sharper transition [96]. Meanwhile the partial substitution of Cl for O showed a depression in T_C [96]. There were reports that the partial substitution of O by F enhanced T_C (~150 K) [97,98], but there was no conformation of this result afterwards.

1.4.3. Bismuth Strontium Calcium Copper Oxide Superconductor

Michel *et al.* reported the existence of superconductivity in bismuth-strontium-copper-oxide system with T_C between 7 and 20 K [99]. But this discovery did not attract much attention at that time because of its low value of T_C. The bismuth based superconductors gained attention when superconductivity above liquid nitrogen temperature was reported by Meda *et al.* [45] and later by Chu *et al.* [100]. They reported that the addition of Ca in Bi-Sr-Cu-O system produced superconductivity above 77 K. Three superconducting phases were subsequently identified in the Bi-Sr-Ca-Cu-O system [99,46,101,102], namely $Bi_2Sr_2Cu_1O_6$ (2201; T_C ~17 K), $Bi_2Sr_2CaCu_1O_8$ (2212; T_C ~82 K) and $Bi_2Sr_2Ca_2Cu_3O_{10}$ (2223; T_C ~110 K). The Bi(2201) phase reported by Michel *et al.* is the least studied because of its low value of T_C.

In bismuth based copper oxide superconductors the structure consists of intergrowths with perovskite like units containing one, two or three CuO_2 planes sandwitched between Bi-O bilayers [4]. The structure

of Bi(2212) deducted from neutron and x-ray diffraction studies revealed that it corresponds to an orthorhombic symmetry with lattice parameters a = 5.414 Å, b = 5.428 Å and c = 30.99 Å [103]. Similarly Bi(2223) also has an orthorhombic structure with lattice parameters a = 5.390 Å, b = 5.410 Å and c = 37.1 Å [104]. The crystal structure of Bi-2201, Bi(2212) and Bi(2223) are given in Fig.1.5. The bismuth compound $Bi_2Sr_2CaCu_2O_{8+\delta}$, $\delta<1$ shows many similarities to the YBCO with a number of significant differences. For instance, the unit cell of Bi(2212) is larger and more complex and it is much more highly anisotropic and forms mica like flaky sheets that easily delaminate [4]. Also unlike the YBCO compound, oxygen annealing is not necessary; a small loss of oxygen does not destroy superconductivity and because of the absence of barium it is less sensitive to atmospheric moisture and CO_2, hence more stable in air. As compared to YBCO, the bismuth compound appears to have a much narrower temperature processing window.

The preparation of bismuth based superconducting compounds as single phase materials is difficult and one of the major constraint is that the different phases are stable only within a small temperature range. It has been reported that a single phase Bi(2223) can be prepared by the precise control of the processing conditions and by the partial substitution of lead for bismuth [105-107].

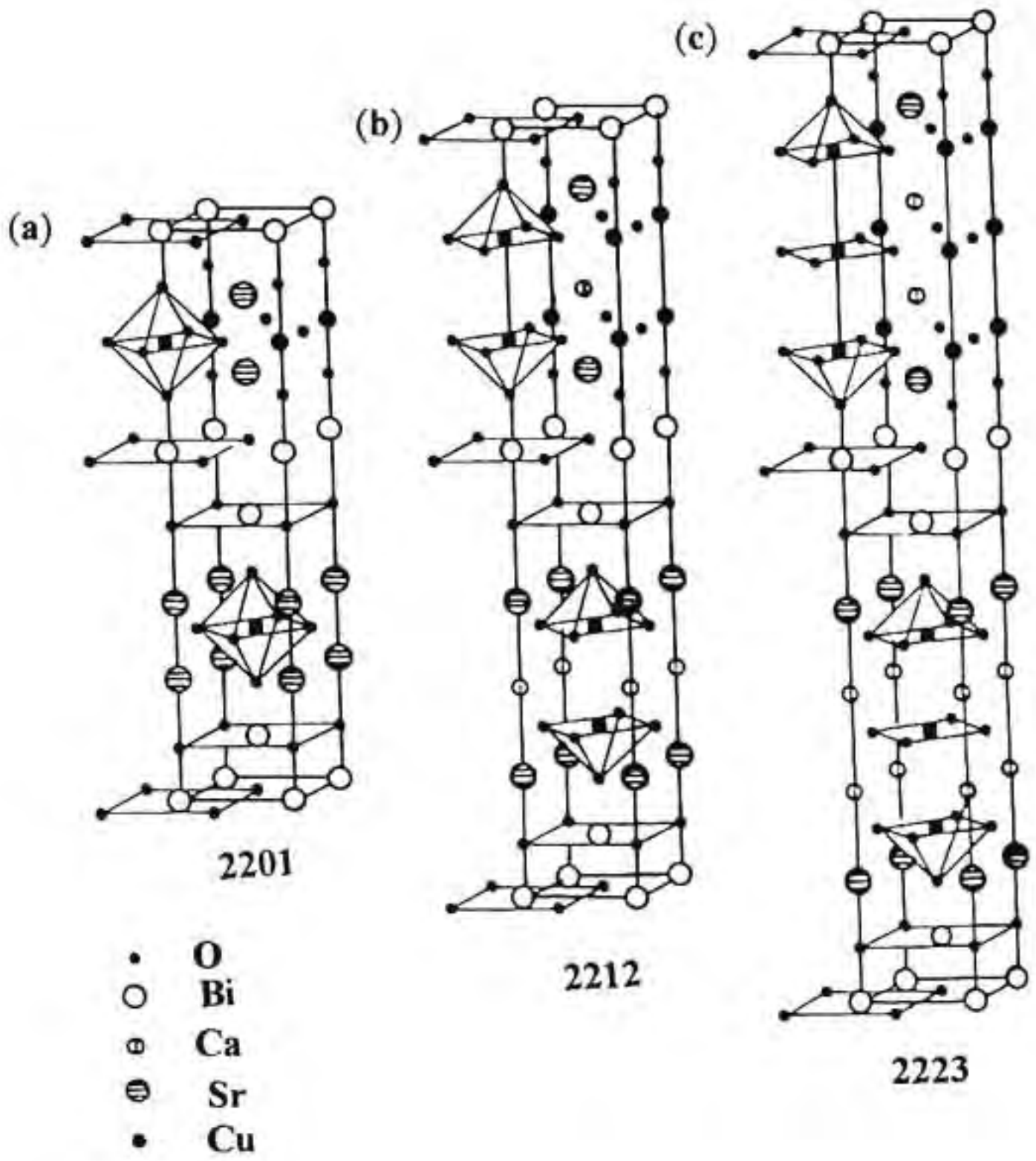

Fig. 1.5 Crystal structure diagram of bismuth superconductors (a) $Bi_2Sr_2CuO_5$, (b) $Bi_2Sr_2CaCu_2O_7$ and (c) $Bi_2Sr_2Ca_2Cu_3O_{10}$.

1.4.4. Thallium Barium Calcium Copper Oxide Superconductor

Sheng and Hermann discovered superconductivity in Tl-Ba-Cu-O system with a T_C above 77 K [108]. They raised the T_C further by adding Ca to the above system and got a T_C onset of ~120 K [47]. Two superconducting phases were identified in Sheng and Hermann's samples by Hazen *et al.* $Tl_2Ba_2CaCu_2O_{8+\delta}$, $Tl_2Ba_2Ca_2Cu_3O_{10+\delta}$ [48]. Then Parkin *et al.* [109] changed the processing conditions to greatly increase the amount of Tl(2223) and produced a T_C of 125 K. Later different superconducting compounds in the family $TlBa_2Ca_{n-1}Cu_nO_{2n+4}$ were discovered [110].

The replacement of bismuth by thallium and strontium by barium in the bismuth system yields a similar set of compounds which are superconducting. In the case of thallium compounds in the series $Tl_2Ba_2Ca_{n-1}Cu_nO_{2n+4+\delta}$, the structure consists of perovskite like units containing one, two or three CuO_2 planes separated by Tl-O by bilayers [4]. On the other hand, the thallium compounds of the series with the formula $TlBa_2Ca_{n-1}Cu_nO_{2n+3+\delta}$, are made up of perovskite like units containing one, two or three CuO_2 planes separated by Tl-O monolayers respectively and have no bismuth analogs. All the thallium compounds have tetragonal structure at room temperature. The thallium compounds with Tl-O monolayers have primitive tetragonal cells whereas the oxides with Tl-O bilayers have body centred tetragonal cells. The crystal structure diagram of $TlBa_2CuO_5$, $TlBa_2CaCu_2O_7$, and $TlBa_2Ca_2Cu_3O_9$ are shown in Fig.1.6. The crystal structure diagram of $Tl_2Ba_2CuO_6$, $Tl_2Ba_2CaCu_2O_8$ and $Tl_2Ba_2Ca_2Cu_3O_{10}$, are similar to that given in Fig.1.5 and can be obtained by replacing bismuth with thallium and strontium by barium.

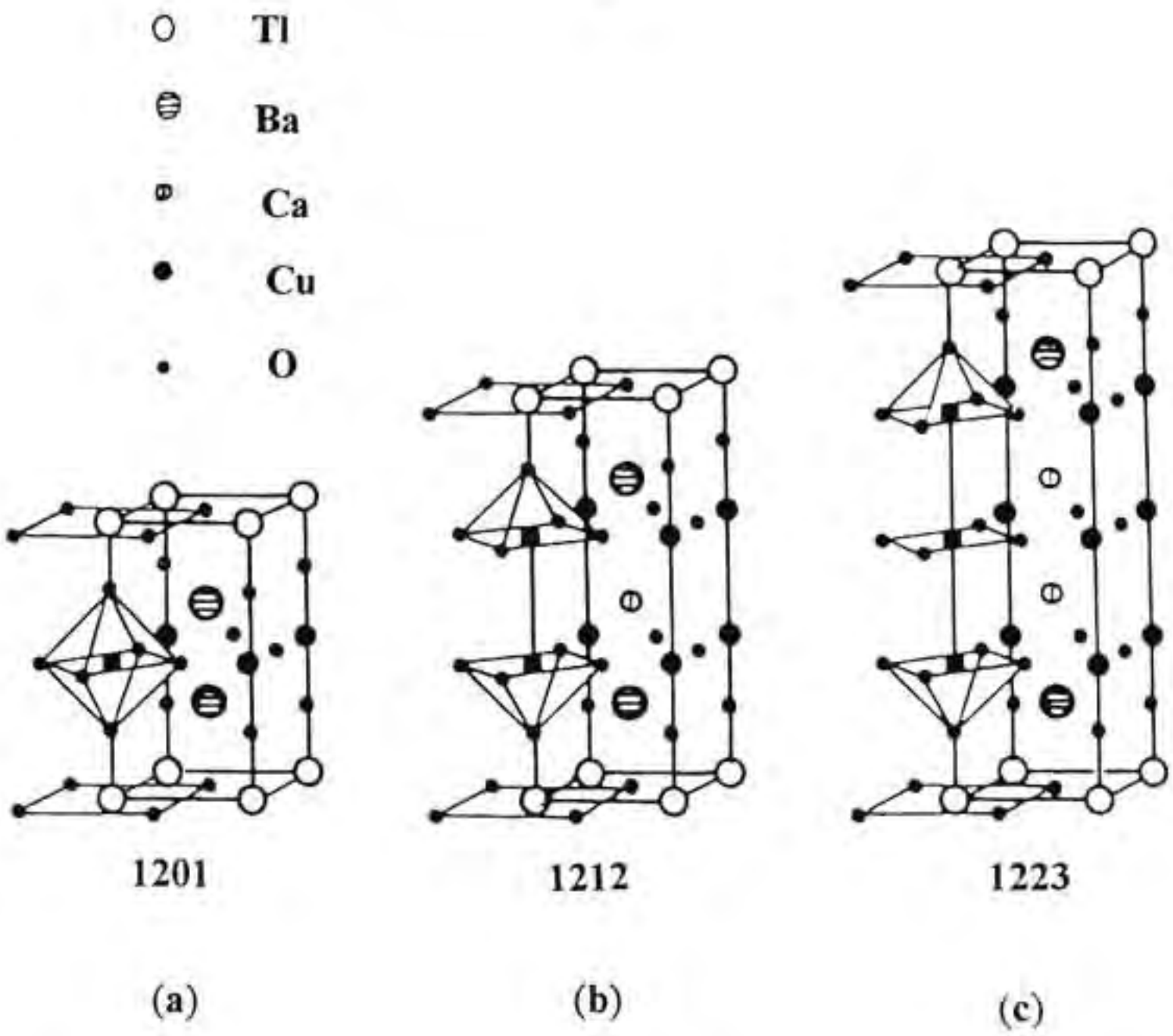

Fig. 1.6 Crystal structure diagram of (a) $TlBa_2CuO_5$, (b) $TlBa_2CaCu_2O_7$ and (c) $TlBa_2Ca_2Cu_3O_9$ superconductors.

1.4.5. Mercury Barium Calcium Copper Oxide Superconductor

The highest T_C obtained so far is in the Hg-Ba-Ca-Cu-O system. In 1993 Putilin *et al.* reported the discovery of superconductivity in $HgBa_2CuO_{4+\delta}$ with a T_C of 94 K [111]. Later the existence of superconductivity above 130 K was reported in a multiphase compound of Hg-Ba-Ca-Cu-O system [49]. Single phase $HgBa_2Ca_2Cu_3O_{8+\delta}$ was subsequently synthesised

and found to be superconducting at a record temperature of 135 K [50]. Due to the high volatility of the mercury compounds, the synthesis of single phase Hg based superconductors is difficult. This problem was overcome by using the high pressure technique [112]. The synthesis of single phase Hg-1223 by a reaction sintering under high pressure and high temperature was reported by Hirabayashi *et al.* [113]. In this technique a precursor with the required composition of Ba, Ca and Cu was calcined and an appropriate amount of HgO is added to it. This is then sealed in an Au capsule for the high pressure synthesis and heated under pressure of ~5 Gpa.

1.5. Substrates for High T_C Superconductors

Copper oxide superconductors are highly attractive for practical applications, since they can superconduct at temperatures above the boiling point of liquid nitrogen. For most of the practical applications large critical current density values of the order of 10^4 to 10^6 A/cm^2 are required in the presence of large magnetic fields. Such high values of critical current density are attainable in the case of high quality films of these oxide superconductors. So the immediate application of these new high T_C ceramic superconductors (HTSC) are mainly in the form of thick and thin films. In order to obtain high quality films, the selection of a suitable substrate and the optimisation of the processing conditions are essential. In the preparation of superconducting films, substrate plays a vital role and one of the issues that presents particular challenges in the

case of HTSC materials is the substrate. Ideally, the substrate should provide only mechanical support but not interact with the film except for sufficient adhesion. In practice, however, the substrate exerts considerable influence on the film characteristics. The search for viable substrate materials is an active area of research.

A number of issues are important in the selection of substrate materials for HTSC films. An ideal substrate for HTSC films should be chemically non-reacting, have a good lattice and thermal match to the film, have low dielectric constant ($\acute{\varepsilon}$) and loss factor (tan δ), cheap in large size single crystals and be easily cut and polished. Also it should be mechanically strong and have a flat, dense surface and be free of twins and other structural inhomogenities [114-116].

The chemical compatibility between the substrate and the film is the first and foremost criterion to be dealt with in determining the suitability of a substrate for HTSC films [116,117]. The high chemical reactivity of HTSC materials and the elevated processing temperature required for the preparation of HTSC films make the compatibility requirements more critical than it would be if high quality films could be prepared at lower temperature. The higher the processing temperature required, the more stringent the requirement for chemical inertness. Regardless of the specific preparation method used, the substrate must be non-reactive in the oxygen rich ambient atmosphere required for HTSC film processing. The high chemical reactivity of YBCO with the conventional substrates such as

Al_2O_3, Si, SiO_2 imposes severe constraints for their use as substrates for YBCO films which might other wise be good candidates. The overriding importance of chemical compatibility over other substrate requirements in determining the suitability of a material as substrate for HTSC film growth have been highlighted in many review articles [116,117]. Therefore, if the chemical compatibility is poor, a good match of other substrate requirements becomes irrelevant.

The next important criterion is the thermal expansion match. A good thermal expansion match is required for obtaining a good quality film. A thermal expansion mismatch may lead to loss of adhesion or film cracking during thermal cycling. The brittleness of the HTSC materials makes cracking of the film surface likely if the mismatch is severe and is especially true if the film is in tension, i.e. if the thermal expansion of the substrate exceeds that of the film. Also the effect of thermal mismatch on the film may depend on film thickness, i.e., a thinner film may confirm to the thermal properties of the substrate, whereas a thicker film may crack. A thermal expansion mismatch may cause the film properties themselves to be altered from what they would be if the mismatch were absent [117]. For substrates application, the high thermal conductivity of the substrate material is considered as an additional advantage [114].

Lattice match of the substrate with the film is an essential requirement for epitaxial growth. The studies of epitaxial growth of films on substrates which are very much different chemically and structurally

from the film to be grown, indicated that a lattice match of less than 15% was required for these to be a possibility of epitaxy [118]. Also very small lattice mismatches are desirable to minimise the effects of dislocations and other defects brought about by lattice dissimilarities. In the case of HTSC materials, it is desirable to minimise the lattice mismatch as much as possible as it seems to improve the ability to obtain singly oriented films [117].

Another important requirement for epitaxial growth is the presence of coincidence sites. The close lattice match between the film and the substrate is simply not enough requirement for good epitaxy, but there must also be a reasonable number of coincidence sites between the two lattices of the film and the substrate on either side of the interface [117]. Coincidence sites are atomic positions, preferably with same or similar atomic sizes and values, that coincide on either side of the interface. In most of the cases this means that the film and the substrate should have similar crystal structures. So, the higher the number of coincidence sites, the better the chance of good epitaxy.

The surface quality of the substrate is important as it is here that the film substrate interaction occurs. A uniform substrate surface is necessary to ensure a uniform and homogeneous film. Therefore, the substrate surface should be free from surface defects like surface warp, cracks, polishing scratches, pores, twin boundaries, dislocation lines, point defects, etc. The surface smoothness is important for a number of

reasons, for example, in some cases scratches or crystallographic steps may influence the orientation of a crystalline film as well as its overall microstructure. So an ideal substrate would have a flat, dense surface and be free of twins and other structural inhomogeneities. Twinning leads to surface corrugations and in the case of HTSC films this leads to the reduction of J_c [119]. Also it is highly desirable that the substrate be thermodynamically stable within the temperature range required to grow and process the film. A phase transition within this region can have dramatic effects on the surface quality of the substrate and the stresses that the film must undergo. So if a phase transition is inevitable, it should be as minor as possible, that is it should be of second order with no discontinuous volume change and minimal structural change [117].

In the case of device applications of HTSC materials another important requirement is that the substrate should have low dielectric constant ($\acute{\varepsilon}$) and loss factor (tan δ). This requirement is more severe in the case of microwave applications. Operation at microwave frequencies imposes the need for substrates with low value of loss tangent [117]. The desired value of $\acute{\varepsilon}$ is related to the length of electromagnetic wave in the substrate material and microwave integrated circuit fabrication tolerances. In order to avoid the destruction of the electromagnetic stability of the circuit, the substrate thickness as well as the width of the co-planner lines should be sufficiently less than the wavelength [114]. By increasing the operating frequency one reduces the maximum of allowed substrate

thickness and line width. However, the substrate thickness cannot be reduced to less than 0.3 to 0.5 mm without comprising much on its mechanical strength. This imposes restrictions on the values of $\acute{\varepsilon}$ of the substrate material and extremely high values of $\acute{\varepsilon}$ and tan δ rule out their application as substrates for microwave circuits [114]. Also in the case of microwave applications where the dielectric properties of the substrate have an important effect on device performance, existence of twining transition in the processing temperature range is unacceptable as it precludes device modelling [120].

For most of the practical applications requires large area single crystal substrates. The single crystal growth of the material requires that it must be congruent melting. Finally in order to be attractive for practical applications, the substrate should be available in large size single crystals, cheap and be easily cut and polished. In practice, the substrate exerts considerable influence on the film characteristics and the crystalline quality of the film will be no greater than that of the substrate.

The survey of the literature shows that many materials have been studied for their suitability as substrates for HTSC films. The conventional substrate materials such as Si, SiO_2, etc react with YBCO at the processing temperature thereby degrading the superconducting properties of the film severely [121,122]. Though Al_2O_3 combines outstanding dielectric properties and high mechanical strength and the commercial availability in high quality twin free large diameter single crystals, the

reaction between Al_2O_3 and YBCO restricts its use as substrate for YBCO superconductor [123-126]. MgO, one of the extensively used substrate material for YBCO thin film growth, form an interlayer of barium salt at the film-substrate interface if the processing temperature is above 700°C, thereby reducing the superconducting transition temperature of the YBCO film considerably [123,125-129]. The other drawbacks of MgO are the lack of mechanical strength, high hygroscopicity and moderate area of the single crystal substrates available [114]. Yttria-stabilised zirconia (YSZ) has been reported as substrate and as a buffer layer between other substrate and YBCO films [114,117]. Considerable success has been achieved in the preparation of YBCO films on YSZ which offers a fair lattice match with YBCO. But there are reports of $BaZrO_3$ formation at the film-substrate interface, indicating chemical reaction [130,131]. The major disadvantage of using YSZ, as far as device applications are concerned, is its high dielectric loss (tan $\delta = 7.5 \times 10^{-3}$ at 10 GHz and 80 K) [132]. $SrTiO_3$ is one of the best substrates which could yield high quality YBCO thin films. Even with the close lattice matching with YBCO, its high dielectric constant [115-117] and loss factor values restricts its use as substrate for microwave device applications. Presently, $LaAlO_3$ have become a substrate of choice for YBCO films. It has a moderately low dielectric constant (~24) and loss factor (~10^{-5}) values, but has the disadvantage that it is available only in twinned crystalline form [116,117,133]. $LaGaO_3$, though has a quite good lattice match and thermal

expansion match with YBCO, and has a serious drawback of having first order phase transition at 420 K [117,134]. Another material, $NdGaO_3$ has a low $\varepsilon' = 20$ and has smaller lattice mismatch than $LaAlO_3$ or $LaGaO_3$. $NdGaO_3$ also has a phase transition at about 1270°C, but the tendency of twinning is much less pronounced than in $LaAlO_3$ or $LaGaO_3$[119]. The properties of some of the important substrate materials reported for HTSC films are summarised in Table.1.4.

1.6. High T_C Superconductor Films

It has been pointed out by several authors that the immediate application of high T_C ceramic superconductors are mainly in the form of thick and thin films [135-139] as these oxide superconductors are brittle; a typical characteristic of ceramic materials. Also, for practical applications, high critical current densities are required and are attainable in the case of high quality films of these superconductors [114,140,141]. For obtaining high quality films of these materials, selection of suitable substrate and the optimisation of processing conditions are crucial. The research in the preparation of high quality films has been motivated by the possibilities of using these HTSC materials in various microelectronic devices like low loss microwave cavities and filters, bolometers, flux transformers, dc and rf superconducting quantum interference devices, HTSC interconnects etc [117]. It is difficult to produce high quality films of these HTSC materials because of the sheer complexity, high anisotropic nature,

Table 1.4 Properties of materials proposed as substrates for HTSC films.

Material	structure	lattice constants a (Å)	b (Å)	c (Å)	dielectric constant (ε)	loss factor (tan δ)	Thermal expansivity x 10^{-6} (K^{-1})
α- Al_2O_3	Cubic				9.4	$3x10^{-5}$ (77 K, 5 GHz)	8
YSZ	Cubic	5.14			25	8×10^{-3} (100 K, 300 GHz)	11
CeO_2	Cubic	5.41			26	-	9.9
MgO	Cubic	4.21			9.6	5×10^{-4} (100 K, 300 GHz)	13.8
$YbFeO_3$	Orthorhombic	5.36	5.5	7.77	5	-	-
BaF_2	Cubic	6.20			7.3	2×10^{-3}	18
$LaAlO_3$	Rhombohedral	3.79			24	3.1×10^{-5}	11
$YAlO_3$	Orthorhombic	3.662	3.768	3.685	16	7.3×10^{-5}	-
$GdAlO_3$	Tetragonal	3.731		3.724	19.5	1×10^{-4}	-
$EuAlO_3$	Tetragonal	3.729		3.734	22.5	1×10^{-4}	-
$SmAlO_3$	Tetragonal	3.737		3.739	19	1×10^{-4}	-
$NdAlO_3$	Cubic	3.750			22.5	5×10^{-5}	-
$EuAlO_3$	Cubic	3.762			25	8×10^{-5}	-
$LaGaO_3$	Orthorhombic	5.519	5.494	7.77	25	10^{-4}	5.6
$NdGaO_3$	Orthorhombic	5.417	5.499	7.717	20	1×10^{-4}	5.8
$PrGaO_3$	Orthorhombic	5.462	5.493	7.740	24	-	8
$SrTiO_3$	Cubic	3.905			277	6×10^{-3} (100 K, 300 GHz)	
$KTaO_3$	Cubic	3.988					6.7
$CaNdAlO_4$	Tetragonal	3.69		12.15	19	1×10^{-4} (77 K, 5 GHz)	
$CaYAlO_4$	Tetragonal	3.648		11.89	20	4×10^{-4} (77 K, 5 GHz)	
$LaSrAlO_4$	Tetragonal	3.754		11.263	17	1.5×10^{-5} (77 K, 10 GHz)	
$LaSrGaO_4$	Tetragonal	3.84		12.676	22	5×10^{-5}	10
Mg_2TiO_4	Cubic	8.44			12	15×10^{-3}	12

close tolerance of the composition required and the high processing temperature which make the chemical compatibility requirement of the substrate with the film more severe. Also the oxygen atmosphere required in the case of *in situ* growth of YBCO thin films imposes additional constraints for the preparation of films, as oxygen is incompatible element with many aspects of traditional thin films growth methods, especially the substrate heating necessary for producing superconducting films.

1.6.1. High T_C Superconductor Thick Films

Thick film technology as we know it today began some forty years ago as a proprietary act, for the manufacture of microcircuits incorporating desired combinations of conductors, dielectrics, resistors, thermistors etc. Thick films are very complex, non-equilibrium systems having physical properties that are intimately related to their microstructure, which in turn is determined by the combination of material properties and processing conditions. Thick films are distinguished from thin films by the method of fabrication and not by thickness [142]. Thick film technology involves two main steps, (a) the deposition of the film of the required material in the desired pattern on to a substrate by common coating methods such as screen printing, spin-coating, dip-coating, spray pyrolysis, paint-on method etc. and (b) the subsequent drying, followed by firing at a higher temperature to produce films of about 3 to 50 μm thick. The final electrical properties of the films depend on the material properties of the

ink ingredients and the substrate as well as the deposition process and time-temperature-atmosphere conditions during firing [142]. Most of the inks contain some active ingredients (the material to be printed), a binder and a screening agent. The primary function of the screening agent is to establish proper rheology for the ink. The thick film inks must have a very high viscosity to retain the particles in suspension and the blending of the organic and inorganic constituents of the ink is required. The rheological properties of the ink are strongly influenced by the size, shape and concentrations of the inorganic particles, but the control of the ink properties is invariably attempted through selection of the organic constituent. In addition to providing suitable rheology, the other major requirement for the organic constituent in the ink is that they are removed completely during the time-temperature-atmosphere required to produce the desired inorganic films. Not only they be removed completely, but they should not influence the chemistry of the inorganic constituents before removal.

Thick films offer mainly two advantages over thin films in certain applications [130,143]. First, the preparation of thick films is inexpensive when compared with thin films which require expensive and sophisticated instrumentation for their deposition. Secondly, they can cover larger areas. Also thick film methods are simple, less costly and easy to apply. Thick films of HTSC materials are of interest for many practical applications such as substrate wiring and magnetic shielding [138,143-145]. Thick

films of HTSC materials have been produced by different methods such as screen printing, spray pyrolysis, spin-coating, dip-coating, paint-on etc. In all these cases post heat treatment is essential. The important requirements for a good HTSC film are adherence to the substrate and its superconducting properties [146]. The later are governed by the alignment and size of the superconducting grains, the presence of grains of foreign phases and the intergrain connectivity etc. In order to achieve good adherence, partial melting of the HTSC material is almost essential [129,130,139,146]. One of the difficulties which come across during the preparation of YBCO thick film is the decomposition of YBCO and its enhanced reaction with the substrate at the partial melting temperature which results in the formation of undesired phases [146].

A survey of the literature shows that considerable amount of success has been achieved in the preparation of superconducting thick films of HTSC materials. Among the different methods used for the preparation of HTSC films, screen printing is more attractive, from application point of view as it is a simple and straight forward method for the preparation of thick films. Also screen printing has an additional advantage over other methods that electronic and microwave circuit patterns and devices can be directly printed on the substrate; thus avoiding the etching and photolithographic steps [126,127,147]. This is of particular importance for films of YBCO superconductor because of its high reactivity with moisture and other chemicals [148]. In the case of screen

printing, the ink (paste for screen printing) is prepared by thoroughly mixing fine HTSC powder with an appropriate amount of organic vehicle. This is then printed on a desired substrate through a screen of suitable mesh size. The printed film is then dried and subjected to controlled heat treatment for obtaining a superconducting thick film [126,139,143,149-152]. For spray pyrolysis, an aqueous solution of the different metal nitrates are prepared in the desired stoichiometric ratio. This desired stoichiometric solution is then sprayed on to a heated substrate placed at a suitable distance from the aerosol nozzle using a carrier gas [153-155]. In the case of spin coating the substrate is attached to a spinning rotor and the thick film paste is allowed to fall on the spinning substrate drop by drop. For dip coating process, the substrate is dipped in the thick film suspension to obtain a thick film coating of the desired material. HTSC thick films have been successfully prepared by both dip coating and spin coating [156-159]. Similarly in paint-on method, the ink is applied on the substrate by means of a fine brush [146,160-161]. In all the above cases the dried film is subjected to heat treatment for obtaining the final adherent superconducting film. In all the above mentioned thick film techniques for the preparation of YBCO films on Si, SiO_2 and Al_2O_3 yielded poor quality films with low T_c and J_c values. The YBCO thick films developed on MgO had low T_c values of ~80 K but was better than the films on Si, SiO_2, Al_2O_3, etc. [123,126,162]. Higher values of T_c have been obtained in the case of YBCO thick films developed on YSZ [130,135,145,151]. In

almost all cases partial melting was found essential for obtaining a good adherent YBCO film and also melt-processing has shown to produce large grains and fewer grain boundaries which in turn improved the J_C of the film. Also this procedure yields films with low surface resistance [139,163]. The results of the silver doped YBCO films shows that the silver addition facilitates the formation of an adherent and denser film by promoting the grain growth. Also this has shown to improve the grain alignment and J_C of YBCO films [135,139,143,146,151]. The addition of silver also improves the stability against environmental degradation and mechanical strength of YBCO films [135,162].

1.6.2. High T_C Superconductor Thin Films

Thin films of HTSC materials are important because of a number of reasons. Thin films have superior properties compared to thick films or bulk material. Also they are required for many electronic applications. Quite a good number of reports of growth of HTSC materials on different substrates are available in the literature now. The properties of thin films of HTSC materials have been reported by different techniques, one requiring high temperature annealing after growth (*ex situ* annealing) and the other grow a film in the correct crystal structure (*in situ* technique). In the preparation of films by *ex situ* annealing, the metallic elements are deposited in approximately the correct composition as an amorphous layer, usually in compound form with oxygen and possibly fluorine, on a

suitable substrate followed by annealing in air or oxygen at high temperature which then lead to the film crystallising by a solid state regrowth mechanism to form a polycrystalline but epitaxial layer [116]. Since the crucial growth step takes place long after deposition, the actual technique used to deposit the layer is of secondary importance. Quite a good number of reports of *ex situ* annealed thin films of HTSC materials are available in the literature [164,165]. The most widely studied HTSC material, YBCO, has now reached the point where state of the art material is mainly made by *in situ* methods. However, careful *ex situ* annealing has been successful in preparing high-order layer compounds of BSCCO and TBCCO families which have so far proved to be very difficult to make by *in situ* techniques [116].

In *in situ* growth the film is deposited in crystalline form and, although it may need some low temperature annealing to achieve the correct oxygen stoichiometry, it requires no substantial rearrangement of the lattice after growth. This has a number of advantages; the lower temperature involved (when compared with the processing temperature of thick films) minimize the chemical interaction between the substrate and the film, single crystal films can be grown, with greatly improved physical properties and with smooth film surface. In the case of YBCO films grown by *in situ* technique, the substrates are usually held at 650 to 800°C and a sufficient oxygen pressure is provided at the substrate surface. Different physical vapour deposition techniques have been successfully

used in this area and among them sputtering, laser ablation and evaporation are widely used for *in situ* growth. YBCO films have also been grown successfully by chemical vapour deposition (CVD) technique from organic precursors [166,167].

Single-target sputtering is the simplest method used to produce YBCO thin films. This technique allows the possibility of large area coating necessary for many device applications. In the case of sputtering the target composition can be reproduced in the film if the problem of resputtering of the deposited film owing to negative oxygen ions can be avoided. The problem of negative ion resputtering can be eliminated if a special geometry is adopted, i.e., by positioning the substrates out of the sputtering plasma (off axis or cylindrical configurations) [116,140]. In any case, the deposition rates are fairly low and the system is not very flexible if multilayer structures have to be used in order to make complex circuits. Another alternative is multitarget sputtering which is more flexible, but it is difficult to optimise the different parameters involved [140] which leads to considerable degree of irreproducibility of the results. Even then, several groups have grown excellent films in this way.

Many evaporation schemes have been proposed including single source and multisource configurations. In all cases, the main problem is related to the incompatibility of the evaporation sources with the high

oxygen partial pressure required for the *in situ* growth of YBCO films. Another difficulty in the case of multisource configuration is the accurate control of the film composition which requires continuous monitoring and active control in a feedback loop. In molecular beam epitaxy (MBE) systems the extreme control of deposition rates and epitaxy conditions is possible. There are quite a number of reports of YBCO film growth by evaporation process [168-170].

In the recent few years, pulsed laser deposition (PLD) has become one of the best PVD techniques for the deposition of films of oxide materials. Pulsed laser ablation has now emerged as the most reliable and easiest deposition technique currently available which could produce consistently high quality superconducting YBCO thin films. In laser ablation, the target composition is accurately reproduced, at least normal to the target being ablated, provided that a short laser pulse is used, the laser wavelength is short and the correct laser power density is used. The deposition configurations are simple and fully compatible with multilayer production. The deposition rates are quite high, but the main problem is the difficulty of coating large surfaces. Another dominant characteristics is the non-uniformity of the thickness of the films grown by pulsed laser ablation. It seems that the high success rate of producing high quality epitaxial YBCO films with optimum characteristics ($T_c(0) = T_c(0)$ bulk, J_c

values higher than 5 x 10^6 A/cm^2 at 7 7 K and zero magnetic field, surface roughness less than 100 Å) and the ease with which the composition can be controlled [116,171-175] has made pulsed laser ablation most popular technique. The *in situ* growth of YBCO films by PLD depends upon many factors such as oxygen pressure during growth, substrate temperature, target-substrate distance, target density, laser pulse energy density, laser wavelength with pulse width and repetition rate etc. [116,174].

A survey of the literature shows that YBCO films with critical current densities in excess of 10^6 A/cm^2 at 77 K have been successfully developed on different substrates. A brief summary of the results obtained in the case of YBCO thin films on various substrates are presented in table 1.5. One of the common parameters in most of the deposition techniques for the growth of YBCO films which determines the film quality is the substrate temperature during film growth. It was found that higher substrate temperature favours growth of oriented YBCO films with c-axis normal to the plane of the substrate, while lower substrate temperature favours growth of a-axis oriented films [189-192]. Significant improvement of J_c of YBCO films have been reported by Ag doping [180]. Also Ag doping has found to enhance the grain growth, grain alignment [180,193] and also reduce surface resistance significantly [194].

Table 1.5 T_C and J_C values of YBCO thin films grown on different substrates.

Substrate	T_C (K)	J_C (A/cm^2) at 77 K	reference
$LaGaO_3$	90	2.3×10^6	176
$YAlO_3$	91	7.2×10^5	177
$LaSrGaO_4$	91	3.5×10^6	178
MgO	90	2.5×10^6	179
$SrTiO_3$	90	5×10^6	176
$LaAlO_3$	90	5×10^6	180
$NdGaO_3$	89	2×10^6	181
$NdAlO_3$	89.7	3×10^4	182
$PrGaO_3$	90	-	183
$KTaO_3$	90	3×10^6	184
$YbFeO_3$	88	1×10^5	185
$CaNdAlO_4$	88	1×10^6	186
YSZ	92	5×10^6	187
$LiNbO_3$	88	2×10^5	188
$LaSrAlO_4$	80	3×10^5	116
$CaYAlO_4$	86	2×10^5	116

1.7. Scope of the Present Work

It was reported that the addition of oxides such as Nb_2O_5, Sb_2O_3, SnO_2, HfO_2, ZrO_2 etc., in YBCO did not have any detrimental effect on the superconducting properties of YBCO superconductor [195-199], though their addition has helped in eliminating the slow cooling procedure which was essential for obtaining superconductivity in YBCO. The addition of these oxides in YBCO resulted in the formation of a second phase, YBa_2MO_6

(M = Nb, Sb, Sn, Hf and Zr), which coexisted with the YBCO superconductor even after severe heat treatment conditions. This non-reacting second phase was later separately synthesised and investigated the possibility of their use as substrate for YBCO superconductor. But it was reported that the YBa_2MO_6 materials could be made single phase by the addition of CuO. Though CuO addition helped in obtaining higher sintered density, it adversely affected the dielectric properties. In this context studies were carried out to overcome this problem by substituting Y by other rare-earths and it was found that a group of ceramic materials, Ba_2RENbO_6 (RE = Pr, Nd, Sm, Eu and Gd), could be prepared and sintered as single phase materials without the addition of CuO. Also these materials were found to be non-reacting with HTSC materials even at the extreme processing conditions and has favourable dielectric properties. These materials were thermodynamically stable and has thermal properties suitable for their use as substrate for HTSC. The percolation studies carried out on superconductor-insulator composites using Ba_2RENbO_6 as the insulator revealed that there is no chemical reaction between the superconductor and Ba_2RENbO_6 materials even at the extreme processing conditions. The suitability of Ba_2RENbO_6 as substrates for HTSC films was demonstrated by developing superconducting HTSC films with excellent superconducting characteristics. Also superconducting YBCO thin films with high $T_C(0)$ and J_C were grown *in situ* on polycrystalline Ba_2RENbO_6 substrates by pulsed laser ablation technique. The experimental details and the results obtained are described in detail in the following chapters of the thesis.

General References

1. J.C. Phillips, Physics of High-T_C Superconductors, Academic Press, Inc. (1992).
2. Superconductivity and Its Applications, Eds. Hoi S. Kwok and David T. Shaw, Elsevier, 1988.
3. Theories of High Temperature Superconductivity, Ed. J. Woods Halley Addison-Wesley Publishing Company, Inc. 1988.
4. Powder Processing of High T_C oxide superconductors, Eds. A.C. Vajpei and G.S. Upadhyaya, Trans. Tech. Publications Ltd., 1992.
5. Chemistry of High-Temperature Oxide Superconductors, Ed. C.N.R. Rao, World Scientific (1991).
6. Superconductivity Source Book, V. Daniel Hunt, John Wiley & Sons (1989).
7. C. Kittal, Introduction to Solid State Physics, 5th Edn. Wiley Eastern Ltd. (1987).
8. R.M. Hazen, Scientific American, **258**, No.6, 52 (1988).
9. W.D. Kingery, H.K. Bowen & D.R. Uhlmann, Introduction to Ceramics, 2nd Edn., John Wiley & Sons, 1976.
10. Progress in High Temperature Superconductivity, Vol.8, Eds. C.G. Burnham and R.D. Kane, World Scientific, 1988.

References

11. J. G. Bednorz and K.A. Muller, Z. Phys. B, **64**, 189 (1986).
12. H. Takagi, S. Uchida, K. Kitazawa and T. Tanaka, Jpn. J. Appl. Phys., **26**, L123 (1987).

13. J.G. Bednorz, M. Takashige and K.A. Muller, Europhys. Lett., 3, 379 (1987).

14. C.W. Chu, P.H. Hor, R.L. Meng, L. Gao and Z.J. Huang, Science, **235**, 567 (1987).

15. C.W. Chu, P.H. Hor, R.L. Meng, L.Gao, Z.J. Huang and Y.Q. Wang, Phys. Rev. Lett., **58**, 405 (1987).

16. R.J. Cava, R.B. van Dover, B. Batlogg and E.A. Rietman, Phys. Rev. Lett., **58**, 408 (1987).

17. J.M. Torascon, L.H. Greene, W.R. McKinnon, G.W. Hull and T.H. Geballe, Science, **235**, 1373 (1987).

18. M.K. Wu, J.R. Ashburn, C.J. Torng, P.H. Hor, R.L. Meng, L. Gao, Z.J. Huang, Y.Q. Wang and C.W. Chu, Phys. Rev. Lett., **58**, 908 (1987).

19. R.J. Cava, B. Batlogg, R.B. van Dover, D.W. Murphy, S. Sunshine, T. Siegrist, J.P. Remeika, E.A. Reitman, S. Zahurak and G.P. Espinosa, Phys. Rev. Lett., **58**, 1676 (1987).

20. P.H. Hor, L. Gao, R.L. Meng, Z.J. Huang, Y.Q. Wang, K. Forster, J. Vassilious and C.W. Chu, Phy. Rev. Lett., **58**, 911 (1987).

21. X. Cai, R. Joynt and D.C. Larbalestier, Phys. Rev. Lett., **58**, 2798 (1987).

22. I.K. Gopalakrishnan, J.V. Yakhmi and R.M. Iyer, Nature, **327**, 604 (1987).

23. S. Dickman, D. Swinbanks, D. Lindley and R. Peese, Nature, **326**, 432 (1987).

24. M. Strongin, D.O. Welch and V.J. Emergy, Nature, **326**, 540 (1987).

25. Y. LePage, W.R. McKinnon, J.M. Tarascon, L.H. Greene, G.W. Hull and D.M. Hwang, Phys. Rev. B, **35**, 7245 (1987).

26. R.M. Hazen, L.W. Finger, R.J. Angel, C.T. Prewitt, N.L. Ross, H.K. Mao and C.G. Hadidiacos, Phys. Rev. B, **35**, 7238 (1987).

27. P.M. Grant, R.B. Beyers, E.M. Engler, G. Lim, S.S.P. Parkin, M.L. Ramirez, V.Y. Lee, A. Nazzal, J.E. Vazques, R.J. Savoy, Phys. Rev. B., **35**, 7242 (1987).

28. W.I.F. David, W.T.A. Harrison, J.M.F. Gum, O. Moze, A.K. Soper, P. Day, J.D. Jorgensen, D.G. Hinks, M.A. Beno, L. Soderholm, D.W. Capona, I.K. Schuller, C.V. Segre, K. Zhang and J.D. Grace, Nature, **327**, 310 (1987).

29. P.H. Hor, R.L. Meng, Y.Q. Wang, L. Gao, Z.J. Huang, J. Bechtold, K. Forster and C.W. Chu, Phys. Rev. Lett., **58**, 1891 (1987).

30. T.P. Orlando, K.A. Delin, S. Foner, E.J. McNiff Jr., J.M. Tarascon, L.H. Greene, W.R. McKinnon and G.W. Hull, Phys. Rev. B, **36** (1987) 2394.

31. L.F. Schneemeyer, J.V. Waszczak, S.M. Zahorak, R.B. van Dover and T. Siegrist, Mat. Res. Bull., **22**, 1467 (1987).

32. J.M. Tarascon, W.R. McKinnon, L.H. Greene, G.W. Hull and E.M. Vogel, Phys. Rev. B, **36**, 226 (1987).

33. A. Poddar, P. Mandal, P. Choudhury, A.N. Das and B. Ghosh, J. Phys. C: Solid State Phys., **20**, L669 (1987).

34. Sung-lk Lee, J.P. Golben, Yi Song, Sang Young Lee, T.W. Noh, X. Chen, J. Testa and J.R. Gaines, Appl. Phys. Lett. **51**, 282 (1987).

35. D.W. Murphy, S. Sunshine, R.B. van Dover, R.J. Cava, B. Batlogg, S.M. Zahurak and L.F. Schneemeyer, Phys. Rev. Lett., **58**, 1888 (1987).

36. K.N. Yang, Y, Dalichaouch, J.M. Ferreira, B.W. Lee, J.J. Neumeier,

M.S. Torikachvili, H. Zhou, M.B. Maple and R.R Hake, Solid State Commun., **63**, 515 (1987).

37. A.R. Moodenbaugh, M. Suenaga, T. Asano, R.N. Shelton, H.C. Ku, R.W. McCallum and P. Klavins, Phys. Rev. Lett., **58**, 1885 (1987).
38. E.A. Hayri, K.V. Ramanujachary, S. Li, M. Greenblatt, S. Simizu and S.A. Friedberg, Solid State Commun., **64**, 217 (1987).
39. S. Hikami, S. Kagoshima, T. Hirai, H. Minami and T. Masumi, Jpn. J. Appl. Phys., **26**, L347 (1987).
40. H. Meda, Y. Tanaka, M. Fukutomi and T. Asano, Jpn. J. Appl. Phys., **27**, L209 (1988).
41. H.W. Zandbergen, Y.K. Huang, M.J.V. Menken, J.N. Li, K. Kadowaki, A.A. Menosky, G. van Tenderloo and S. Amelinckx, Nature, **332**, 620 (1988).
42. Z.Z. Sheng and A.M. Hermann, Nature, **332**, 138 (1988).
43. R.M. Hazen, L.W. Finger, R.J. Angel, C.T. Prewitt, N.L. Ross, C.G. Hadidiacos, P.J. Henney, D.R. Veblen, Z.Z. Sheng, A. El Ali and A.M. Hermann, Phys. Rev. Lett., **60**, 1657 (1988).
44. A. Schilling, M. Cantoni, J.D. Gao and H.R. Ott, Nature, **363**, 56 (1993).
45. L. Gao, Z.J. Huang, R.L. Meng, J.G. Lin, F. Chen, L. Beauvais, Y.Y. Sun, Y.Y. Xue and C.W. Chu, Physica C, **213**, 261 (1993).
46. C.W. Chu, L. Gao, F. Chen, Z.J. Huang, R.L. Meng and Y.Y. Xue, Nature, **365**, 323 (1993).
47. H. Ihara, K. Tokiwa, H. Ozawa, M. Hirabayashi, H. Matuhata, A. Negishi and Y.S. Song, Jpn. J. Appl. Phys. **33**, L300 (1994).
48. H. Ihara, K. Takiwa, H. Ozawa, M. Hirabayashi, A. Negishi, H.

Matuhata and Y.S. Song, Jpn. J. Appl. Phys., **33**, L503 (1994).

49. R.J. Cava, B. Batlogg, J.J. Krajewski, R. Farrow, L.W. Rupp Jr., A.E. White, K. Short, W.F. Peck and T. Kometani, Nature, **332**, 814 (1988).
50. K.A. Muller and J.G. Bednorz, Science, **237**, 1133 (1987).
51. F.S. Galasso and J. Pyle, Inorg. Chem., **2**, 482 (1963).
52. F.K. Patterson, C.W. Moeller and R. Ward, Inorg. Chem., **2**, 196 (1963).
53. X. Zheng, Q. Wang and B. Gu, J. Am. Ceram. Soc., **74**, 2846 (1991).
54. C. Randall, D. Barber, R. Whatmore and P. Groves, Ferroelectrics, **76**, 277 (1987).
55. G. King, E. Goo, T. Yamamoto and K. Okazaki, J. Am. Ceram. Soc., **71**, 454 (1988).
56. B.G. Hyde, J.G. Thompson, R.L. Withers, J.G. Fitz Gerald, A.M. Stewart, D.G.M. Bevan, J. Bitmead and M.S. Paterson, Nature, **327**, 402 (1987).
57. M.A. Beno, L. Soderholm, R.W. Capone, D.G. Hinks, J.D. Jorgensen, I.K. Schuller, C.V. Segre, K. Zhang and J.D. Grace, Appl. Phys. Lett., **51**, 57 (1987).
58. F. Beech, S. Miraglion, A. Santoro and R.S. Roth, Phys. Rev. B, **35**, 8778 (1987).
59. W. Schafer, E. Jansen, G. Will, J. Faber Jr. and B.Veal, Mat. Res. Bull., **23**, 1439 (1988).
60. J.D. Jorgensen, D.G. Hinks, H. Shaked, B. Dabrowski, B.W. Veal, A.P. Paulikas, C.J. Nowicki, G.W. Gabtree, W.K. Kwok, A. Umezawa, L.H. Nunez and B.D. Dunlap, Physica B, **156-157**, 877 (1989).

61. J.E. Greedan, A.H. O'Reilly and C.V. Stager, Phys. Rev. B, **35**, 8770 (1987).

62. Y. LePage, T. Siegrist, S.A. Sunshine, L.K.F. Schneemeyer, D.W. Murphy, S.M. Zahurak, J.V. Waszczak, W.R. McKinnon, J.M. Tarascon, G.H. Hull and L.H. Greene, Phys. Rev. B, **36**, 3617 (1987).

63. G. Celestani and C. Rizzoli, Nature, **328**, 606 (1987).

64. M.L. Fornasini, G.A. Costa, M. Ferretti and G.L. Olcese, Solid State Commun., **65**, 1121 (1988).

65. T. Siegrist, S.A. Sunshine, D.W. Murphy, R.J. Cava and S.M. Zahurak, Phys. Rev. B, **36**, 7137 (1987).

66. F.P. Okamura, S. Sneno, I. Nakai and A. Ouo, Mat. Res. Bull., **22**, 1081 (1987).

67. R.M. Hazen, L.W. Finger, R.J. Angel, C.T. Prewitt, N.L. Ross, H.K. Mao, C.G. Hardidicos, P.H. Hor, R.L. Meng and C.W. Chu, Phys. Rev. B, **36**, 3966 (1987).

68. A. Manthiram, J. Swinnea, Z.T. Sui, H. Steinfink and J.B. Goodenough, J. Am. Chem. Soc., **109**, 6667 (1987).

69. H.M. O'Bryan and P.K. Gallagher, Adv. Ceram. Mater., **2**, 640 (1987).

70. K. Kishio, J. Shimoyama, T. Hasegawa, K. Kitazawa and K. Fueki, Jpn. J. Appl. Phys., **26**, L1228 (1987).

71. Y. Ueda and K. Kosuge, Physica C, **156**, 281 (1988).

72. R.J. Cava, B. Batlogg, C.H. Chen, E.A. Rietman, S.M. Zahurak and D. Wender, Phys. Rev. B, **36**, 5719 (1987).

73. B.G. Bagley, L.H. Greene, J.M. Tarascon and G.W. Hull, Ap . Phys. Lett., **51**, 622 (1987).

74. P. Menffels, B. Rupp and E. Porschke, Physica C, **156**, 441 (1988).

75. R.J. Cava, B. Batlogg, C.H.Chen, E.A. Rietman, S.M. Zahurak and D. Wender, Nature, **329**, 423 (1987).

76. A.M.T. Bell, Supercond. Sci. Technol., **3**, 55 (1990).

77. S.W. Tozex, A.W. Kleinsasser, T. Penney, D. Kaiser and F. Holtzberg, Phys. Rev. Lett. **59**, 1768 (1987).

78. T.R. McGuirie, T.R. Dinger, P.J.P. Freitas, W.J. Gallagher, T.S. Plaskett, R.L. Sandstorm and J.M. Shaw, Phys. Rev. B, **36**, 4032 (1987).

79. J.R. Moodera, R. Messervey, J.E. Tkaczyk, O.X. Hao, G.A. Gibs and P.M. Tedrow, Phys. Rev. B, **36**, 619 (1987).

80. T.R. Dinger, T.K. Worthington, W.J. Gallagher and R.L. Sandstorm, Phys. Rev. Lett., **58**, 2687 (1987).

81. G.W. Crabtree, J.Z. Liu, A. Umezawa, M.K. Kwok, C.H. Sowers and S.K. Malik, Phys. Rev. B, **36**, 4021 (1987).

82. A.P. Malozemoff, W.J. Gallagher and R. Schwall, ACS Symp. Series, **351**, Chap.27 (1987).

83. J. Heremans, D.T. Morelli, G.W. Smith and S.C. Strite III, Phys. Rev. B, **37**, 1604 (1988).

84. N. McN. Alford, T.W. Button and J.D. Birchall, Supercond. Sci. Technol., 3, 1 (1990).

85. M.F. Yan, R.L. Barns, H.M. O'Bryan Jr., P.K. Gallagher, R.C. Sherwood and S. Jin, Appl. Phys. Lett., **51**, 532 (1987).

86. J.G. Thomson, B.G. Hyde, R.L. Withers, J.S. Anderson, J.D.F. Gerald, J. Bitmead, M.S. Paterson and A.M. Stewart, Mat. Res. Bull., **22**, 1715 (1987).

87. B.W. Veal, W.K. Kwok, A. Umezawa, G.W. Crabtree, J.D. Jorgensen, J.W.

Downey, L.J. Nowicki, A.W. Mitchell, A.P. Paulikas and C.H. Sowers, Appl.Phys. Lett., **51**, 279 (1987).

88. G. Ferey, A. Le Bail, Y. Laligant, M. Hervieu, B. Raveau, A. Sulpice and R. Tournier, J. Solid State Chem., **73**, 610 (1988).
89. D. Shindo, K. Hiraga, M. Hirabayashi, A. Tokiwa, M. Kikuchi, Y. Syono, O. Nakatsu, N. Kabayashi, Y. Muto and E. Aoyagi, Jpn. J. Appl. Phys., **26**, L1667 (1987).
90. T. Kajitani, K. Kusaba, M. Kikuchi, Y. Syono and M. Hirabayashi, Jpn. J. Appl. Phys., **27**, L354 (1988).
91. I. Sankawa, M. Sato and T. Konaka, Jpn. J. Appl. Phys., **27**, L28 (1988).
92. Y.K. Tao, J.S. Swinnea, A. Manthiram, J.S. Kim, J.B. Goodenough and Steinfink, J. Mater. Res., **3**, 248 (1988).
93. P. Strobel, C. Paulsen and J.L. Tholence, Solid State Commun., **65**, 585 (1988).
94. M.F. Yan, W.W. Rhodes and P.K. Gallagher, J. Appl. Phys., **63**, 821 (1988).
95. N. Zhu, X. Jiang, H. Qi, H. Yu, X. Zeng and G. Qiao, Philosophical Magazine Letters, **56**, 271 (1987).
96. I. Felner, I. Nowik and Y. Yeshurun, Phys. Rev. B, **36**, 3923 (1987).
97. S.R. Ovshinsky, R.T. Young, D.D. Allred, G. DeMaggio and G.A. Van der Leeden, Phys. Rev. Lett., **58**, 2579 (1987).
98. M. Xian-Ren, R. Yan-Ru, L. Ming-zhu, T. Qing-Yun, L. Zhen-Jin, S. Li-Hua, D. Wei-Qing, F. Min-Hua, M. Qing-Yun, L. Chang-Jiang, L. Xiu-Hai, Q. Guan-Liang and C. Mou-Yuan, Solid State Commun., **64**, 325 (1987).

99. C. Michel, M. Hervieu, M.M. Berel, A. Grandin, F. Deslandes, J. Provost and B. Raveau, Zeitschrift f. Physik, B, **68**, 421 (1987).

100. C.W. Chu, J. Bechtold, L. Gao, P.H. Hor, Z.J. Huang, R.L. Meng, Y.Y.Sun, Y.Q. Wang and Y.Y. Xue, Phys. Rev. Lett., **60**, 941 (1988).

101. R.M. Hazen, C.T. Prewitt, R.J. Angel, N.L. Ross, L.W. Finger, C.G. Hardidicos, D.R. Veblen, P.J. Heaney, P.H. Hor, R.L. Meng, Y.Y. Sun, Y.Q. Wang, Y.Y. Xue, Z.J. Huang, L. Gao, J. Bechtold and C.W. Chu, Phys. Rev. Lett., **60**, 1174 (1988).

102. C.Y. Yang, J.G. Wen, Y.F. Yan and K.K. Fung, Physica C, **160**, 161 (1989) and references therein.

103. P. Bordet, J.J. Capponi, C. Chaillout, J. Chenavas, A.W. Hewat, E.A. Hewat, J.I. Hodeau, M. Marezio, J.L. Tholence and D. Tranqui, Physica C, **156**, 189 (1988).

104. H.W. Zandbergen, W.A. Groen, F.C. Mijlhoff, G. van Tendeloo and S. Amelinckx, Physica C, **156**, 325 (1988).

105. S.A. Sunshine, T. Siegrist, L.F. Schneemeyer, D.W. Murphy, R.J. Cava, B. Batlogg, R.B. van Dover, R.M. Fleming, S.M. Glarum, S. Nakahara, R. Farrow, J.J. Krajewski, S.M. Zahurak, J.V. Waszczak, J.H. Marshell, P. Marsh, L.W. Rupp and W.F. Peck, Phys. Rev. B, **38**, 893 (1988).

106. H.K. Liu, S.X. Dou, N. Savvides, J.P. Zhou, N.X. Tan, A.J. Bourdillon, M. Kuiz and C.C. Sorrell, Physica C, **157**, 93 (1989).

107. B. Zhu, L. Lei, S.L. Yuan, S.B. Tang, W. Wang, G.G. Zhang, W.Y. Guan and J.Q. Zheng, Physica C, **157**, 370 (1989).

108. Z.Z. Sheng and A.M. Herman, Nature, **332**, 55 (1988).

109. S.S.P. Parkin, V.Y. Lee, E.M. Engler, A.I. Nazzal, T.C. Huang, G. Gorman, R. Savoy and R. Beyers, Phys. Rev. Lett., **60**, 2539 (1988).

110. H. Ihara, R. Sugise, M. Hirabayashi, N. Terada, M. Jo, K. Hayashi, A. Negishi, M. Tokumoto, Y. Kimura and T. Shimomura, Nature, **334**, 510 (1988).

111. S.N. Putilin, E.V. Antipov, O. Chmaissem and M. Marezio, Nature, **362**, 226 (1993).

112. M. Hirabayashi, K. Tokiwa, M. Tokumoto and H. Ihara, Jpn. J. Appl. Phys. **32**, 1206 (1993).

113. M. Hirabayashi, K. Tokiwa, H. Ozawa, Y. Noguchi, M. Tokumoto and H. Ihara, Physica C, **219**, 6 (1994).

114. E.K. Hollmann, O.G. Vendik, A.G. Zaitsev and B.T. Melekh, Supercond. Sci. Technol., **7**, 609 (1994).

115. C.D. Brandle and V.J. Fratello, J. Mater. Res., **5**, 2160 (1990).

116. R.G. Humphreys, J.S. Satchell, N.G. Chew, J.A. Edwards, S.W. Goodyear, S.E. Blenkinsop, O.D. Dosser and A.G. Cullis, Supercond. Sci., Technol., **3**, 38 (1990).

117. J.M. Phillips, J. Appl. Phys., **79**, 1829 (1996).

118. D.W. Rashley, in: "Epitaxial Growth", edited by J.W. Mathews (Academic Press, New York, 1975).

119. H.J. Scheel, M. Berkowski and B. Chabot, Physica C, **185-189**, 2095 (1991).

120. W.G. Lyons, R.S. Withers, J.M. Hamm, A.C. Anderson, D.E. Oates, P.M. Mankiewich, M.L. O'Malley, R.R. Bonetti, A.E. Williams and N. Newman, Proceedings of the Fifth Conference on Superconductivity and Applications, edited by T.H.Kao, H.S. Kowh and A.E. Kaloyeros, **251**, 639 (1992).

121. H. Koinuma, K. Fukuda, T. Hashimoto and K. Fueki, Jpn. J. Appl. Phys., **27**, L1216 (1988).

122. I. Shih and C.X. Qiu, Processing and applications of high T_C superconductors, Edited by W.E. Mayo, (The Metallurgical Society, Inc. 1988) p.223.

123. X.M. Li, Y.T. Chou, Y.H. Hu and C.L. Booth, J. Mater. Sci., **26**, 3057 (1991).

124. X.M. Li, Y.T. Chou, Y.H. Hu and C.L. Booth, J. Mater. Sci. Lett., **9**, 669 (1990).

125. M. Naito, R.H. Hammond, B. Oh, M.R. Halin, J.W.P. Hsu, P. Rosenthal, A.F. Marshall, M.R. Beasley, T.H. Geballe and A. Kapitulnik, J. Mater. Res., **2**, 713 (1987).

126. N.P. Bansal, R.N. Simons and D.E. Farrel, Appl. Phys. Lett., **53**, 603 (1988).

127. M.F. Yan, W.W. Rhodes and P.K. Gallagher, J. Appl. Phys., **63**, 821 (1988).

128. C.T. Cheong and E. Ruckenstein, J. Mater. Res., **4**, 1 (1989).

129. N.P. Bansal, Mater. Lett. **13**, 7 (1992).

130. T.C. Shields and J.S. Abell, Supercond. Sci. Technol., **5**, 627 (1992).

131. M.J. Cima, J.S. Schneider, S.C. Paterson and W. Coblenz, Appl. Phys. Lett., **53**, 710 (1988).

132. J. Talvacchio and G.R. Wagner, Supercond. Appl. Infrared Microwave Dev., **1**, 1292 (1990).

133. H.M. O'Bryan, P.K. Gallagher, G.W. Berkstresser and C.D. Brandle, J. Mater. Res., **5**, 183 (1990).

134. A. Mogro-Campero, B.D. Hunt, L.G. Turner, M.C. Burell and W.E. Balz, Appl. Phys. Lett. **52**, 584 (1988).

135. Y. Matsuoka, E. Ban, H. Ogawa and K. Kurosawa, Supercond. Sci. Technol., **4**, 528 (1991).

136. C.L. Bohn, J.R. Delayen, U. Balachandran and M.D. Langan, Appl. Phys. Lett., **55**, 304 (1989).

137. A.Z. Lin, H.Q. Li, F.W. Liu and L. Tang, Jpn. J. Appl. Phys., **27**, L1204 (1988).

138. P. Campbell, Nature, **330**, 21 (1987).

139. N. McN. Alford, T.W. Button, M.J. Adams, S. Hedges, B.Nicholson and W.A. Phillips, Nature, **349**, 680 (1991).

140. R. Vaglio, Ceram. Inter., **19**, 421 (1993).

141. G. Kozlowski, S. Rele, D.F. Lee and K. Salama, J. Mater. Sci., **26**, 1056 (1991).

142. R.W. Vest, Ceram. Bull. **65**, 631 (1986).

143. M. Miyajima, T. Nakamoto, S. Nagaya, I. Hirabayashi and S. Tanaka, Supercond. Sci. Technol., **5**, S292 (1992).

144. L. Strom, E. Carnall, S. Ferranti and J. Mir, J. Mater. Sci., **26**, 1577 (1991).

145. Y. Matsuoka, E. Ban, H. Ogawa and A. Suzumura, Supercond. Sci. Technol., **4**, 62 (1991).

146. D.K. Aswal, S.K. Gupta, A.K. Debnath, G.P. Kothiyal, S.C. Sabharwal and M.K. Gupta, Supercond. Sci. Technol., **4**, 188 (1991).

147. N.P. Bansal, R.N. Simons and D.E. Farrel, in: Ceramic Superconductors, Vol.2, ed. M.F. Yan (American Ceramic Society,Westerville, OH, 1988) p.474.

148. N.P. Bansal and A.L. Sandkuhl, Appl. Phys. Lett., **52**, 323 (1988).

149. R.C. Budhani, S.M.H. Tzeng, H.J. Doerr and R.F. Bunshah, Appl. Phys. Lett., **51**, 1277 (1987).

150. H. Koinuma, T. Hashimoto, T. Nakamura, K. Kishio, K. Kitazawa and K. Fueki, Jpn. J. Appl. Phys., **26**, L761 (1987).

151. N. Khare, A.K. Gupta, S. Chaudhry and V.S. Tomar, Supercond. Sci. Technol. **4**, 107 (1991).

152. N. McN. Alford, T.W. Button and D. Opie, Supercond. Sci. Technol., **4**, 33 (1991).

153. G.B. Blanchet and C.R. Fincher Jr., Supercond. Sci. Technol., **4**, 69 (1991).

154. M. Jergel, S. Chromik, V. Strbik, V. Smatko, F. Hanic, G. Plesch, S. Buchta and S. Valtyniova, Supercond. Sci. Technol., **5**, 225 (1992).

155. A. Gupta, G. Koren, E.A. Giess, N.R. Moore, E.J.M. O'Sullivan and E.I. Copper, Appl. Phys. Lett., **52**, 163 (1988).

156. T. Nonaka, K. Kaneko, T. Hasegawa, K. Kishio, Y. Takahashi, K. Kobayashi, K. Kitazawa and K. Fueki, Jpn. J. Appl. Phys., **27**, L867 (1988).

157. T. Nonaka, M. Green, K. Kishio, T. Hasegawa, K. Kitazawa, K. Kaneko and K. Kobayashi, Physica C, **160**, 517 (1989).

158. M.E. Gross, M. Hong, S.H. Liou, P.K. Gallagher and J. Kwo, Appl. Phys. Lett., **52**, 160 (1988).

159. J.V. Mantese, A.H. Hamdi, A.L. Micheli, Y.L. Chen, C.A. Wong, J.L. Johnson, M.M. Darmarkar and K.R. Padmanabhan, Appl. Phys. Lett., **52**, 1631 (1988).

160. P. May, D. Jedamzik, W. Boyle and P. Miller, Supercond. Sci. Technol., **1**, 1 (1988).

161. I. Shih and C.X. Qiu, Appl. Phys. Lett., **52**, 748 (1988).

162. H. Murakami, J. Nishino, S. Yaegashi, Y. Shiohane and S. Tanaka, Jpn. J. Appl. Phys., **30**, L185 (1991).

163. E. Saiz and J.S. Moya, Supercond. Sci. Technol., **5**, 130 (1992).

164. M. Gurvitch and A.T. Fiory, Appl. Phys. Lett. **51**, 1027 (1987).

165. A. Mogro-Campero and L.G. Turner, Appl. Phys. Lett., **52**, 1185 (1988).

166. K. Watanabe, H. Yamane, H. Kurosawa, T. Hirai, N. Kobayashi, H. Iwasaki, K. Noto and Y. Muto, Appl. Phys. Lett., **54**, 575 (1989).

167. I.V. Khoroshum, E.V. Karyaev, V.T. Moshnyaga, G.A. Kiosse, M.A. Krachun, V.M. Zakosarento and V.Y. Davydov, Supercond. Sci. Technol., **3**, 493 (1990).

168. J. Azoulay and D. Gooldschmidt, Appl. Phys.Lett., **54**, 2467 (1989).

169. P. Berberich, B. Utz, W. Prusseit and H. Kinder, Physica C, **219**, 497 (1994).

170. P. Chaudhari, R.H. Koch, R.B. Laibowitz, T.R. McGuire and R.J. Gambino, Phys. Rev. Lett., **58**, 2684 (1987).

171. X.D. Wu, B. Dutta, M.S. Hegde, A. Inam, T. Venkatesan, E.W. Chase, C.C. Chang and R. Howard, Appl. Phys. Lett., **54**, 179 (1989).

172. A. Inam, M.S. Hegde, X.D. Wu, T. Venkatesan, P. England, P.F. Miceli, E.W. Chase, C.C. Chang, J.M. Tarascon and J.B. Watchman, Appl. Phys. Lett., **53**, 908 (1988).

173. R. Pinto, S.P. Pai, C.P. D'Souza, L.C. Gupta, R. Vijayaraghavan, D. Kumar and M. Sharon, Physica C, **196**, 264 (1992).

174. R. Pinto and R. Vijayaraghavan, Ind. J. Pure Appl. Phys., **30**, 692 (1992).

175. S.R. Foltyn, R.E. Muenchausen, R.C. Dye, X.D. Wu, L. Luo and D.W. Cooke, Appl. Phys. Lett., **59**, 1374 (1991).

176. P.R. Broussard, V.C. Cestone, L.H. Allen and M.E. Reeves, Mater. Res. Soc. Symp. Proc., **275**, 507 (1992).

177. H. Asano, S. Kubo, O. Michikami, M. Satoh and T. Konaka, Jpn. J.Appl. Phys., **29**, L1452 (1990).

178. A.W. McConnel, R.A. Hughes, A. Dabkowski, H.A. Dabkowska, J.S. Preston, J.E. Greedan and T.Timusk, Physica C, **225**, 7 (1994).

179. S. Tanaka and H. Itozaki, Jpn. J. Appl. Phys., **27**, L622 (1988).

180. D. Kumar, M. Sharon, R. Pinto, P.R. Apte, S.P. Pai, S.C. Purandare, L.C. Gupta and R. Vijayaraghavan, Appl. Phys. Lett., **62**, 3522 (1993).

181. H.Y. To, G.J. Valco and K.B. Bhasin, Supercond. Sci. Technol., **5**, 421 (1992).

182. J.M. Phillips, M.P. Siegal, R.B. van Dover, T.H. Tiefel, J.H. Mershall, C.D. Brandle, G. Berkstresser, A.J. Strauss, R.E. Fahey, S. Sengupta, A. Cassanho and J.P. Jenssen, J. Mater. Res., **7**, 2650 (1992).

183. M. Sasura, M. Mukaida and S. Miyazawa, Appl. Phys. Lett., **57**, 2728 (1990).

184. W. Prusseit, L.A. Boutner and D. Rutz, Appl. Phys. Lett., **63**, 3376 (1993).

185. R. Remesh, A. Inam, W.A. Bonner, P. England, B.J. Wilkens, B.J. Meagher, L. Nazar, X.D. Wu, M.S. Hegde, C.C. Chang and T. Venkatesan, Appl. Phys. Lett., **55**, 1138 (1989).

186. K.H. Young, G.V. Negrete, M.M. Eddy, J.Z. Sun, T.W. James, McD. Robinson and E.J. Smith,Thin Solid Films, **206**, 116 (1991).

187. J.A. Alarco, G. Brorsson, Z.G. Iranov, P.A. Nilsson, E. Olsson and M. Lofgren, Appl. Phys. Lett., **61**, 723 (1992).

188. P. Gurptasarma, S.T. Bendre, S.B. Ogale, M.S. Multani and R. Vijayaraghavan, Physica C, **203**, 209 (1992).

189. H. Asano, M. Asahi and O. Michikami, Jpn. J. Appl. Lett., **28**, L981 (1989).

190. Y. Terashima, M. Sagoi, K. Kubo, Y. Mizutani, T. Miura, J. Yoshida and K. Mizushima, Jpn. J. Appl. Phys., **28**, L653 (1989).

191. T. Terashima, Y. Bando, K. Iijima, K. Yamamoto and K. Hirata, Appl. Phys. Lett., **53**, 2232 (1988).

192. G. Linker, X.X. Xi, O. Meyer, Q. Li and J. Geerk, Solid State Commun., **69**, 249 (1989).

193. R. Pinto, P.R. Apte, S.P. Pai and D. Kumar, Physica C, **207**, 13 (1993).

194. R. Pinto, N. Goyal, S.P. Pai, P.R. Apte, L.C. Gupta and R. Vijayaraghavan, J. Appl. Phys., **73**, 5105 (1993).

195. K.V. Paulose, J. Koshy and A.D. Damodaran, Jpn. J. Appl. Phys., **30**, L458 (1991).

196. K.V. Paulose, J. Koshy and A.D. Damodaran, Supercond. Sci. Technol., **5**, 31 (1992).

197. K.V. Paulose, P. Murugaraj, J. Koshy and A.D. Damodaran, Jpn. J. Appl. Phys., **31**, 1323 (1992).

198. K.V. Paulose, J. Koshy and A.D. Damodaran, Supercond. Sci. Technol., **4**, 98 (1991).

199. J. Koshy, J.K. Thomas, J. Kurian, Y.P. Yadava and A.D. Damodaran, Mater. Lett., **15**, 298 (1992).

CHAPTER 2

PREPARATION AND CHARACTERISATION TECHNIQUES

2.1. Introduction

The processing of ceramics, both substrate materials and high T_C superconductors (HTSC), involves preparation of high purity single phase powders of the material (calcination) followed by densification and texturing at high temperatures (sintering). The microstructure and the final properties are critically dependent on the powder preparation procedure. The major problems encountered in the preparation of powder are inhomogeneity, non-uniformity in terms of particle size and shape, high impurity levels and lack of reproducibility in the final product [1]. A brief description of the method of preparation of ceramic materials in the form of both bulk and films, and the different techniques used for their characterisation are given in this chapter. However, the specific details regarding the sample preparation and characterisation are described in detail in the respective chapters.

2.2. Preparation of Ceramic Materials

The powder synthesis methods adopted for ceramics can be broadly classified into three major categories. They are solid phase synthesis, liquid phase synthesis and gas phase synthesis [2]. The solid phase synthesis (solid state reaction method) for the synthesis of ceramics employs a series

of mixing, grinding and heating cycles with varying heating schedule. The solid state reaction method, though widely used because of its simplicity has certain disadvantages. The presence of agglomerates in calcined powders would result in high porosity and poor mechanical properties of the final product. Inadequate mixing of powders can lead to compositional inhomogeneities, insufficient stoichiometry control and formation of extraneous phases. Solid state reaction method thus needs optimisation in terms of constituents and choice of the type, purity and form of constituents, wet or dry mixing. In the case of multi-component system, the mixing of the constituent salts or compounds is a very important part in solid state method and one of the problems associated with conventional mixing of powders is that it may not result in sufficient communication of powders which in turn may prevent a complete solid state reaction during calcination. In the ball milled powders it is difficult to obtain reproducible uniform distribution of materials especially when one constituent fraction is present in small amounts. The methods based on liquid and vapour phase synthesis have the advantage of obtaining greater homogeneity and reproducibility as compared to the conventional solid state synthesis method. In the case of liquid phase synthesis it is often possible to achieve in solution much more intimate mixing of constituents prior to high temperature processing. Also finer powder particles of uniform morphology and microstructure can be produced through solution routes. Recently

vapour phase methods have received considerable attention as a route for the preparation of bulk powders of ceramic superconductors, besides their use in thick and thin film preparation [1]. The advantage is that ultra fine particles of uniform size and distribution can be synthesised directly from appropriate vapours in a short time. Close control of the process is required to obtain the powders of desired morphology and stoichiometry.

In the present study, the ceramic materials were prepared by the conventional solid state reaction method. Stoichiometric amounts of high purity (99.9%) constituent oxides/carbonates/nitrates were weighed and thoroughly mixed in an agate mortar with acetone as wetting medium. The mixture was dried in an oven at about 150°C for 2 to 4 h. The dried mixture was calcined in air at a desired temperature for 12 to 15 h in a alumina/platinum crucible. The resulting powder was ground well and the calcination step was repeated 2 to 3 times. The details of annealing temperature, rate of heating, duration of heating etc. for the specific cases are described in the respective chapters. The calcined materials were then ground well and pelletised in required dimensions. These pellets were then sintered in air at a desired temperature for a specific duration and slow cooled at a required rate to room temperature. Figure 2.1 summarises the procedure adopted in the present study for the preparation of ceramic materials by solid state reaction method.

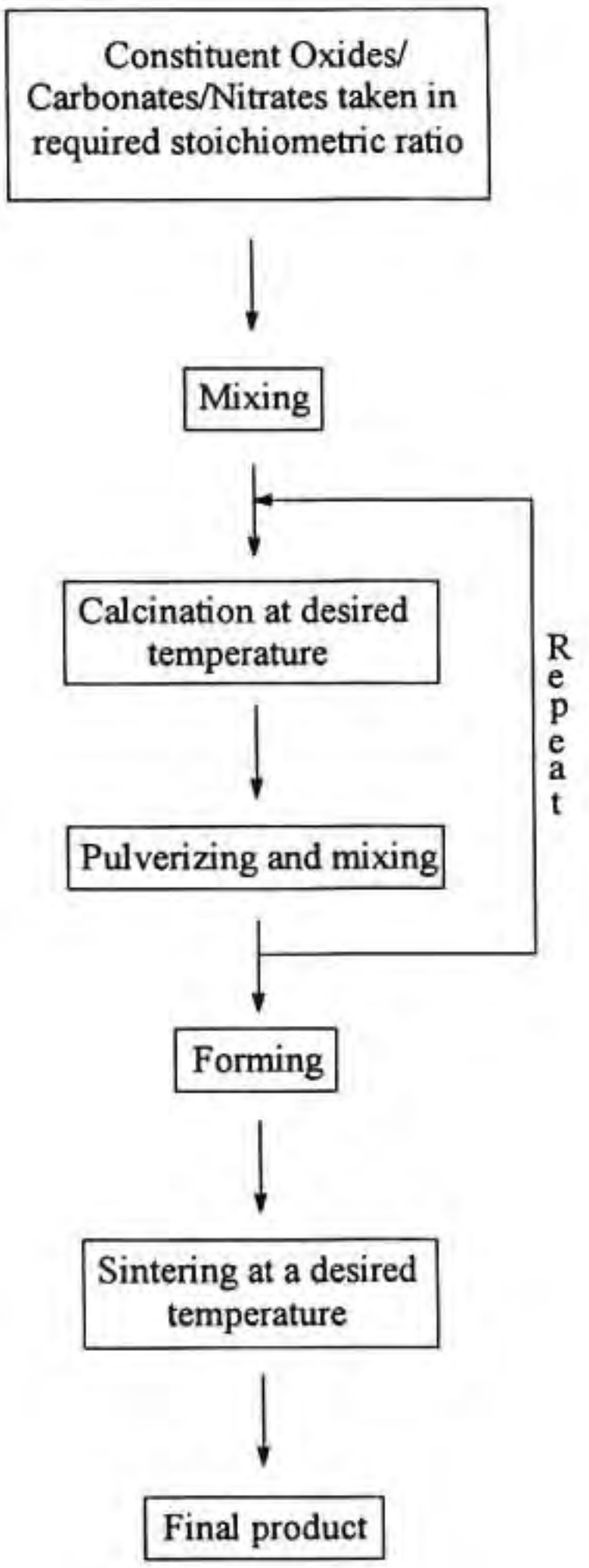

Fig. 2.1 Procedure for the preparation of ceramic materials by solid state reaction.

2.3. Preparation of Thick Films

Thick films of HTSC materials have been prepared by different techniques such as screen printing, dip-coating, spin coating, spray pyrolysis, paint-on method etc. Thick films of superconductors in the present study have been prepared by screen printing and dip-coating techniques. Screen printing technique is advantageous as compared to other thick film preparation methods in that electronic and microwave circuits can be directly printed on the substrate. On the other hand dip-coating is a relatively simpler technique and can be used for preparing thinner films (2 to 4 μm) and coating surfaces which are not plane. Another advantage of dip-coating is that both the surfaces of the substrate can be coated, if desired.

In the case of screen printing of HTSC thick film, an ink of the HTSC material is prepared by thoroughly mixing fine HTSC powder with an appropriate amount of an organic vehicle (usually isopropyl alcohol or n-butanol). The viscosity of the ink is controlled by the addition of commercially available fish oil. This ink is then printed on a desired polished substrate using a screen of suitable mesh size, usually 325 mesh. The printed film is dried in a hot air oven and subjected to controlled heat treatment. For dip-coating, a suspension of the HTSC material was prepared by thoroughly mixing fine HTSC powder with isopropyl alcohol or n-butanol. For obtaining the film, the polished and cleaned substrate is dipped in the thick film suspension and the dipping process is repeated till the required thickness is attained. The resulting film is then dried in a hot air oven and

is subjected to controlled heat treatment. The actual temperature, time of annealing, rate of heating and cooling are described in the respective chapters.

2.4. *In situ* Growth of YBCO Thin Films

YBCO thin films have been successfully grown by physical vapour deposition (PVD) as well as chemical vapour deposition (CVD) techniques. Among the different PVD techniques, pulsed laser deposition (PLD) has become the most successful and reliable technique for the deposition of YBCO thin films [3-7]. In the preparation of YBCO thin films by PLD, different lasers have been employed like Nd:YAG laser, Ruby laser, excimer lasers etc., [8-13] and among them KrF excimer laser was the most successful and widely used [3,4,7].

In the present study, YBCO thin films were grown *in situ* using a Lambda Physik 301 KrF 248 nm excimer laser and a 30 cm focal length quartz lens for laser beam focusing. A 30 cm diameter stainless steel chamber with a quartz window pumped with a turbo pump module was used for the growth of YBCO films. The substrates were heated to the required temperature using a platinum strip heater. The laser beam was allowed to fall on a rotating target of ~1.5 cm diameter at an angle of 45° normal to the target. The substrate was arranged in such a way that the front surface of the substrate faced the target. A stoichiometric YBCO target was used for the *in situ* growth of YBCO films. Schematic diagram of laser ablation technique employed is given in Fig. 2.2. The quality of the *in situ* grown YBCO films by laser ablation depends on a number of

factors like laser pulse energy density, laser pulse width and repetition rate, geometric configuration between the target and the substrate, substrate temperature, substrate target distance, oxygen partial pressure etc. The specific growth conditions and parameters used for the *in situ* growth of YBCO and YBCO-Ag thin films are given in the respective chapters.

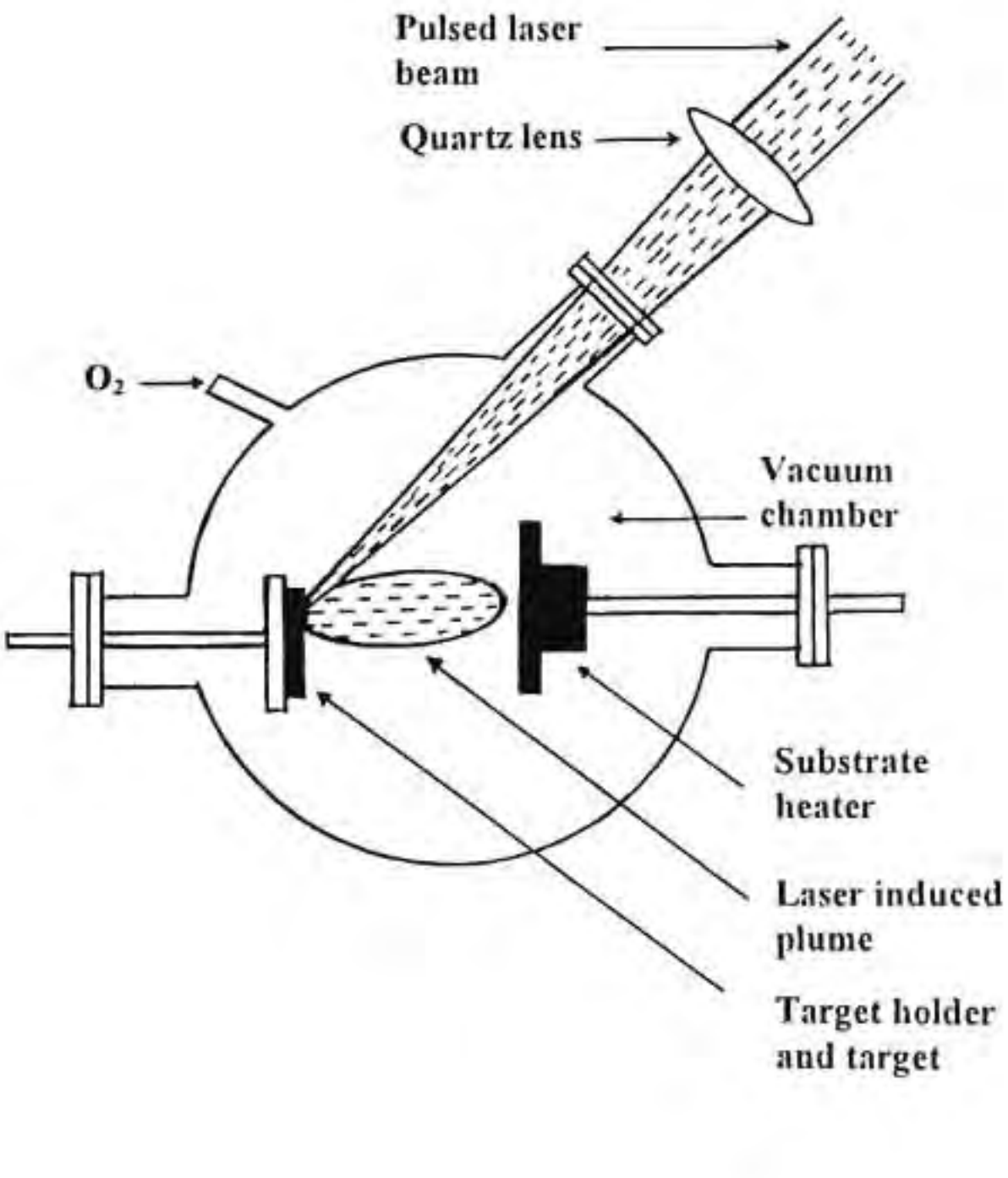

Fig. 2.2 Schematic diagram of laser ablation setup.

2.5. Characterisation Techniques

The ceramic materials prepared in the present study are crystalline in nature. The various techniques used for the characterisation of the ceramic materials prepared in the present study are X-ray diffraction technique, scanning electron microscopy, differential thermal analysis, differential scanning calorimetry, thermomechanical analysis and photoacoustics method. The dielectric properties of the ceramic substrate samples were studied by using a complex impedance analyser. The superconductivity studies were carried out by temperature-resistivity and critical current density measurements by four point probe method.

2.5.1. X-ray Diffraction Technique

Since ceramic materials are crystalline in nature, the X-ray diffraction technique is a powerful tool for the determination of crystal structure and the analysis of phases present in the specimen. Characteristic X-ray diffraction (XRD) patterns are produced when the wavelength (λ) of the electromagnetic radiation interacting with the specimen is comparable to that of the interatomic spacing in crystals. Radiations of longer wavelength cannot resolve the details of structure on an atomic scale, and that of shorter wavelength is diffracted through inconveniently smaller angles. X-rays have wavelengths comparable with the interatomic spacing in crystals. When X-rays of wavelength comparable or smaller than the lattice constants are allowed to incident on a crystal, one or more diffracted beams are

observed in directions quite different from that of the incident beam. W.L. Bragg explained the observed angles of the diffracted X-rays from a crystal in which the incident waves are reflected specularly from parallel planes of atoms in the crystal, with each plane reflecting a very small fraction of the radiation. The diffracted beams are found only when the reflections from the parallel planes of atoms interfere constructively.

Bragg showed that when an X-ray radiation is incident on a series of parallel (hkl) planes spaced equal distances d_{hkl} apart, and when the path difference for the X-rays reflected from adjacent planes, $2\ d_{hkl} \sin\theta$ (where θ is the angle which the incident beam makes with the plane of the crystal), is an integral multiple of the wavelength λ, constructive interference of the radiation reflected from the successive planes occurs. Thus the condition for constructive interference of the reflected radiation is given by $2d_{hkl} \sin\theta = n\lambda$. It is observed that, although the reflections from each plane is assumed to be specular, only for certain values of θ will the reflections from all parallel planes add up in phase to give a strong reflected (diffracted) beam. The Bragg law is a consequence of the periodicity of the space lattice. Bragg reflections can occur for wavelengths $\lambda < 2d_{hkl}$ [14].

In the present study, powder method is employed for the identification of the crystalline phases present in the specimen sample. The XRD pattern is a unique characteristic property of a material resulting from the arrangement of atoms. Thus different materials have different atomic

arrangements or crystal structure which in turn produces characteristic XRD patterns. The identification of the phases is done by comparing the d spacing and (I/I_o) of the observed XRD pattern of the sample with standard reference data. In the present study, the samples for XRD studies were prepared by smearing polycrystalline powder of the specimen on a flat glass sample holder (provided with a grove for holding the powder). A computerised Rigaku X-ray diffractometer (model Dmax/2C, Japan) with Ni filtered CuKα radiation (λ = 1.5406 Å) was used for the characterisation of the samples.

2.5.2. Scanning Electron Microscopy

The properties of ceramic materials are closely associated with its microstructure and hence the analysis of its microstructure can yield useful information like surface defects, cracks, pores, presence of additional phases, grain morphology and size, etc. In the present study, the microstructural analysis have been carried out using a Hitachi (model S2400, Japan) scanning electron microscope (SEM).

The SEM employs electromagnetic lenses, vacuum systems, apertures and electron guns. A schematic diagram illustrating the basic parts of an SEM is given in Fig. 2.3. In an SEM, the electrons emitted by a heated filament is accelerated and then collimated into a narrow beam. It is then allowed to fall upon the specimen surface, producing several different imaging possibilities. Because of the aperture size and short wavelength of electrons, tremendous depth of field can be realised.

A narrow beam of electrons from the electron gun is focused by electromagnetic lenses into a small spot (less than 10 nm) on the surface of the specimen. Deflector coils then scan the beam across the specimen. In the most common imaging mode, secondary electron imaging (SEI), the high energy primary beam dislodges electrons from the atoms near the surface of the specimen (secondary electrons), some of which then strike

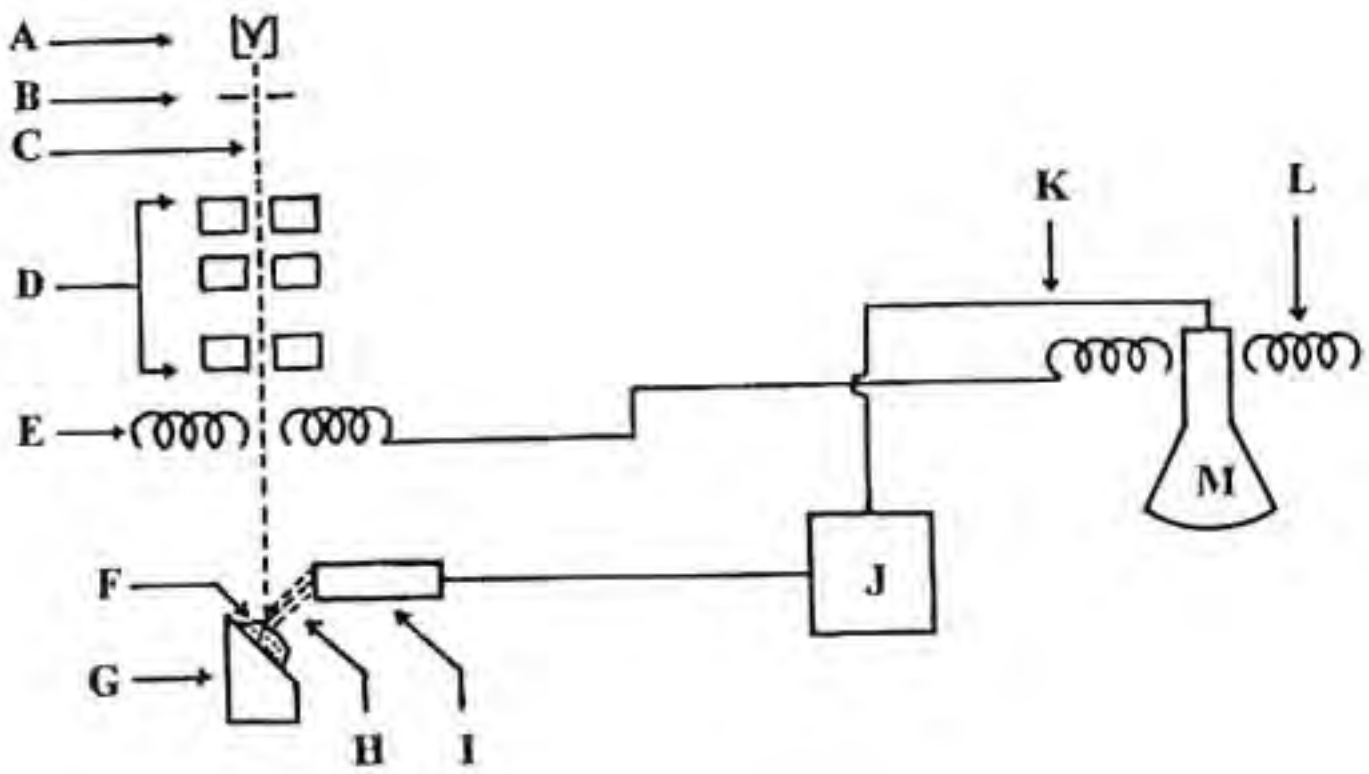

Fig. 2.3 Diagrammatic sketch of an SEM showing Wehnelt assembly with filament (A), anode aperture (B), electron beam (C), condenser lenses (D), deflector coils on column (E) connected to deflector coils (L) of CRT (M), specimen (F) on stage (G), producing secondary electrons (I) striking collector (H) connected to amplifier (J) feeding voltage through cable (K) to CRT (ref. 15).

the SEI collector. Electrons which strike the collector produce photons that then processed by a photoamplifier circuit connected to the cathode ray tube (CRT). An electron that interacts with the collector results in a voltage applied to the gun of the CRT, which produces a point of illumination on the CRT screen. The scan generator that operates the scanning coils controlling the electron beam within the SEM column is connected to the deflector plates of the CRT. Thus, as the SEM beam is scanned over the specimen, the CRT gun is simultaneously scanned over the CRT screen. The output of the photoamplifier (voltage) is employed to modulate the brightness of the CRT beam in synchronisation with the SEM electron beam. The current of secondary electrons recorded by the collector at a given point in time produces a given voltage after processing by the photomultiplier circuit, determining the brightness of the spot of the CRT. Any variation in elemental composition, texture or topography can result in a variation in the current reaching the collector. The specimen magnification is determined by the relationship between the distance scanned on the specimen surface by the primary beam and the distance scanned on the CRT during the same period [15].

The use of an electron gun needs a vacuum system and the type of the gun used determines the type of the vacuum system needed. Most of the SEM's have accelerating voltages adjustable from 0-35 kV and have three electromagnetic lenses, the first two of which defocus the beam, the third being used to determine the final diameter of the beam striking the

specimen surface. Working distance can be varied by placing the specimen higher or lower in the column, which also places the specimen nearer to or further away from the electron source and collector, respectively. Moving the specimen further away from the lens and collector increases the depth of field and can reduce charging to some extent. The insulator samples for SEM analysis are coated with gold in order to improve the surface conductivity which prevents the accumulation of negative surface charge which might interact with the secondary electrons. The coating of non-conducting specimens improves the signal. For the SEM analysis of conducting specimens no coating is required.

2.5.3. Thermal Characterisation

The thermal characterisation of ceramic samples is important especially when used for substrate applications. In the present study, differential thermal analysis was carried out for the ceramic substrate samples to find whether there is any phase transition occurring in the temperature range from room temperature to 1300°C. The specific heat capacity (c) and the thermal expansion coefficient of ceramic substrate samples were determined by differential scanning calorimetry and thermomechanical analysis respectively. The thermal diffusivity (α) of the substrate samples were determined by photoacoustics method. The thermal conductivity of the substrate samples were calculated using the experimentally obtained values of α, ρ' and C, where ρ' is the density of the material.

2.5.3.1. Differential Thermal Analysis

Differential thermal analysis (DTA) is a thermal technique in which the temperature of the sample, compared with the temperature of a thermally inert material, is recorded as a function of the sample, inert material, or furnace temperature as the sample is heated or cooled at a uniform rate. The temperature changes occurring during chemical or physical changes are detected by a differential method using thermocouples. In DTA, highly sensitive thermocouples detect the temperature difference (ΔT) between the sample and the inert reference and is plotted against temperature. Thus a knowledge of the endothermic or exothermic effects occurring in the sample during the heat treatment can be obtained from the DTA curve. The reference sample used is alpha alumina which undergoes no enthalpy change till its melting point [16]. In the present study, a Shimadzu DTA (model 50H) was used for the DTA analysis. The DTA studies were carried out in Ar atmosphere and the heating rate used was 10°C/min.

2.5.3.2. Differential Scanning Calorimetry

In the case of differential scanning calorimetry (DSC), the sample and the reference material are maintained isothermally by means of individual heaters by proper application of electrical energy. The parameter recorded is the difference in power inputs to the heaters, (dH/dt) with reference to temperature [16]. This is the basic difference of DSC to that of DTA where the temperature difference between the sample and the

reference material is recorded as a function of temperature. In the present study the DSC experiments were carried out using a Mettler DSC 20 standard cell with Mettler TA3000 programmer. A known mass of the powdered ceramic sample whose specific heat is to be measured is taken in an aluminium pan and sealed. The pan is then placed inside the calorimeter and the heat flow into the sample is plotted as a function of temperature. The DSC scans were carried out in nitrogen atmosphere with a heating rate of 10°C/min. The specific heat capacity of the samples were calculated from the DSC data.

2.5.3.3. Thermomechanical Analysis

The thermal expansion of the ceramic samples were studied by thermomechanical analysis (TMA). Compared to many other thermal analytical techniques, the instrumentation involved in TMA is quite simple. In a TMA, the changes in the dimensions of the sample are detected by a mechanical, optical or electrical transducer although the transducer is usually a linear variable differential transducer (LVDT). The sample may be positioned either vertically or horizontally. The latter usually induces friction between the sample and the support tube, which may be reduced to acceptable levels but never totally eliminated [16]. Vertical dilatometers overcome the problem of friction, but achievement of zero loading is difficult. The LDVT core must make light but positive contact with the

sample and its mass must be counter balanced by flotation or spring loading. In TMA, the vertical arrangement is easily adapted for use under applied loads. The thermal expansion coefficients of the ceramic samples were measured using a Perkin-Elmer Thermomechanical Analyser (TMA 7) with thermal analysis controller TAC 7/DX. The thermal expansion of the samples as a function of temperature was recorded in the temperature range 20 to 100°C at a heating rate of 10°C/min. The thermal expansion coefficient of the samples were calculated from the TMA plots.

2.5.3.4. Thermal Diffusivity Study

The photoacoustic effect was discovered by Alexander Graham Bell [17] who found that an acoustic signal was produced when a sample in an enclosed cell was illuminated with light having a periodically varying intensity [18]. Later this was developed as a sensitive and non-destructive method for measuring the optical [19] and thermal [20] properties of material due to the availability of coherent optical sources and advancement in signal processing and data acquisition systems. The photoacoustic (PA) effect in the generation of acoustic signals when a sample placed inside a cell is illuminated by an intensity modulated beam of light. The absorption of light and the subsequent non-radiative relaxation process generate thermal waves having the same frequency in the sample. The thermal waves in the sample is converted into a periodic pressure variation or an acoustic

wave in the gas medium which can be detected by means of a sensitive microphone. The basic theory of PA effect in condensed medium has been described by Rosencwaig and Gersho [21-22]. One of the parameters which determine the PA signal amplitude is the thermal diffusion length (μ) and is given by the relation $\mu^2 = \alpha/\pi f$, where a is the thermal diffusivity and f the chopping frequency (modulation frequency). In the case of thermally thick regime ($\mu < l$, where l is the thickness of the sample), the PA signal is independent of the thermal properties of the backing material whereas in the case of thermally thin regime ($\mu > l$) the PA signal is modified by the thermal properties of the backing material. For an appropriate sample thickness, it is possible to obtain a transition from the thermally thin regime to the thermally thick regime by increasing the chopping frequency. The PA signal amplitude verses chopping frequency plot shows a distinct change in slope at the characteristic frequency f_c at which the transition takes place [23-25]. The thermal diffusivity α of the sample can be determined from the relation $\alpha = l^2 f_c$ [26].

Figure 2.4 shows the schematic diagram of experimental setup used for photoacoustic spectroscopy [27]. In the present study, an Argon ion laser was used as the light source. The amplitude of the laser beam was modulated using an electromechanical chopper. The modulated laser beam was allowed to fall on the sample placed inside the PA cell and the PA signal generated was detected by means of a sensitive microphone. The PA cell used is a cylindrical, small volume, non-resonant cell made out of

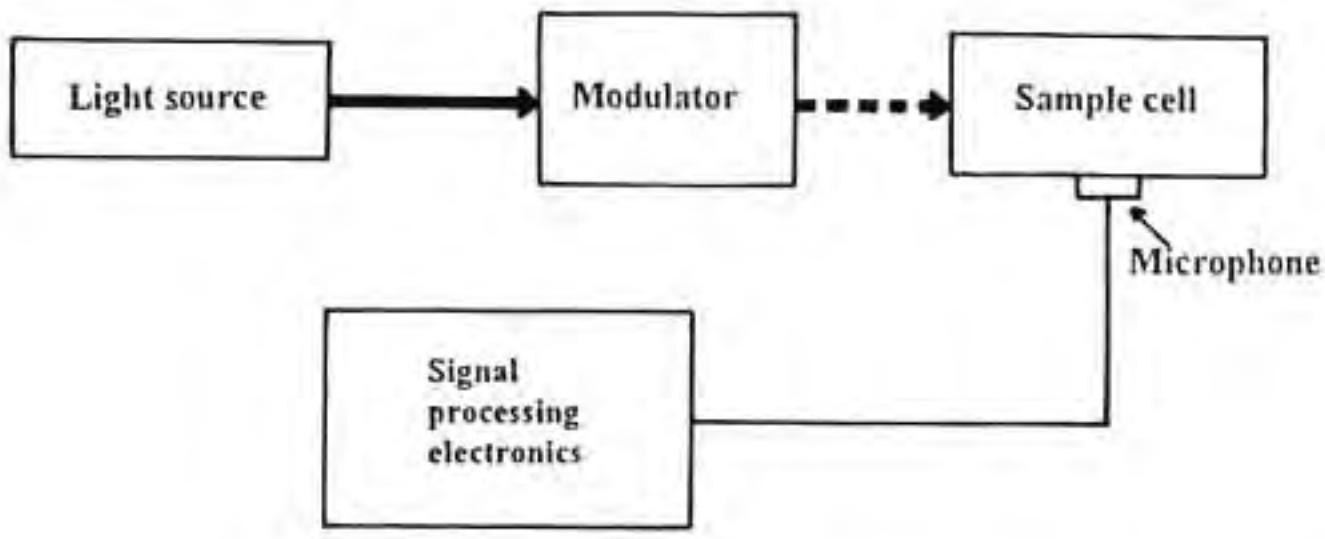

Fig. 2.4 Essential experimental setup for photoacoustic spectroscopy (ref. 27).

aluminium [25]. The sample is fixed on an aluminium disc which acts as the thermally thick backing material and a proper thermal contact is ensured between the sample and the backing material. The microphone output is processed by means of a digital lock-in-amplifier. The block diagram of the experimental setup is shown in Fig. 2.5. The amplitude of the PA signal is plotted against chopping frequency and the characteristic frequency, f_c, is determined from the plot. By substituting the values of f_c and l, the thermal diffusivity can be found.

The thermal conductivity, κ, of the sample is given by the relation $\kappa = \alpha\rho' c$, where c in the specific heat capacity and ρ' is the density of the sample. In the present study, κ is calculated using the above relation by substituting the experimentally obtained values of α, ρ' and c.

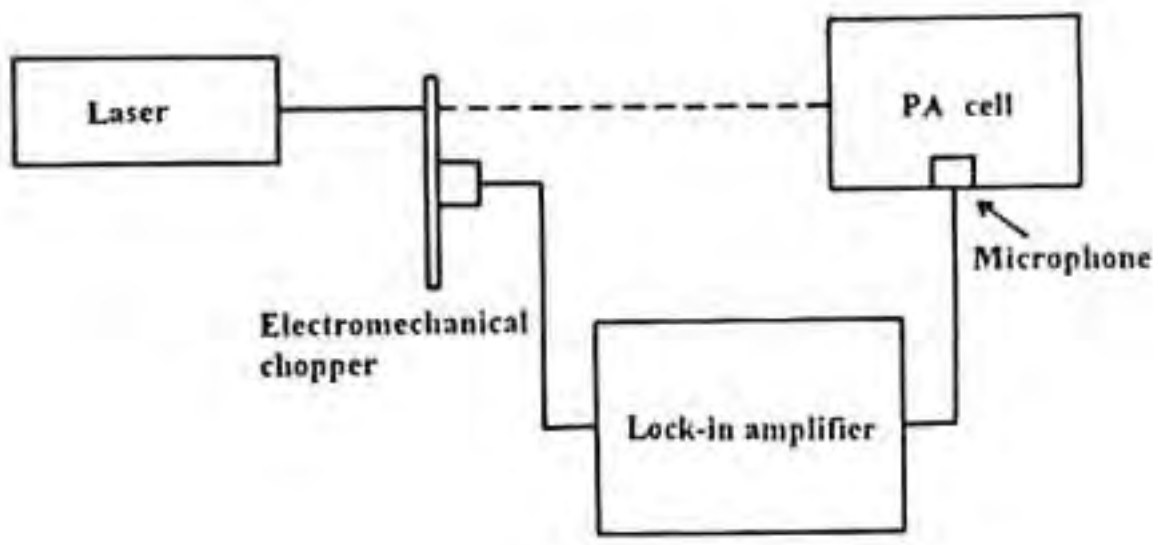

Fig. 2.5 Block diagram of the experimental setup.

2.5.4. Dielectric Measurements

The dielectric properties of the ceramic compounds have been studied using a complex impedance analyser (Hewlett-Packard model 4192A) in the frequency range 30 Hz to 13 MHz. The samples for dielectric measurements were prepared in the form of circular discs with dimensions 13 mm diameter and ~0.5 to 1.0 mm thickness. Both the faces of the substrate were polished and cleaned. A thin coating of silver paste was applied on both the faces of the circular disc and copper leads of suitable length were fixed on each face of the disc using silver paste. The discs were dried in an oven. The capacitance (C) and the dissipation factor (tan δ) were directly measured from the impedance analyser and the measurement is carried out by varying the frequency. The dielectric constant (ε') of the

samples were calculated by substituting the values of capacitance in the formula $C = \varepsilon_o \varepsilon' A/d$, where ε_o is the permittivity of free space ($\varepsilon_o = 8.854 \times 10^{-12}$ F/m), d, the thickness of the sample and A, the area of cross section of the disc.

2.5.5. Resistivity Measurements

Resistivity measurements is one of the important tool to characterise a superconductor sample. The superconducting transition temperature (T_C) can be directly determined by the resistivity measurement of the sample as a function of temperature. In the present study, the standard four probe method was employed for the resistivity measurements of superconductor samples. The four probe method of measuring the resistance has the advantage over two probe method that the effects due to contact resistance, lead resistance, etc., can be avoided.

Four probe technique in van der Pauw geometry permits the measurement of the resistivity of an isotropic sample of uniform flat thickness but with arbitrary shape if it meets the following criteria [28,29]. The different criteria are, the contacts are at the periphery of the sample, the contacts are sufficiently small, the sample is uniform in thickness, the sample does not contain holes and the sample is homogeneous. The measurement relies on a theorem proved for a sample of arbitrary shape with leads shown in Fig. 2.6. The resistance R_{MN} is defined as the potential difference $V_P - V_O$ between the contacts O and P when unit current is put through the contacts M and N, i.e.,

$$R_{MN,OP} = (V_P - V_O)/I_{MN} \tag{2.1}$$

Analogously,

$$R_{NO,PM} = (V_M - V_P)/I_{NO} \tag{2.2}$$

The new method of measurement is based on the theorem that between $R_{MN,OP}$ and $R_{NO,PM}$, there exists the simple relation,

$$\exp(-\pi d R_{MN,OP}/\rho) + \exp(-\pi d R_{NO,PM}/\rho) = 1 \tag{2.3}$$

where d is the thickness of the lamella and ρ the resistivity of the material. If d and the resistances $R_{MN,OP}$ and $R_{NO,PM}$ are known, then equation (2.3) yields an equation in which ρ is the only unknown quantity. The solution is particularly straight forward if the sample possesses a line of symmetry. In that case, M and O are placed on the line of symmetry, while N and P are disposed symmetrically with respect to this line. Then,

$$R_{NO,PM} = R_{MN,OP} \tag{2.4}$$

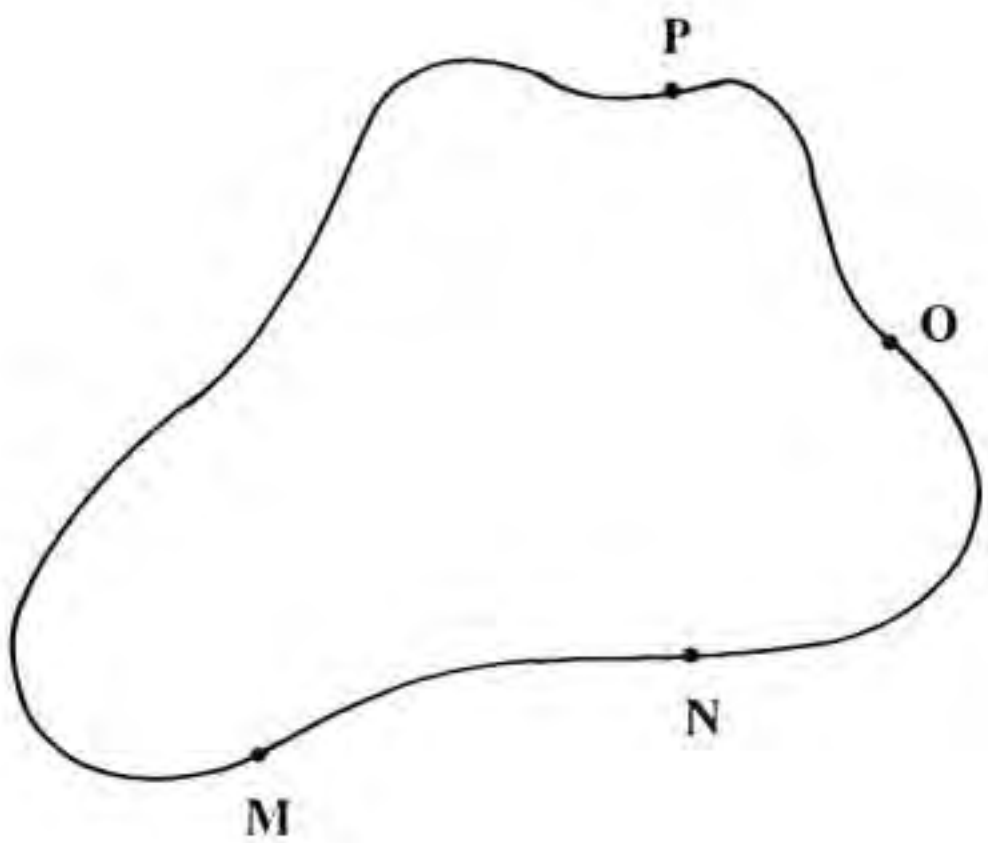

Fig. 2.6 Lead arrangement for van der Pauw with four contacts M, N, O and P on the periphery for resistivity measurements (ref. 29).

R can then easily be found from equation (2.3)

$$\rho = (\pi d/\ln 2)\, R_{MN,OP} \tag{2.5}$$

In general, it is not possible to express ρ explicitly in known functions. The solution can however be written in the form

$$\rho = (\pi d/\ln 2)\, \{(R_{MN,OP} + R_{NO,PM})/2\}\, f \tag{2.6}$$

where f is a function of the ratio of resistance such that

$$\{(R_{MN,OP} - R_{NO,PM})/(R_{MN,OP} + R_{NO,PM})\} = f \operatorname{arccosh}\{[\exp(\ln 2/f)]/2\} \tag{2.7}$$

van der Pauw has given a graphical representation for f (fig. 2.7). Thus to determine ρ, we first calculate $(R_{MN,OP}/R_{NO,PM})$, read from Fig. 2.7, the corresponding value of f and then find ρ from equation (2.6).

In the spherical case of samples and contacts which are invariant under rotation of 90°, the sheet resistance $R_S = \rho/d$ reduces to the form

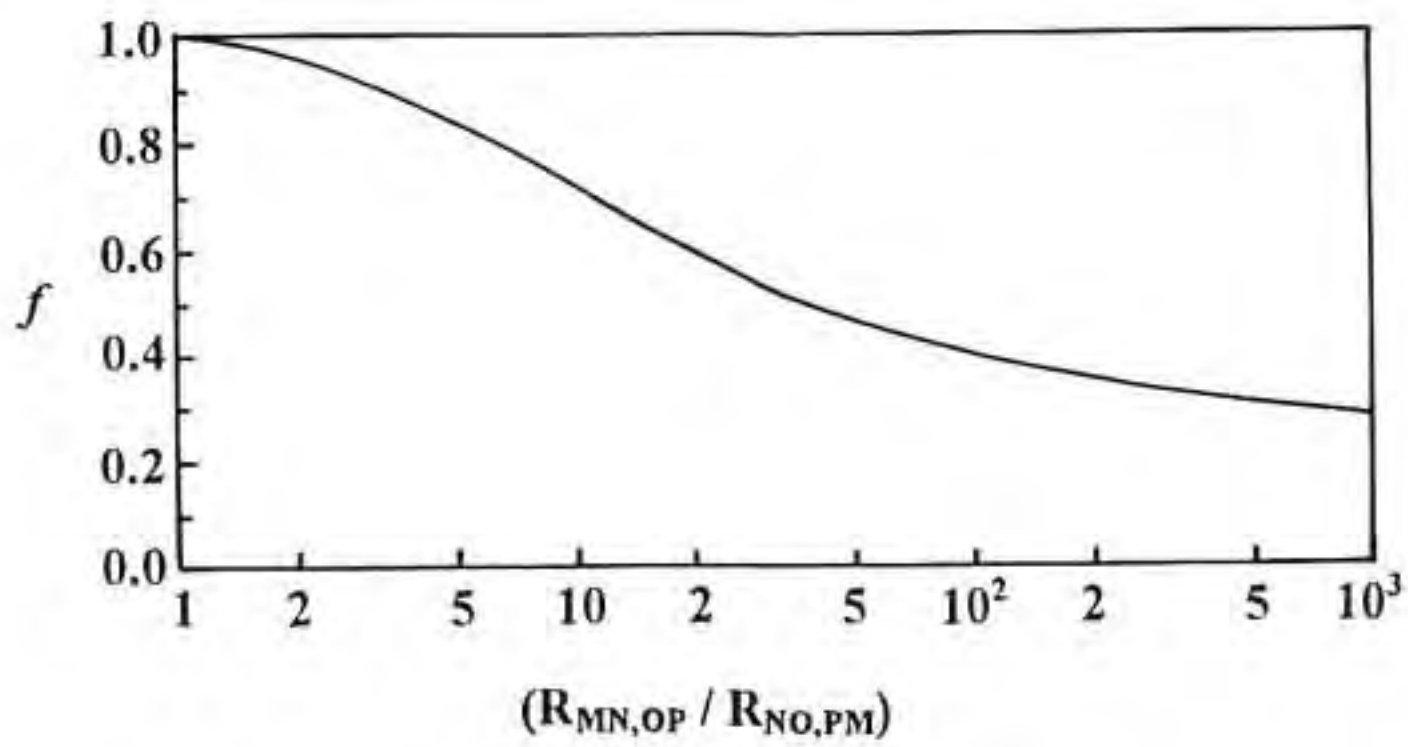

Fig. 2.7 Plot of factor f versus $(R_{MN,OP}/R_{NO,PM})$ (ref. 29).

$$R_S = (\pi/\ln 2)\ (V/I) = (\pi/\ln 2)\ R_{MN,OP} = (\pi/\ln 2)\ R_{MN,NP} \qquad (2.8)$$

Specimens with such symmetry are often easily prepared. Here V is the voltage between voltage contacts and I is the current flowing between two current contacts. Versnel [30] has extended this equation to include the case of finite length contacts on structures which are invariant under 90° rotation.

In the present study, the specimen whose resistivity to be measured was mounted using a thin layer of insulating varnish on a copper block attached at the end of a copper tube. Four copper leads were attached on the periphery of the sample using conducting silver paste. A calibrated copper constantan thermocouple attached to the copper block very close to the sample was used for the temperature measurements. The whole setup was enclosed in a cylindrical vessel (Fig. 2.8). The vessel was evacuated and a small amount of nitrogen gas was introduced. The whole setup was then introduced into the liquid nitrogen dewar. The resistivity measurement with respect to temperature was conducted by cooling the sample at a slow rate and taking the readings at close intervals. The temperature of the specimen was varied by raising or lowering the cylindrical vessel. To measure the resistance, a known current was passed through the current leads (usually 1 to 10 mA) and the voltage drop across the voltage leads was measured. A Keithley Current source (model 220) and a Keithley nanovoltmeter (model 181) were used for the above purpose. In the present study the resistivity of the samples were studied in the temperature range 300 to 77 K. The thickness of the bulk samples were measured using a screw gauge.

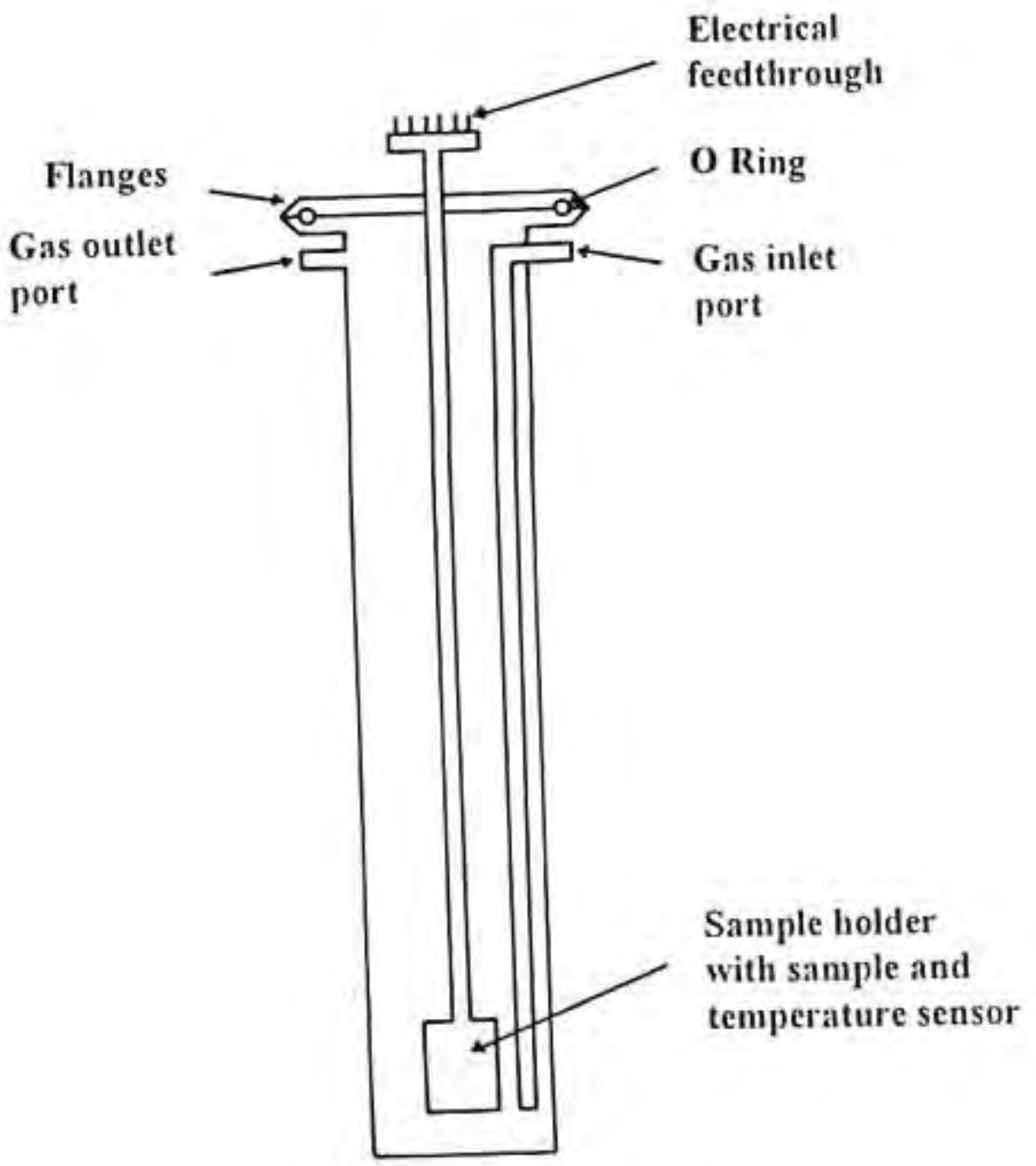

Fig. 2.8 Schematic diagram of resistivity measurement setup.

2.5.6. Current Density Measurements

The critical current density (J_C) of the superconducting films were measured at 77 K in zero magnetic field by direct method. Superconducting films developed on a rectangular substrate of dimension

15 mm (length) x 2 mm (width) were used for the current density measurements. Four contacts were given linearly as shown in Fig. 2.9. In the present study 1 μV/cm criterion was followed for the determination of J_c. All other setup for current density measurements were same as that employed for resistivity measurements except the current source and the linear contacts.

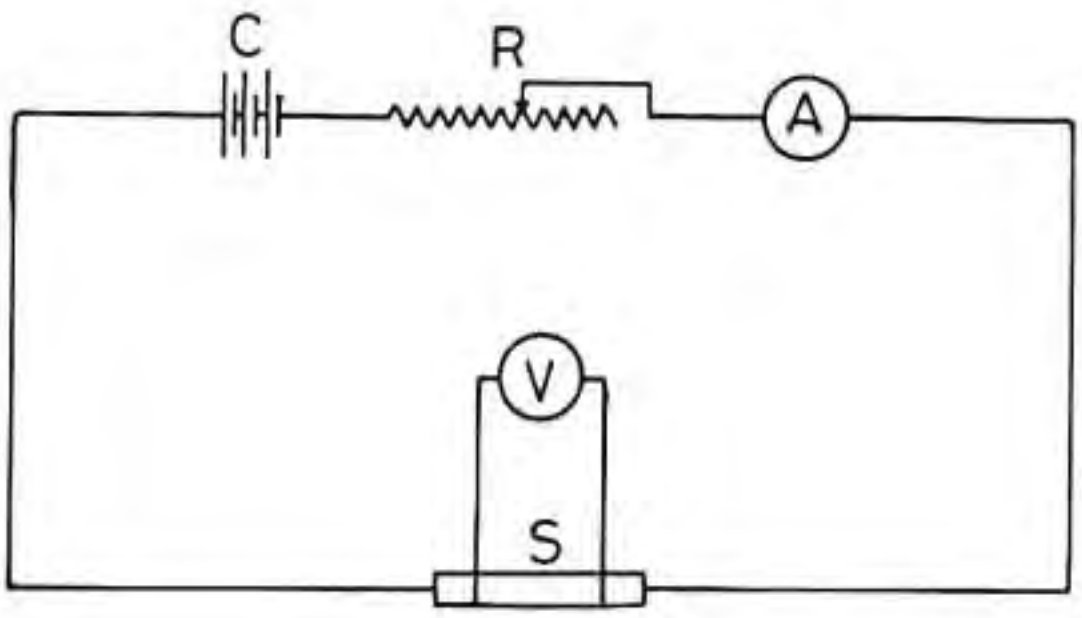

Fig. 2.9 Schematic diagram of current density measurement showing sample (S), storage cell (C), rheostat (R), ammeter (A) and nanovoltmeter (V).

References

1. A.C. Vajpei and G.S. Upadhyaya, Powder processing of high T_c superconductors, Trans. Tech. Publications, 1992, Chapter 2.
2. N. Ichinose, K. Komeya, N. Ogino, A. Tsuge and Y. Yokomizo, Introduction to Fine Ceramics; applications in engineering, ed. N. Ichinose, John Wiley and sons ltd., 1987.
3. D.M. Hwang, L. Nazar and T. Venkatesan, Appl. Phys. Lett., **52** 1834 (1988).
4. R. Pinto, S.P. Pai, C.P. D'Souza, L.C. Gupta, R. Vijayaraghavan, D. Kumar and M. Sharon, Physica C, **196**, 264 (1992) and references therein.
5. S.R. Foltyn, R.E. Muenchausen, R.C. Dye, X.D. Wu, L. Luo and D.W. Cooke, Appl. Phys. Lett., **59**, 1374 (1991).
6. R. Vaglio, Ceramics International, **19**, 421 (1993).
7. R.G. Humphreys, J.S. Stachell, N.G. chew, J.A. Edwards, S.W. Goodyear, S.E. Blenkinsop, O.D. Dosser and A.G. Cullis, Supercond. Sci. Technol., **3**, 38 (1990) and references therein.
8. C. Bjormander, A.M. Grishin, B.M. Moon, J. Lee and K.V.Rao, Appl. Phys. Lett., **64**, 3646 (1994).
9. T. Koga, B.M. Moon, I. Zakharchenko, K.V. Rao and H. Medelius, IEEE Trans. Mag., **29**, 3601 (1993).
10. R. Naidoo, R. Pretorius and C.M. Comrie, Supercond. Sci. Technol. **7**, 57 (1994).
11. O. Martinez, J. Jimenez, P. Martin, A.C. Prieto, S. Degog, D. Chambonnet,

C. Belouet, S. Nicoletti and L. Correra, Physica C, **270**, 144 (1996).

12. T. Manamikawa, M. Tazoe, K. Segawa, Y. Yonezawa, A. Morimoto and T. Shimizu, Physica C, **267**, 330 (1996).
13. X.D. Wu, B. Dutta, M.S. Hegde, A. Iman, T. Venkatesan, E.W. Chase, C.C. Chang and R. Howard, Appl. Phys. Lett., **54**, 179 (1989).
14. C. Kittel, Introduction to Solid State Physics, IV edition, John Wiley and Sons, Inc., 1971, Chapter 2.
15. M.J. Dykstra, Biological Electron Microscopy: Theory, Techniques and Trouble Shooting, Plenum Press, 1992, Chapter 9.
16. W.W. Wendlandt, Thermal Analysis, 3rd edition, John Wiley and Sons, 1986.
17. A.G. Bell, Am. J. Sci., **20**, 305 (1880).
18. F.A. McDonald and G.C. Wetsel Jr., J. Appl. Phys., **49**, 2313 (1978).
19. C.C. Ghizoni, M.A. Siqueira, H. Vargas and L.C.M. Miranda, Appl. Phys. Lett., **32**, 554 (1978).
20. A. Lachaine and P. Poulet, Appl. Phys. Lett., **45**, 953 (1984).
21. A. Rosencwaig and A. Gersho, J. Appl. Phys., **47**, 64 (1976).
22. A. Rosencwaig, Photoacoustics and Photoacoustic Spectroscopy, Wiley, New York, 1980, Chapter 9.
23. K.N. Madhusoodanan, J. Philip, G. Parthasarathy, S. Asokan and E.S.R. Gopal, Philosophical Magazine B, **58**, 123 (1988).
24. J. Issac, J. Philip and B.K. Chaudhuri, Pramana J. Phys., **32**, L167 (1989).
25. S.S. Raman, V.P.N. Nampoori, C.P.G. Vallabhan, G. Ambadas and S.

Sugunan, Appl. Phys. Lett., **67**, 2939 (1995).

26. P. Charpentier, F. Lepoutre and L. Bertrand, J. Appl. Phys., **53**, 608 (1982).
27. G.A. West, J.J. Barrett, D.R. Siebert and K.V. Reddy, Rev. Sci. Instrum. **54**, 797 (1983).
28. L.J. van der Pauw, Philips Res. Repts., **13**, 1 (1958).
29. L.J. van der Pauw, Philips Tech. Rev., **20**, 220 (1958).
30. W. Versuel, Solid State Electron, **21**, 1261 (1978).

CHAPTER 3

PREPARATION AND CHARACTERISATION OF Ba_2RENbO_6 (RE=Pr, Nd, Sm, Eu and Gd): A GROUP OF PEROVSKITES SUITABLE AS SUBSTRATES FOR $YBa_2Cu_3O_{7-\delta}$ SUPERCONDUCTOR

3.1. Introduction

The discovery of high temperature superconductivity above liquid nitrogen temperature in some of the ceramic perovskite oxides has led to considerable amount of research activities on the preparation of these materials in the form of thick and thin films for device applications. For the successful preparation of films of these materials, selection of a suitable substrate material is an important factor. One of the most important criteria for the selection of any material as a substrate for high T_c superconductor (HTSC) films is the chemical non-reactivity between the substrate and the film at the processing temperature. The over riding importance of the chemical compatibility of the substrate with the film over other substrate parameters has been highlighted in many articles [1-4]. In addition to the chemical inertness, the substrate should have low dielectric constant and loss factor for their application in microwave devices [1-2]. Also, the substrate should have good thermal and lattice match with HTSC film and be free from any phase transition [4]. All the currently available substrates represent some kind of compromise, i.e., they either offer a good lattice match and a high dielectric constant, or a low dielectric constant and a poor lattice match, or twinning or a large divergence in thermal expansion coefficient [4]. Hence the search for a suitable and economically viable

substrate for HTSC films is an active area of research. The conventional substrate materials such as Si, SiO_2, Al_2O_3, etc., react with YBCO at the processing temperature thereby reducing the superconducting transition temperature of YBCO considerably [5-10]. MgO, one of the extensively used substrate material for the epitaxial growth of YBCO thin films, forms an interlayer of barium salt at the film-substrate interface if the processing temperature is above 700°C, thereby reducing the transition temperature of YBCO film [7,9-14]. $SrTiO_3$, though has a good lattice matching with YBCO, its high dielectric constant and loss factor values restricts its use as substrate for microwave device applications [15-17]. Yttria-stabilised zirconia has been used as a substrate for YBCO films, but there are reports of the formation of $BaZrO_3$ at the film-substrate interface due to reaction with YBCO [18-19]. The major disadvantage of yttria-stabilised zirconia is its high dielectric loss [20]. Presently, $LaAlO_3$ has become a substrate of choice for the growth of YBCO films. Though $LaAlO_3$ has a moderately low dielectric constant and loss factor values, it has the disadvantage that it is available only in twinned crystalline form [16-17,21]. In the course of our work on the development of novel substrates for $YBa_2Cu_3O_{7-\delta}$ (YBCO) superconductor, we have identified a group of complex perovskites $Ba_2R_ENbO_6$☆ (where R_E = Pr, Nd, Sm, Eu and Gd) having a general formula $A_2BB'O_6$ which are chemically non-reacting with YBCO superconductor even at the extreme processing conditions. BR_ENO were found to have dielectric constant and loss factor values in a range suitable

☆ Published in *Jpn. J. Appl. Phys.* **33**, 117 (1994) and *Materials Letters*, **17**, 393 (1993)

for their use as substrates for microwave applications. Also, these materials were found to have suitable thermal properties for substrate application making BReNO as ideal candidates as substrates for YBCO superconductors. A detailed description regarding the preparation and characterisation of BReNO is given in the following sections of this chapter.

3.2. Preparation of BReNO

BReNO were prepared following the conventional solid state reaction technique. Stoichiometric amounts of high purity (99.9%) rare-earth oxide (Re_2O_3), barium carbonate ($BaCO_3$) and niobium oxide (Nb_2O_5) were weighed and thoroughly wet mixed in an agate mortar with acetone as wetting medium. The mixture was dried and calcined in an alumina crucible at a temperature between 1100°C and 1200°C for 36 h in air with two intermediate grindings. The phase purity of these materials were examined by X-ray diffraction technique and these phase pure materials were ground well so as to make them in the form of fine powders. These finely ground powder of BReNO were mixed with appropriate amount of polyvinyl alcohol (PVA) [added as binder] and pressed in the form of circular discs with dimensions of 10 mm (or 13 mm) diameter and about 1.5 mm thickness by applying a pressure of 350 to 450 MPa by uniaxial pressing. These circular discs were then sintered at a temperature between 1400°C to 1500°C for 12 h in air. The individual values corresponding to calcination temperature and time, sintering temperature and time, etc, are presented in Table 3.1.

Table 3.1 Calcination temperature, duration of calcination, sintering temperature and duration of sintering of Ba_2RENbO_6

Material	Calcination temperature(°C)	Duration of calcination(h)	Sintering temperature(°C)	Duration of sintering(h)
Ba_2PrNbO_6	1100	36	1420	12
Ba_2NdNbO_6	1150	36	1480	12
Ba_2SmNbO_6	1100	36	1450	12
Ba_2EuNbO_6	1100	36	1500	12
Ba_2GdNbO_6	1150	36	1480	12

3.3. Structural Characterisation of BRENO

The structural characterisation of BRENO samples was carried out using powder X-ray diffraction (XRD) technique. In the present study the XRD patterns were recorded using a computerised Rigaku X-ray diffractometer (Dmax/2C, Japan) employing nickel filtered Cu Kα radiation (λ = 1.5406 Å). Figures 3.1(a) to 3.1(e) show the powder XRD patterns of sintered Ba_2PrNbO_6 (BPNO), Ba_2NdNbO_6 (BNNO) and Ba_2GdNbO_6 (BGNO) respectively taken for 2θ values between 5 and 90 degrees. The detailed computerised XRD data comprised of 2θ, d values, I/I_o and hkl values of BRENO are given in Table 3.2. The XRD patterns and the data of BRENO materials clearly show that these materials are isostructural and the

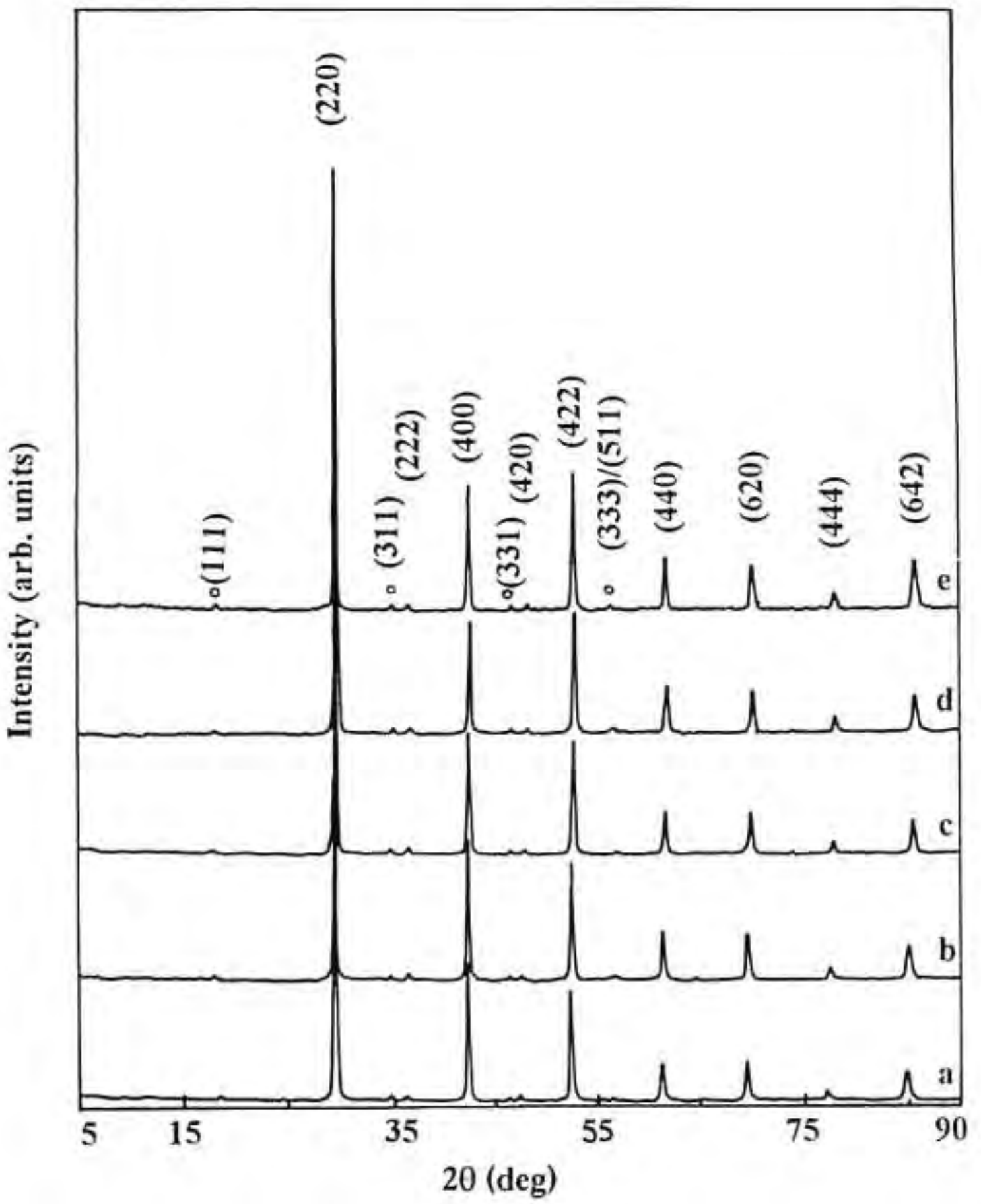

Fig. 3.1 Powder X-ray diffraction patterns of phase pure sintered (a) Ba_2PrNbO_6, (b) Ba_2NdNbO_6, (c) Ba_2SmNbO_6, (d) Ba_2EuNbO_6 and (e) Ba_2GdNbO_6. Superstructural lines are marked by '∘'.

Table 3.2(a) Powder X-ray diffraction data of sintered Ba_2PrNbO_6☆

No.	2θ (deg.)	Width	'd' (Å)	I/I_o	h k l
1	17.860	0.423	4.962	3	111
2	29.540	0.450	3.022	100	220
3	34.800	0.330	2.576	3	311
4	36.400	0.390	2.466	4	222
5	42.280	0.450	2.136	37	400
6	46.350	0.389	1.957	3	331
7	47.380	0.360	1.917	3	420
8	52.390	0.630	1.745	29	422
9	55.940	0.405	1.642	3	333/511
10	61.360	0.780	1.510	11	440
11	69.510	0.615	1.351	12	620
12	77.520	0.285	1.230	3	444
13	85.040	0.360	1.140	8	642

☆ accepted for publication in JCPDS file

Table 3.2(b) Powder X-ray diffraction data of sintered Ba_2NdNbO_6 ✡

No.	2θ (deg.)	Width	'd' (Å)	I/I_o	h k l
1	17.920	0.393	4.946	3	111
2	29.670	0.435	3.009	100	220
3	34.970	0.330	2.564	3	311
4	36.550	0.405	2.456	5	222
5	42.440	0.435	2.128	36	400
6	46.650	0.369	1.945	3	331
7	47.640	0.345	1.907	3	420
8	52.600	0.555	1.739	30	422
9	56.380	0.412	1.631	3	333/511
10	61.550	0.585	1.505	13	440
11	69.770	0.645	1.347	12	620
12	77.700	0.270	1.228	4	444
13	85.040	0.780	1.140	9	642

✡ *accepted for publication in JCPDS file*

Table 3.2(c) Powder X-ray diffraction data of sintered Ba_2SmNbO_6☆

No.	2θ (deg.)	Width	'd' (Å)	I/I_o	h k l
1	18.020	0.384	4.919	3	111
2	29.720	0.420	3.004	100	220
3	35.010	0.345	2.561	4	311
4	36.620	0.405	2.452	6	222
5	42.550	0.465	2.123	35	400
6	46.520	0.321	1.951	4	331
7	48.050	0.300	1.892	4	420
8	52.760	0.510	1.734	34	422
9	56.180	0.354	1.636	3	333/511
10	61.730	0.585	1.502	13	440
11	70.010	0.585	1.343	13	620
12	77.850	0.645	1.226	6	444
13	85.460	0.570	1.135	12	642

☆ *accepted for publication in JCPDS file*

Table 3.2(d) Powder X-ray diffraction data of sintered Ba_2EuNbO_6

No.	2θ (deg.)	Width	'd' (Å)	I/I_o	h k l
1	18.200	0.369	4.870	4	111
2	29.880	0.420	2.996	100	220
3	35.160	0.330	2.550	4	311
4	36.790	0.459	2.441	7	222
5	42.720	0.465	2.115	31	400
6	46.710	0.343	1.943	4	331
7	48.360	0.480	1.881	5	420
8	52.960	0.510	1.728	33	422
9	56.620	0.389	1.624	3	333/511
10	61.920	0.555	1.497	14	440
11	70.220	0.465	1.339	13	620
12	78.020	0.345	1.224	6	444
13	85.690	0.465	1.133	12	642

Table 3.2(e) Powder X-ray diffraction data of sintered Ba_2GdNbO_6☆

No.	2θ (deg.)	Width	'd' (Å)	I/I_o	h k l
1	17.920	0.381	4.946	4	111
2	29.610	0.495	3.015	100	220
3	34.930	0.390	2.567	6	311
4	36.570	0.465	2.455	8	222
5	42.490	0.525	2.126	37	400
6	46.290	0.409	1.960	3	331
7	48.230	0.465	1.885	7	420
8	52.760	0.540	1.734	40	422
9	55.910	0.379	1.643	3	333/511
10	61.770	0.555	1.501	21	440
11	70.080	0.615	1.342	17	620
12	77.930	0.705	1.225	9	444
13	85.600	0.780	1.134	17	642

☆ *accepted for publication in JCPDS file*

characteristic XRD peaks have almost the same intensity ratio. **Also** BREnO are found to be isostructural with other rare-earth complex **cubic** perovskites with general formula $A_2BB'O_6$ such as Ba_2ErSbO_6, Ba_2YNbO_6, Ba_2DySbO_6, etc., reported in JCPDS file, in which the doubling of the basic perovskite unit cell (ABO_3) is observed. The doubling of the basic perovskite unit cell in BREnO is due to the ordering of RE and Nb atoms at the octahedral sites [22-23]. The presence of superstructural lines in the XRD patterns shown in Fig. 3.1 indicates the ordering of the basic ABO_3 perovskite unit cell in BREnO materials. The crystal structure diagram of BREnO is shown in Fig. 3.2. The XRD peaks including the minor peaks

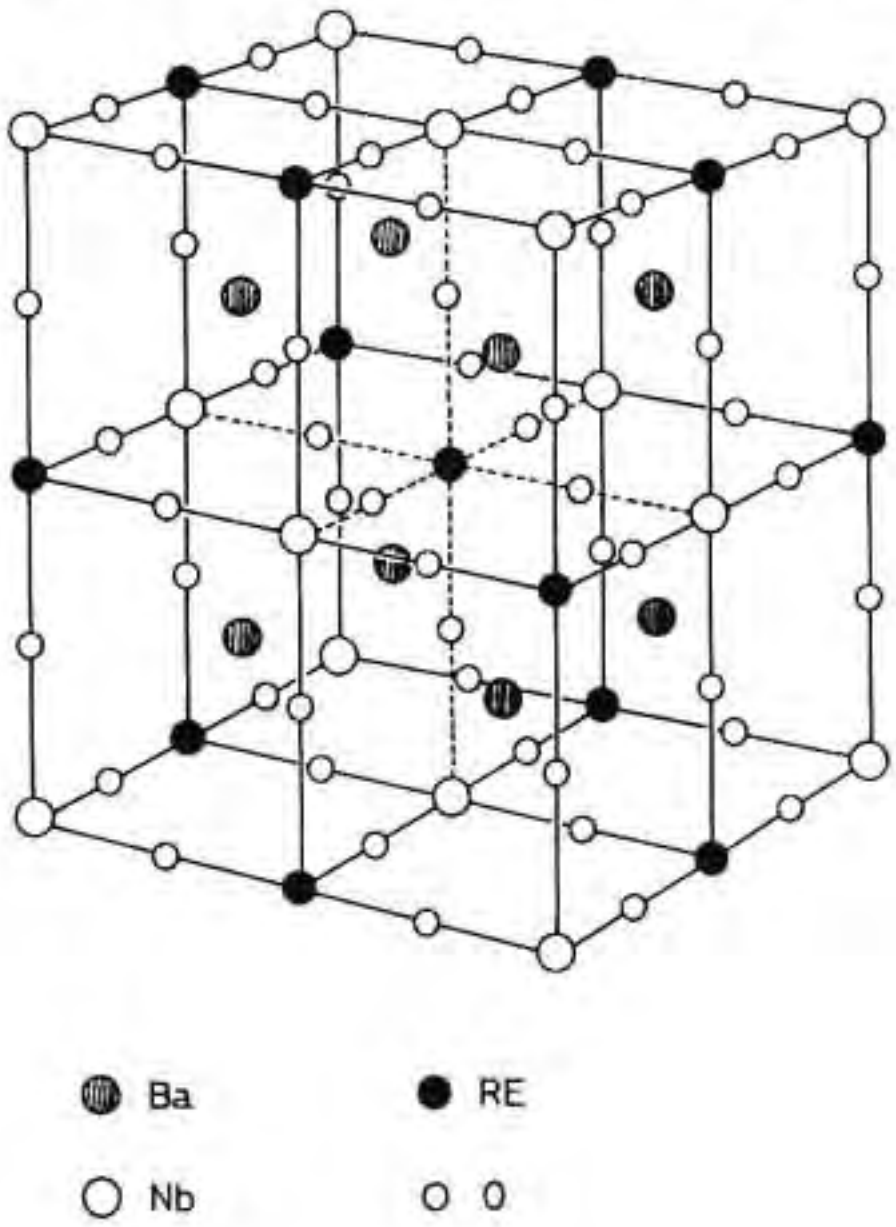

Fig. 3.2 Crystal structure diagram of Ba_2REnbO_6 materials.

of BREnO are indexed for a complex cubic perovskite structure and the lattice constant values of BREnO are given in Table 3.3. Based on the doubling of the simple perovskite unit cell, the lattice constant values of BREnO are comparable to that of MgO, which is used as a substrate for epitaxial growth of YBCO thin films.

It may be noted that Ba_2EuNbO_6 is reported as a cubic perovskite [24] and Ba_2SmNbO_6 is reported as an orthorhombic perovskite [25]. However, our XRD results clearly shows that Ba_2SmNbO_6 also has a cubic symmetry. On the other hand, Ba_2NdNbO_6 [26] is reported in JCPDS (Joint Committee on Powder Diffraction Standards) as a cubic perovskite, but the I/I_o of the peaks were very much different from the I/I_o which we obtained in our XRD data. In the case of Ba_2GdNbO_6 [27], the structure is reported in JCPDS file as perovskite with tetragonal symmetry. But our XRD results shows that Ba_2GdNbO_6 has a cubic perovskite structure and the d values of the characteristic peaks were different from the reported data.

3.4. Density Measurements of BREnO

The sintered density of BREnO discs was measured by Archimedes method. The sintered density of BREnO compounds was >97% of the theoretical density for the materials sintered at the optimum sintering temperature. The individual sintering temperatures of BREnO are given in Table 3.1. The theoretical density (ρ') of BREnO was calculated by substituting the corresponding values of lattice constant, a, obtained from

XRD analysis in the equation $\rho' = (Z.M)/(N.V)$, where Z = 4 (in the present case), M, the molecular weight of BRENO, V, volume of unit cell, and N, the Avogadro number. The values of theoretical density and sintered density of BRENO materials are given in Table 3.3. The variation of sintered density with sintering

Table 3.3 Lattice constant, theoretical density and sintered density of Ba_2RENbO_6

Material	Lattice constant(Å)	Theoretical density(gm/cm^3)	Sintered density(gm/cm^3)
Ba_2PrNbO_6	8.592	6.330	6.159
Ba_2NdNbO_6	8.573	6.407	6.219
Ba_2SmNbO_6	8.524	6.584	6.443
Ba_2EuNbO_6	8.455	6.764	6.462
Ba_2GdNbO_6	8.587	6.512	6.362

temperature for Ba_2GdNbO_6 material with a green density (density of the disc measured before sintering) of ~68% of the theoretical density sintered at different temperature for 12 h in air is shown in Fig. 3.3 as a typical example.

The BRENO samples were mechanically strong and stable in air. BRENO could be sliced into thin pieces of 0.5 mm thickness by a diamond cutter. Good reflecting surfaces were obtained by mechanical polishing and organic solvents such as alcohol, acetone, carbon tetrachloride, trichloro-ethylene, etc., could be used as effective cleaning agents.

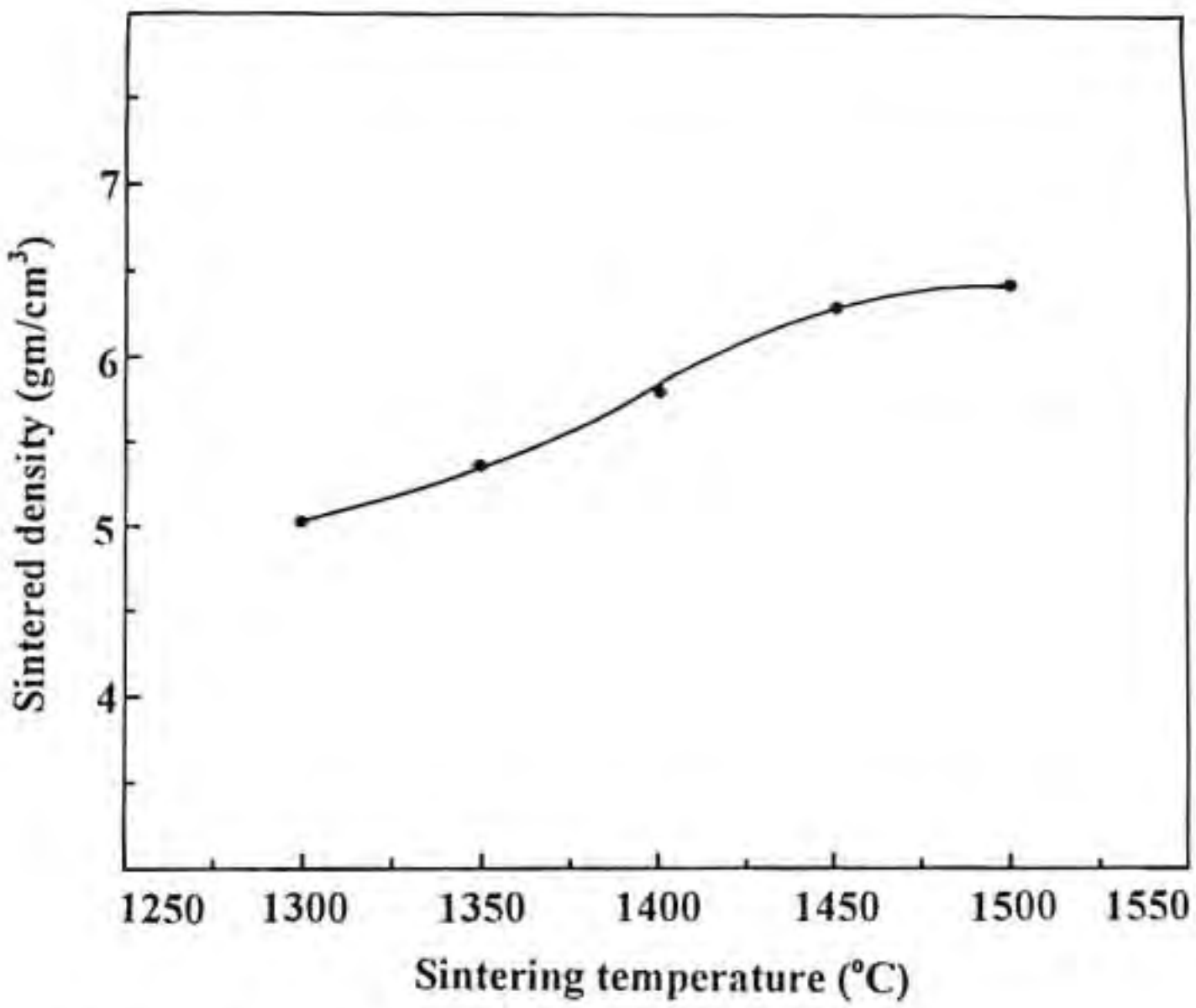

Fig. 3.3 Variation of sintered density with sintering temperature for Ba_2GdNbO_6 sintered in air for 12 h.

3.5. Microstructural Studies of BRENO

The surface morphology of sintered BRENO samples was examined by a Hitachi (S2400, Japan) scanning electron microscope (SEM). The sintered BRENO samples were polished well and subjected to chemical etching using a 5% HCl solution. BRENO samples were dried and the polished surface was coated with gold before observing them by SEM. The typical surface SEM micrographs of BRENO samples are shown in Fig. 3.4. The microstructural analysis of the surface of the sintered BRENO samples shows that these samples are dense and almost free from porosity. The surface grain structure of BRENO shows that they are of uniform size.

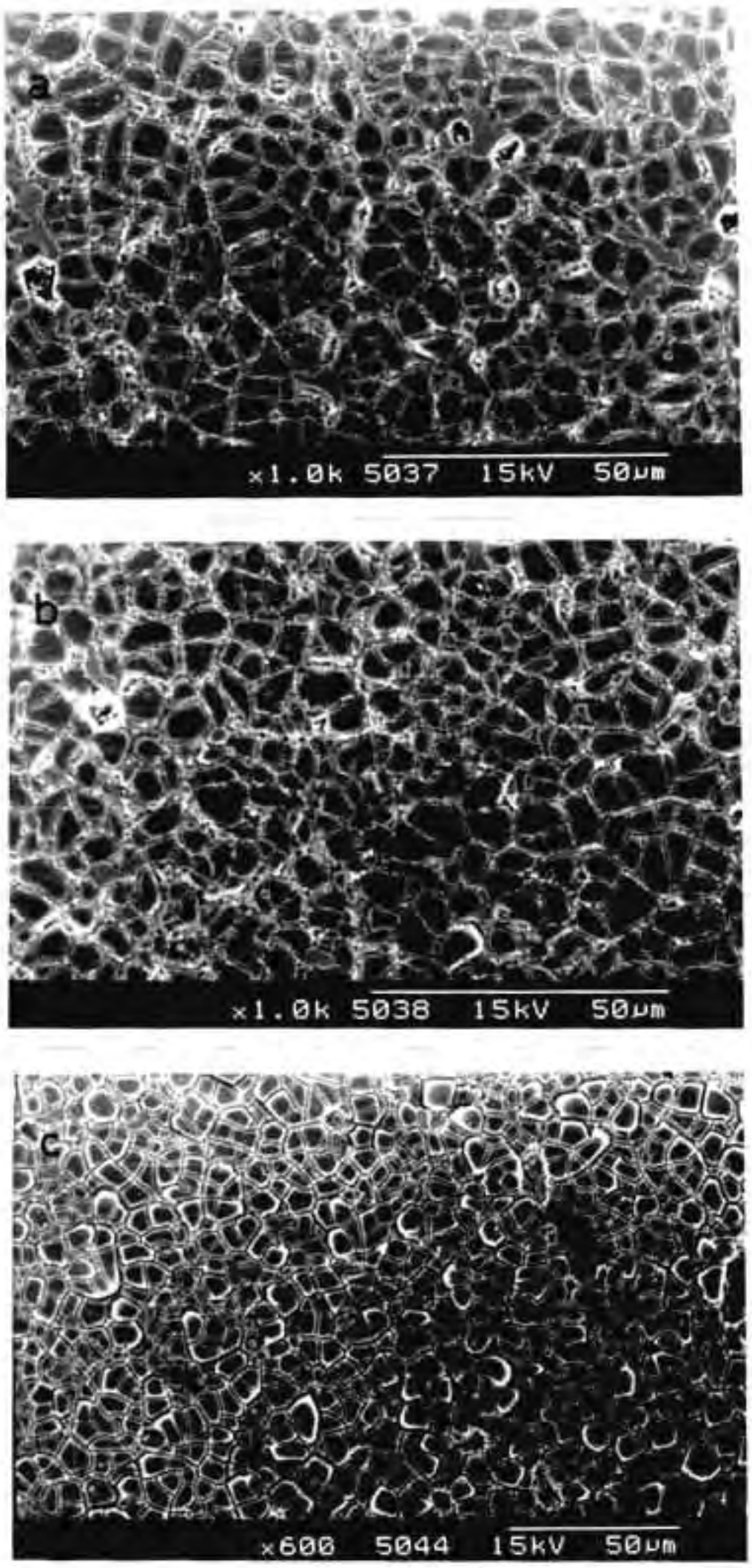

Fig. 3.4 The SEM micrograph of polished and subsequently etched surface of sintered (a) Ba_2NdNbO_6, (b) Ba_2SmNbO_6 and (c) Ba_2GdNbO_6

3.6. Dielectric Characterisation of BRENO.

The dielectric constant (έ) and loss factor (tan δ) of polycrystalline BRENO (sintered density >97%) were measured using an HP 4192 A Complex Impedance Analyser in the frequency range 30 Hz to 13 MHz. Sintered circular discs of BRENO with 10 mm diameter (or 13 mm diameter) and about 1 mm thickness with silver electrodes on both sides of the discs were used for the dielectric measurements. The variation of dielectric constant and loss factor with frequency at room temperature are shown in Figs. 3.5 and 3.6, respectively. The study of variation of έ and

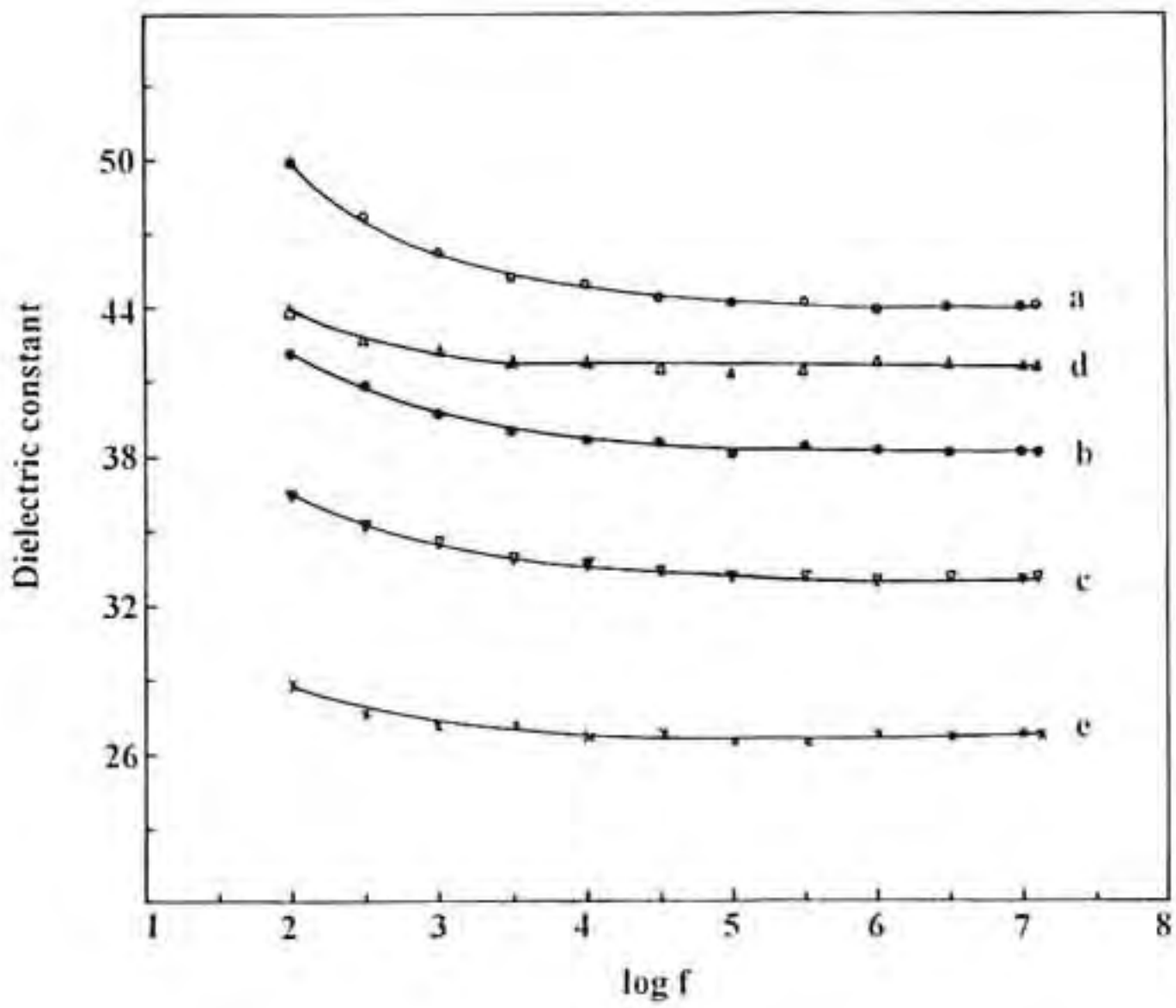

Fig. 3.5 Variation of dielectric constant (έ) with frequency for (a) Ba_2PrNbO_6, (b) Ba_2NdNbO_6, (c) Ba_2SmNbO_6, (d) Ba_2EuNbO_6 and (e) Ba_2GdNbO_6.

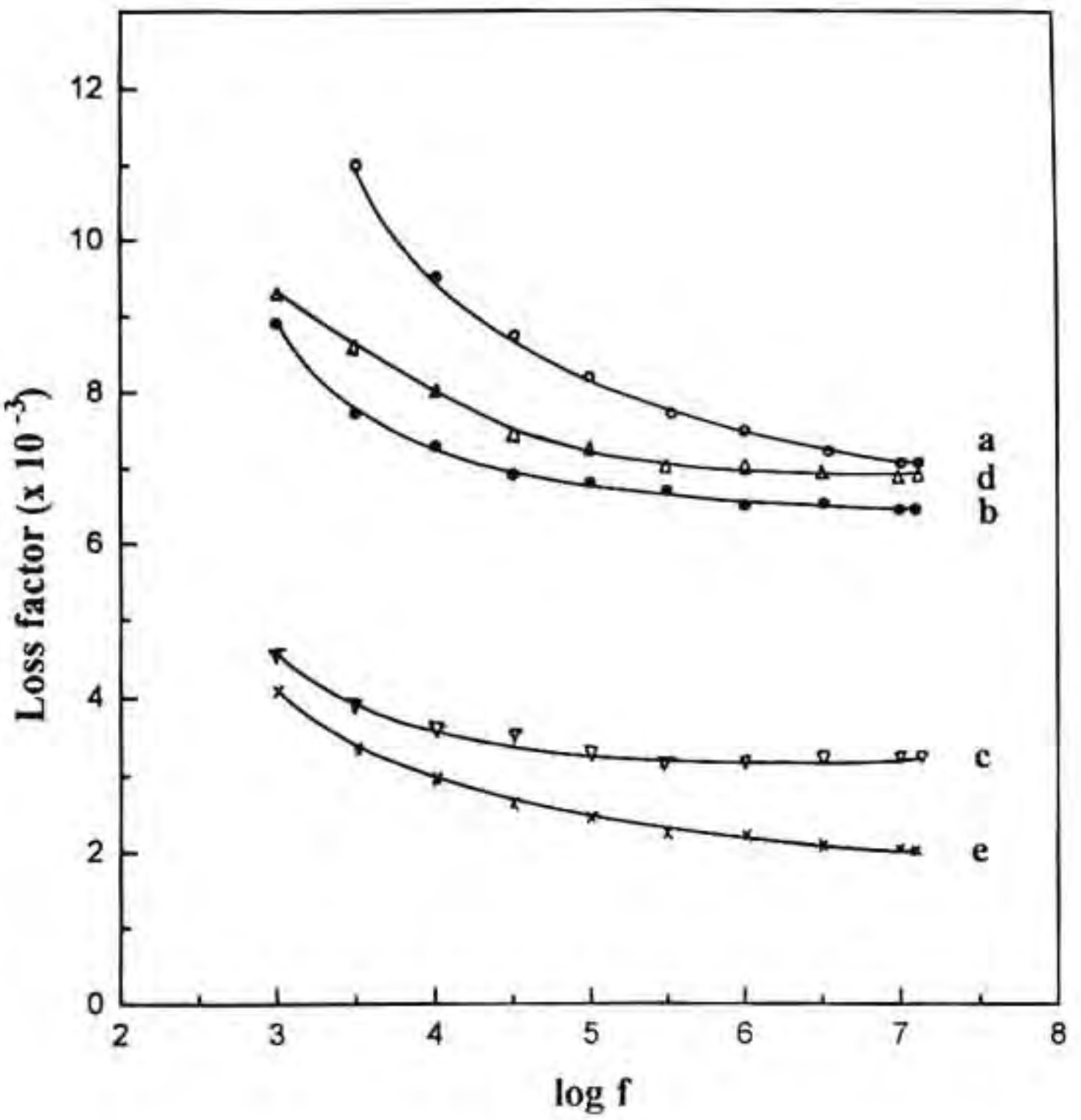

Fig. 3.6 Variation of loss factor (tan δ) with frequency for (a) Ba_2PrNbO_6, (b) Ba_2NdNbO_6, (c) Ba_2SmNbO_6, (d) Ba_2EuNbO_6 and (e) Ba_2GdNbO_6 measured at room temperature.

tan δ of BRENO with frequency at liquid nitrogen temperature (77 K) in the frequency range 13 Hz to 13 MHz showed that the value of tan δ decreased almost by one order whereas there were no substantial change in the έ values of BRENO materials. The variation of tan δ with frequency of BRENO at liquid nitrogen temperature is shown in Fig. 3.7. The values of έ and tan δ of BRENO measured at 10 MHz are given in Table 3.4.

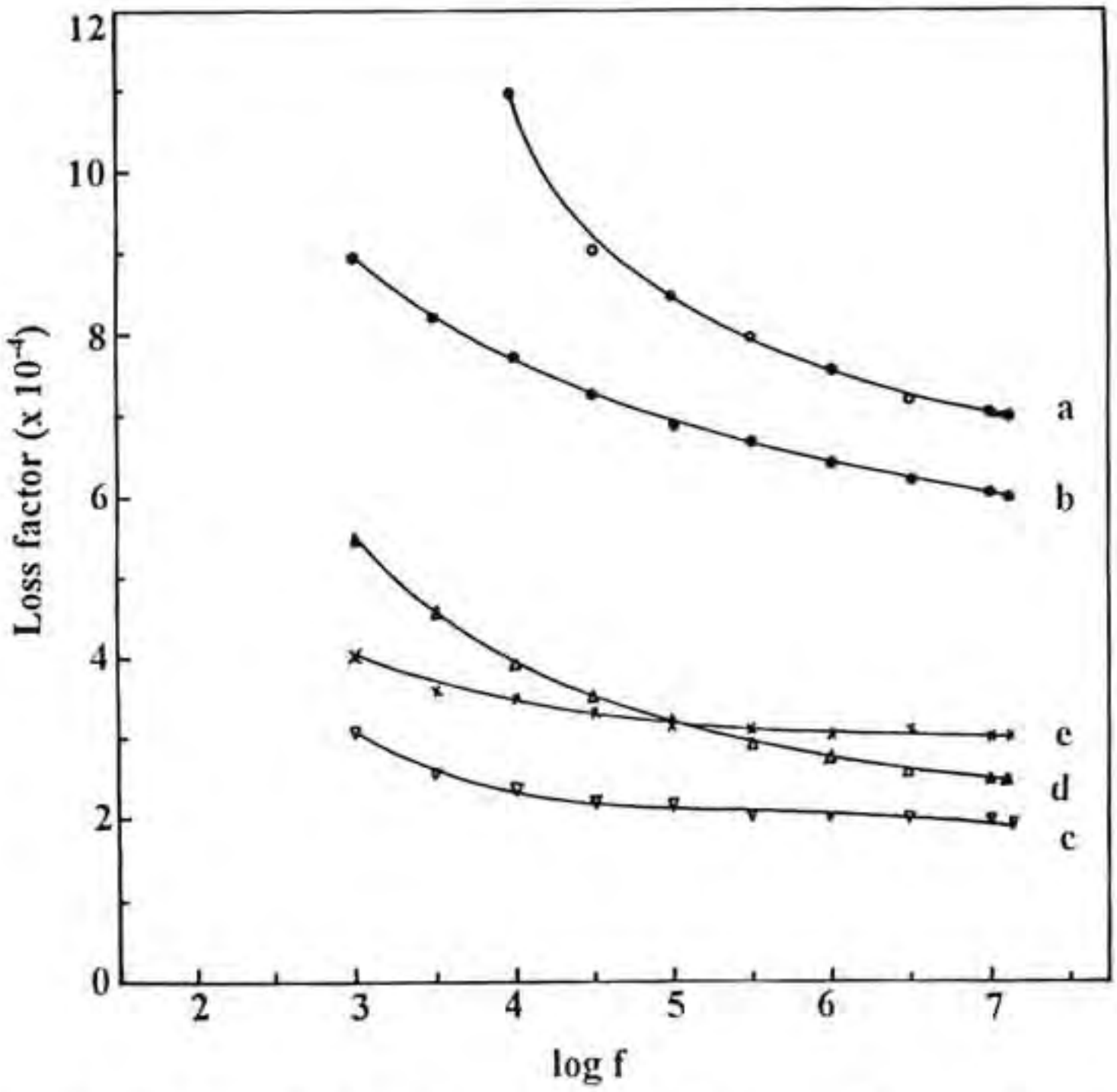

Fig. 3.7 Variation of loss factor (tan δ) with frequency for (a) Ba_2PrNbO_6, (b) Ba_2NdNbO_6, (c) Ba_2SmNbO_6, (d) Ba_2EuNbO_6 and (e) Ba_2GdNbO_6 measured at liquid nitrogen temperature (77 K).

Table 3.4 Dielectric constant (έ), loss factor (tan δ) and dc resistivity of Ba_2RENbO_6

Material	Dielectric constant (έ)	Loss factor (tan δ) 300 K	Loss factor (tan δ) 77 K	dc resistivity (10^{10} Ω.cm)
Ba_2PrNbO_6	43.9	7.1×10^{-3}	7.0×10^{-4}	3.4
Ba_2NdNbO_6	38.1	6.5×10^{-3}	6.0×10^{-4}	4.8
Ba_2SmNbO_6	32.8	3.2×10^{-3}	2.0×10^{-4}	8.9
Ba_2EuNbO_6	41.4	6.9×10^{-3}	2.5×10^{-4}	7.8
Ba_2GdNbO_6	26.9	2.0×10^{-3}	3.0×10^{-4}	9.2

The electrical resistivity measurements of BRENO samples were carried out using Keithley solid state electrometer model 602. The room temperature resistivities were in the range 10^{10} Ω.cm and the individual values are given in Table 3.4. The atmospheric stability of BRENO samples were studied by keeping the sintered BRENO discs in boiling water for 1 h and measuring the electrical resistivity of the humidity treated samples after drying. The electrical resistivity measurements of the humidity treated samples showed no change in resistivity values indicating that these materials are highly stable under atmospheric conditions and no degradation was observed in the stability of the samples.

3.7. Thermal Characterisation of BReNO

The thermal characterisation of polycrystalline BReNO materials was carried out using differential thermal analysis, differential scanning calorimetry, thermomechanical analysis and photoacoustic techniques.

Differential thermal analysis (DTA) of BReNO samples was carried out using Shimadzu DTA model 50 H (Japan) in the temperature range 30 to 1300°C. The DTA scans of phase pure powdered BReNO samples were taken from 30 to 1300°C at a rate of 10°C/min in nitrogen atmosphere. The DTA plots of these samples did not show any indication of a phase transition (within the precision of DTA) up to a temperature of 1300°C. The DTA curve of Ba_2SmNbO_6 is shown in Fig. 3.8 as a representative example.

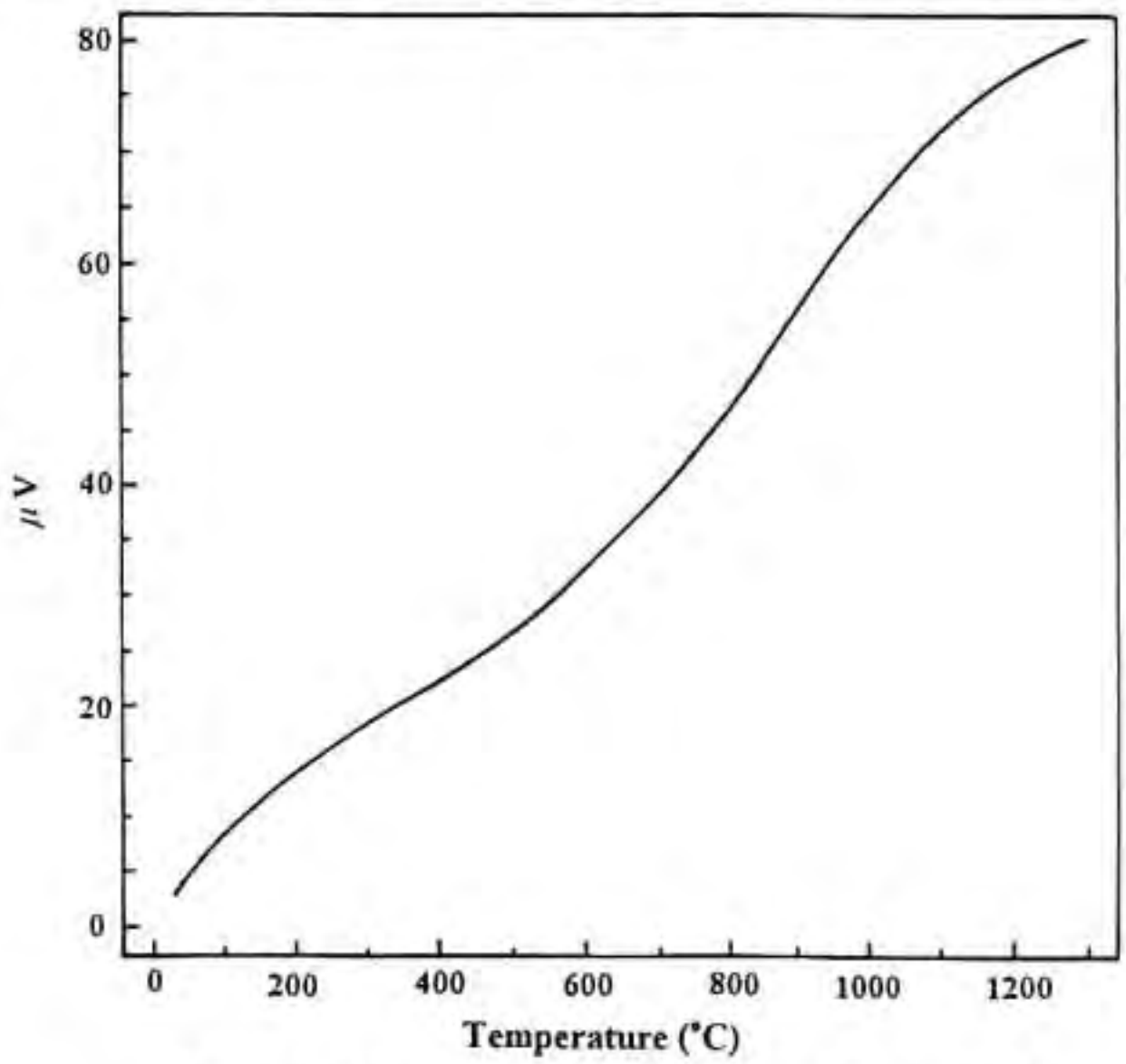

Fig. 3.8 DTA curve of phase pure Ba_2SmNbO_6

The thermal expansion coefficient of BRENO samples was measured using a Perkin Elmer Thermomechanical Analyser (TMA 7) with thermal analysis controller model TAC 7/DX. Sintered BRENO samples with dimension 5 mm (length) x 5 mm (breadth) x ~7 mm (height) were used for the thermal expansion studies. The expansion of the samples verses temperature was recorded in the temperature range 20 to 100°C at a heating rate of 10°C/min. The thermal expansion coefficients of BRENO samples were calculated from the TMA plots. A typical TMA expansion plot of Ba_2NdNbO_6 sample is shown in Fig. 3.9. The thermal expansion coefficient of BRENO samples are given in Table 3.5.

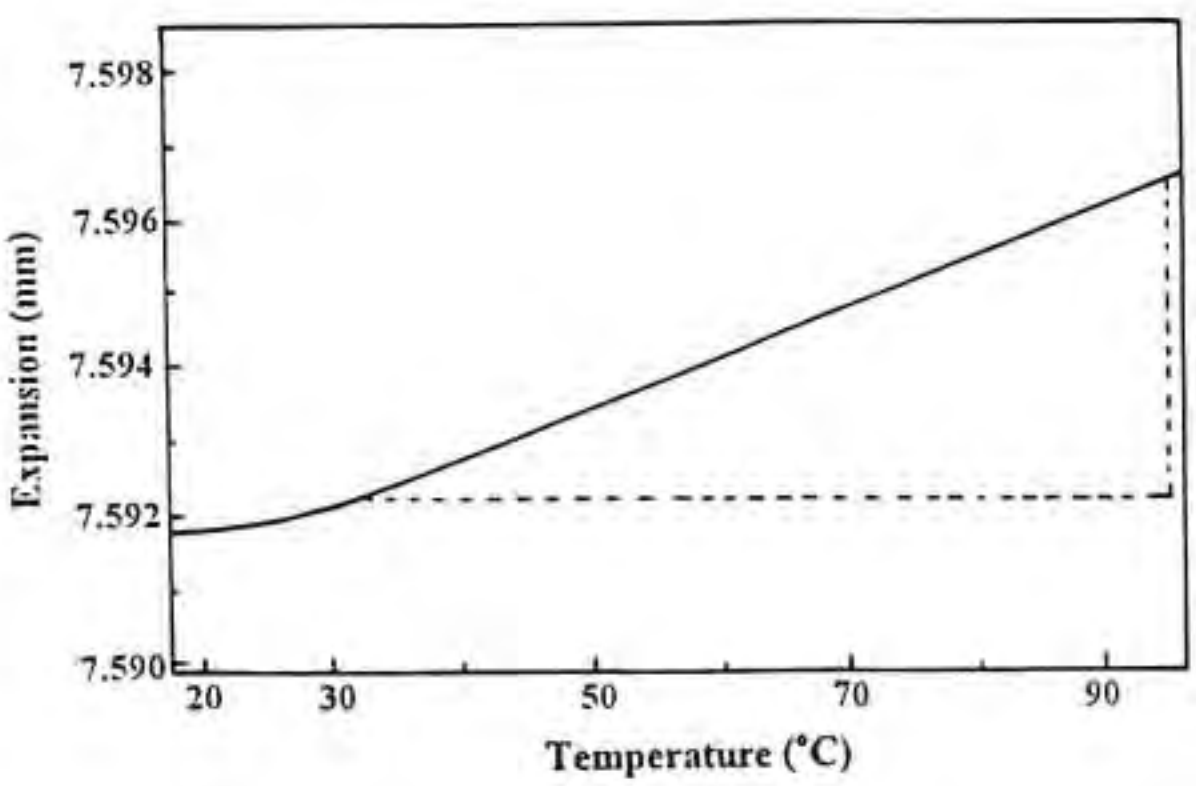

Fig. 3.9 TMA expansion plot of sintered Ba_2NdNbO_6 sample with dimension 5 x 5 x 7.592 mm taken at room temperature.

Table 3.5 Thermal expansion coefficient of Ba_2RENbO_6 at room temperature

Material	Thermal expansion coefficient($x10^{-6}$ °C^{-1})
Ba_2PrNbO_6	8.572
Ba_2NdNbO_6	8.620
Ba_2SmNbO_6	7.818
Ba_2EuNbO_6	8.272
Ba_2GdNbO_6	7.913

The specific heat capacity of BRENO samples was found out using differential scanning calorimetry (DSC) studies. In the present study DSC experiments were carried out using Mettler DSC 20 standard cell with Mettler TA 3000 programmer. The BRENO samples in the form of fine powder were taken in an aluminium pan and sealed. The pan is then placed inside the calorimeter and the heat flow into the sample is plotted as a function of temperature. The DSC studies were carried out in nitrogen atmosphere and the heating rate used was 10°C/min. A typical DSC plot of BRENO is shown in Fig. 3.10. The specific heat capacity of BRENO samples were calculated from the DSC plots. The specific heat capacity of BRENO samples are given in Table 3.6.

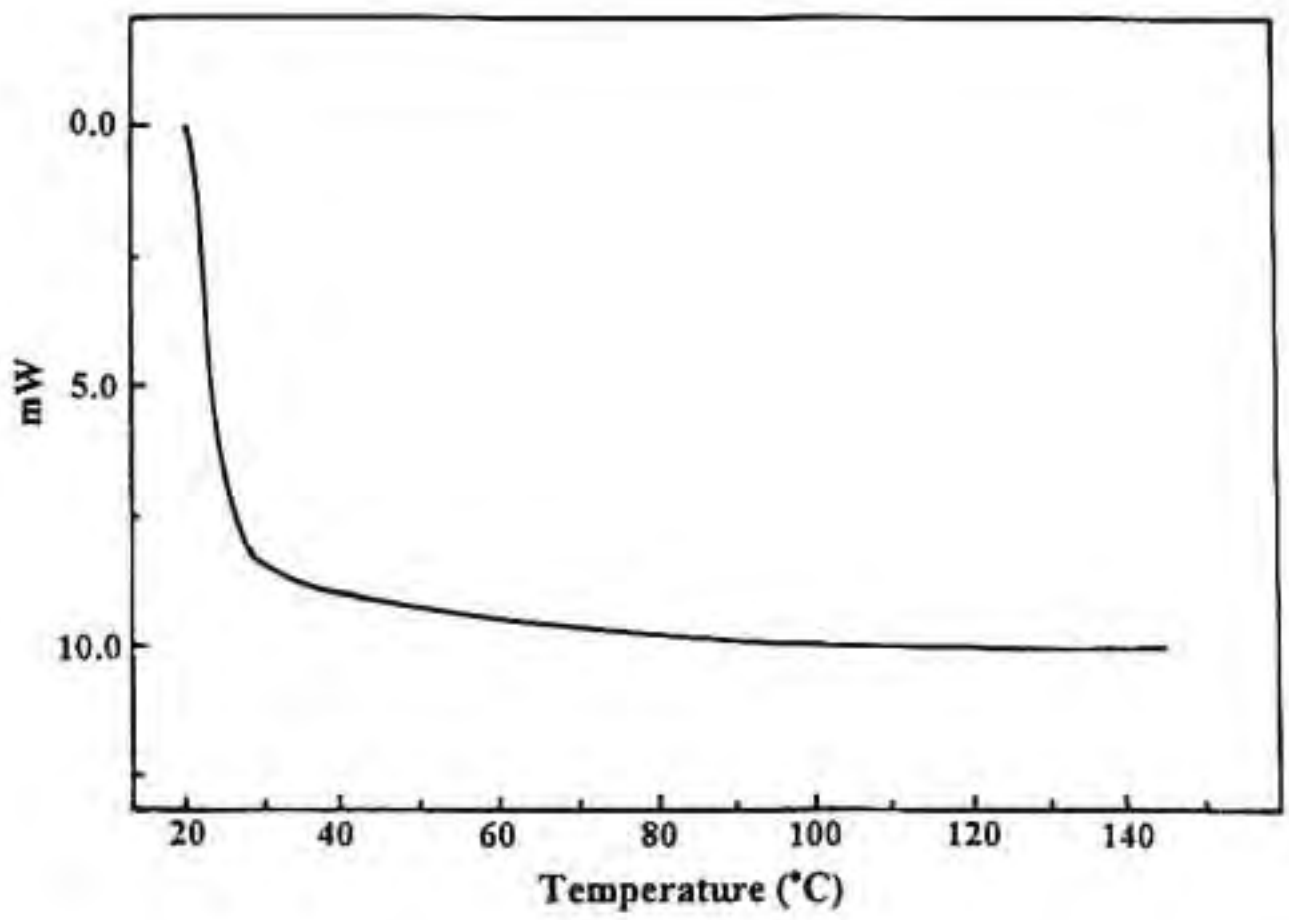

Fig. 3.10 DSC curve of phase pure Ba_2GdNbO_6 material.

Table 3.6 Specific heat capacity of $Ba_2R_ENbO_6$

Material	Specific heat capacity(J kg^{-1} K^{-1})			
	35°C	50°C	70°C	90°C
Ba_2PrNbO_6	460	460	470	460
Ba_2NdNbO_6	510	520	530	510
Ba_2SmNbO_6	530	560	570	540
Ba_2EuNbO_6	480	490	480	480
Ba_2GdNbO_6	430	450	450	440

The thermal diffusivity of BREnO samples was measured following the photoacoustic technique. BREnO samples of dimension 13 mm diameter and ~0.5 mm thickness were used for the thermal diffusivity studies. In the present study 488 nm radiation of an Ar ion laser (Spectra Physics model 171-17) with 500 mW power was used as the light source. The laser beam was modulated by an electromechanical chopper (Stanford Research Systems model SR 540). The photoacoustic cell used is a cylindrical, small volume, non-resonant cell made out of aluminium. The modulated laser beam was allowed to fall on the specimen kept inside the cell and the photoacoustic signals generated were detected by a sensitive microphone (Knowles 1834 having a sensitivity of 6 mV/Pa and a flat frequency response up to 3 KHz). The photoacoustic signals were processed by a digital lock-in-amplifier (Stanford Research Systems model SR 850DSP). The photoacoustic amplitude is recorded as a function of modulating frequency. The critical frequency, f_c (frequency at which a slope change is observed), corresponding to each samples were determined from the photoacoustic amplitude versus modulating frequency plot. The thermal diffusivity, α, of BREnO samples was calculated by substituting the values of f_c in the relation $\alpha = l^2 f_c$, where l is the thickness of the sample. A plot of photoacoustic amplitude versus frequency for Ba_2SmNbO_6 is shown in Fig. 3.11 as a typical example. The thermal diffusivity values of BREnO samples are given in Table 3.7.

The value of thermal conductivity (κ) of BREnO samples was calculated by substituting the values of specific heat (c), thermal diffusivity (α) and density (ρ') in the relation $\kappa = \alpha\rho' c$. The thermal diffusivity values of BREnO materials are given in Table 3.7. Melting experiments were carried out to see whether BREnO materials melts congruently by using oxy-hydrogen flame. The XRD patterns of completely melted and subsequently quenched BREnO were identical to those of sintered samples, indicating that those materials melt congruently, making single crystal growth from the melt possible.

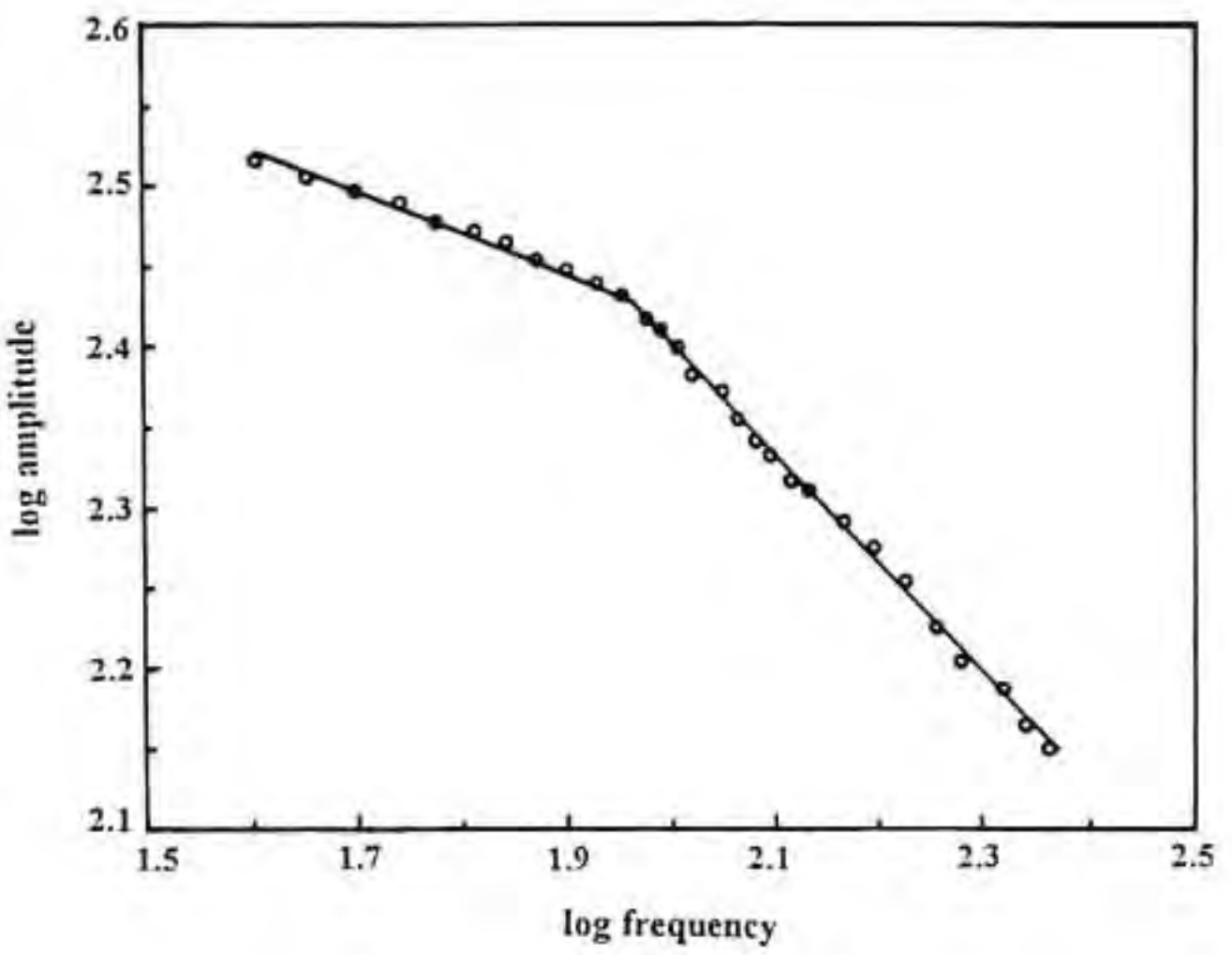

Fig. 3.11 Variation of photoacoustic amplitude with frequency for Ba_2EuNbO_6 sample at room temperature.

Table 3.7 Characteristic frequency (f_C), sample thickness (l), thermal diffusivity (α) and thermal conductivity (κ) of Ba_2RENbO_6.

Material	Characteristic frequency (Hz)	Sample thickness (cm)	Thermal diffusivity (cm^2/s)	Thermal conductivity ($Wm^{-1}K^{-1}$)
Ba_2PrNbO_6	122.18	0.044	0.236	68.72
Ba_2NdNbO_6	95.89	0.053	0.269	87.90
Ba_2SmNbO_6	506.89	0.021	0.223	77.82
Ba_2EuNbO_6	88.96	0.054	0.259	84.09
Ba_2GdNbO_6	89.12	0.053	0.250	70.00

3.8. Chemical Compatibility Studies of BRENO with YBCO

The chemical compatibility of the substrate and the film is the first and foremost criterion to be dealt with in determining the suitability of any material as substrate for HTSC films [16-17]. The high chemical reactivity of HTSC materials at the elevated processing temperature required for the preparation of films make the compatibility requirements more critical. Therefore the study of chemical reactivity of BRENO with YBCO is important in determining the suitability of BRENO as substrates for YBCO superconductor. The chemical reactivity of BRENO with YBCO was studied at temperatures up to 950°C. Superconducting YBCO powder for the chemical reactivity study was prepared following the conventional solid state route. Stoichiometric amounts of high purity (99.9%) Y_2O_3, $BaCO_3$ and CuO were weighed and thoroughly wet mixed in acetone medium and

dried. The dried mixture was calcined in air at 940°C for 48 h with three intermediate grindings. The phase purity of YBCO samples were examined by XRD and the phase pure YBCO samples were used for the chemical reactivity studies.

Superconducting YBCO powder was mixed with BRENO powder in the 1:1 volume ratio and pressed in the form of pellets. These pellets were then annealed at 950°C for 15 h and cooled slowly. If YBCO reacts with BRENO at such annealing conditions new additional phases besides YBCO and BRENO could be observed in the X-ray diffraction patterns of annealed YBCO-BRENO composites. On the other hand, if YBCO does not react with BRENO, the crystalline phases after annealing will be just two phases of YBCO and BRENO. The powder XRD patterns of annealed samples of 1:1 volume mixture of YBCO and BRENO are shown in Fig. 3.12. The XRD patterns of the two phases in the annealed samples {Fig. 12(b) to 12(f)} were compared with those of pure YBCO {Fig. 3.12(a)} and pure BRENO (Fig. 3.2). It is clear from the XRD patterns of 1:1 YBCO-BRENO composite samples {Fig. 3.12(b) to Fig. 3.12(f)} that there were no new additional phases formed, within the precision of powder XRD technique, besides YBCO and BRENO in the YBCO-BRENO composites. This indicates that there is no detectable reaction taking place between YBCO and BRENO even under severe heat treatment conditions.

The effect of addition of BRENO on the superconducting properties of YBCO was studied by temperature-resistivity measurements using standard four probe technique. A Keithley current source model 221 and

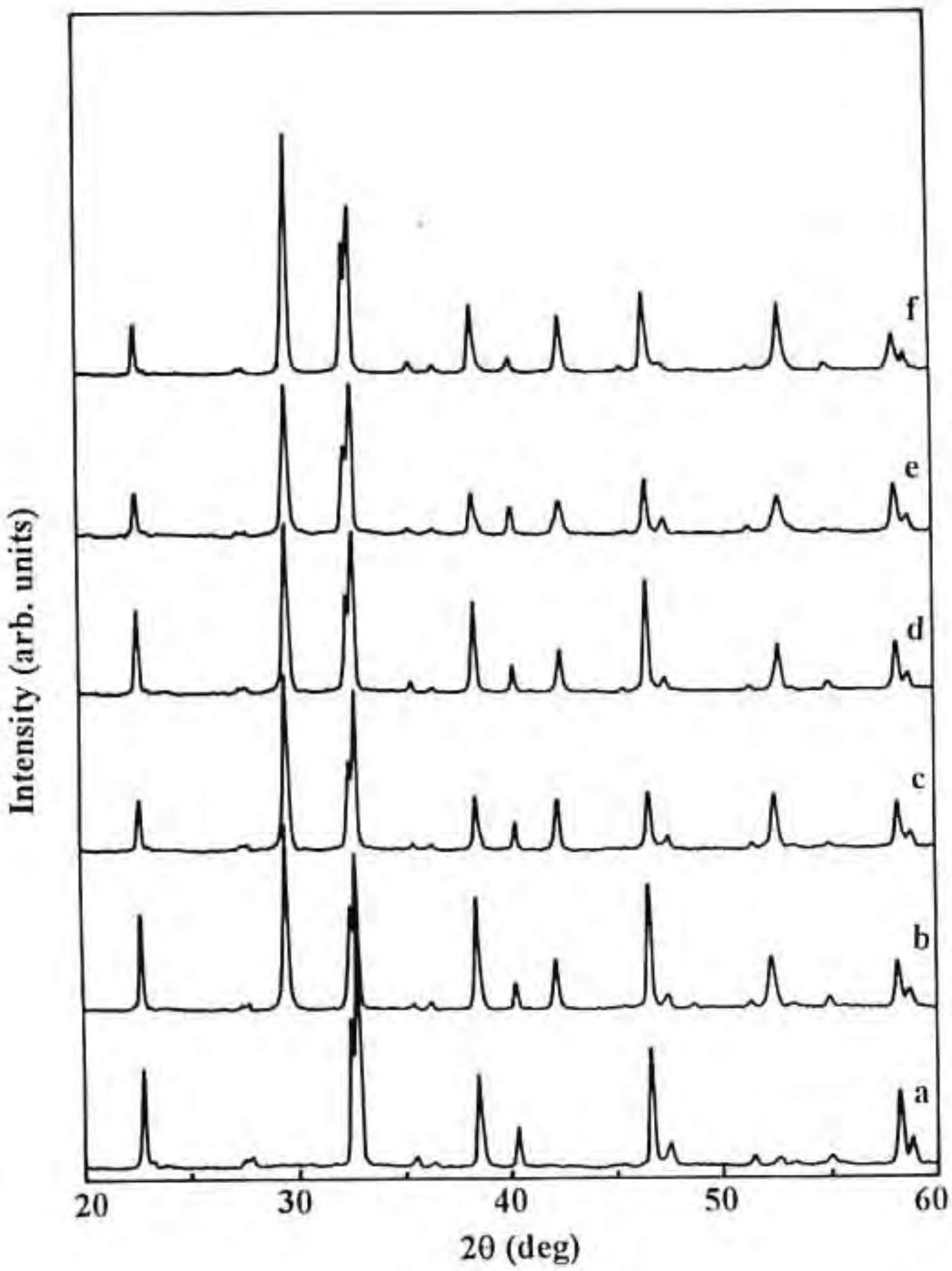

Fig. 3.12 Powder X-ray diffraction patterns of (a) pure YBCO (b) 1:1 volume mixture of YBCO and Ba_2PrNbO_6 (c) 1:1 volume mixture of YBCO and Ba_2NdNbO_6 (d) 1:1 volume mixture of YBCO and Ba_2SmNbO_6 (e) 1:1 volume mixture of YBCO and Ba_2EuNbO_6 and (f) 1:1 volume mixture of YBCO and Ba_2GdNbO_6 ; all annealed at 950°C for 15 h in air.

a Keithley nanovoltmeter model 181 were used for resistance measurements and the temperature of the samples was measured by a calibrated copper constantan thermocouple. Figure 3.13 shows the temperature versus resistivity curves for YBCO-BRENO composites containing 20 volume precent of BRENO pelletised and annealed at 950°C for 15 h.

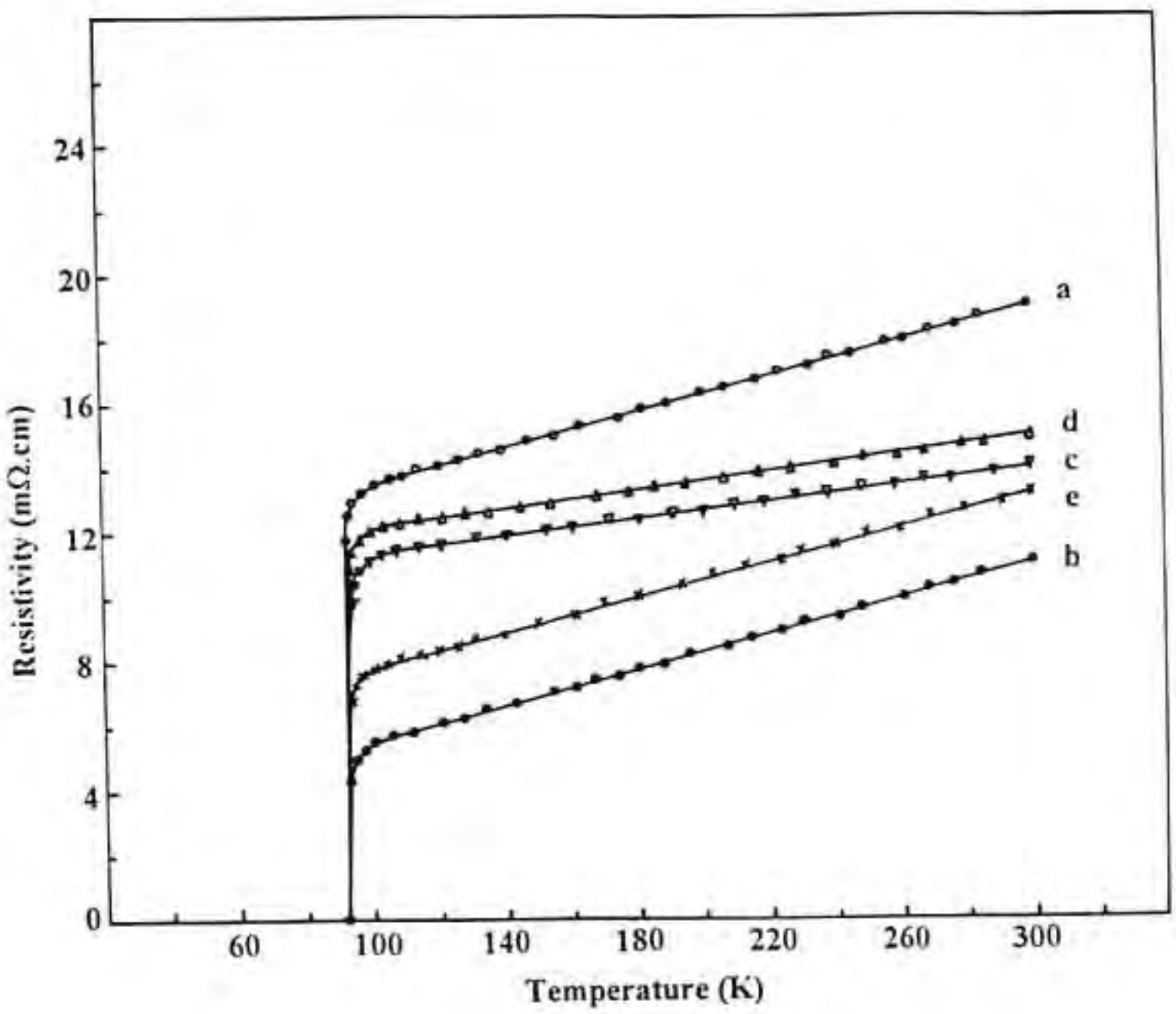

Fig. 3.13 Temperature-resistivity curves for YBCO-Ba_2RENbO_6 composites containing 20 vol% of (a) Ba_2PrNbO_6, (b) Ba_2NdNbO_6, (c) Ba_2SmNbO_6, (d) Ba_2EuNbO_6 and (e) Ba_2GdNbO_6.

Superconducting transition of 92 K was observed in all these composite samples, showing that the addition of an insulating phase BREnO in YBCO and annealing at 950°C did not have any detrimental effect on the superconducting transition temperature of YBCO even after a prolonged heat treatment at 950°C. It may be noted that an addition of even one vol% of MgO in YBCO and annealing at 900°C reduces the superconducting transition temperature of YBCO below 77 K [28-30].

3.9. Conclusion

Ba_2PrNbO_6, Ba_2NdNbO_6, Ba_2SmNbO_6, Ba_2EuNbO_6 and Ba_2GdNbO_6 were prepared and sintered as single phase materials by solid state reaction method. These materials are isostructural and have a perovskite structure with cubic symmetry and the lattice constant values are comparable with that of MgO. The dielectric constant and loss factor values of sintered BREnO materials are in a range suitable for there use as substrates for microwave applications. The thermal expansion values of BREnO are comparable to that of YBCO superconductor thereby offering a reasonable thermal expansion match with YBCO. The DTA studies reveals that there is no phase transition occurring in BREnO in the temperature range 30 to 1300°C and the thermal conductivity values comparable to that of MgO. BREnO materials melts congruently, making single crystal growth from melt possible. It is found that YBCO does not react with BREnO even at the extreme annealing conditions. Addition of BREnO up to 20 vol% in

YBCO did not show any detrimental effect on the superconducting property of YBCO as revealed by the temperature-resistivity measurements. The chemical compatibility, favourable dielectric and thermal properties of BRENO makes them potential candidates as substrate for YBCO superconductor films.

References

1. E.K. Hollmann, O.G. Vendik, A.G. Zaitsev and B.T. Melekh, Supercond. Sci. Technol., **7**, 609 (1994).
2. R.G. Humphreys, J.S. Satchell, N.G. Chew, J.A. Edwards, S.W. Goodyear, S.E. Blenkinsop, O.D. Dosser and A.G. Cullis, Supercond. Sci. Technol., **3**, 38 (1990).
3. H.J. Scheel, M. Berkowski and B. Chabot, Physica C, **185-189**, 2095 (1991)
4. J.M. Phillips, J. Appl. Phys. **79**, 1829 (1996).
5. H. Koinuma, K. Fukuda, T. Hashimoto and K. Fueki, Jpn. J. Appl. Phys., **27**, L1216 (1988).
6. I. Shih and C.X. Qiu, Processing and applications of high T_C superconductors, Edited by W.E. Mayo, (The Metallurgical Society, Inc. 1988) p.223.
7. X.M. Li, Y.T. Chou, Y.H. Hu and C.L. Booth, J. Mater. Sci., **26**, 3057 (1991).
8. X.M. Li, Y.T. Chou, Y.H. Hu and C.L. Booth, J. Mater. Sci. Lett., **9**, 669 (1990).
9. M. Naito, R.H. Hammond, B. Oh, M.R. Halin, J.W.P. Hsu, P. Rosenthal, A.F. Marshall, M.R. Beasley, T.H. Geballe and A. Kapitulnik, J. Mater. Res., **2**, 713 (1987).
10. N.P. Bansal, R.N. Simons and D.E. Farrel, Appl. Phys. Lett., **53**, 603 (1988).
12. M.F. Yan, W.W. Rhodes and P.K. Gallagher, J. Appl. Phys., **63**, 821 (1988).
13. C.T. Cheong and E. Ruckenstein, J. Mater. Res., **4**, 1 (1989).
14. N.P. Bansal, Mater. Lett. **13**, 7 (1992).
15. C.D. Brandle and V.J. Fratello, J. Mater. Res., **5**, 2160 (1990).
16. R.G. Humphreys, J.S. Satchell, N.G. Chew, J.A. Edwards, S.W. Goodyear,

S.E. Blenkinsop, O.D. Dosser and A.G. Cullis, Supercond. Sci., Technol., **3**, 38 (1990).

17. J.M. Phillips, J. Appl. Phys., **79**, 1829 (1996).
18. T.C. Shields and J.S. Abell, Supercond. Sci. Technol., **5**, 627 (1992).
19. M.J. Cima, J.S. Schneider, S.C. Paterson and W. Coblenz, Appl. Phys. Lett., **53**, 710 (1988).
20. J. Talvacchio and G.R. Wagner, Supercond. Appl. Infrared Microwave Dev., **1**, 1292 (1990).
21. H.M. O'Bryan, P.K. Gallagher, G.W. Berkstresser and C.D. Brandle, J. Mater. Res., **5**, 183 (1990).
22. A.F. Wells, Structural Inorganic Chemistry, 5th ed. Drendon, Oxford, 279 (1986).
23. X. Zhang and Q. Wang, J. Am. Ceram. Soc.,(1991), 2846 (1991).
24. Joint Committee on Powder Diffraction Standards, No. 31-137.
25. Joint Committee on Powder Diffraction Standards, No. 37-857.
26. Joint Committee on Powder Diffraction Standards, No. 14-116.
27. Joint Committee on Powder Diffraction Standards, No. 34-976.
28. H. Koinuma, K. Fukuda, T. Hashimoto and K. Fueki, Jpn. J. Appl. Phys. **27**, L1216 (1988).
29. C.T. Cheung and E. Ruckenstein, J. Mater. Res. **4**, 1 (1989).
30. L.H. Preng, T.S.Chin, K.C.Chen and C.H. Lin, Supercond. Sci. Technol., **3**, 233 (1990).

CHAPTER 4

ELECTRICAL TRANSPORT AND PERCOLATION BEHAVIOUR OF SUPERCONDUCTOR-INSULATOR COMPOSITE SYSTEM

4.1. Introduction

The study of superconducting small aggregates, clusters or particles are very important both from fundamental as well as technological point of view [1-2]. Due to the short coherence length [3-6] and large penetration depth [2,7] along with the granular nature of high T_C superconductors, it will be interesting to study the percolation and fractal properties, quantum size effects, thermal fluctuations and size effects on superconductivity. The preparation of a superconductor-insulator composite system without deteriorating the characteristic properties of the individual compounds can provide valuable information from fundamental and technological view points. Recently, there were few studies on the percolation behaviour of superconductor-noble metal composites based on electrical transport and magnetisation properties [8-12]. These studies revealed that noble metals such as silver and gold form composites with $YBa_2Cu_3O_{7-\delta}$ (YBCO) without deteriorating its characteristic properties. The percolation model equations cannot be strictly applied to such a system due to the low resistivity ratio, ρ_s/ρ_n (where ρ_s and ρ_n are the resistivities of the superconductor and normal metal respectively) of the two components, superconductor and noble metal, at room temperature. The critical exponents describing the electrical transport

properties of YBCO-Ag composites show deviations from the theoretically expected values and these deviations were shown to be due to the low resistivity ratio of a metal to superconductor compared to that of a metal to insulator [13]. Recently there are a few reports of studies, on composites consisting of high T_c superconductor powder embedded in an insulating medium, available in the literature [14-17]. The main constraint on the study of a high T_c superconductor-insulator composite system is the high chemical reactivity of high T_c superconductor (HTSC) with most of the known ceramic insulators at the elevated processing temperatures, thereby destroying the superconducting properties [2]. In the course of our studies on the development of novel ceramic substrates for HTSC superconductors, we have found that the insulating ceramic materials Ba_2RENbO_6 (BRENO) do not react with YBCO superconductor even at the extreme processing conditions (details of which are given in the previous chapter) and hence can form ideal superconductor-insulator composite systems. This chapter describes in detail the electrical transport properties and the percolation behaviour of $YBa_2Cu_3O_{7-\delta}$-Ba_2GdNbO_6 composite system based on the X-ray diffraction and electrical resistivity studies as a typical example.

4.2. Percolation Theory

The percolation model was originally proposed [18] to describe different phenomena like spreading of a fluid through a porous media, branching polymers forming a gel, migration of electrons in a solid, etc.

Because of the generality and relative simplicity, the percolation theory has found many applications ranging from physics of quarks to the extraction of oil from sand stones. Percolation theory deals with different phenomena such as clustering, criticality, diffusion, fractals, phase transitions, disordered systems, etc. It provides a quantitative and conceptual model for understanding these phenomena and gives a theoretical and statistical background to many of the physical and natural problems dealing with randomness [19].

In order to have a better understanding of the percolation theory, let us consider a regular lattice where the lattice sites have two states; either black or white [18]. A cluster is defined as a group of black sites connected by neighbour distances [20]. There is a critical point $V = V_c$ below which only finite clusters exist, but for $V > V_c$ a fraction of the black sites belong to an infinite cluster and a percolation is possible. Below the percolation threshold, $V < V_c$, there is no infinite cluster of black sites. From V_c the fraction of sites belonging to the infinite cluster grows drastically, it has a non-analytic point at V_c. This non-analyticity is a characteristic for the percolation threshold and is usually described by a power law asymptotically close to V_c.

Consider the case of a metal-insulator composite system. The resistivity of the insulator is very high when compared to that of the metal. If we add a metal to an insulator, the resistivity of the composite remains

more or less same as that of the insulator, up to a critical volume fraction of the metal in the composite. When the volume fraction of the metal in the composite increases beyond a critical value, the resistivity of the composite reduces to a value that of the metal. The critical volume fraction of the metal required in the metal-insulator composite to have a continuous network, or in other words, to have an infinite cluster is called the percolation threshold value. The electrical transport properties of the metal-insulator composite system can be described by a set of exponential relations below and above the critical volume fraction [2,18,21]. The relations are,

$$\rho = \rho_o (V_m - V_C)^{-t} \quad \text{for } V_m > V_C \tag{4.1}$$

$$\rho' = \rho_o' (V_C - V_m)^{u} \quad \text{for } V_m < V_C \tag{4.2}$$

where ρ_o and ρ_o' are constants, V_C is the critical volume fraction of the metal at which the electrical transport properties change drastically (percolation threshold), V_m is the volume fraction of the metal in the metal-insulator composites and t and u are critical exponents describing the electrical transport properties of the composite system. In the case of a perfect metal-insulator system where there is no interaction or reaction between the two components, the value of percolation threshold is ~17 vol.% of the metal in the system. The theoretically expected values of critical exponents are t ~1.7 and u ~0.7 [2].

4.3. Preparation of $YBa_2Cu_3O_{7-\delta}$–Ba_2GdNbO_6 Composites

Phase pure YBCO powder was prepared following the conventional solid state route. Stoichiometric amounts of high purity (99.9%) Y_2O_3, $BaCO_3$ and CuO were weighed and thoroughly wet mixed in an agate mortar with acetone as the wetting medium. The mixture was dried and calcined at 940°C for 48 h in air with 2 to 3 intermediate grindings. The phase purity of the YBCO powder was examined by X-ray diffraction technique. The YBCO powder was slow cooled after the final calcination. The detailed preparation procedure of the ceramic insulator Ba_2GdNbO_6 (BGNO) is given in Chapter 3. The YBCO-BGNO composites containing different vol.% of YBCO were prepared by thoroughly mixing appropriate amounts of YBCO and BGNO, taking into account the theoretical densities of YBCO (6.4 gm/cm^3) and BGNO (6.51 gm/cm^3). The thoroughly mixed YBCO-BGNO samples were pressed in the form of circular discs with 10 mm diameter and ~1.5 mm thickness with a pressure of ~300 MPa. These samples were then sintered at an optimum temperature for 12 h in air and slow cooled to room temperature. The details regarding the sintering temperature, sintered density, etc., of YBCO-BGNO composites containing different volume fraction of YBCO are given in Table 4.1.

Table 4.1 Composition of YBCO-BGNO composites and the corresponding sintering temperature and sintered densities.

Vol% of YBCO	Vol% of BGNO	Sintering temperature(°C)	Sintered density (gm/cm^3)
100	0	950	5.81
90	10	950	5.82
80	20	950	5.80
70	30	960	5.82
60	40	975	5.79
50	50	980	5.72
40	60	995	5.70
30	70	1010	5.67
20	80	1020	5.60
15	85	1030	5.60
10	90	1035	5.45

4.4. X-ray Diffraction Studies of YBCO-BGNO Composites

X-ray diffraction (XRD) studies of YBCO-BGNO composites were carried out using a Rigaku (Dmax/2C, Japan) diffractometer with Ni filtered Cu Kα radiation to examine the reaction between YBCO and BGNO compounds. Fig. 4.1 shows the powder XRD patterns of YBCO-BGNO composites containing different volume percentage of YBCO. In the XRD pattern of the YBCO-BGNO composites, the characteristic peaks corresponding to BGNO and an orthorhombic phase of YBCO are clearly visible indicating that there is no reaction taking place between YBCO and BGNO (within the precision of XRD technique) in the composite system even after severe heat treatment above 950°C. No additional peaks were

observed in the XRD pattern of the composites. Therefore, the two compounds, YBCO and BGNO, remains as a composite throughout the composition range.

4.5. Resistivity Studies of YBCO-BGNO Composites

The resistivity of YBCO-BGNO composites containing different vol.% of YBCO was studied in the temperature range 300-77 K by standard four probe technique. For superconducting samples, resistance measurements were carried out using a Keithley nanovoltmeter model 181 and a Keithley current source model 220. For the high resistance range, resistance measurements were carried out using a Keithley solid state electrometer model 602 at room temperature. The temperature of the samples were measured using a calibrated copper-constantan thermocouple.

Figure 4.2 shows the temperature versus normalised resistivity (ρ/ρ_r) of YBCO-BGNO composites containing different vol.% of YBCO. For clarity and readability, the variation of ρ/ρ_r with respect to temperature has been shown, where ρ_r is the room temperature resistivity of the sample. From the Fig. 4.2 it is clear that for low values of vol.% of BGNO (V_N) in the composites, the variation of resistivity with respect to temperature shows a metallic behaviour and gave a superconducting transition. But for higher values (>70%) of BGNO in the YBCO-BGNO composites, the composite samples showed semiconducting behaviour and did not show any superconducting transition up to 77 K. This can be due to the absence of

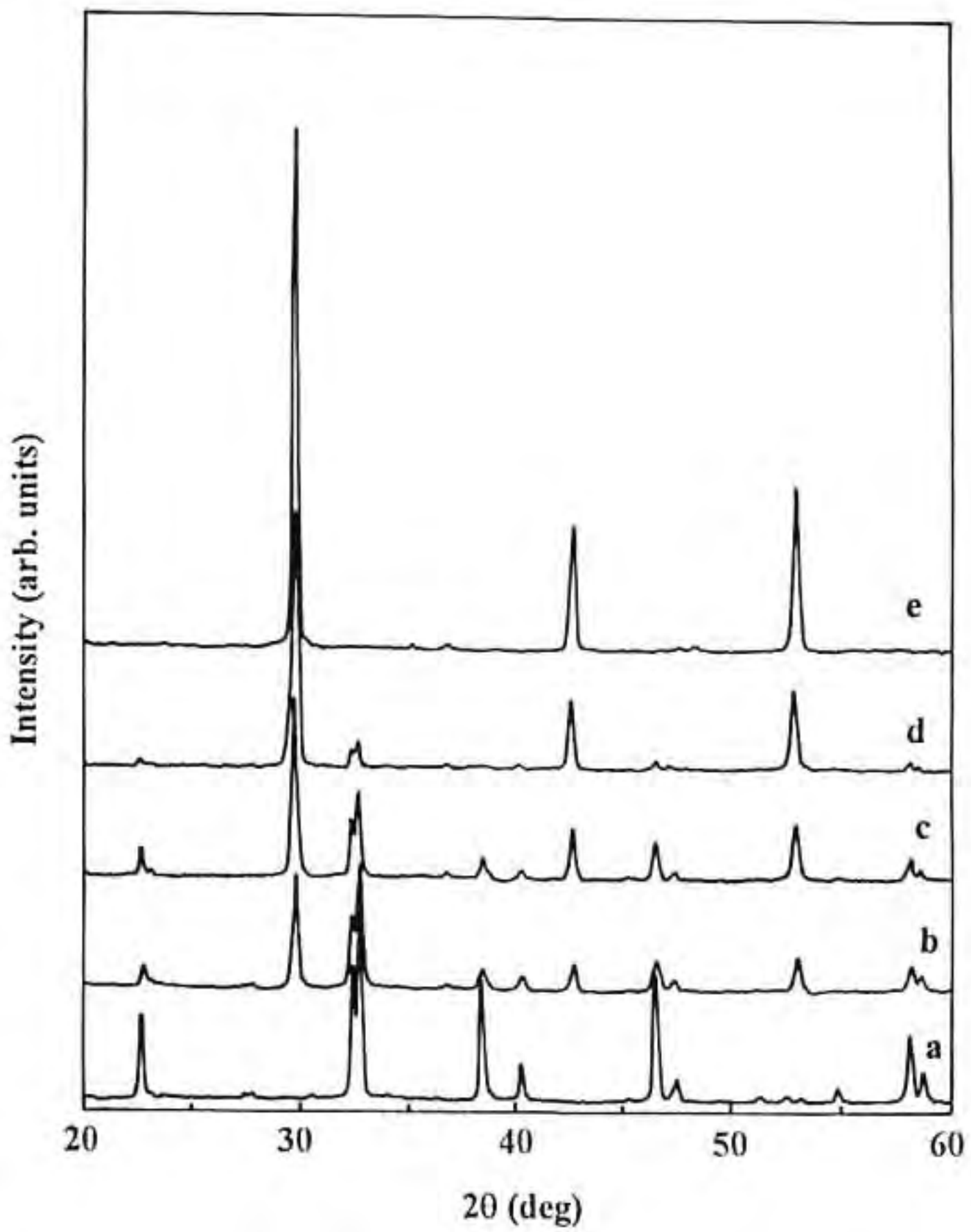

Fig. 4.1 Powder X-ray diffraction patterns of sintered YBCO-BGNO composites containing different vol% of BGNO (a) 0 % (b) 20 % (c) 40 % (d) 70 % and (e) 100%.

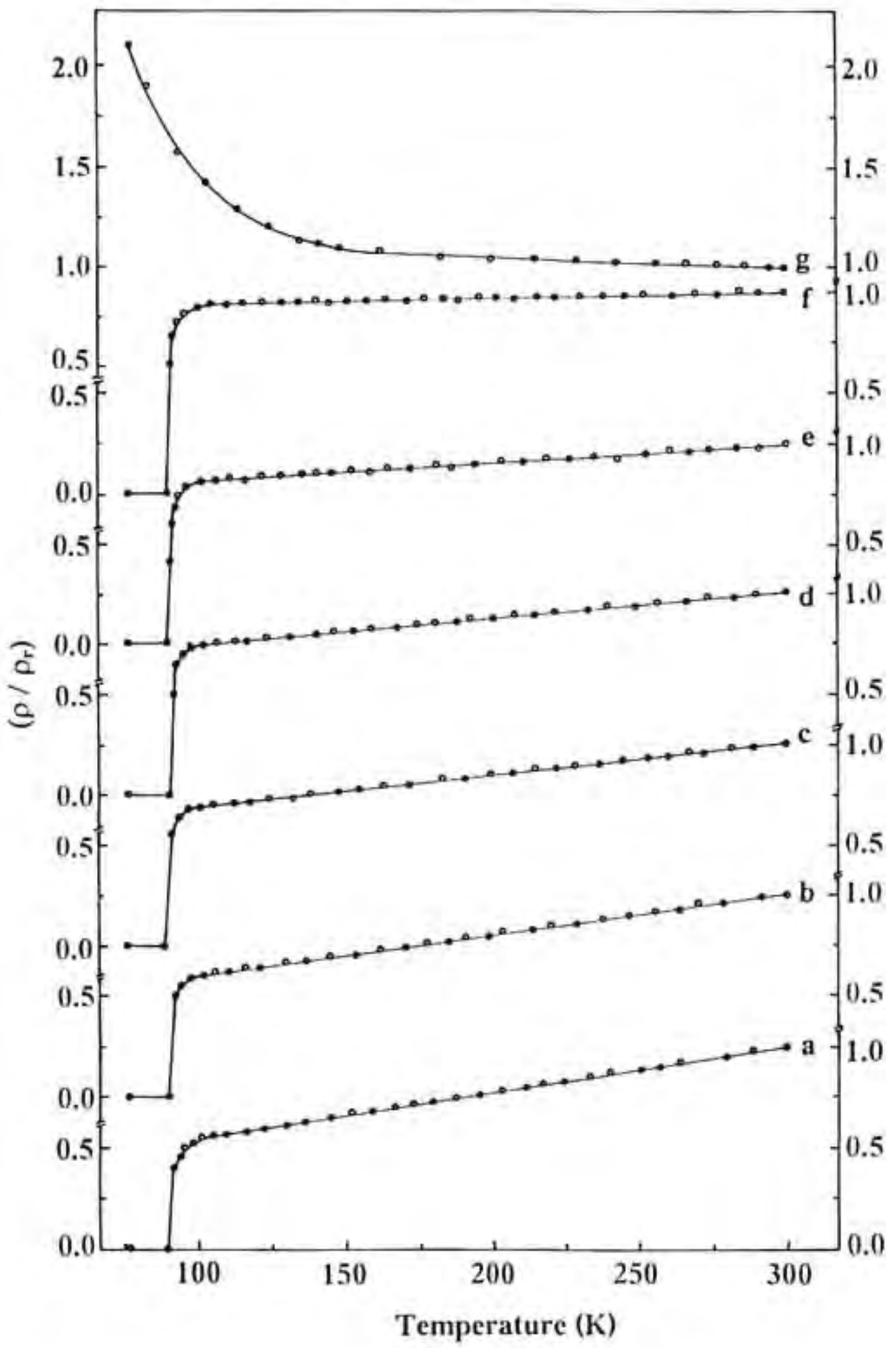

Fig. 4.2 Variation of normalised resistivity ρ/ρ_r with temperature for different vol % of BGNO in the YBCO-BGNO composites (a) 0 %, (b) 10 %, (c) 40 %, (d) 50 %, (e) 60 %, (f) 70 % and (g) 80 %.

a superconducting network through the matrix of the composite, because of the low vol.% of YBCO. Thus, the superconducting percolation threshold for YBCO-BGNO composites lies between 20 and 30 vol% of YBCO in the composite.

The variation of normal state (room temperature) resistivity (ρ) and the temperature coefficient of resistivity $\{\alpha = (1/\rho)\ (d\rho/dT)\}$ with the volume percentage of YBCO (V_s) in the YBCO-BGNO composite are shown in Fig. 4.3. In the normal state, YBCO behaves like a metallic conductor and its resistivity is nearly 13 orders of magnitude lower than that of the ceramic insulator BGNO. The normal state resistivity of YBCO-BGNO composites is dominated by YBCO with a significant drop of resistivity occurring near V_s~20 vol.%, where V_s is the vol.% of YBCO in the composite. The behaviour of ρ correlates with that of α which increases sharply towards that of YBCO for V_s ~20 vol.%. Therefore, the percolation threshold value, V_c, for the normal state transport properties of the composites is ~20 vol% of YBCO. The exact value of percolation threshold is found from the percolation model relations described in section 4.2 by considering the superconductor YBCO as a metal and the ceramic BGNO as an insulator.

The electrical transport properties of a superconductor-insulator composite system in the normal state can be represented by the relations

$$\rho = \rho_o\,(V_s - V_c)^{-t} \quad \text{for } V_s > V_c \tag{4.3}$$

$$\rho = \rho_o'(V_c - V_s)^{u} \quad \text{for } V_s < V_c \tag{4.4}$$

where V_s is the volume percentage of the superconductor in the composite,

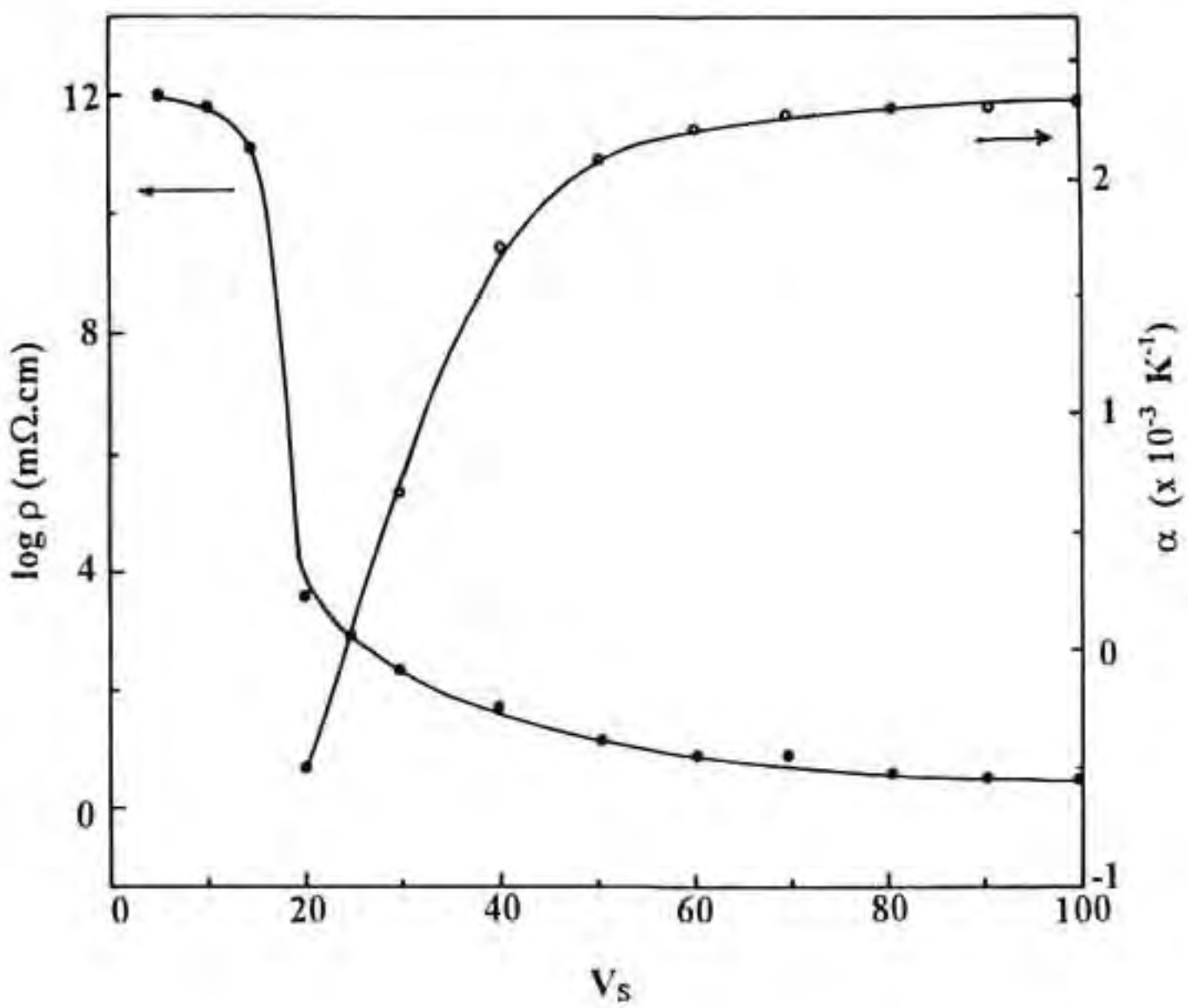

Fig. 4.3 (a) Variation of normal state resistivity (ρ), and temperature coefficient of resistivity $\{\alpha = (1/\rho)(d\rho/dT)\}$ of YBCO-BGNO composites at room temperature for different vol% of YBCO (V_s) in the composite.

ρ and ρ' are resistivity of the composites above and below the percolation threshold, V_c and t and u are critical exponents describing the transport properties of the composite system. The values of t, u, ρ_o and ρ_o' are calculated from the log-log plots of ρ versus $(V_s - V_c)$ and ρ' versus $(V_c - V_s)$

both of which gives straight lines. The exact value of V_C is taken such that the log-log plots of equations (4.3) and (4.4) gives a straight line. Figures 4.4 and 4.5 shows the log-log plots of ρ versus $(V_S - V_C)$ and ρ' versus $(V_C - V_S)$, respectively. The values of the exponents t and u were found out from Figs. 4.4 and 4.5 and are 1.65 and 0.88, respectively with a percolation threshold, $V_C = 0.17$. The values of ρ_o and ρ_o' are found to be equal to 8.318 mΩ.cm and 5.24 x 10^{12} mΩ.cm, respectively. The value of the critical exponents obtained for the YBCO-BGNO composite system agrees reasonably well with the theoretically expected values for an idealised metal-insulator percolation system.

4.6. Conclusion

Results obtained from the X-ray diffraction and resistivity studies of YBCO-BGNO composites indicate that YBCO do not react with BGNO even at the extreme annealing conditions. In the YBCO-BGNO composite system, it is found that YBCO and BGNO remains as two separate phases with their own characteristics even after the severe heat treatment conditions. The normal state percolation threshold and superconducting percolation threshold of YBCO-BGNO composite system were found to be ~17 vol.% and ~30 vol.% of YBCO in the composite system, respectively. The value of the critical exponents t and u describing the electrical transport properties of YBCO-BGNO composite system were found to be 1.65 and 0.88 respectively. The values of the constants ρ_o and ρ_o' were

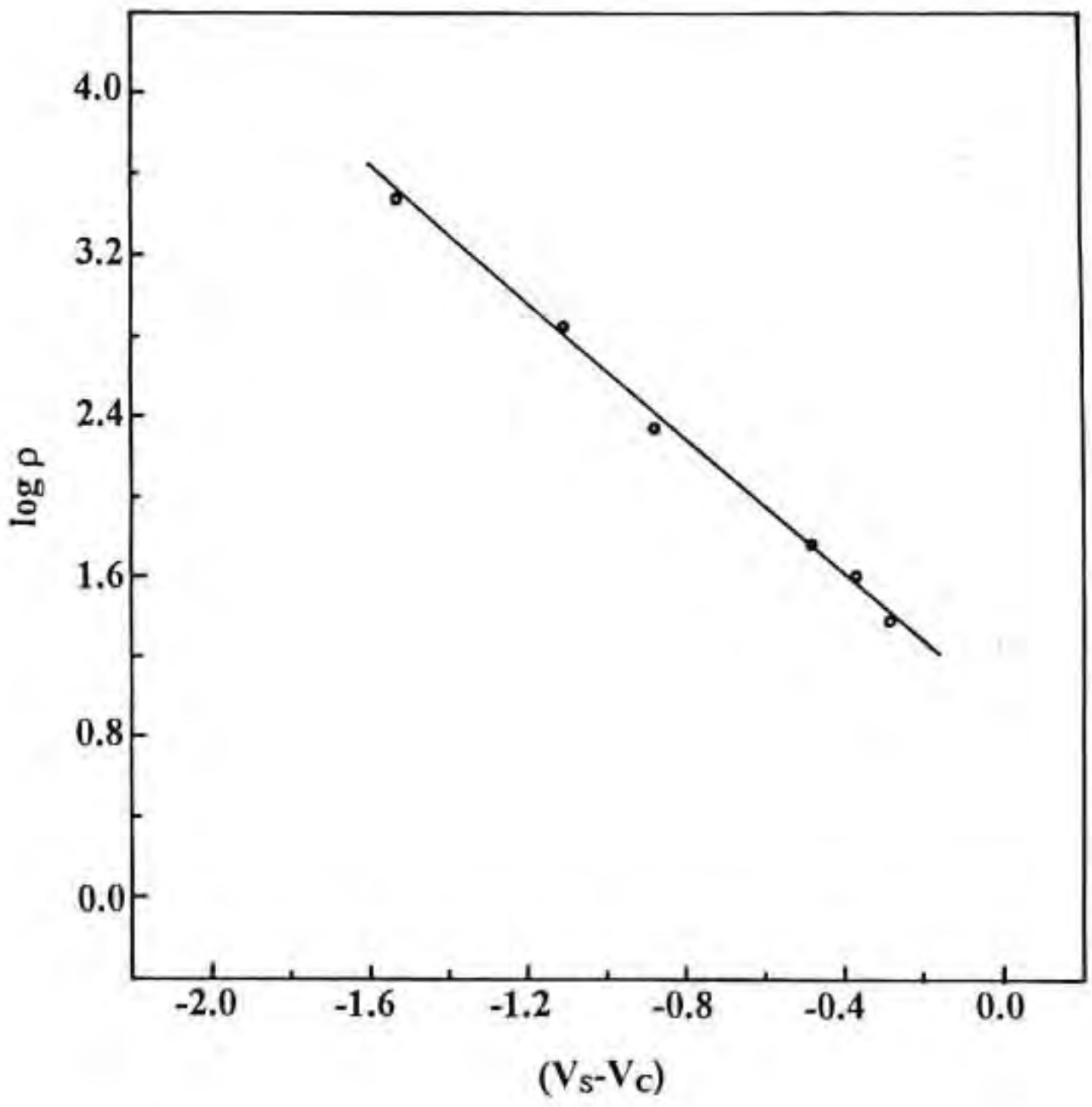

Fig. 4.4 log-log plot of resistivity ρ of the YBCO-BGNO composites versus (V_S-V_C) where V_S is the vol% of YBCO in the composite and V_C is the percolation threshold value.

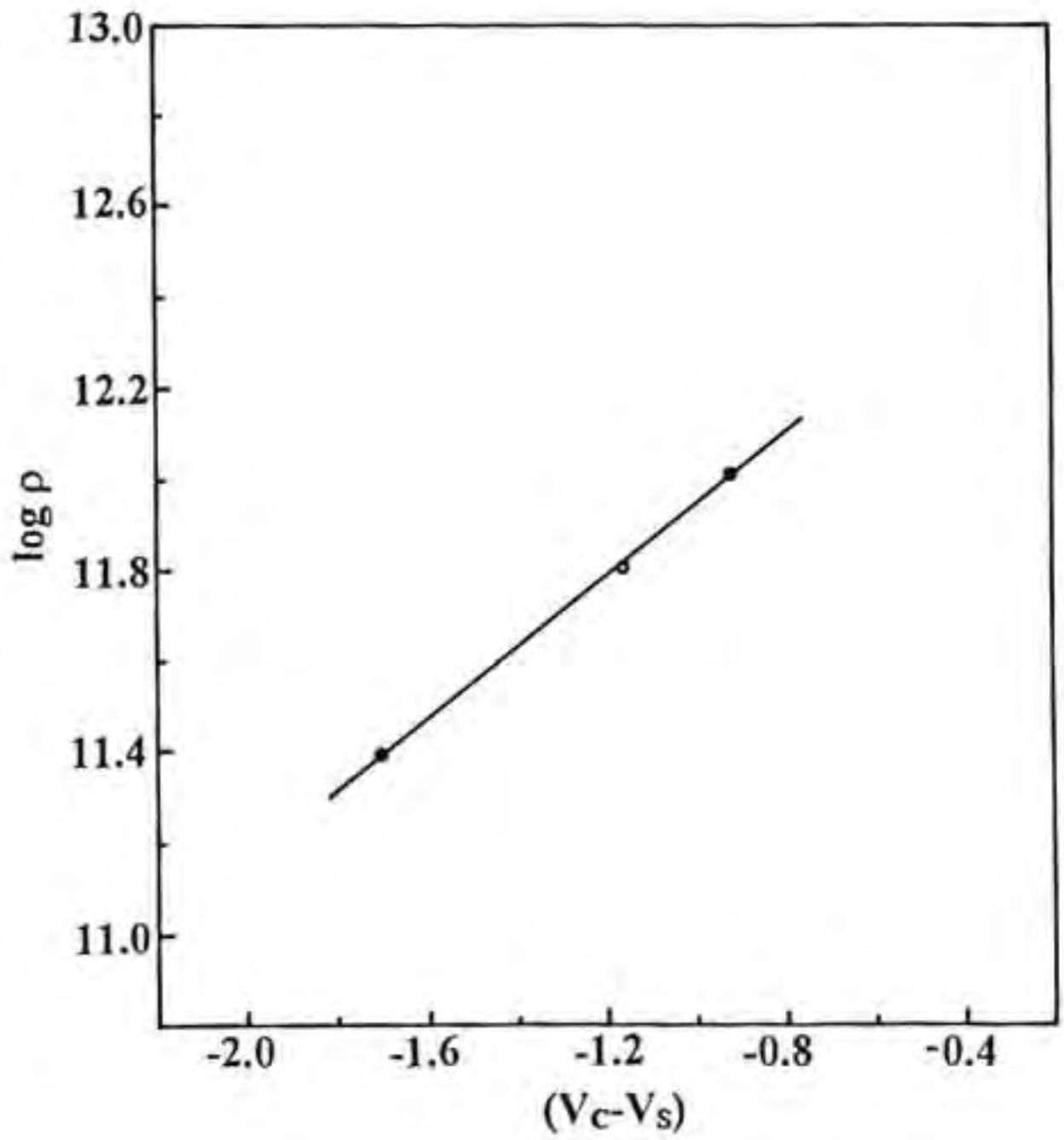

Fig. 4.5 log-log plot of resistivity ρ of the YBCO-BGNO composites versus (V_C-V_S) where V_S is the vol% of YBCO in the composite and V_C is the percolation threshold value.

8.318 mΩ.cm and 5.24 $\times 10^{12}$ mΩ.cm respectively. The normal state percolation threshold value and the critical exponents describing the transport behaviour of the YBCO-BGNO composite system match fairly well with those expected for a perfect metal-insulator composite system. The chemical non-reactivity of BGNO with YBCO even at the extreme processing conditions makes BGNO a potential substrate material for YBCO superconducting films.

References

1. G. Deutscher, Mat. Res. Soc. Symp. Proc., **195**, 303 (1990) and references therein.
2. G. Xiao, F.H. Streitz, M.Z. Cieplak, A. Bakhashai, A.Gavrin and C.L. Chien, Phys. Rev. B, **38**, 776 (1988).
3. G. Deutscher and K.A. Muller, Phys. Rev. Lett., **59**, 1745 (1987).
4. T.K. Worthington, W.J. Gallagher and T.R. Dinger, Phys. Rev. Lett. **59**, 1160 (1987).
5. G. Geutscher, Highlights in Condensed Matter Physics and Future Prospects, Ed. L.Esaki, Plenum Press, 399 (1991).
6. G. Deutscher, Physics and Material Science of High Temperature Superconductors, Eds. R. Kosswsky et al., Kluwer Academic Publishers, 19 (1990).
7. D.R. Harshman, G.Aeppli, E.J. Ansaldo, B.Batlogg, J.H. Brewar, J.F. Arolan, R.J. Cava, M. Celio, A.C.D. Chaklader, W.H. Hardy, S.R. Kreitzman, G.M. Luke, D.R. Noakes and M. Sneba, Phys. Rev. B., **36**, 2386 (1987).
8. L. Ganapathi, A. Kumar and J. Narayanan, J. Appl. Phys., **66**, 5935 (1989).
9. B. Ropers, R. Cannet, F. Carmona and S. Flandrois, Solid State Commun. **75**, 791 (1990).
10. T. Nisho, Y. Itoh, F. Ogasawa, M. Suganuma, Y. Yamada and V. Mizutani, J. Mater. Sci., **24**, 3228 (1988).
11. A. Goyal, S.J. Burns and P.D. Funkenbusch, Physica C, **168**, 405 (1990).
12. P.U. Muralidharan, K.V. Paulose, J. Koshy and A.D. Damodaran, J. Am. Ceram. Soc. **74**, 2679 (1991).
13. J.J. Lin, Phys. Rev. B., **44**, 789 (1991).

14. J. Koshy, K.V. Paulose, M.K. Jayaraj and A.D. Damodaran, Phys. Rev. B., **47**, 15304 (1993).

15. J. Koshy, K.S. Kumar, J. Kurian, Y.P. Yadava and A.D. Damodaran, Phys. Rev. B., **51**, 9096 (1995).

16. M. Golosvosky, M. Tsindlekht and D. Davidov, Phys. Rev. B., **46**, 11439 (1992).

17. K.V. Paulose, Ph. D thesis, Cochin University of science and Technology, 1992.

18. J. Kerteszi and T. Vicsek, Sintering theory and Practice, Eds. D. Kolar et al., Elsevier Scientific, 53 (1982).

19. D. Stauffer and A. Ahrarony, Introduction to Percolation Theory, 2nd edition, Taylor and Francis, 1992.

20. G. Deutscher, Applications of percolation, eds. J. Souletie, J. Vannimenus and R. Stora, Elsevier Science Publishers B.V, 1987.

21. D. Stauffer, Phys. Rep., **54**, 1 (1979).

CHAPTER 5

PREPARATION AND CHARACTERISATION OF YBCO AND YBCO-Ag THICK FILMS ON Ba_2RENbO_6 (RE = Pr, Nd, Sm, Eu and Gd) SUBSTRATES

5.1. Introduction

The preparation of high quality copper oxide superconductor films is of crucial importance both from fundamental and technological view points. Thick films of high T_C superconductors are of interest for many applications such as magnetic shielding, substrate wiring, various high speed microelectronic devices and microwave electronic circuits [1-6]. The particular advantages of the thick film route are the simplicity and the low cost of the process, and the ability to apply the coating on curved surfaces and on large areas [7-8]. For the preparation of $YBa_2Cu_3O_{7-\delta}$ (YBCO) thick films, different techniques like screen-printing, dip-coating, spin-coating, spray-pyrolysis, paint-on-method, etc. are used. For the successful preparation of superconductor thick films, the selection of suitable substrate material and the optimisation of the processing conditions are crucial [1,9-10]. The state of art of YBCO thick films is described in detail in chapter 1. It is found from our detailed studies on percolation behaviour of YBCO with Ba_2RENbO_6 (BRENO) that BRENO are chemically non-reacting with YBCO superconductor even under severe heat treatment conditions which is the most important criterion for the selection of a material as substrate for YBCO superconductor films. In

dielectric properties, thermal expansion match, thermodynamical stability, etc. We have successfully prepared superconducting YBCO thick films with $T_c(0) = 92$ K and high critical current density on BRENO☆ substrates by both screen-printing and dip-coating techniques. The details of preparation of YBCO and YBCO-Ag thick films on BRENO and their characterisation are described in the following sections of this chapter.

5.2. Preparation of YBCO Thick Films on BRENO

In the present study, YBCO thick films were prepared on polycrystalline BRENO substrates by screen-printing and dip-coating techniques. Screen printing technique has the advantage over other thick film techniques that desired circuit patterns can be directly printed on to the substrate, thereby avoiding the etching and photolithographic steps. On the other hand, dip-coating technique is relatively simpler and films can be prepared on curved or non-planar surfaces and also thinner films (~2 μm) can be obtained. Even though the initial coating techniques is different for screen printing and dip-coating, both requires careful and controlled processing at high temperatures for obtaining a well adhered superconducting YBCO film.

For the preparation of YBCO thick films on BRENO by screen printing, a thick film ink of YBCO was prepared by thoroughly mixing fine YBCO powder with appropriate amount of isopropyl alcohol or

☆ Published in *Physica C*, **215**, 209 (1993) and *Materials Letters*, **17**, 393 (1993)

n-butanol. The viscosity of the ink was controlled by the addition of commercially available fish oil. This ink was then printed on to a polished and cleaned BRENO substrate using a screen of 325 mesh size. The printed films were then dried in a hot air oven at 150°C for 2 h and subjected to controlled heat treatment in a programmable furnace. In the case of dip-coating, a suspension of YBCO was prepared by thoroughly mixing fine YBCO powder with appropriate amount of isopropyl alcohol or n-butanol. Here also the viscosity of the suspension was controlled by the addition of commercially available fish oil. The well polished and cleaned BRENO substrate was then dipped in the YBCO suspension and was allowed to dry. This step was repeated till a required thickness is attained. The dip coated YBCO thick films were dried in a hot air oven and subjected to controlled heat treatment as in the case of screen printed films.

As mentioned earlier, for the successful preparation of superconducting YBCO thick films, the optimisation and close control of the heat treatment conditions are essential. In the present study, for the preparation of YBCO thick films on polycrystalline BRENO, the optimised processing conditions are as follows. The dried YBCO thick films on BRENO substrates were heated in a programmable furnace at a rate of 5°C/min up to 1000°C and annealed at that temperature for ~2 min. The films were cooled from 1000°C at a rate of 2°C/min up to 940°C and were annealed at 940°C for 30 to 60 min. The films were then slow cooled to

room temperature at a rate of 1°C/min. The diagrammatic representation of heating and cooling schedule adopted for the preparation of superconducting YBCO thick films on BREnO is shown in Fig. 5.1. The

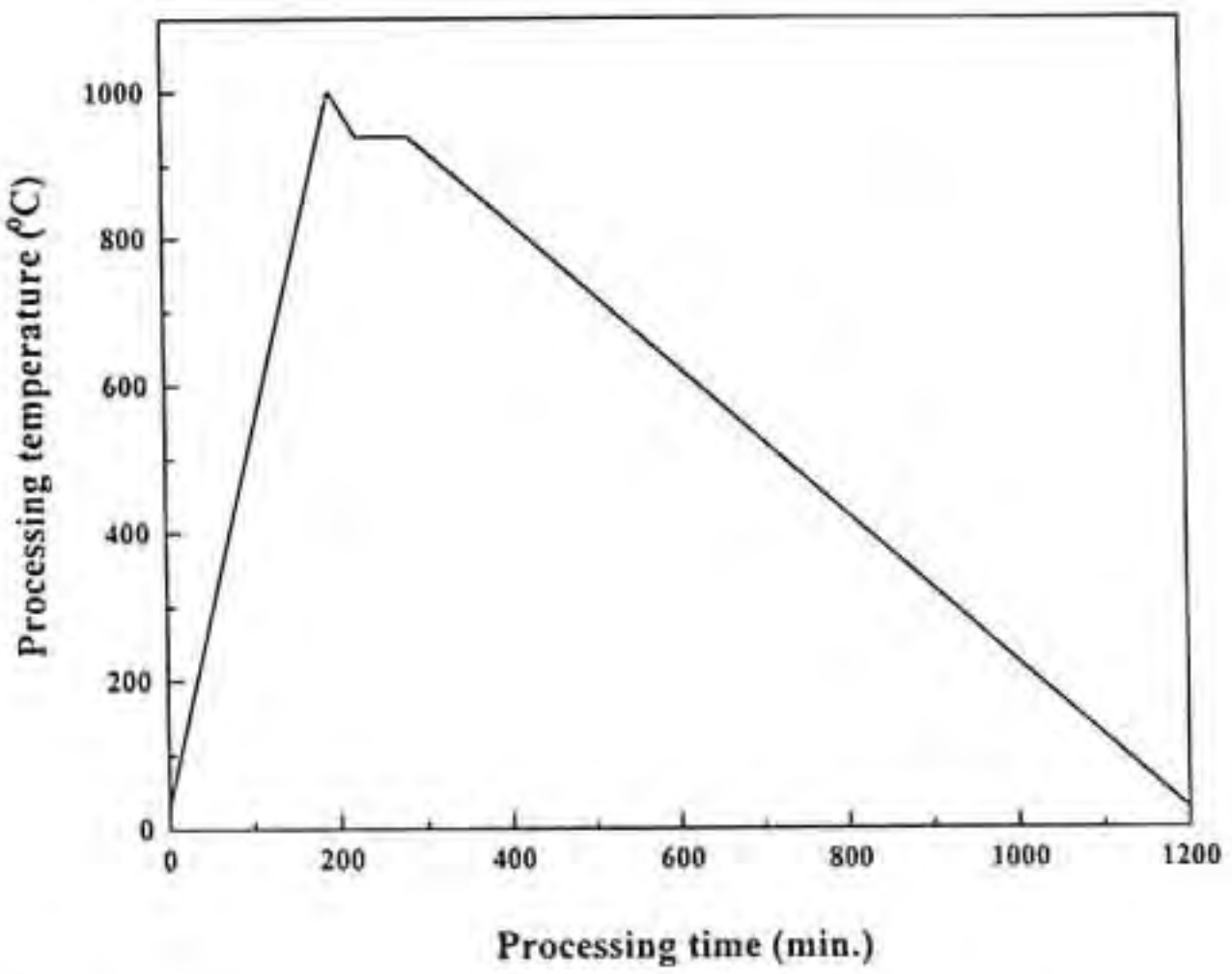

Fig. 5.1 Heating and cooling schedule for the preparation of YBCO thick films on Ba_2REnbO_6 substrates.

heating of the YBCO films up to the partial melting temperature of YBCO (1000°C) was necessary to get good adherence of YBCO film to the substrate and also for obtaining highly textured films with smooth surfaces. The slow cooling procedure adopted was essential to facilitate oxygenation. Also it has been found that the annealing temperature close to the melting point of YBCO phase and relatively short annealing time enhanced the c-axis orientation of YBCO films. The screen printed YBC(

thick films had thickness of about 10 to 30 μm, whereas the dip-coated films had thickness in the range 2 to 4 μm. In all the cases the film surface looked black and the peal off test carried out using an adhesive tape showed that the film on BRENO had good adhesion to the substrate.

5.3. Characterisation of YBCO Thick Film on BRENO

The structure and the surface morphology of YBCO thick films prepared on BRENO substrates by screen printing and dip-coating were characterised by X-ray diffraction and scanning electron microscopy. The superconductivity of the films was studied by temperature-resistivity and critical current density measurements. The X-ray diffraction (XRD) patterns of YBCO thick films on BRENO are given in Fig. 5.2. It is clear

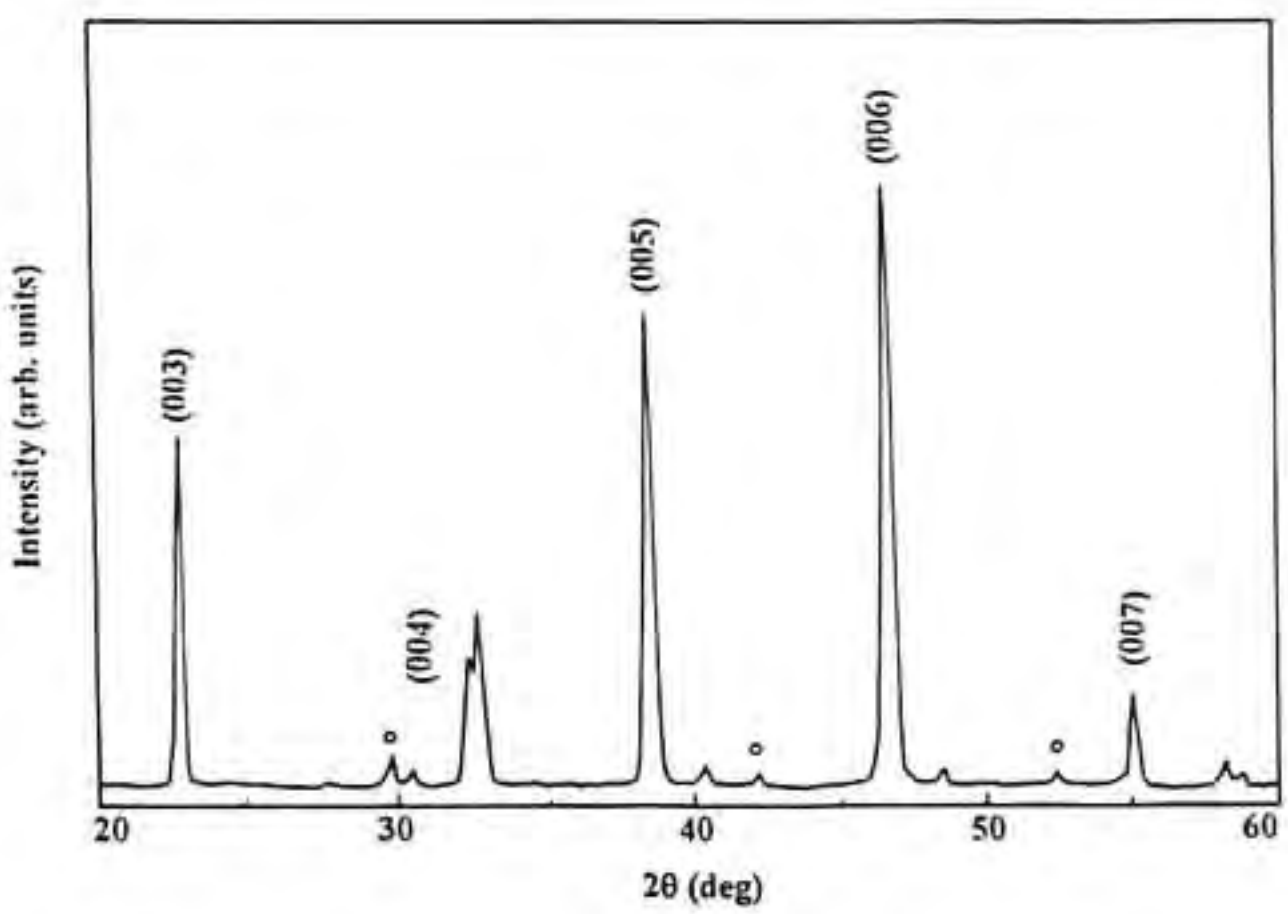

Fig. 5.2(a) XRD pattern of Screen printed YBCO film on Ba_2PrNbO_6. The substrate peaks are marked by 'o'.

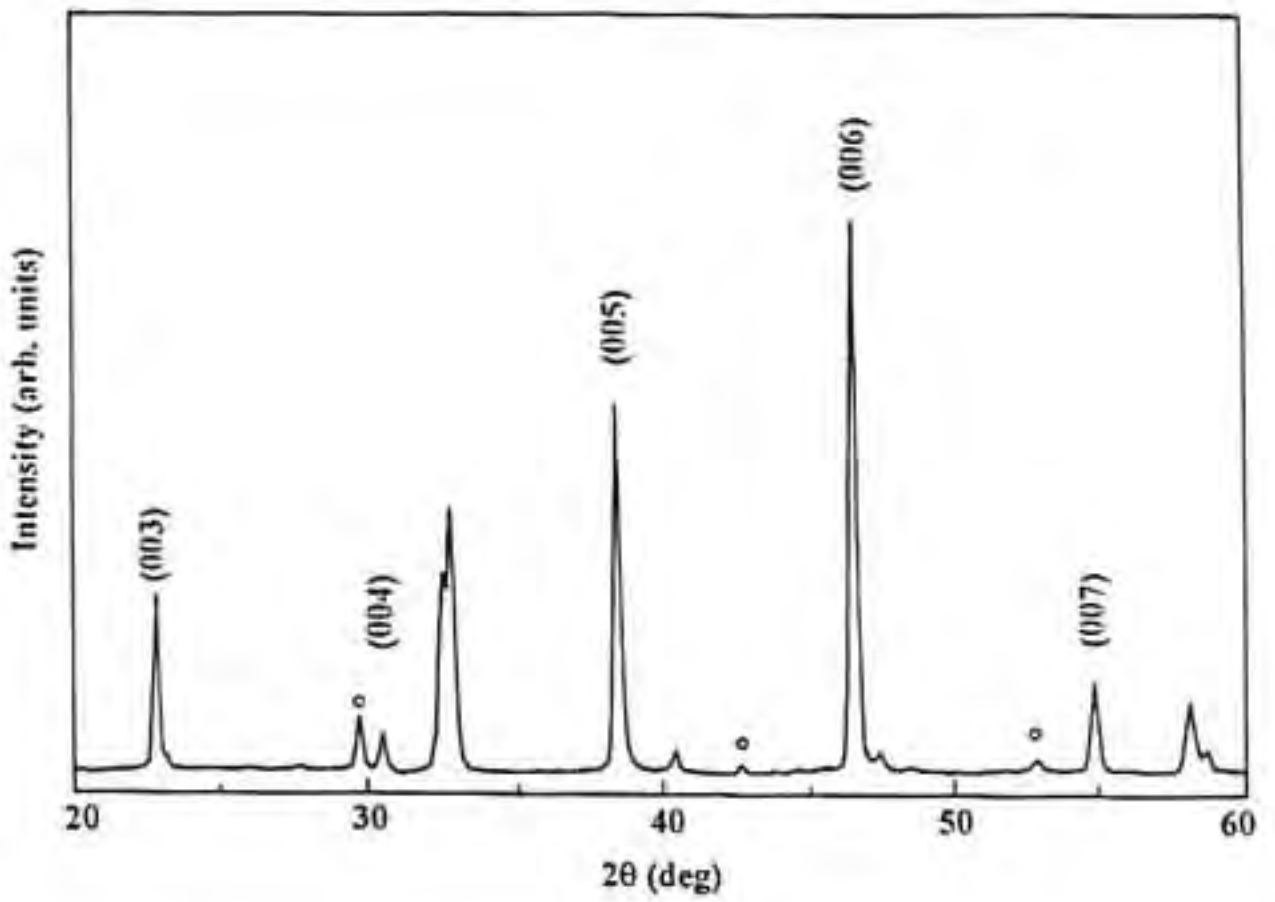

Fig. 5.2(b) XRD pattern of Screen printed YBCO film on Ba_2NdNbO_6. The substrate peaks are marked by 'o'.

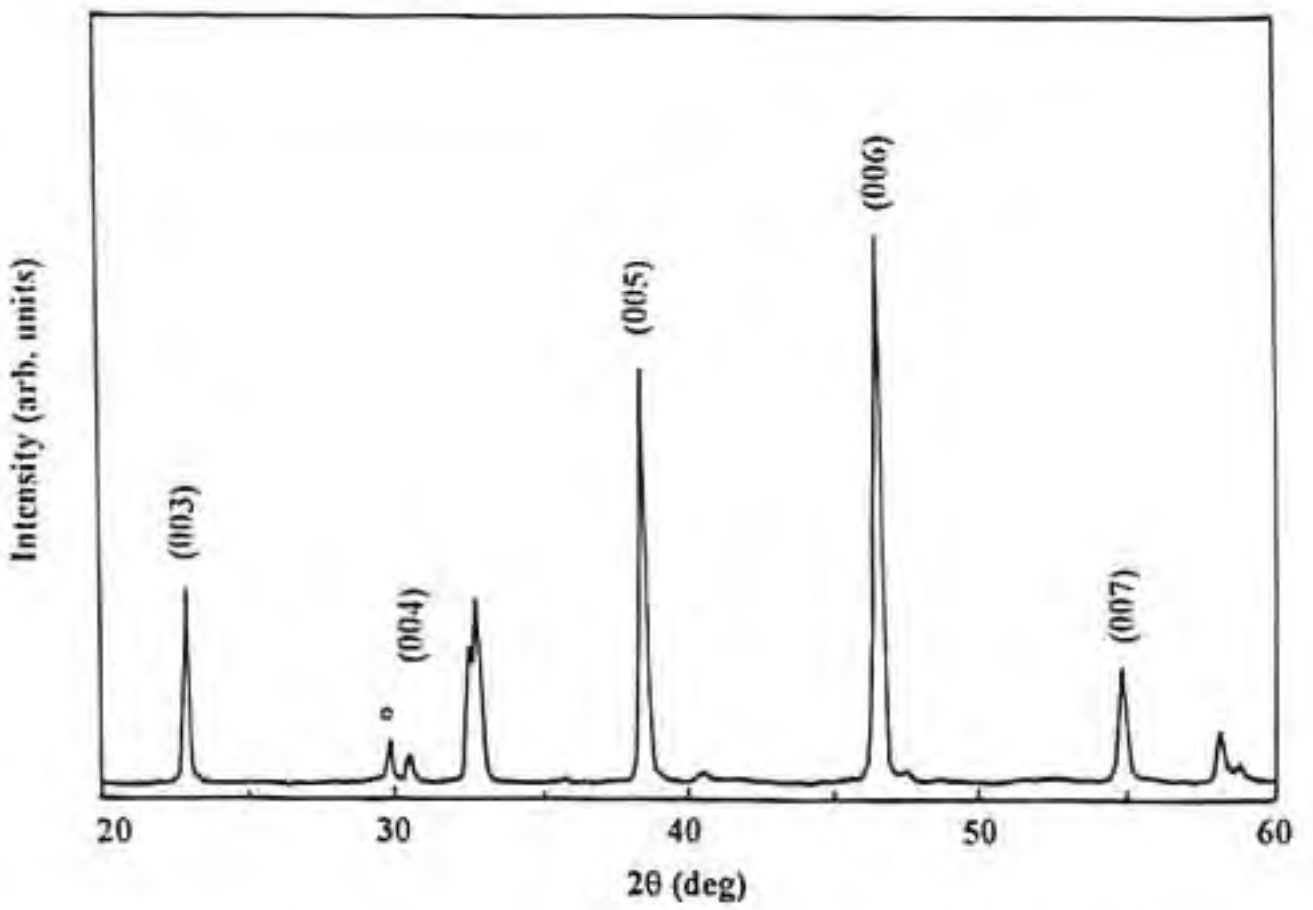

Fig. 5.2(c) XRD pattern of Screen printed YBCO film on Ba_2SmNbO_6. The substrate peaks are marked by 'o'.

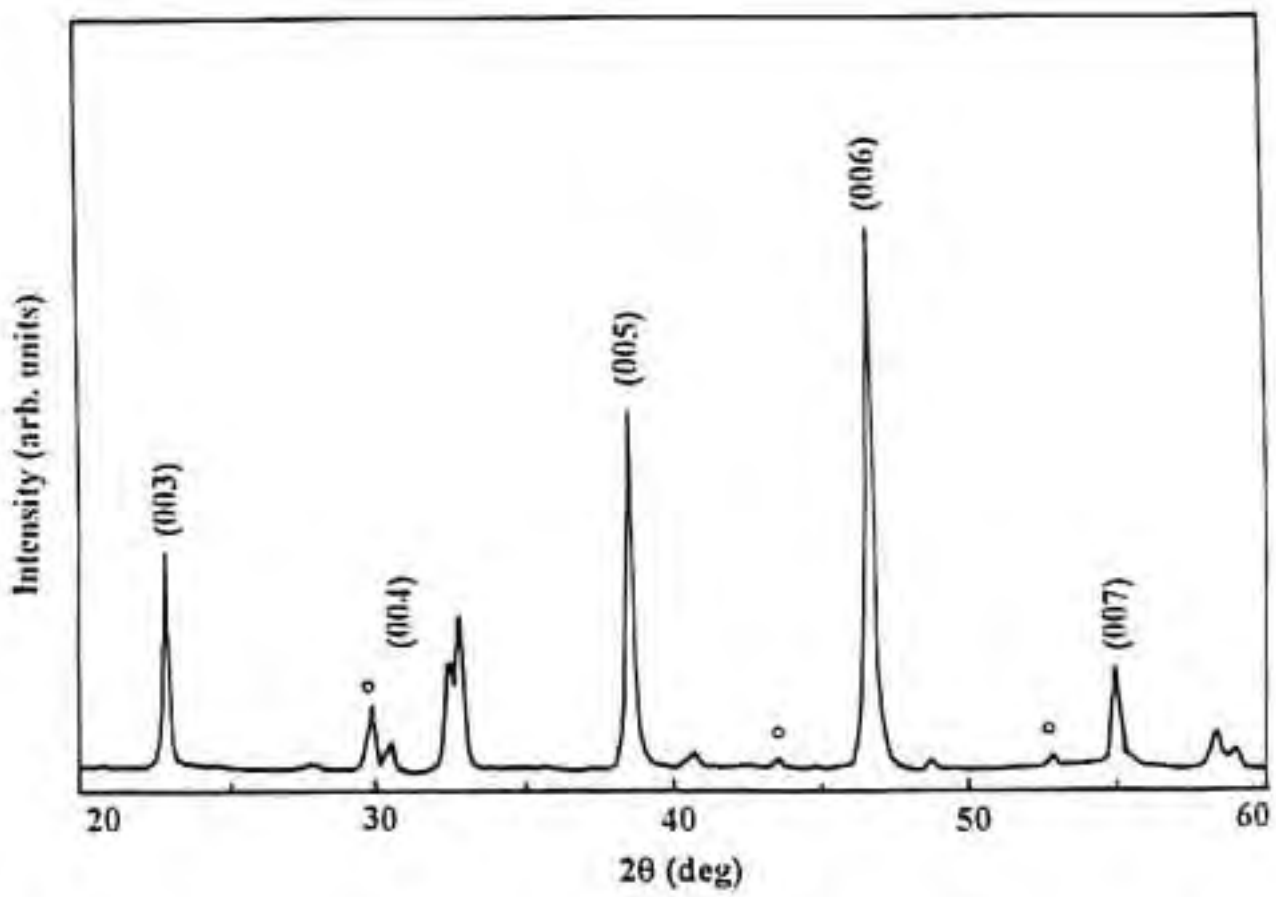

Fig. 5.2(d) XRD pattern of Screen printed YBCO film on Ba_2EuNbO_6. The substrate peaks are marked by 'o'.

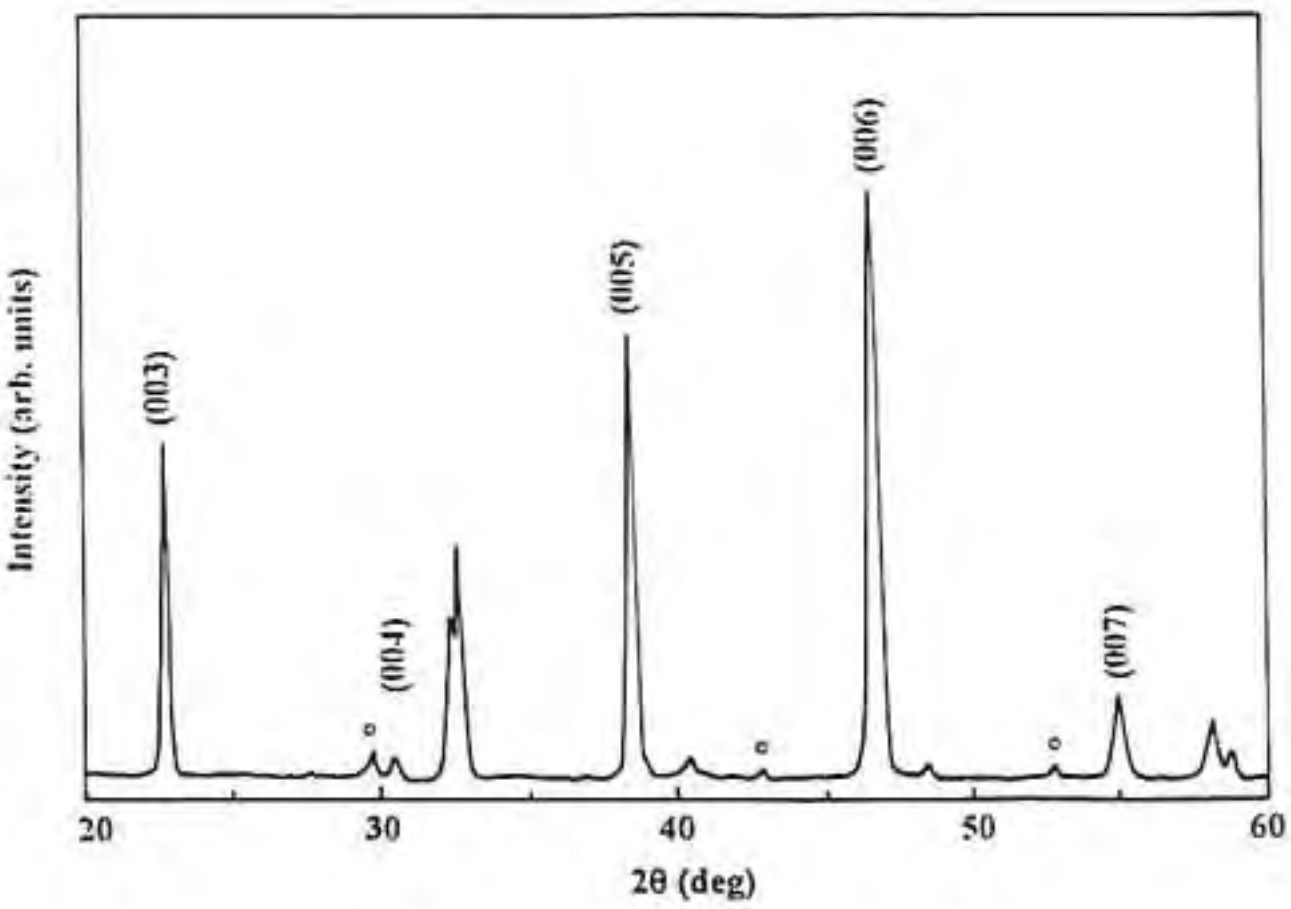

Fig. 5.2(e) XRD pattern of screen printed YBCO film on Ba_2GdNbO_6. The substrate peaks are marked by 'o'.

from Fig.5.2 that except for the characteristic peaks of BRENO, all the other peaks are those of the orthorhombic YBCO superconductor. The intensities of the (00*l*) reflection of YBCO superconductor indicates that the film is highly textured with respect to the ordering of the crystallographic c-axis. The absence of any other peaks other than that of BRENO and YBCO indicate that there is no detectable chemical reaction between YBCO and BRENO even at the partial melting temperature of YBCO. The high degree of c-axis texturing observed in the XRD patterns of YBCO films on BRENO are due to the partial melt processing method adopted.

The surface morphology and film-substrate interface of YBCO thick films on BRENO were examined by scanning electron microscope (SEM). The surface SEM micrographs of YBCO thick films on BRENO are shown in Fig. 5.3. It is evident from the SEM micrographs that the YBCO films on BRENO substrates have smooth and dense surface and large grains. This type of microstructure is associated with a high degree of preferred orientation of the film, with the c-axis perpendicular to the plane of the substrate [7]. The SEM micrographs did not show any indication of other secondary phases like Y_2BaCuO_5 and also the existence of microcracks. The cross-sectional SEM micrographs of YBCO thick films on BRENO are shown in Fig. 5.4. It is evident from Fig. 5.4 that there is no detectable chemical reaction between the film and the substrate at the film-substrate interface.

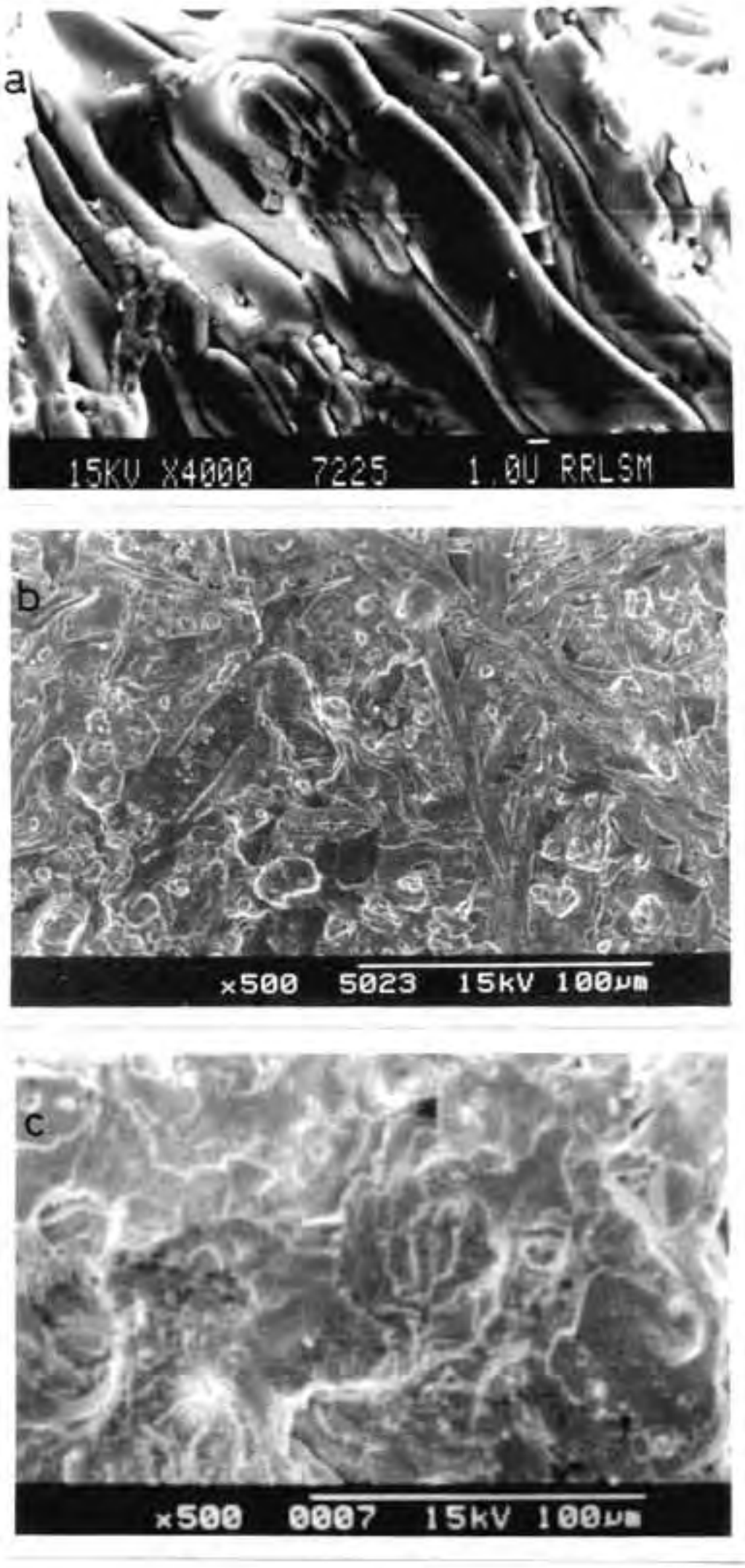

Fig. 5.3 Surface SEM micrograph of YBCO thick film on (a) Ba_2PrNbO_6, (b) Ba_2EuNbO_6 and (c) Ba_2GdNbO_6 substrates.

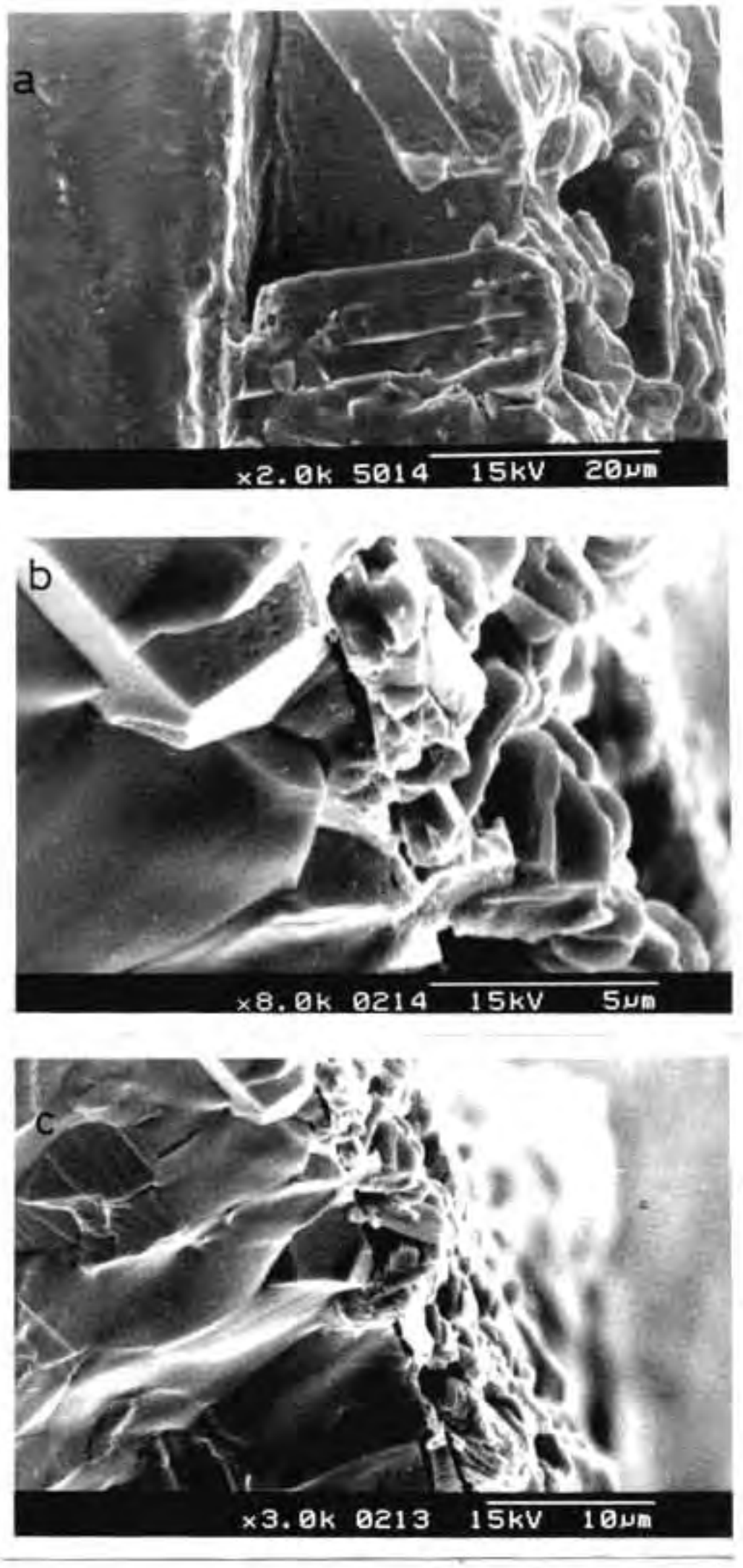

Fig. 5.4 Crosssectional SEM micrograph of YBCO thick film on (a) screen printed on Ba_2PrNbO_6, (b) dip-coated on Ba_2EuNbO_6 and (c) dip-coated on Ba_2GdNbO_6 substrates.

The superconductivity of the YBCO thick films prepared on BRENO was studied by standard four probe technique. A Kiethley current source model 220 and a Keithley nanovoltmeter model 181 were used for the resistance measurements. The temperature of the films were measured by a copper-constantan thermocouple with an accuracy of ±0.2 K. The temperature-resistance curves of YBCO thick films on BRENO are shown in Fig. 5.5. The YBCO films showed a metallic behaviour in the normal state and gave a zero resistance transition at 92 K with a transition width of ~2 K. The critical current density (J_c) of the films at 77 K and zero magnetic field were ~10^4 A/cm^2. The values of T_c, J_c and ΔT obtained for YBCO thick films on BRENO substrates are summarised in Table 5.1.

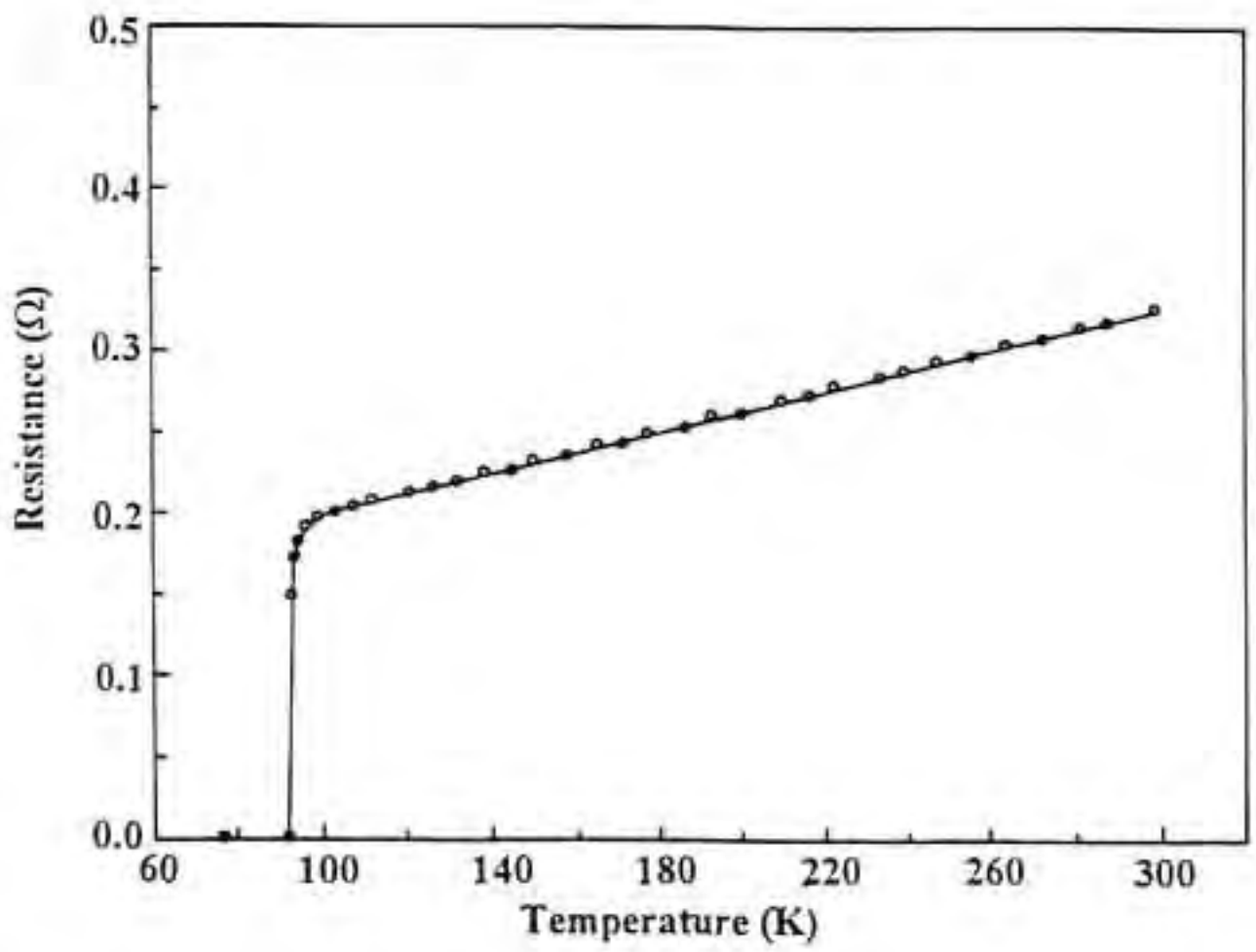

Fig. 5.5(a) Temperature-resistance curve of screen printed YBCO film on Ba_2PrNbO_6 substrate.

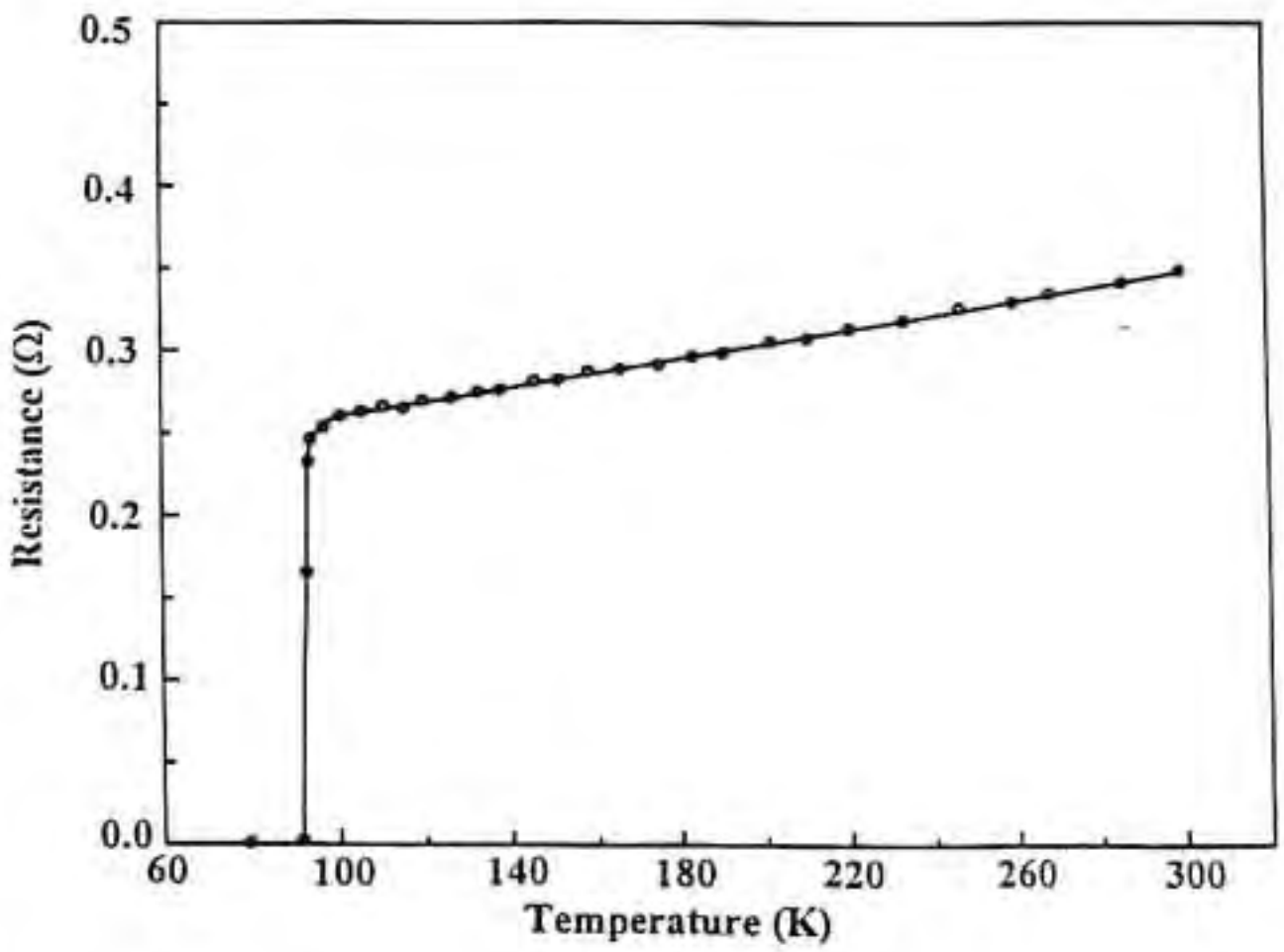

Fig. 5.5(b) Temperature-resistance curve of screen printed YBCO film on Ba_2NdNbO_6 substrate.

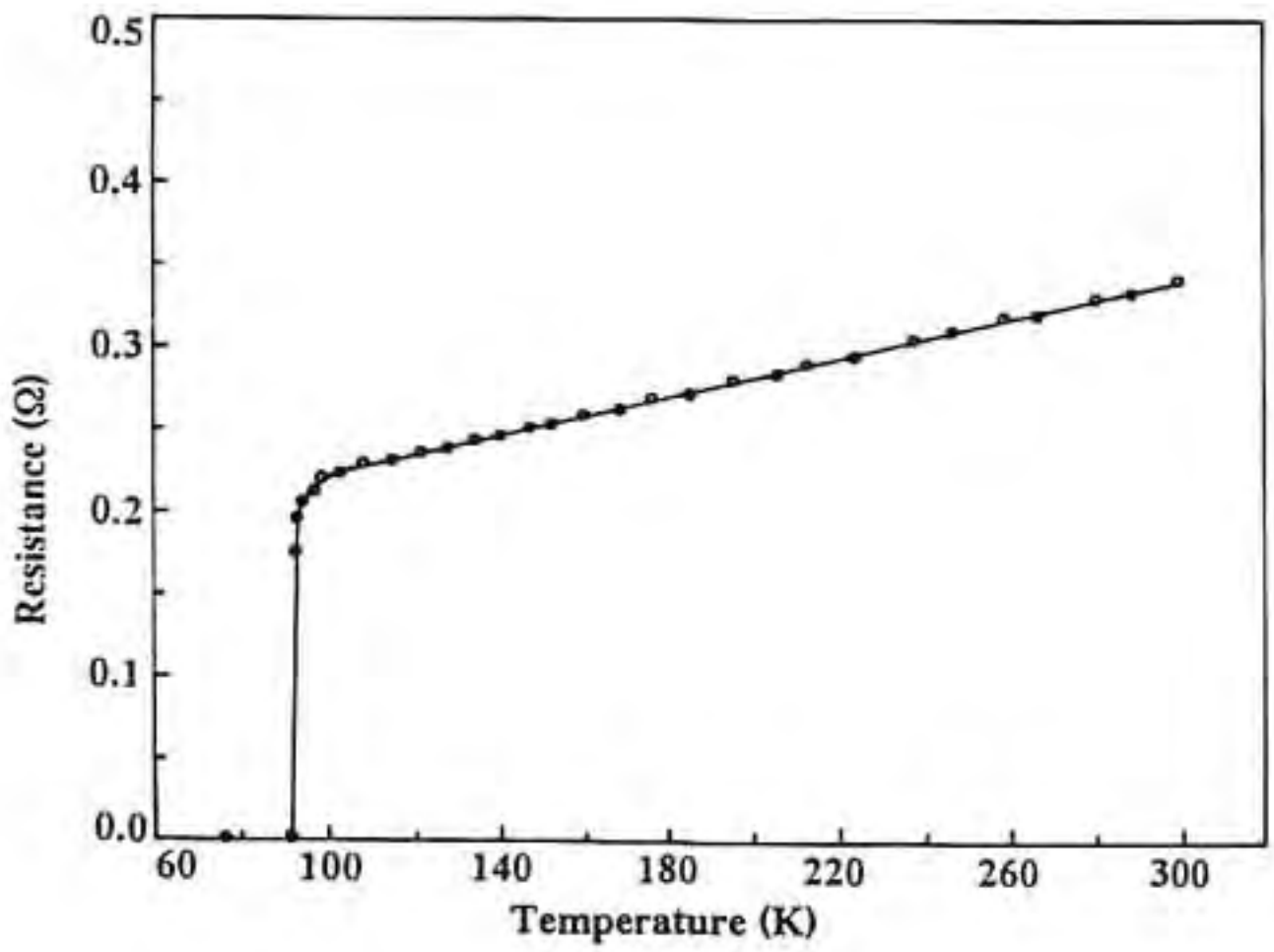

Fig. 5.5(c) Temperature-resistance curve of screen printed YBCO film on Ba_2SmNbO_6 substrate.

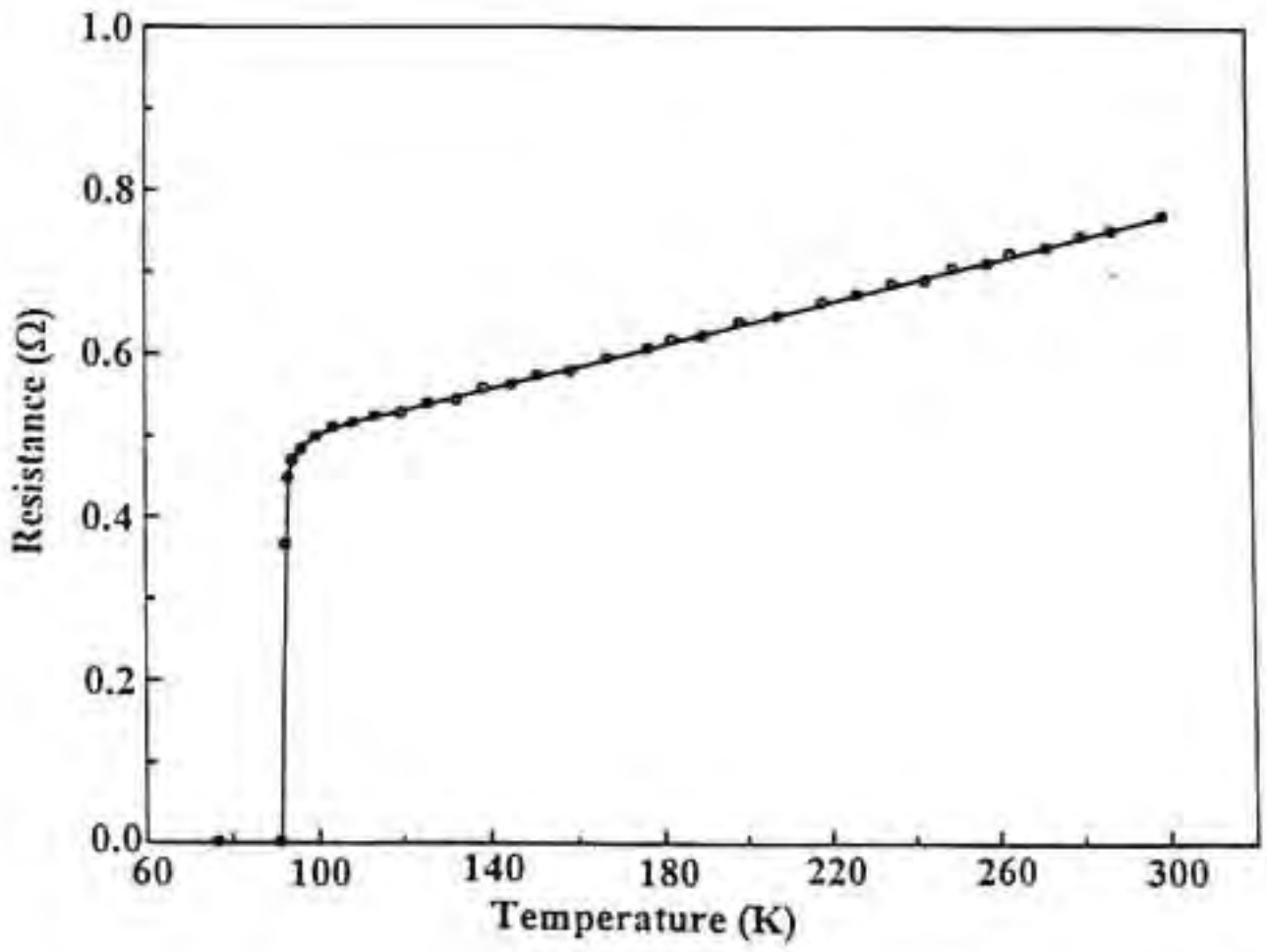

Fig. 5.5(d) Temperature-resistance curve of screen printed YBCO film on Ba_2EuNbO_6 substrate.

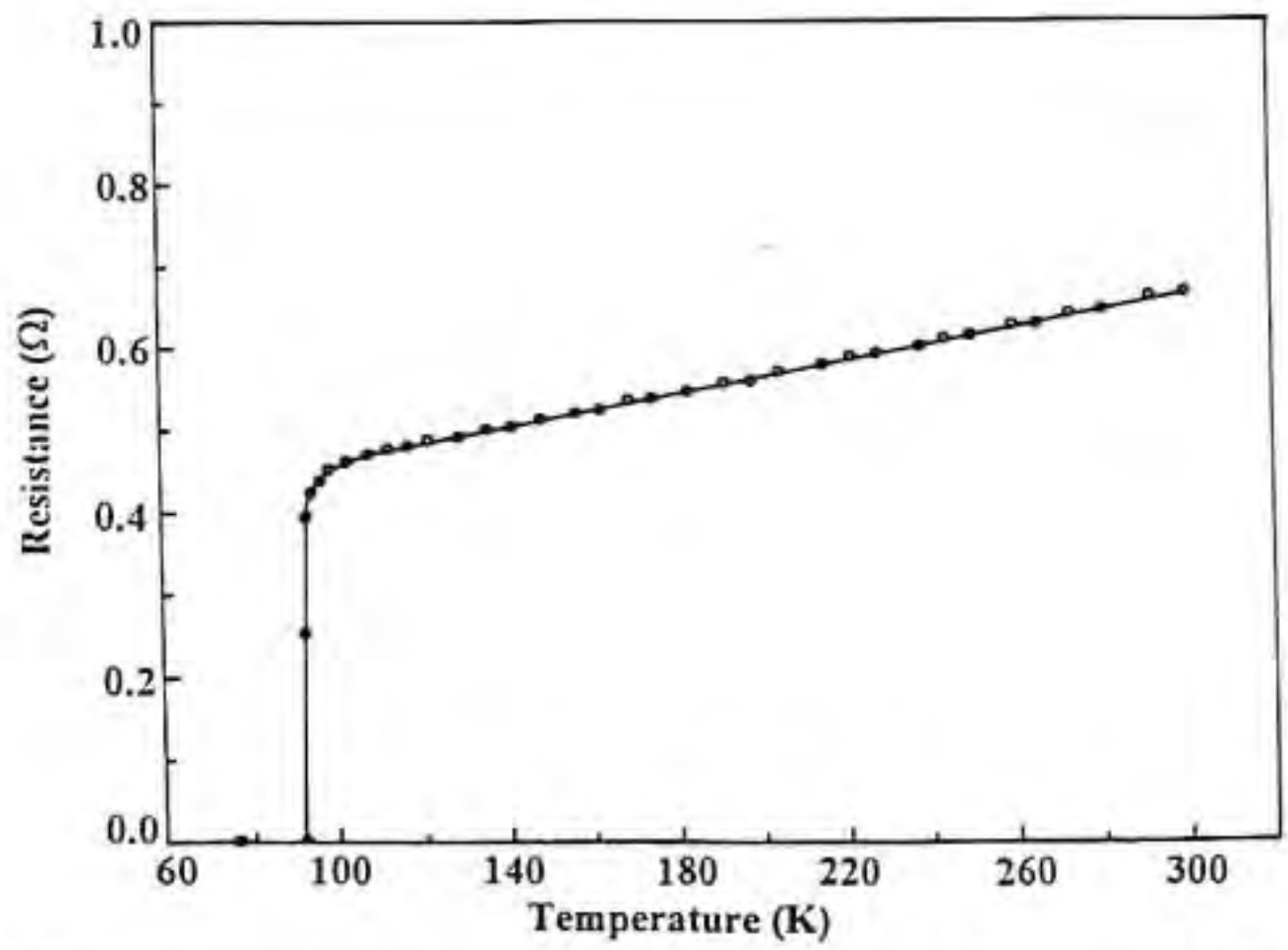

Fig. 5.5(e) Temperature-resistance curve of screen printed YBCO film on Ba_2GdNbO_6 substrate.

5.4. Preparation of YBCO-Ag Composite Thick Films on BRENO

It is reported in literature that the silver addition in YBCO enhances the superconducting characteristics and also improves its microstructure both in thick films and in bulk [2,4,7,8,10]. In the case of silver added YBCO thick films it is reported that the J_c of the YBCO films increases with percentage of silver and reaches a maximum at about 7 wt% of silver in the composite [10,12-13]. In the present study YBCO-Ag (7 wt%) powder was used for the preparation of thick films on BRENO by dip-coating technique.

YBCO-Ag (7 wt%) composites were prepared by the conventional solid state sintering route. Appropriate amount of $AgNO_3$ was thoroughly mixed with phase pure calcined YBCO powder and mixture was annealed at 920°C for 12 h and then slow cooled to room temperature. The YBCO-Ag suspension for dip-coating was prepared by thoroughly mixing fine YBCO-Ag powder with isopropyl alcohol or n-butanol and the viscosity of the suspension was controlled by the addition of fish oil. The YBCO-Ag thick films were prepared by dipping highly polished and cleaned BRENO substrates in the YBCO-Ag suspension followed by drying. The procedure adopted in the case of YBCO-Ag thick films were same as that for YBCO thick films except those for the annealing temperatures. The dried YBCO-Ag thick films were heated in a programmable furnace up to 980°C at a rate of 5°C/min and annealed at 980°C for ~2 min and cooled to 930°C at a rate of 2°C/min. The films

were annealed at 930°C for 30 to 60 minutes and slow cooled to room temperature at a rate of 1°C/min.

5.5. Characterisation of YBCO-Ag Thick Films on BRENO

The structure of the YBCO-Ag thick films on BRENO were examined by X-ray diffraction technique and the XRD patterns of YBCO-Ag thick films on BRENO are shown in Fig. 5.6. It is clear from the XRD patterns of YBCO-Ag thick films that except for the characteristic peaks of BRENO, all the other peaks are those of an orthorhombic YBCO superconductor. The XRD patterns of YBCO-Ag thick films show a high degree of (00*l*) orientation and is an indication of preferred c-axis texturing of the YBCO films with c-axis normal to the surface of the substrate.

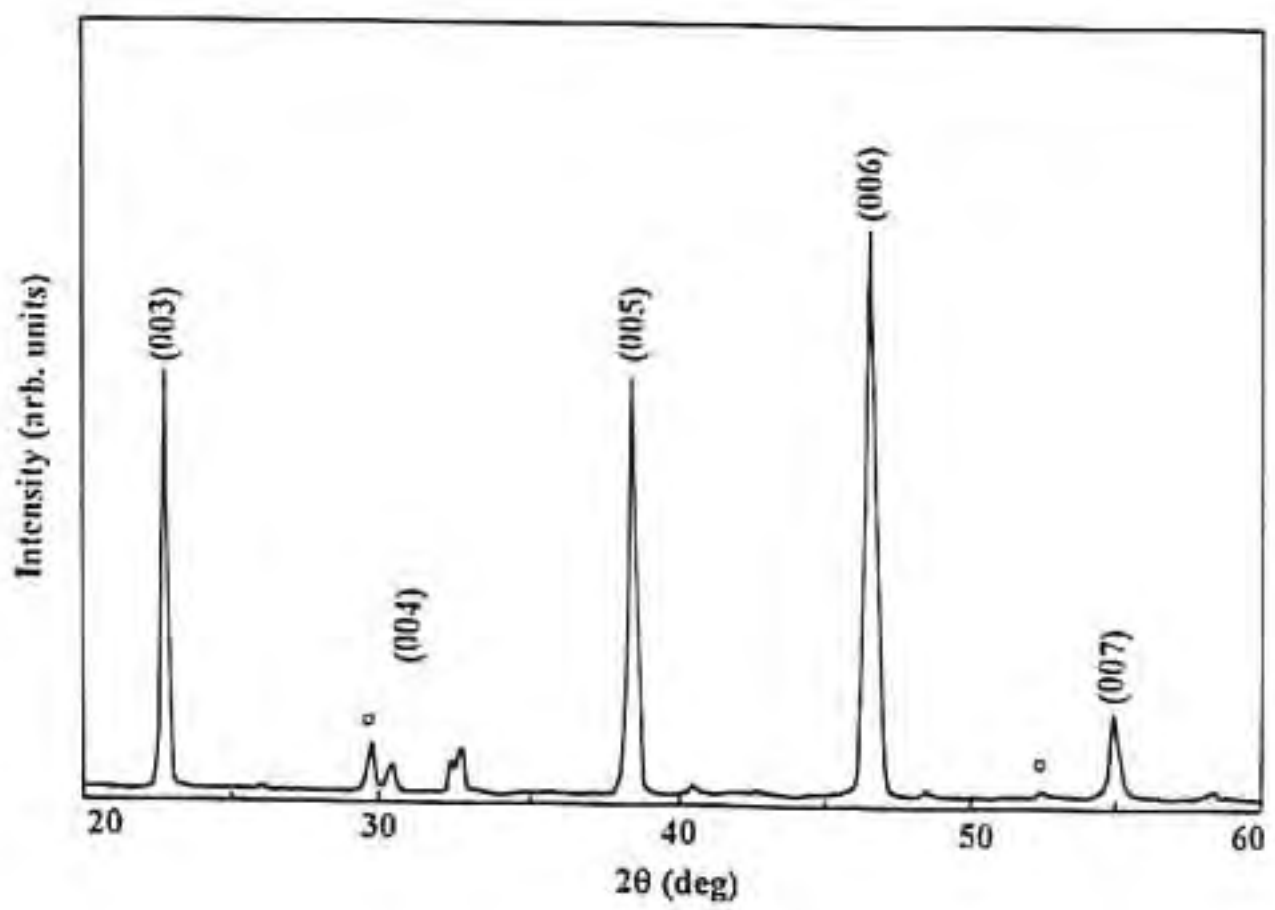

Fig. 5.6(a) XRD pattern of YBCO-Ag thick film dip-coated on Ba_2PrNbO_6 substrate. The substrate peaks are marked by 'o'.

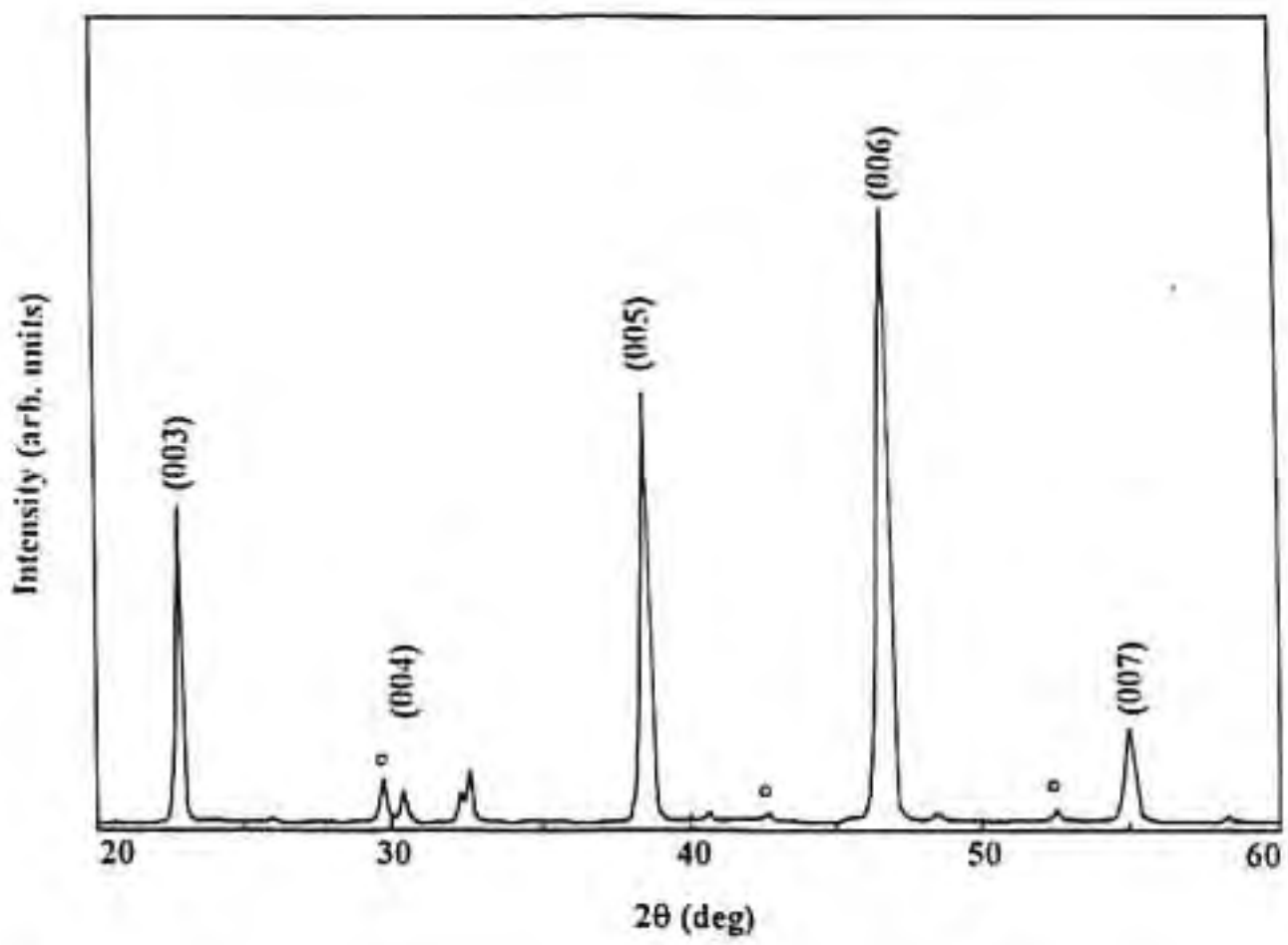

Fig. 5.6(b) XRD pattern of YBCO-Ag thick film dip-coated on Ba_2NdNbO_6 substrate. The substrate peaks are marked by 'o'.

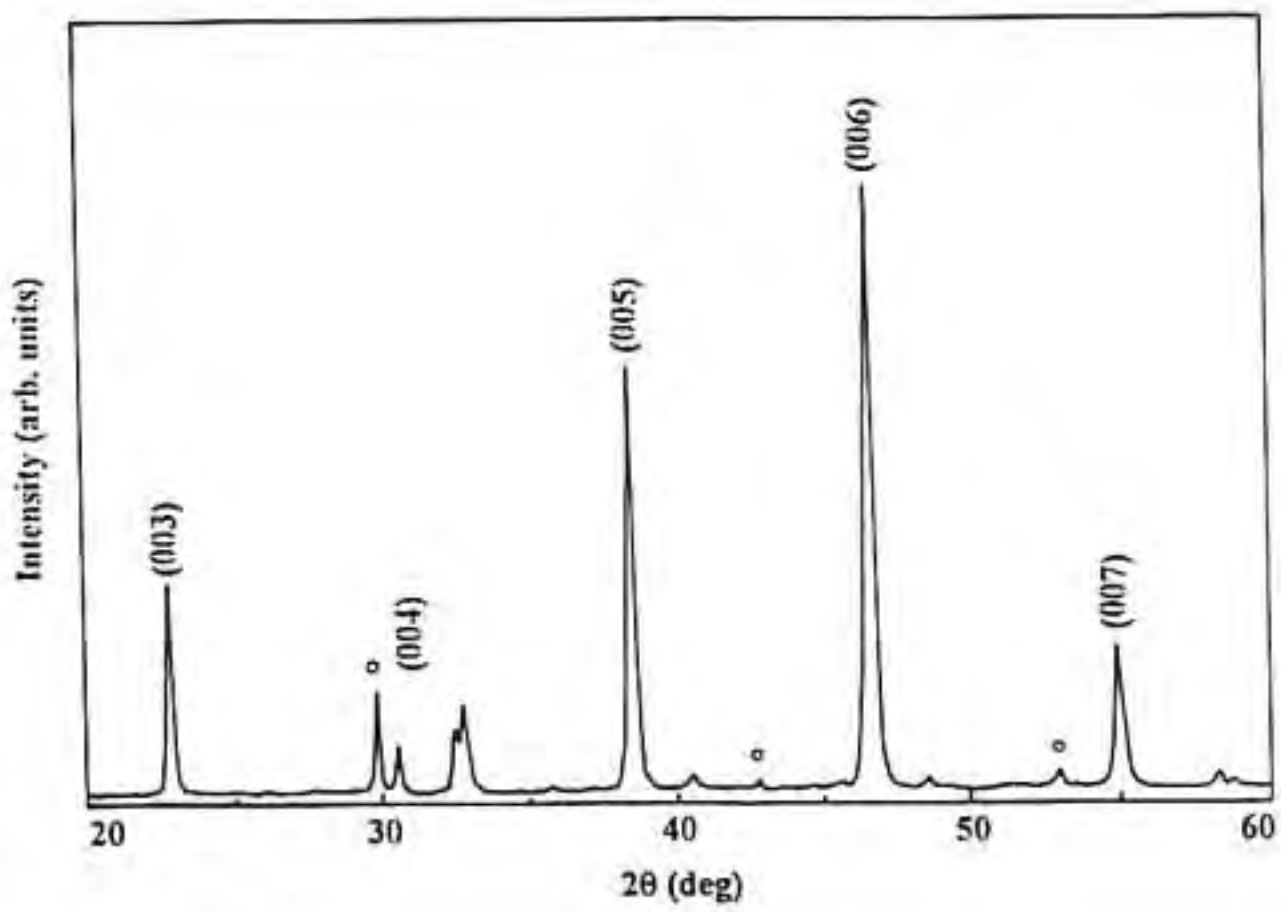

Fig. 5.6(c) XRD pattern of YBCO-Ag thick film dip-coated on Ba_2SmNbO_6 substrate. The substrate peaks are marked by 'o'.

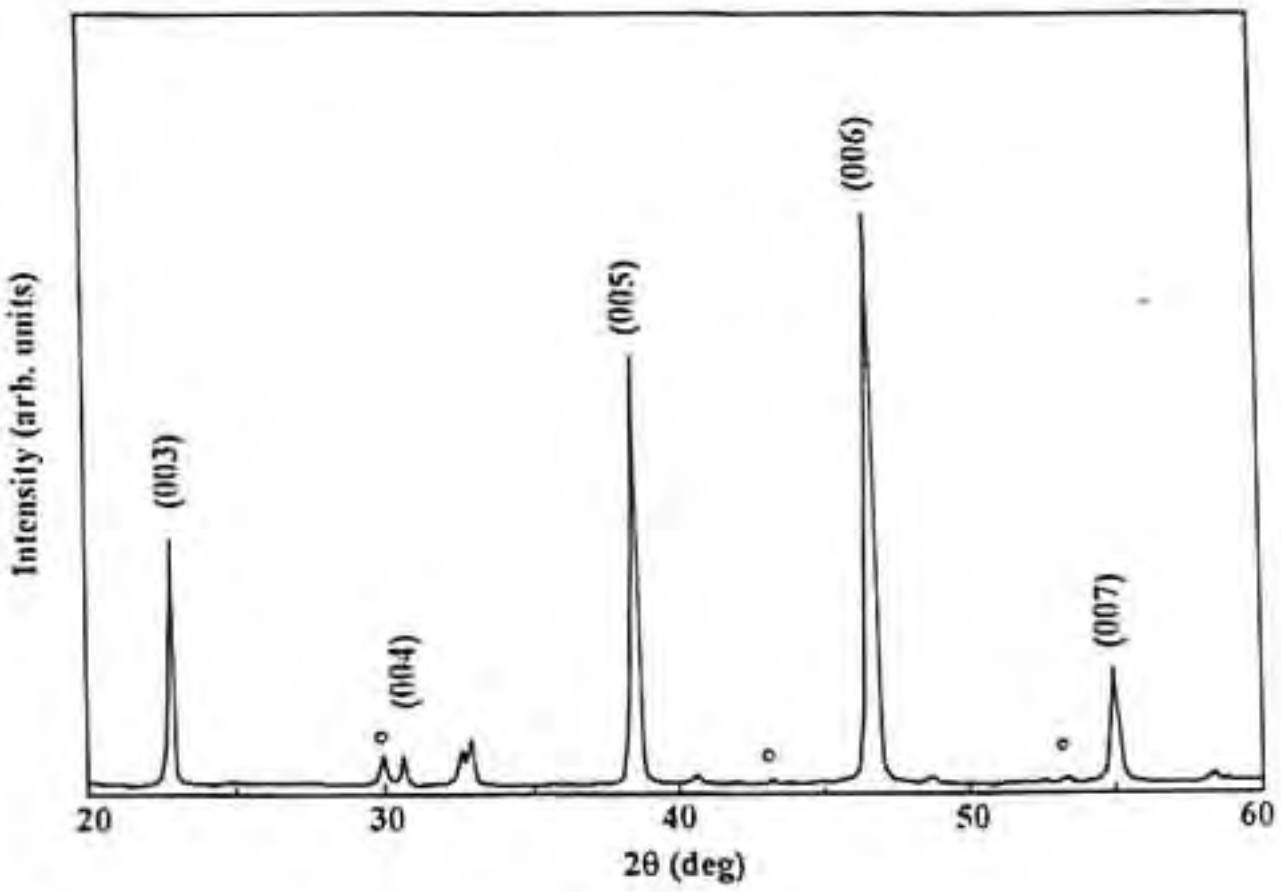

Fig. 5.6(d) XRD pattern of YBCO-Ag thick film dip-coated on Ba_2EuNbO_6 substrate. The substrate peaks are marked by 'o'.

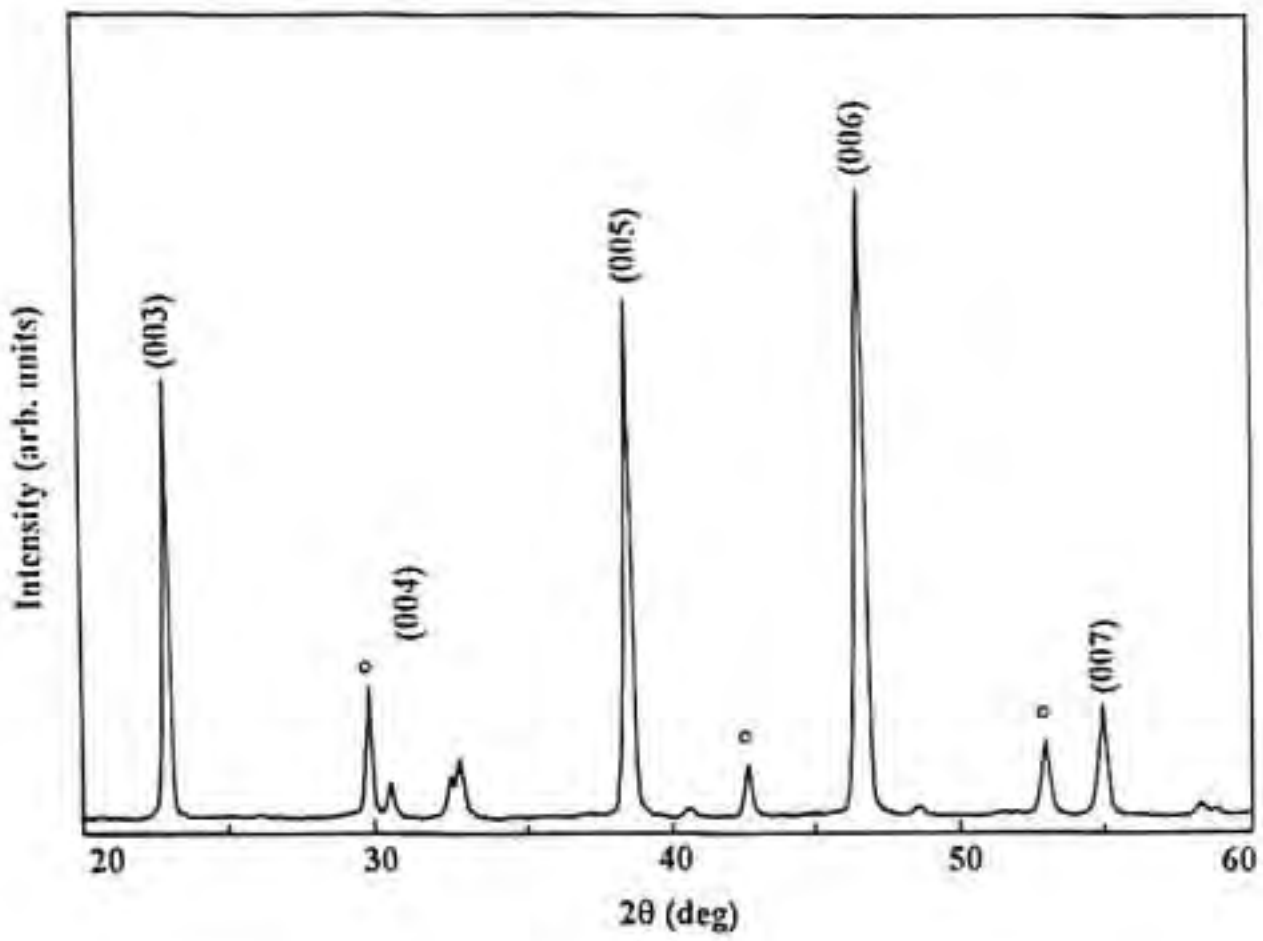

Fig. 5.6(e) XRD pattern of YBCO-Ag thick film dip-coated on Ba_2GdNbO_6 substrate. The substrate peaks are marked by 'o'.

The SEM micrographs of the YBCO-Ag films show the presence of large grains and smooth surface. Surface SEM micrograph of YBCO-Ag thick film on BRENO are shown in Fig. 5.7. The SEM analysis of the surface of the YBCO-Ag films showed no indication of any microcracks. It was seen that the crystal orientation and the density of YBCO films have improved by the addition of silver. In addition to these results, the optimum annealing temperature decreases from 1000°C to 980°C by the addition of silver.

The superconductivity in YBCO-Ag thick films on BRENO was studied by temperature-resistance measurements. Fig. 5.8 shows the temperature-resistance curve for dip-coated YBCO-Ag thick films on BRENO. It was observed that in all the cases the superconducting transition temperature [$T_c(0)$] of 92 K was obtained. The room temperature resistivity for the silver added YBCO films were lower than that of the undoped YBCO thick films. Also it was observed that the critical current density values of YBCO-Ag films improved by nearly 3 times to that of the pure YBCO thick films. The individual values of J_c obtained for YBCO-Ag thick films are given in Table 5.1.

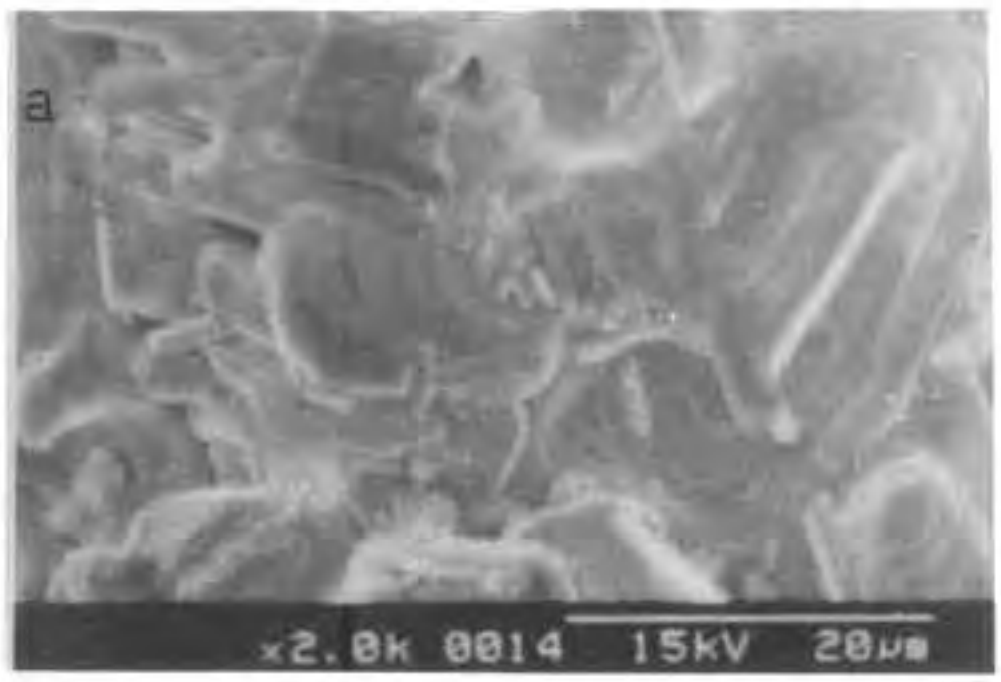

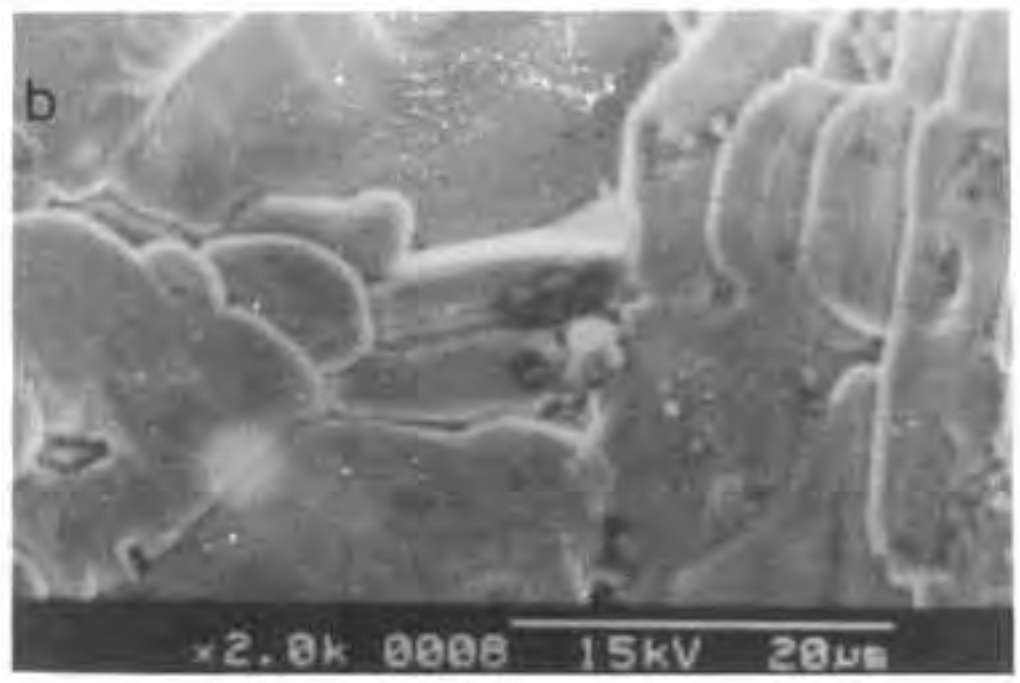

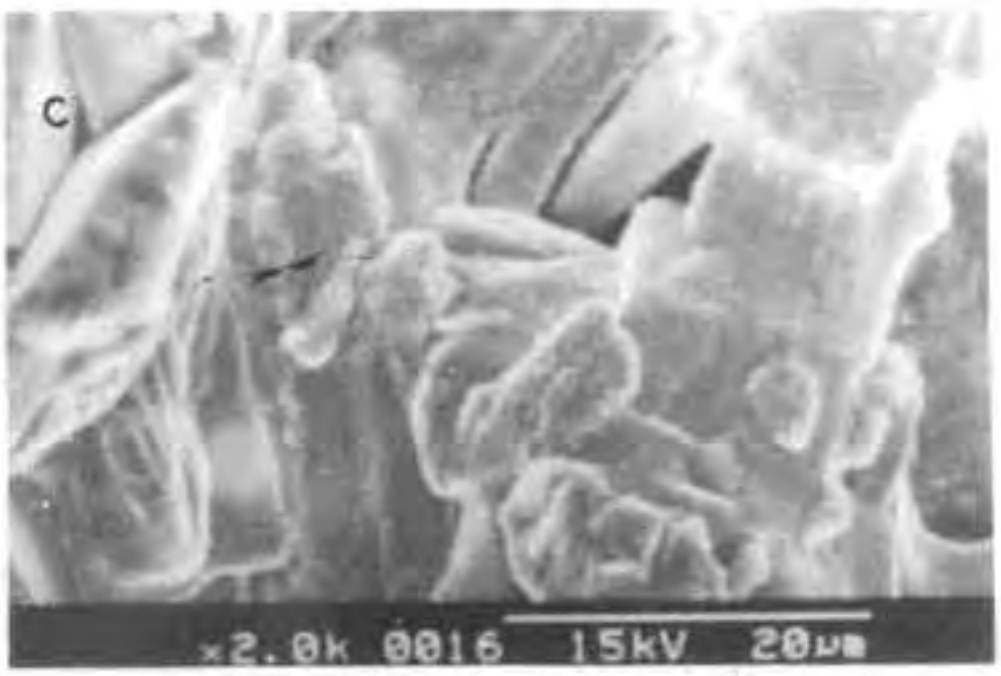

Fig. 5.7 Surface SEM micrograph of YBCO-Ag thick film dip-coated on (a) Ba_2NdNbO_6, (b) Ba_2EuNbO_6 and (c) Ba_2GdNbO_6 substrate.

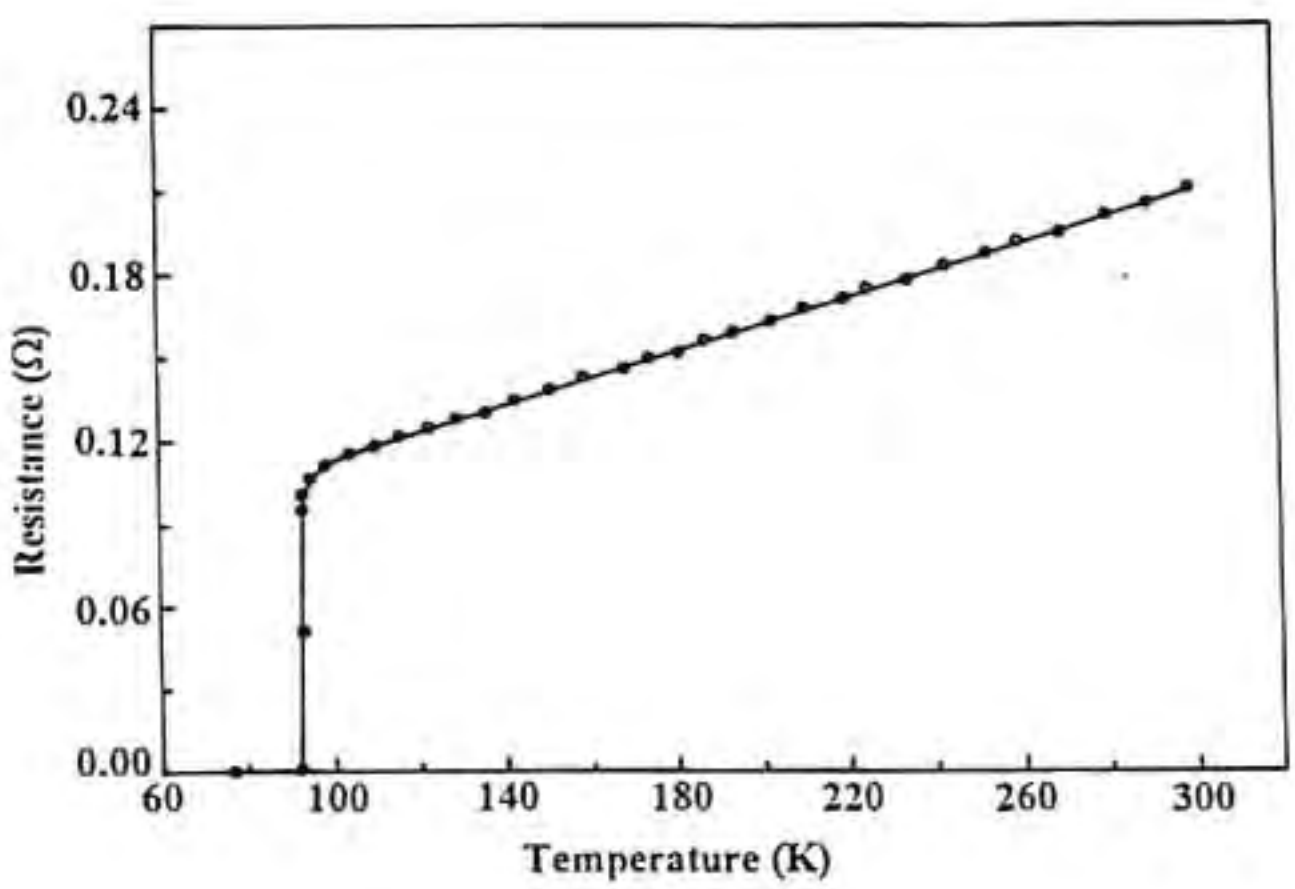

Fig. 5.8(a) Temperature-resistance curve of YBCO-Ag thick film dip-coated on Ba_2PrNbO_6 substrate.

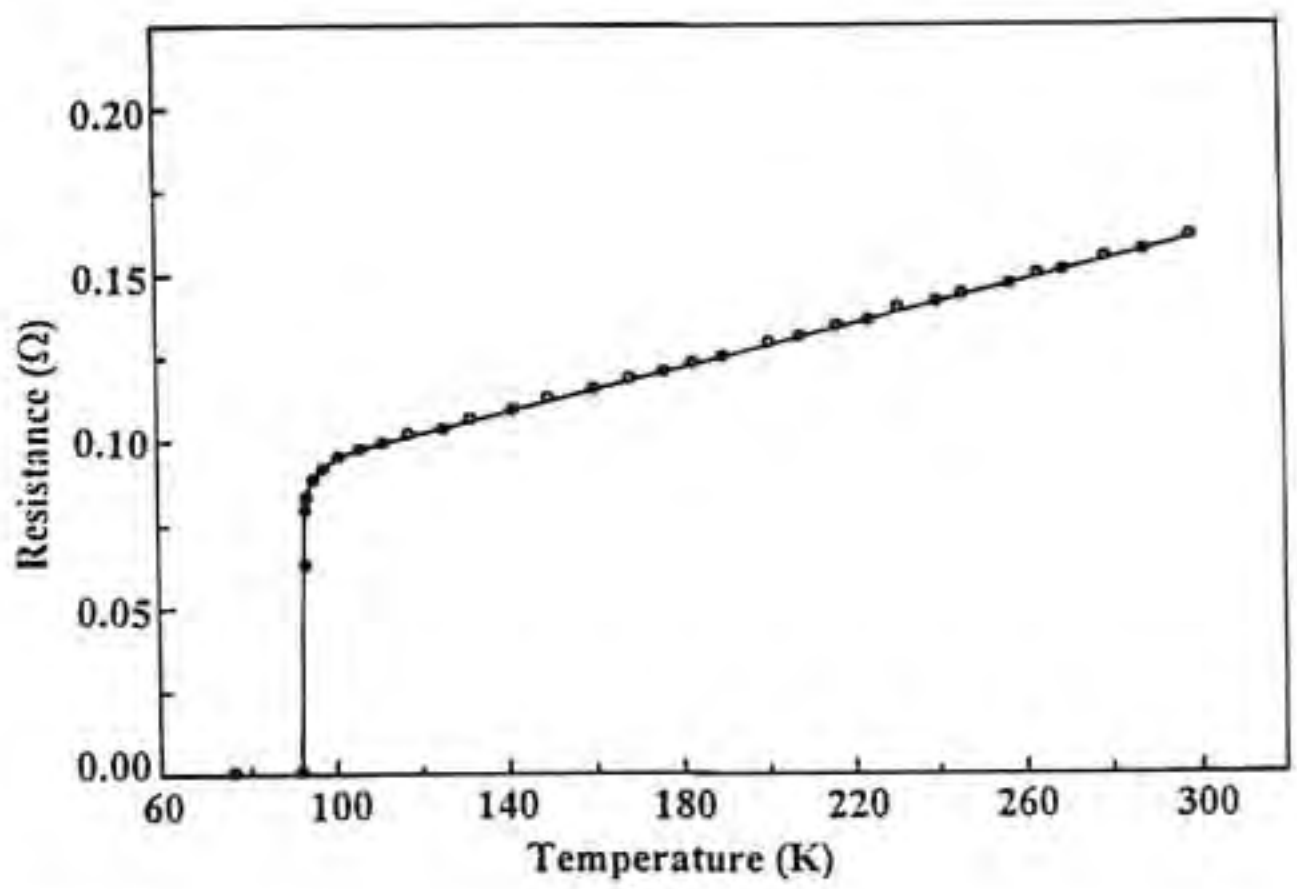

Fig. 5.8(b) Temperature-resistance curve of YBCO-Ag thick film dip-coated on Ba_2NdNbO_6 substrate.

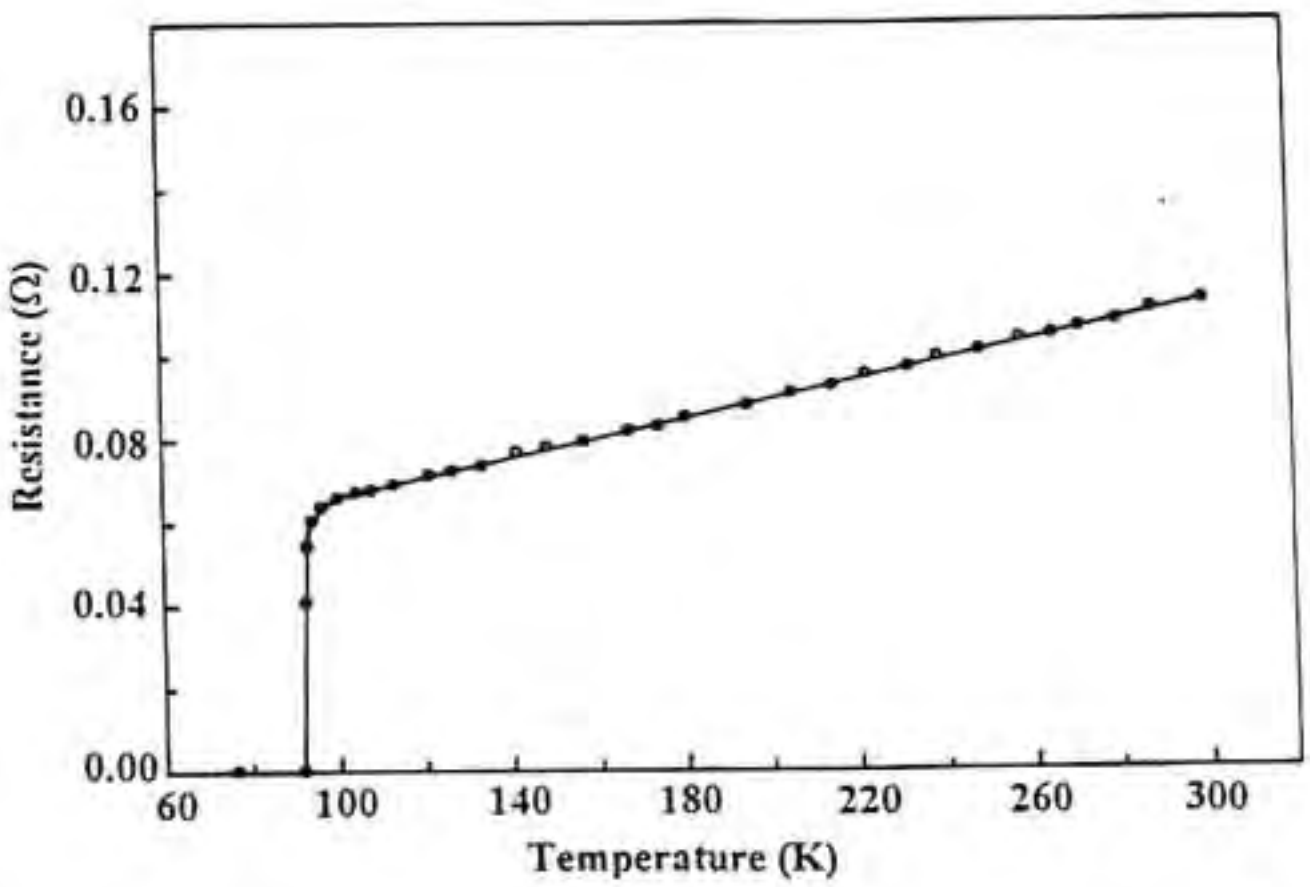

Fig. 5.8(c) Temperature-resistance curve of YBCO-Ag thick film dip-coated on Ba_2SmNbO_6 substrate.

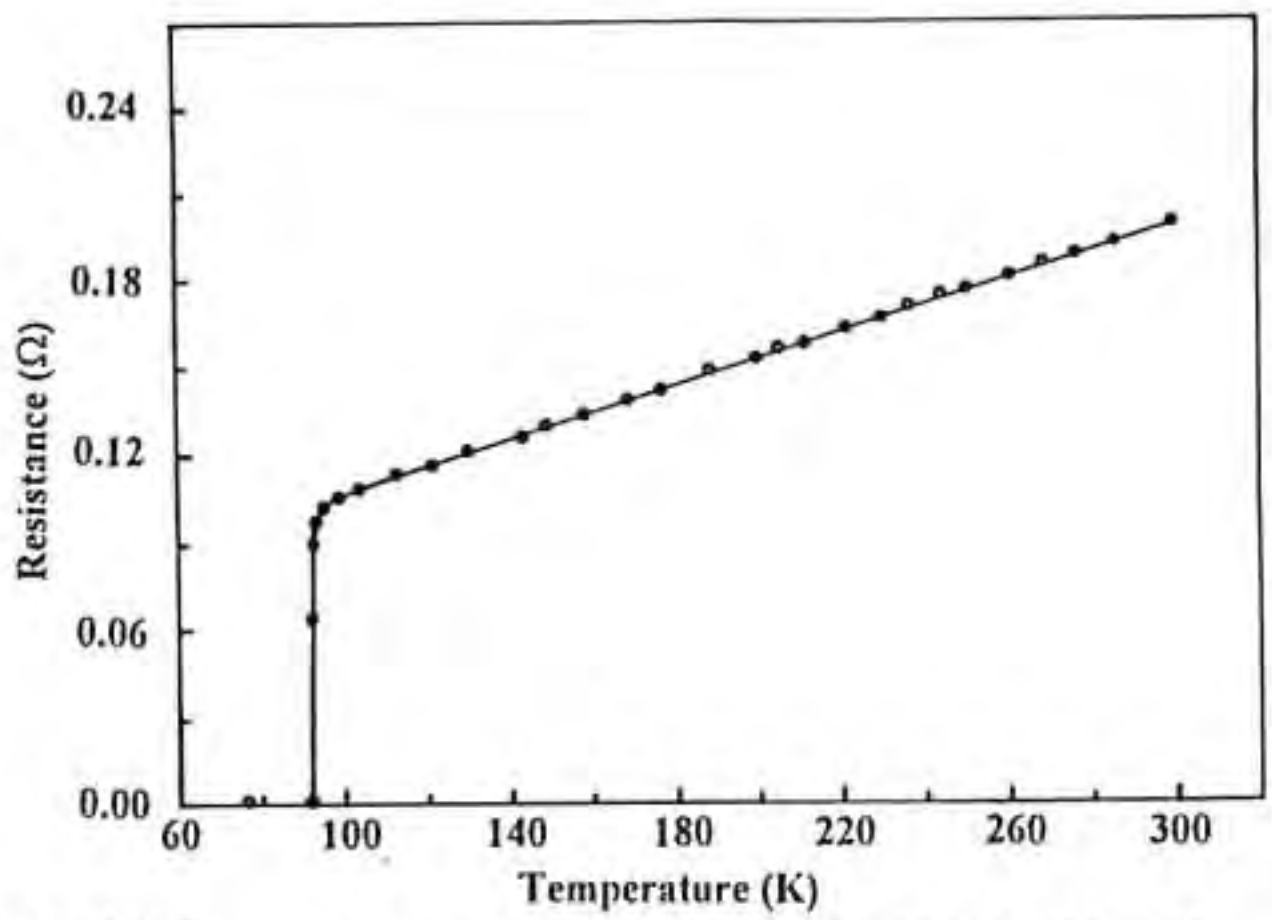

Fig. 5.8(d) Temperature-resistance curve of YBCO-Ag thick film dip-coated on Ba_2EuNbO_6 substrate.

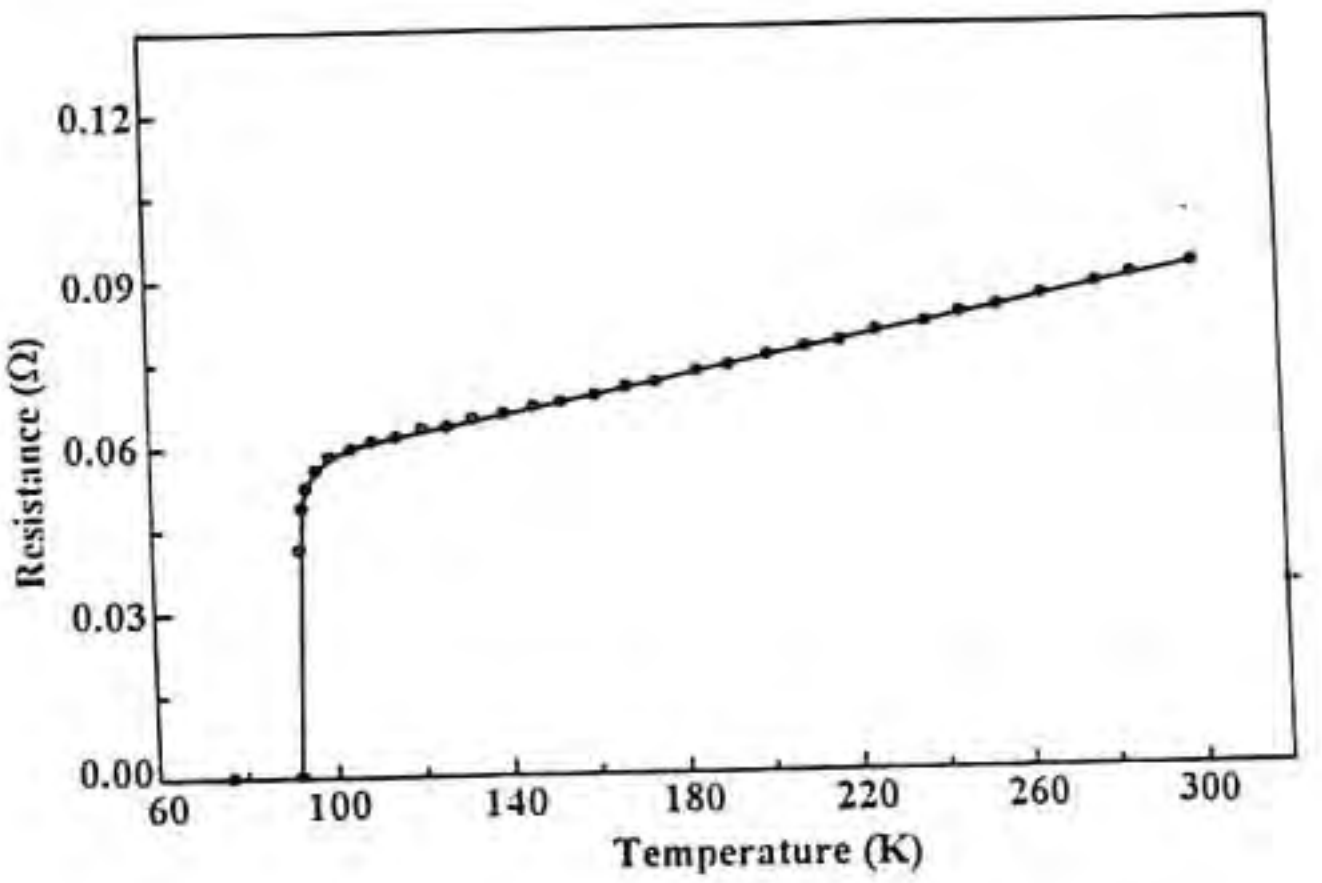

Fig. 5.8(e) Temperature-resistance curve of YBCO-Ag thick film dip-coated on Ba_2GdNbO_6 substrate.

Table 5.1 The superconducting transition temperature $\{T_c(0)\}$, transition width (ΔT), critical current density (J_c) at 77 K for the YBCO and YBCO-Ag thick films on Ba_2RENbO_6 substrates.

Substrate	$T_c(0)$ (K)	ΔT (K)	J_c (A/cm^2) at 77 K for YBCO	YBCO-Ag
Ba_2PrNbO_6	92	2.0	2.9×10^3	9.0×10^3
Ba_2NdNbO_6	92	2.0	4.1×10^3	1.1×10^4
Ba_2SmNbO_6	92	1.9	5.4×10^3	2.1×10^4
Ba_2EuNbO_6	92	2.1	3.2×10^3	1.1×10^4
Ba_2GdNbO_6	92	1.9	5.5×10^3	1.8×10^4

5.6. Conclusion

Superconducting YBCO and YBCO-Ag composite thick films were successfully prepared on polycrystalline BRENO substrates by both screen printing and dip-coating techniques. The successful preparation of superconducting YBCO thick films is found to be critically dependent on the processing conditions and the best results were obtained for films annealed at 1000°C for ~2 min. in air. The processing of the YBCO thick films at the partial melting point of YBCO enhanced the texturing of the YBCO films and also improved the adhesion of the film with the substrate. The X-ray diffraction studies shows a high degree of c-axis orientation for the YBCO films developed on BRENO substrates and there were no evidence of the formation of any second phase within the precision of X-ray diffraction technique. The microstructural analysis of the surface of the YBCO films by SEM shows that the film surface is smooth and almost free from pores. Also there were no evidence of any microcracks. The SEM analysis of the cross section of the YBCO thick films shows no indication of any reaction between the film and the substrate at the film-substrate interface. The YBCO thick films developed on BRENO substrates gave zero resistance superconducting transition [$T_c(0)$] of 92 K with a transition width of ~2 K and a critical current density (J_c) value of ~10^4 A/cm^2 at 77 K and zero magnetic filed. The YBCO-Ag composite (7 wt.% of Ag) thick films developed on BRENO gave $T_c(0)$ of 92 K and a J_c of ~$3x10^4$ A/cm^2 at 77 K and zero magnetic

field. It was evident from the X-ray analysis that the addition of silver improves the c-axis texturing of the YBCO film. Also the SEM analysis shows that the silver addition results in the formation of a much smoother and denser film. The silver addition also enhances the J_c of the YBCO thick films by about three times. The high value of T_c and J_c obtained for YBCO films developed on BReNO substrates can be attributed to the chemical non-reactivity of BReNO with YBCO at the elevated processing temperature of 1000°C. The successful preparation of YBCO thick films free from any microcracks indicates that BReNO offers a reasonable thermal expansion match with YBCO.

References

1. N.B. Bansal, R.N. Simon and D.E.Farrell, Appl. Phys. Lett. **53** 603 (1988).
2. Y. Matsuoka, E. Ban, H. Ogawa and A.Suzumura, Supercond. Sci. Technol. **4**, 62 (1991).
3. N. Khare, A.K.Gupta, S. Chaudhry and V.S. Tomar, Supercond. Sci. Technol. **4**, 107 (1991).
4. N. McN. Alford, T.W. Button and D. Opie, Supercond. Sci. Technol. **4**, 433 (1991).
5. N.P. Bansal, Materials Letters. **13**, 7 (1992).
6. E. Saiz and J.S. Moya, Supercond. Sci. Technol. **5**, 130 (1992).
7. N. McN. Alford, T.W. Button, M.J. Adams, S. Hedges, B. Nicholson and W.A. Phillips, Nature, **349**, 680 (1991).
8. M. Miyajima, T. nakamoto, S. Nagaya, I. Hirobayashi and S. Tanaka, Supercond. Sci. Technol., **5**, 5292 (1992).
9. T.C. Shields and J.S. Abell, Supercond. Sci. Technol., **5**, 130 (1992).
10. D.K. Aswal, S.K. Gupta, A.K. Debnath, G.P.Kothiyal, S.C. Sabharwal and M.K. Gupta, Supercond. Sci. Technol., **4**, 188 (1991).
11. G. Kozlowski, S. Rele, D.F. Lee and K. Salama, J. Mater. Sci., **26**, 1056 (1991).
12. K.S. Kumar, J. Kurian, P.K. Sajith, J. Koshy, Physica C, **256**, 312 (1996).
13. K.S. Kumar, Ph.D. thesis, University of Kerala, 1996.

CHAPTER 6

GROWTH AND CHARACTERISATION OF YBCO AND YBCO-Ag THIN FILMS ON POLYCRYSTALLINE Ba_2RENbO_6 (RE = Nd, Sm, Eu and Gd) BY PULSED LASER ABLATION

6.1. Introduction

Since the discovery of high T_C superconductors (HTSC) the study of high T_C superconductor films has become one of the most important areas in the field of high temperature superconductivity. In particular, thin films of YBCO compounds have been the most attractive mainly because it is relatively easier to get its single phase film and also its simplicity of fabrication when compared with other HTSC compounds [1]. The growth of thin films of HTSC materials has been motivated by two major possibilities. One is the potential of HTSC thin films to give insight into the fundamental mechanism governing HTSC compounds and the other involves numerous applications of high quality thin films in bolometers, flux transformers, dc and rf superconducting quantum interference devices (SQUIDS), interconnects and in various microwave devices such as delay line, resonators, antennas, filters, etc [2-9]. Some of the challenges encountered in the production of high quality films of HTSC materials are the shear complexity of HTSC materials, the high reactivity, the role of oxygen, the anisotropic nature, etc. The large anisotropic properties of HTSC materials needs that the films should be grown with specific crystallographic orientation [9]. High quality YBCO thin films have been

grown by different methods such as sputtering, pulsed laser ablation, co-evaporation, molecular beam epitaxy, chemical vapour deposition etc [10-15]. Among the various techniques, pulsed laser deposition (PLD) have become the most popular and easiest deposition technique for the *in situ* growth of high quality YBCO thin films [16-20]. In the present study YBCO and YBCO-Ag thin films were grown *in situ* on polycrystalline Ba_2ReNbO_6* (BReNO) {RE = Nd, Sm, Eu and Gd} substrates by pulsed laser ablation technique. The growth and characterisation of YBCO and YBCO-Ag thin films grown on polycrystalline BReNO substrates are described in detail in the different sections of this chapter.

6.2. *In situ* Growth of YBCO Thin Films on BReNO

YBCO thin films were grown *in situ* on polycrystalline BReNO substrates by pulsed laser ablation technique. In the present study laser ablation experiments were carried out using Lambda Physik 301 KrF 242 nm excimer laser. A 30 cm focal length quartz lens was used for laser beam focusing. The excimer laser pulse had a maximum energy of 1200 mJ with a pulse width of 25 ns and a 1 to 10 Hz variable repetition rate. Since the intensity profile of the 3 cm (width) and 1 cm (height) laser beam has a gaussian distribution along the short (vertical) axis, only 0.5 cm of the central region of the beam along the short axis was allowed

---

* Published in *Physica C*, **225**, 101 (1994)

to pass through the quartz lens using an aperture 0.5 cm height and width variable from 1 to 2 cm. The width of the aperture was varied from 1 to 2 cm in order to vary the spot size of the laser beam on the target. The angle between the laser beam and the normal to the target was 45°.

A 30 cm diameter stainless steel chamber having a quartz window and pumped with a turbo pump module was used for the growth of YBCO films. A platinum strip heater with a temperature capability up to ~850°C was used for the *in situ* growth and YBCO films. Highly polished polycrystalline BRENO substrates of size 1x0.5x0.5 cm cleaned by isopropyl alcohol and an ultrasonic cleaner were mounted on to the substrate heater at a distance of 4.5 cm from the YBCO target. The chamber was initially pumped to a base pressure of 10^{-6} Torr and later oxygen was introduced into the chamber after throttling the turbo pump for film deposition. The YBCO target, 1.5 cm diameter and 0.3 cm thickness was prepared by solid state sintering method. The target was rotated at a rate of 15 rpm. The substrate temperature was measured using an optical pyrometer. The YBCO films were grown on BRENO at a substrate temperature of 780 to 800°C for about 20-30 min and cooled in ~500 Torr of oxygen after the termination of growth. The energy density of the laser beam was 2.2 J/cm^2 for the deposition of YBCO films. The film thickness was measured using a surface profilometer and the films had thickness between 3000 Å and 4000 Å.

6.3. Characterisation of YBCO Thin Films

The YBCO thin films grow *in situ* on polycrystalline BRENO substrates by pulsed laser ablation technique were characterised by X-ray diffraction and temperature-resistance measurements. The microstructural analysis of the YBCO films was carried out by scanning electron microscope.

The structure of the YBCO thin films *in situ* grown on BRENO substrates was examined by X-ray diffraction (XRD) using nickel filtered Cu Kα radiation. Figure 6.1 shows the XRD patterns of *in situ* grown YBCO thin film on polycrystalline BRENO substrates by PLD. It is clear from fig.6.1 that except for the characteristic peaks of BRENO, all other peaks in the X-ray spectra are those of (00*l*) reflections of an

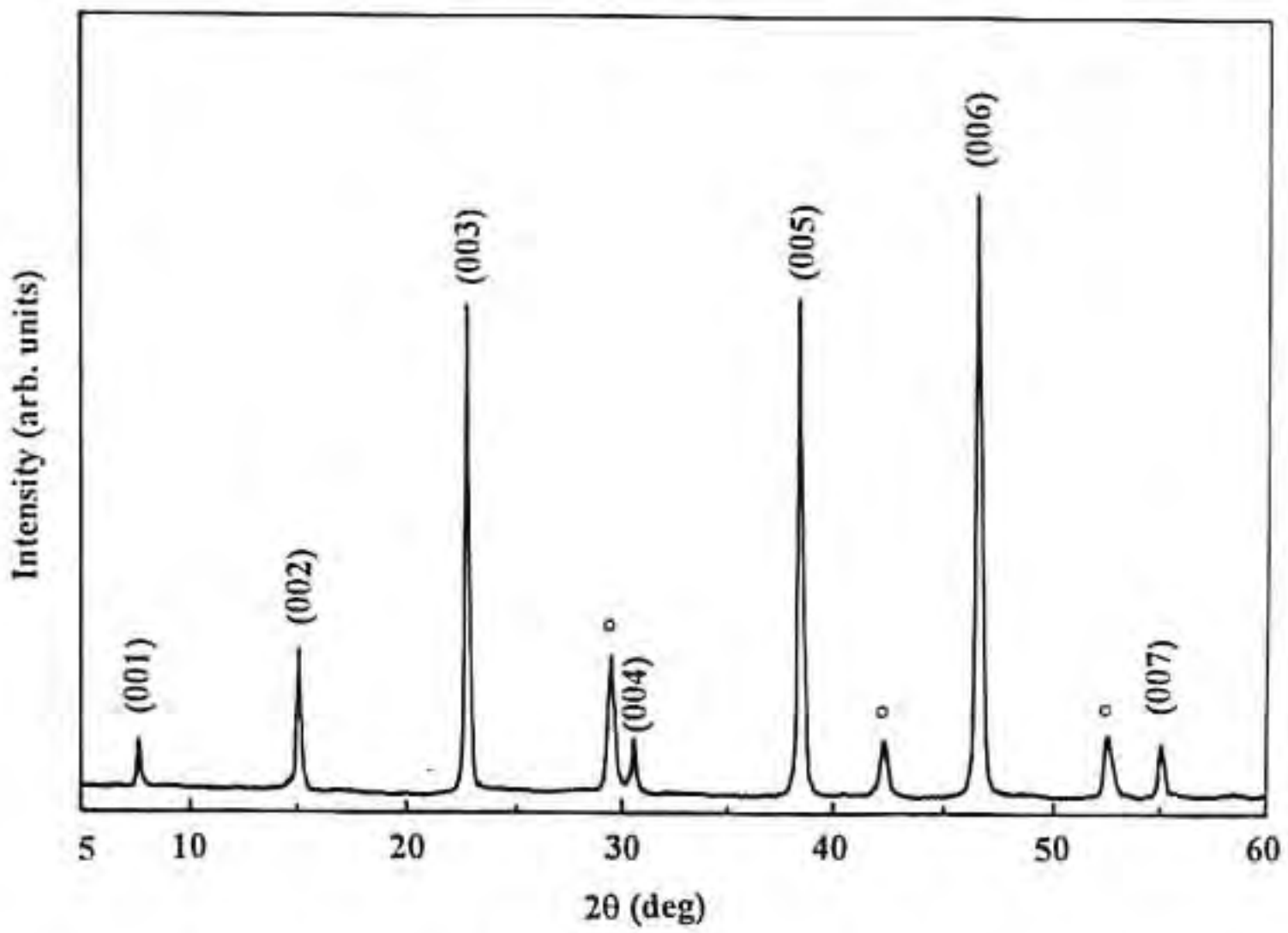

Fig. 6.1(a) XRD pattern of laser ablated YBCO thin film on polycrystalline Ba_2NdNbO_6 subsatrate. The substrate peaks are marked by '∘'.

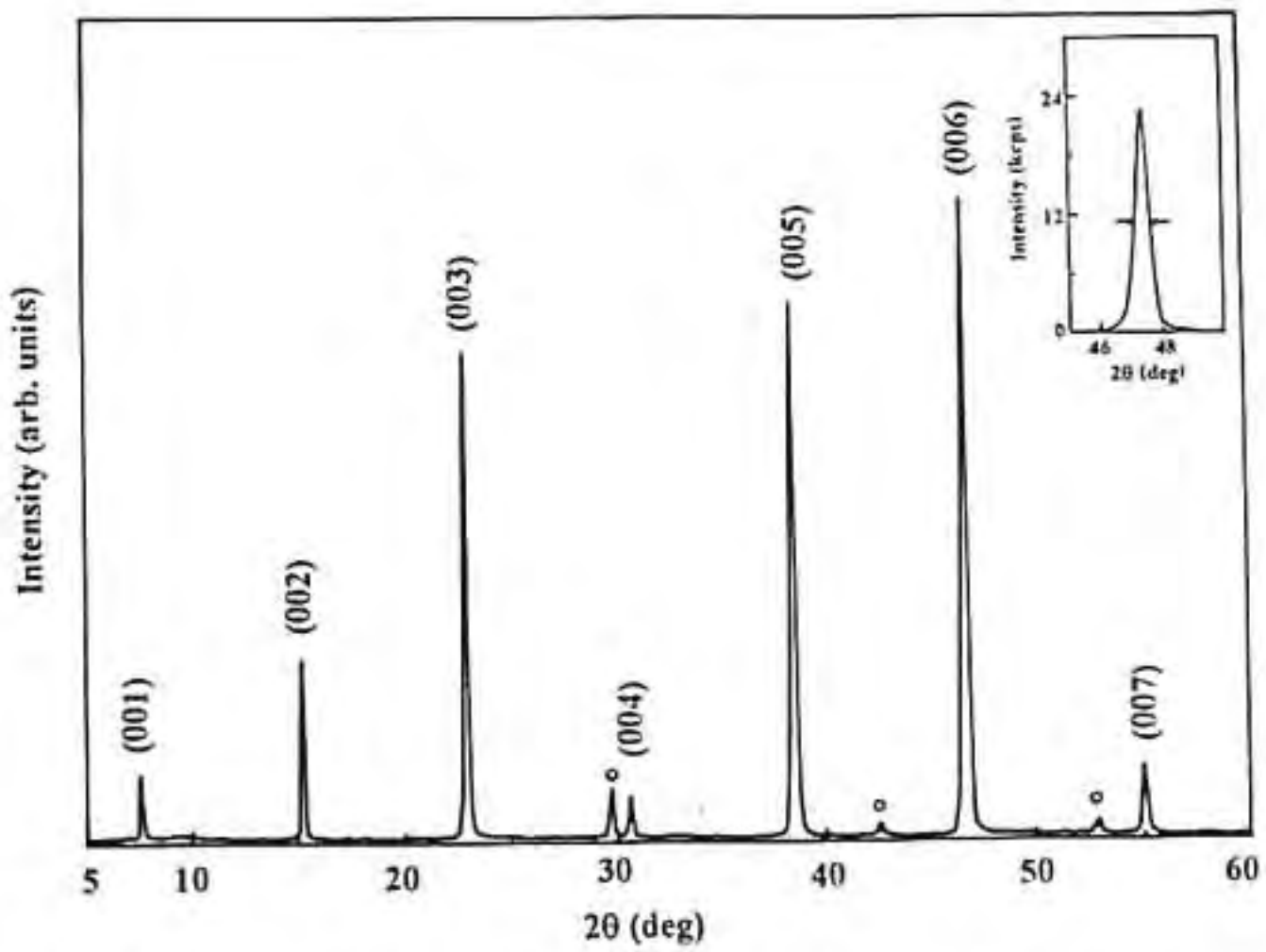

Fig. 6.1(b) XRD pattern of laser ablated YBCO thin film on polycrystalline Ba_2SmNbO_6 subsatrate. The substrate peaks are marked by '∘'. The profile of (006) reflection is superposed showing the intensity in kilocounts per second.

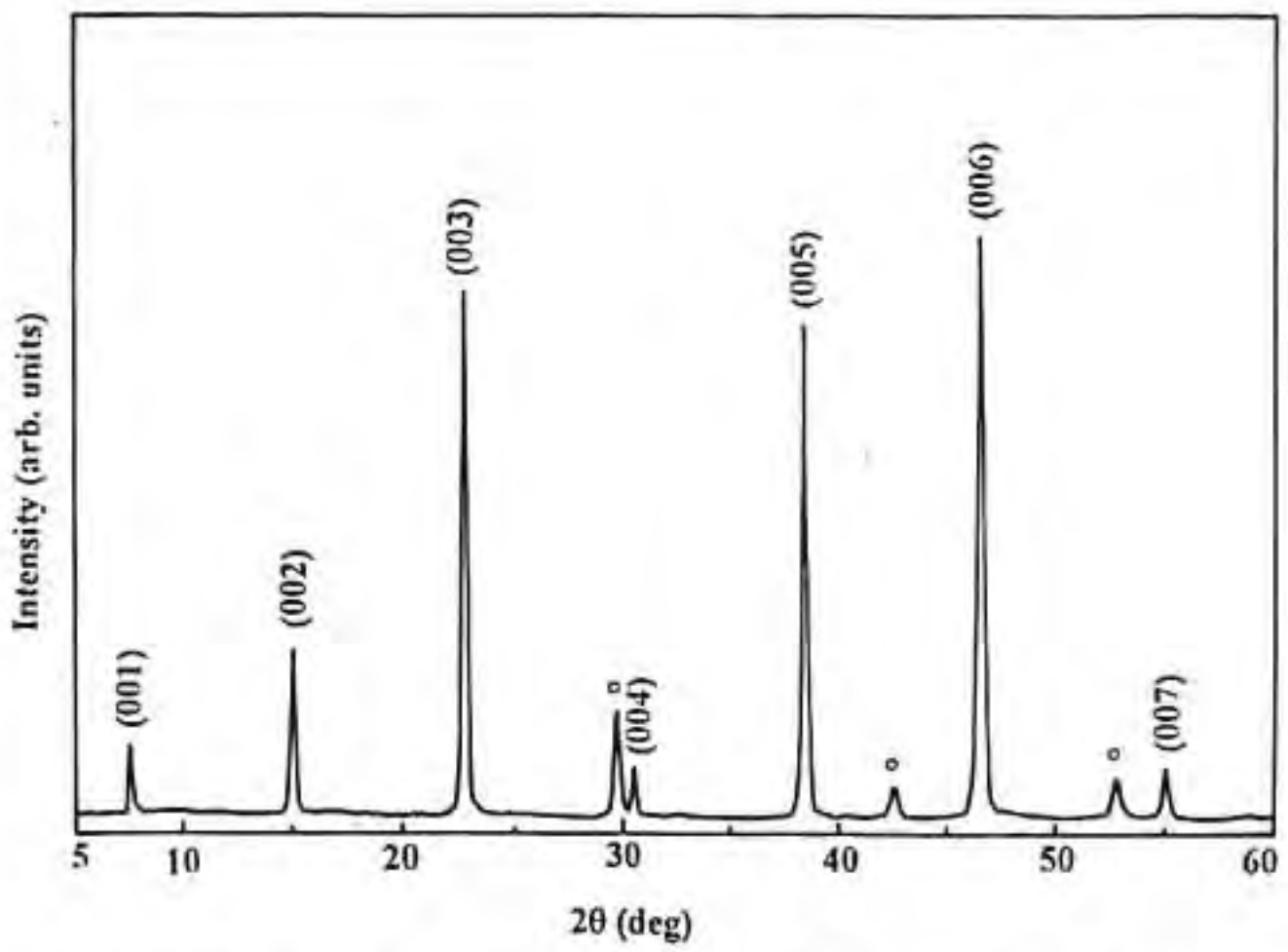

Fig. 6.1(c) XRD pattern of laser ablated YBCO thin film on polycrystalline Ba_2EuNbO_6 subsatrate. The substrate peaks are marked by '∘'.

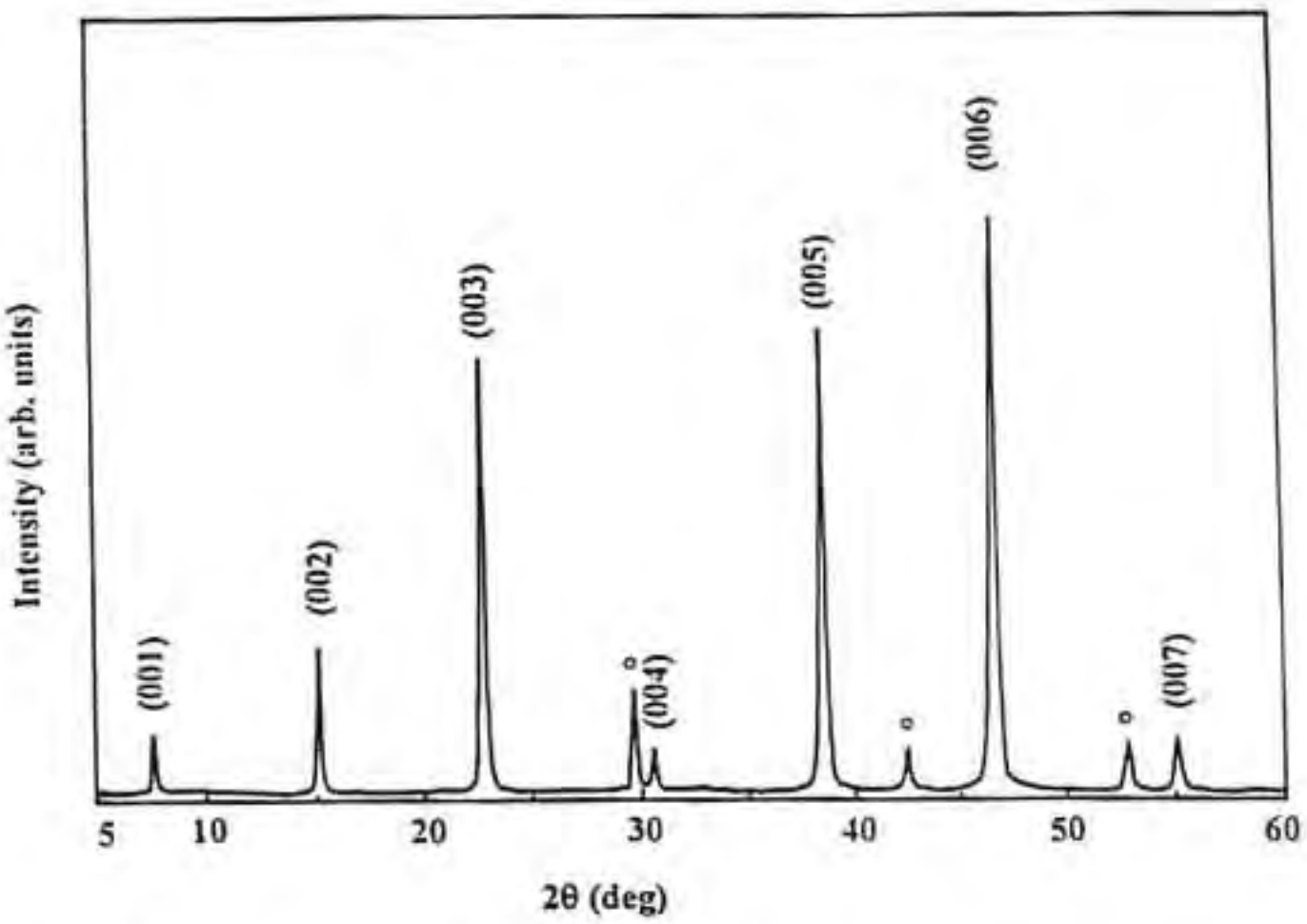

Fig. 6.1(d) XRD pattern of laser ablated YBCO thin film on polycrystalline Ba_2GdNbO_6 subsatrate. The substrate peaks are marked by '∘'.

orthorhombic YBCO superconductor. All the XRD patterns of YBCO thin films on BRENO were similar and showed a high degree of c-axis orientation. The peaks corresponding to (00*l*) orientation of YBCO are as sharp and intense as those of YBCO films on (100) $LaAlO_3$ substrate indicating good crystallinity of grains of YBCO films. Inset of Fig. 6.1(b) shows the (006) reflection in the XRD spectra of YBCO thin film grown on Ba_2SmNbO_6 substrate with Y axis showing the real intensity in kilocounts per second(kcps) {the XRD patterns were recorded with XRD instrument conditions of 40 kV, 20 mA and a scan speed of 4 deg/min

with a sampling interval of 0.01 deg.}. The full width at half maximum (FWHM) of (005) and (006) reflections (measured in 2θ scale) of YBCO in the YBCO thin films grown on BRENO substrates are given in Table 6.1. The FWHM of the (005) and (006) reflections of YBCO films grown on BRENO substrates are comparable with those of YBCO films grown on (100) $LaAlO_3$, indicating the crystalline quality of YBCO films grown on BRENO.

Table 6.1 Full width at half maximum (FWHM) for (005) and (006) reflections in the XRD of YBCO thin films grown on BRENO substrates by laser ablation.

Substrate	FWHM in 2θ scale for	
	(005)	(006)
Ba_2NdNbO_6	0.210	0.259
Ba_2SmNbO_6	0.218	0.262
Ba_2EuNbO_6	0.217	0.262
Ba_2GdNbO_6	0.219	0.263

The surface morphology of the YBCO thin films grown on BRENO substrates was examined by SEM. The microstructure of the surface of the YBCO thin films *in situ* grown on polycrystalline BRENO taken on a Hitachi (model S2400) Scanning Electron Microscope are shown in Fig.6.2. The surface SEM micrographs of the YBCO thin films on BRENO shows a smooth and continuous surface. Also there was no evidence of any microcrack.

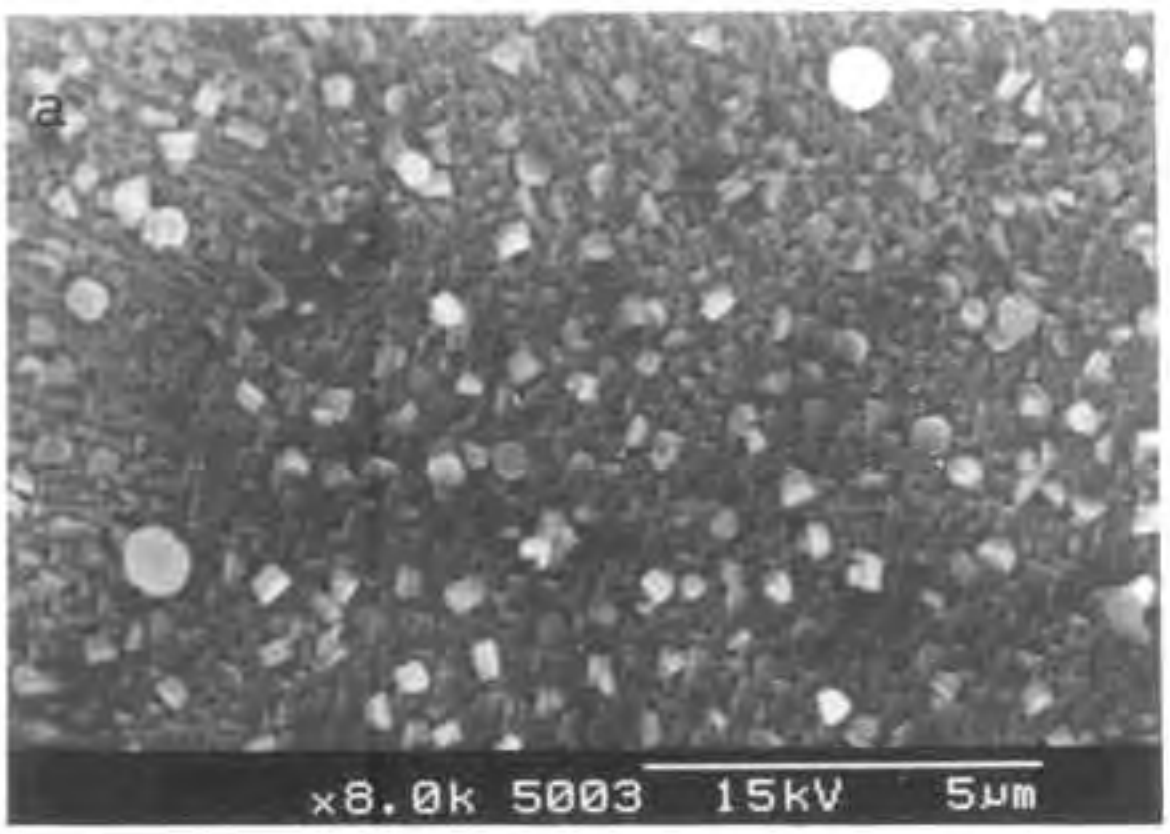

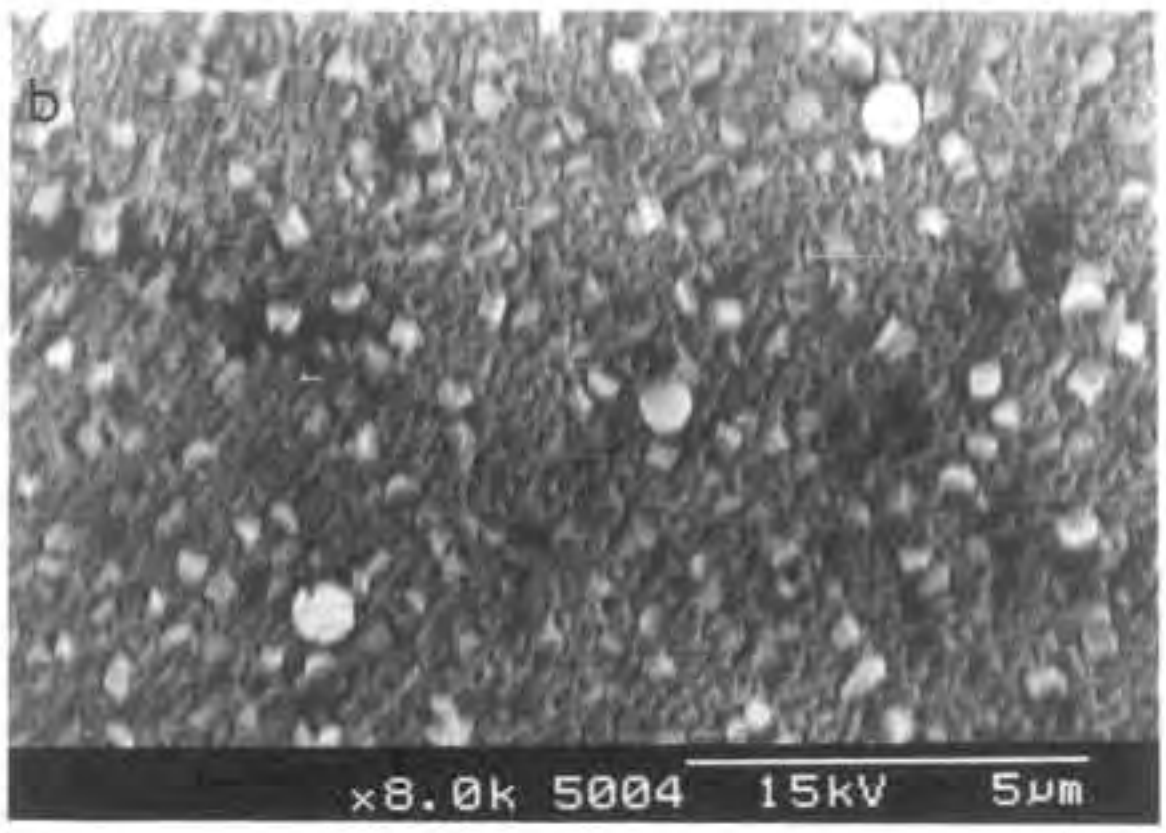

Fig. 6.2 Surface SEM micrograph of YBCO thin film on (a) Ba_2NdNbO_6, and (b) Ba_2EuNbO_6.

The superconductivity of the laser ablated YBCO thin films on BRENO substrates was studied by temperature-resistance measurements using the standard four probe technique. A Keithley current source model 220 and a Keithley nanovoltmeter model 181 were used for the resistance measurements. The temperature of the films was measured using a calibrated copper-constantan thermocouple. The temperature-resistivity curves of YBCO thin films grown on BRENO substrates are given in Fig.6.3. The YBCO thin films on all the BRENO substrates gave a T_c(onset) of ~91.5 K and a T_c(o) of ~90 K with a transition width of ~1.5 K. The electrical transport Jc of the YBCO films estimated at 77 K and zero magnetic field following 1 μV/cm criterion were ~$3x10^4$ A/cm^2.

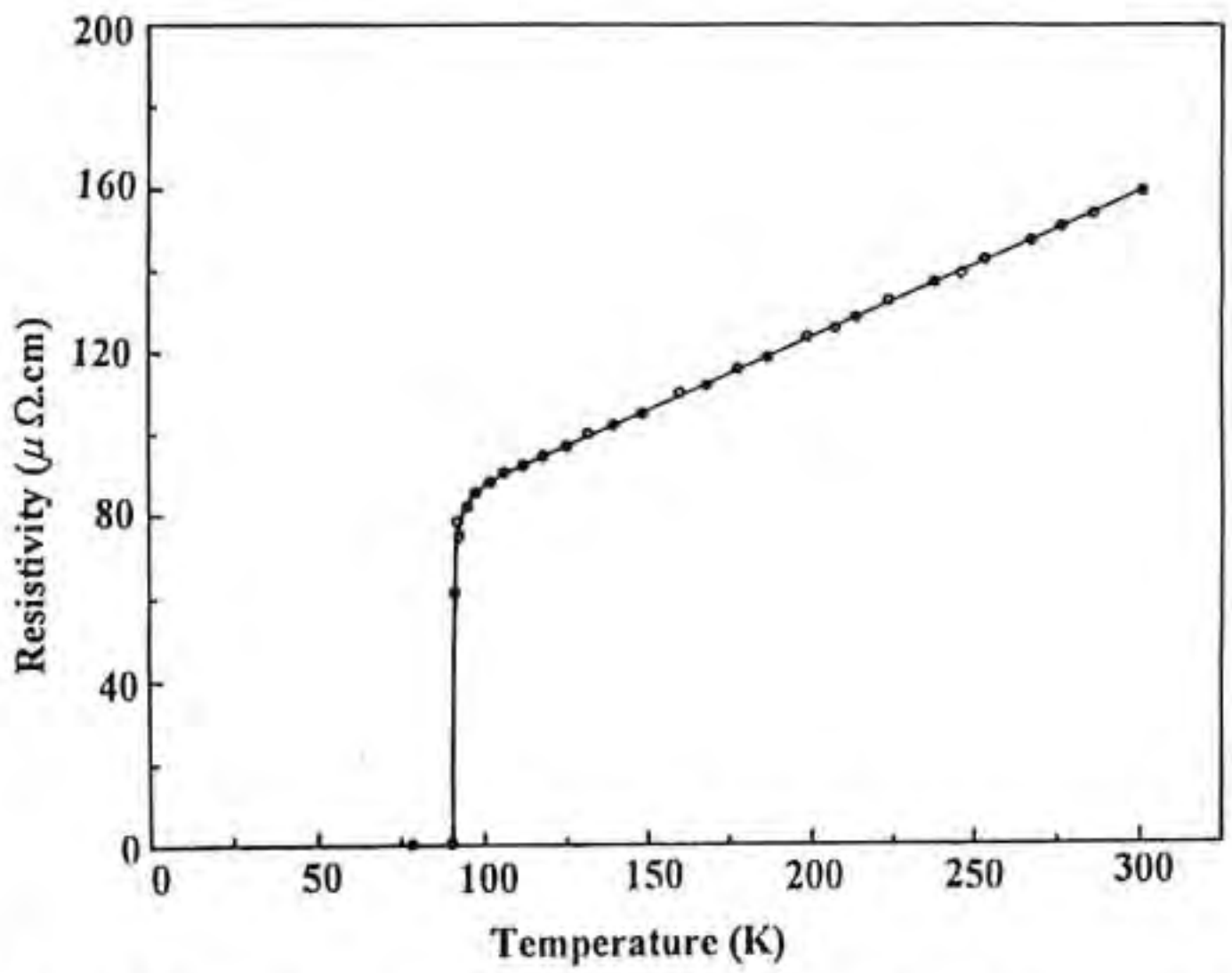

Fig. 6.3(a) Temperature-resistivity curve for laser ablated YBCO thin film on polycrystalline Ba_2NdNbO_6 substrate.

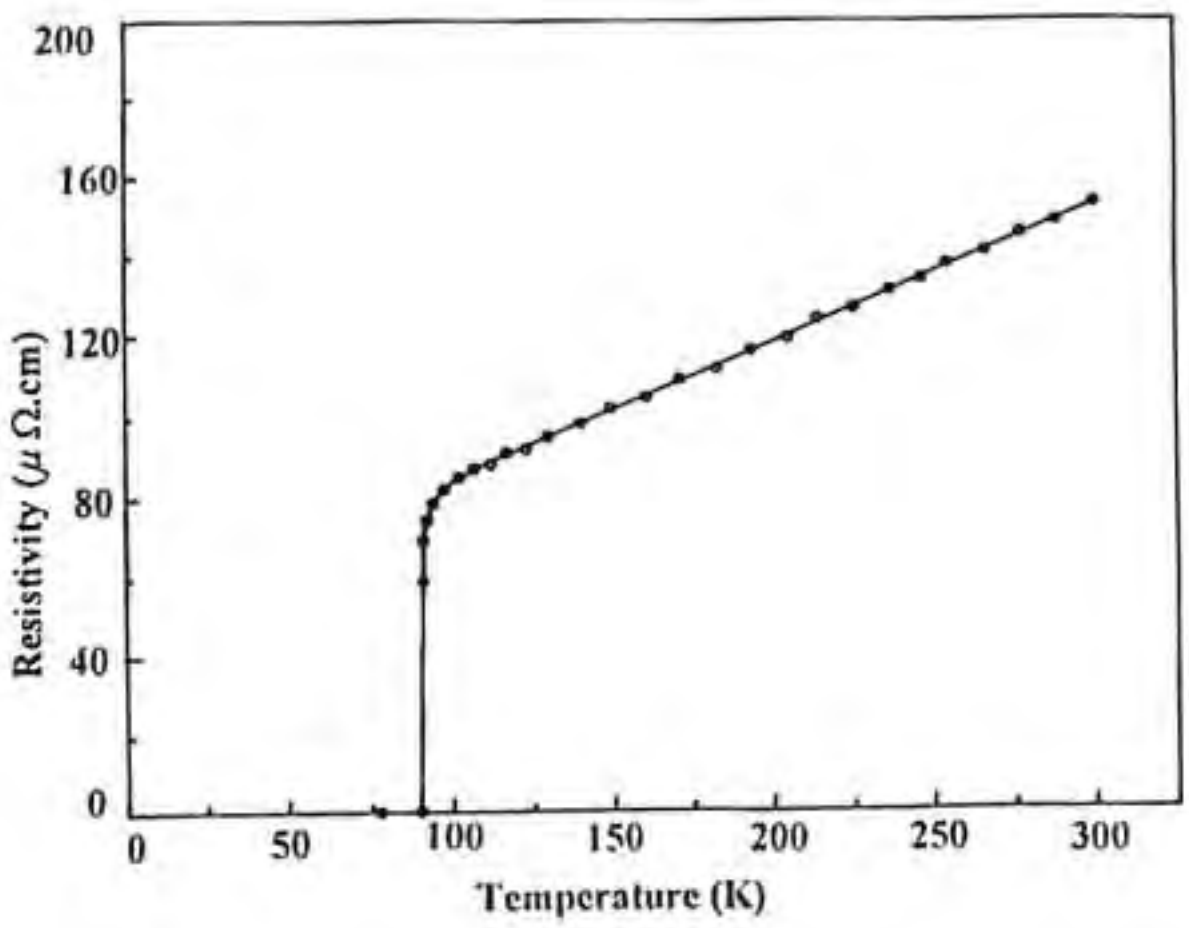

Fig. 6.3(b) Temperature-resistivity curve for laser ablated YBCO thin film on polycrystalline Ba_2SmNbO_6 substrate.

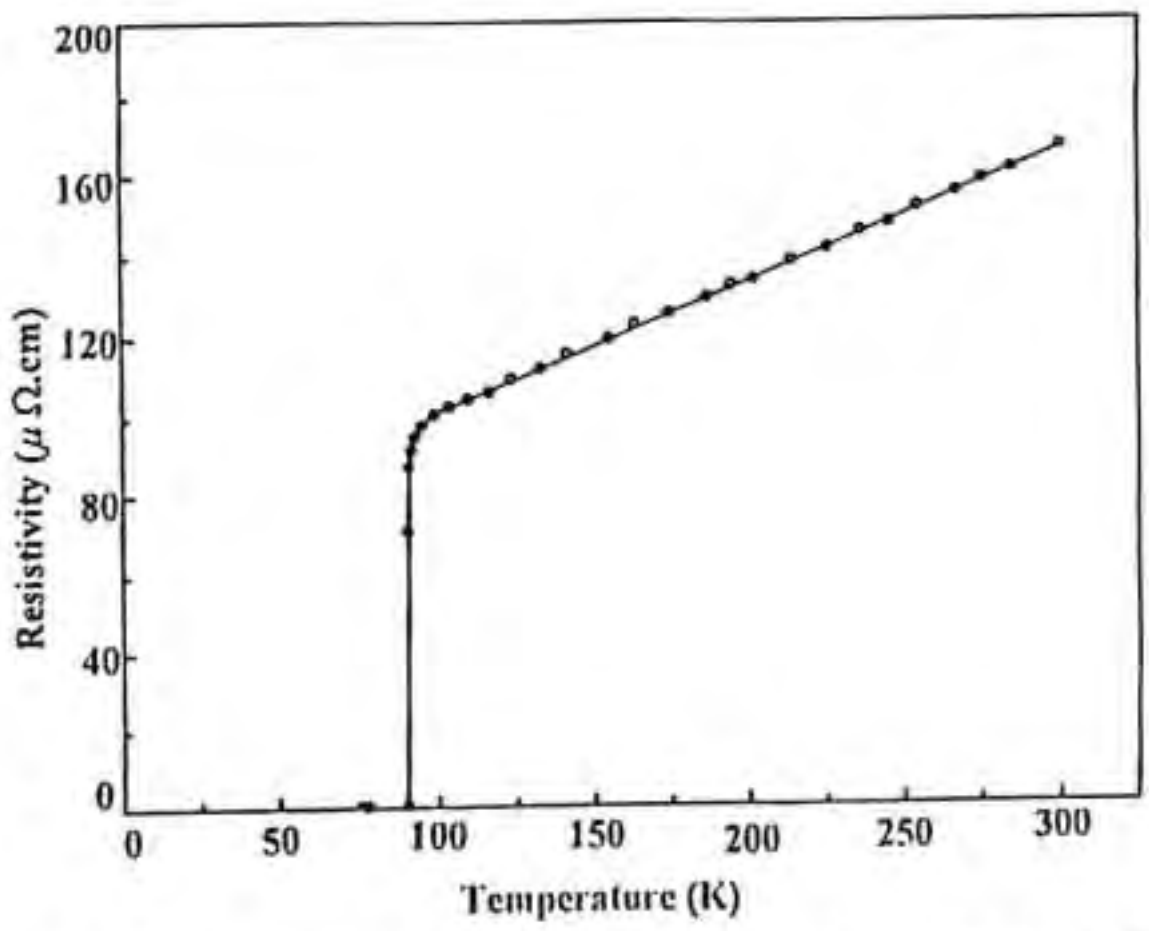

Fig. 6.3(c) Temperature-resistivity curve for laser ablated YBCO thin film on polycrystalline Ba_2EuNbO_6 substrate.

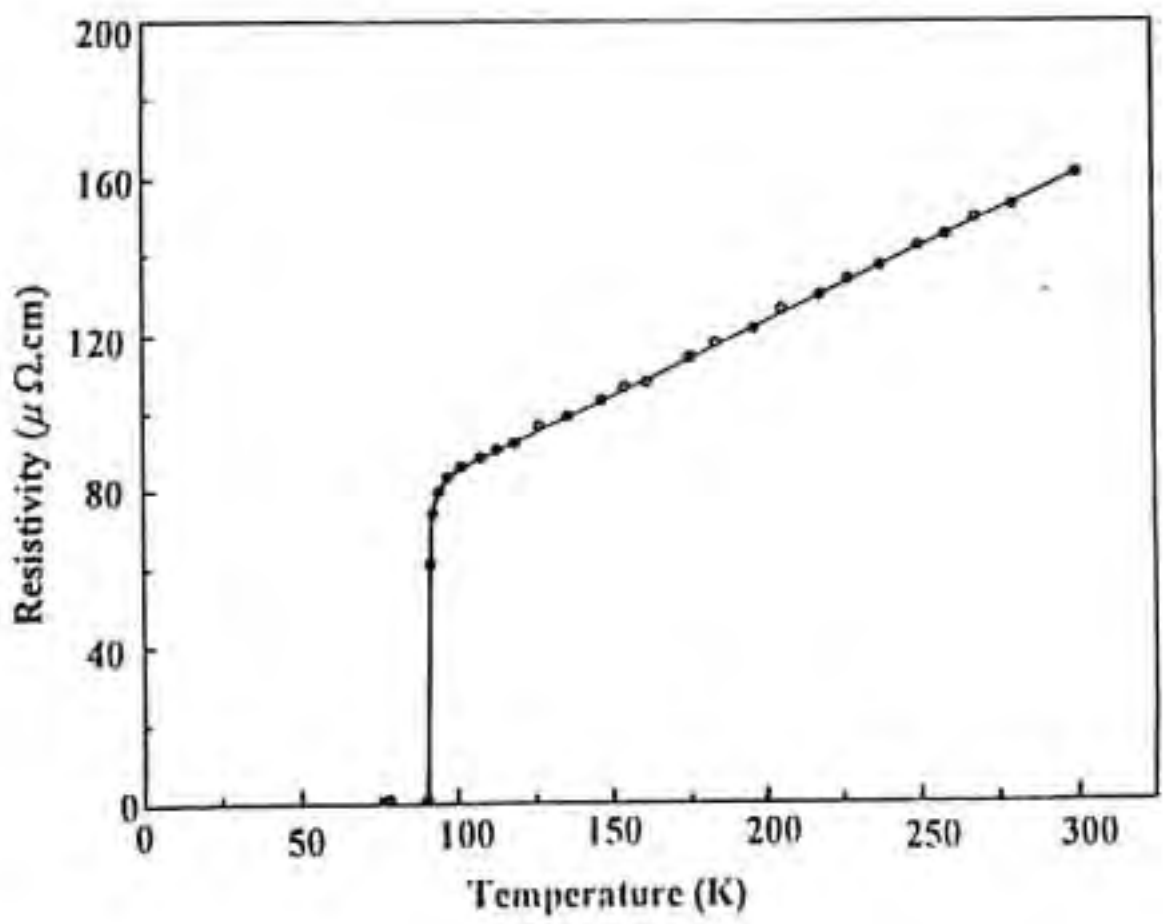

Fig. 6.3(d) Temperature-resistivity curve for laser ablated YBCO thin film on polycrystalline Ba_2GdNbO_6 substrate.

6.4. *In situ* Growth of YBCO-Ag Thin Films on BRENO

It is reported that the critical current density, J_c, of HTSC thin films depends strongly on its microstructure [21-22]. Silver addition has shown considerable benefit in bulk YBCO material [23] as well as in YBCO films. The YBCO-Ag thin films are reported to have better crystallinity, microstructure and low surface resistance and the optimum percentage of Ag in YBCO was reported to be 5 wt.% [24-27]. The YBCO-Ag thin films were grown *in situ* on polycrystalline BRENO substrates also by pulsed laser ablation technique. The procedure adopted for the growth of YBCO-Ag films was similar to that described for the

in situ growth of YBCO thin films in the previous section. The only difference is that the substrate temperature and the target used were different. In the present study, a YBCO-Ag target containing 5 wt% of Ag was used for the preparation of YBCO-Ag thin films. The YBCO-Ag targets containing 5 wt% Ag was prepared by adding appropriate amounts of $AgNO_3$ to phase pure YBCO powder and heating the mixture at 930°C for 24 h. This was then pressed in the form of circular discs with 1.5 cm diameter and ~0.3 cm thickness and sintered at 930°C for 12 h. YBCO-Ag films were *in situ* grown on polycrystalline BRENO substrates at a substrate temperature of 760°C for about 20 to 25 min and cooled in 500 Torr of oxygen after the termination of growth. The energy density of the laser beam for YBCO-Ag film deposition was 2.2 J/cm^2. The YBCO-Ag film thicknesses were about 3000 to 3500 Å.

6.5. Characterisation of YBCO-Ag Thin Films

The structure of the YBCO-Ag thin films *in situ* grown on polycrystalline BRENO substrates was examined by XRD. The XRD patterns of YBCO-Ag thin films *in situ* grown on BRENO are shown in Fig. 6.4. From the Fig. 6.4, it is clear that all the peaks except those of the characteristic peaks of BRENO are due to (00*l*) reflections of an orthorhombic YBCO phase. Also a high degree of c-axis orientation is evident from the XRD patterns of YBCO-Ag films. The peaks corresponding to (00*l*) reflection of YBCO are sharp and intense and are

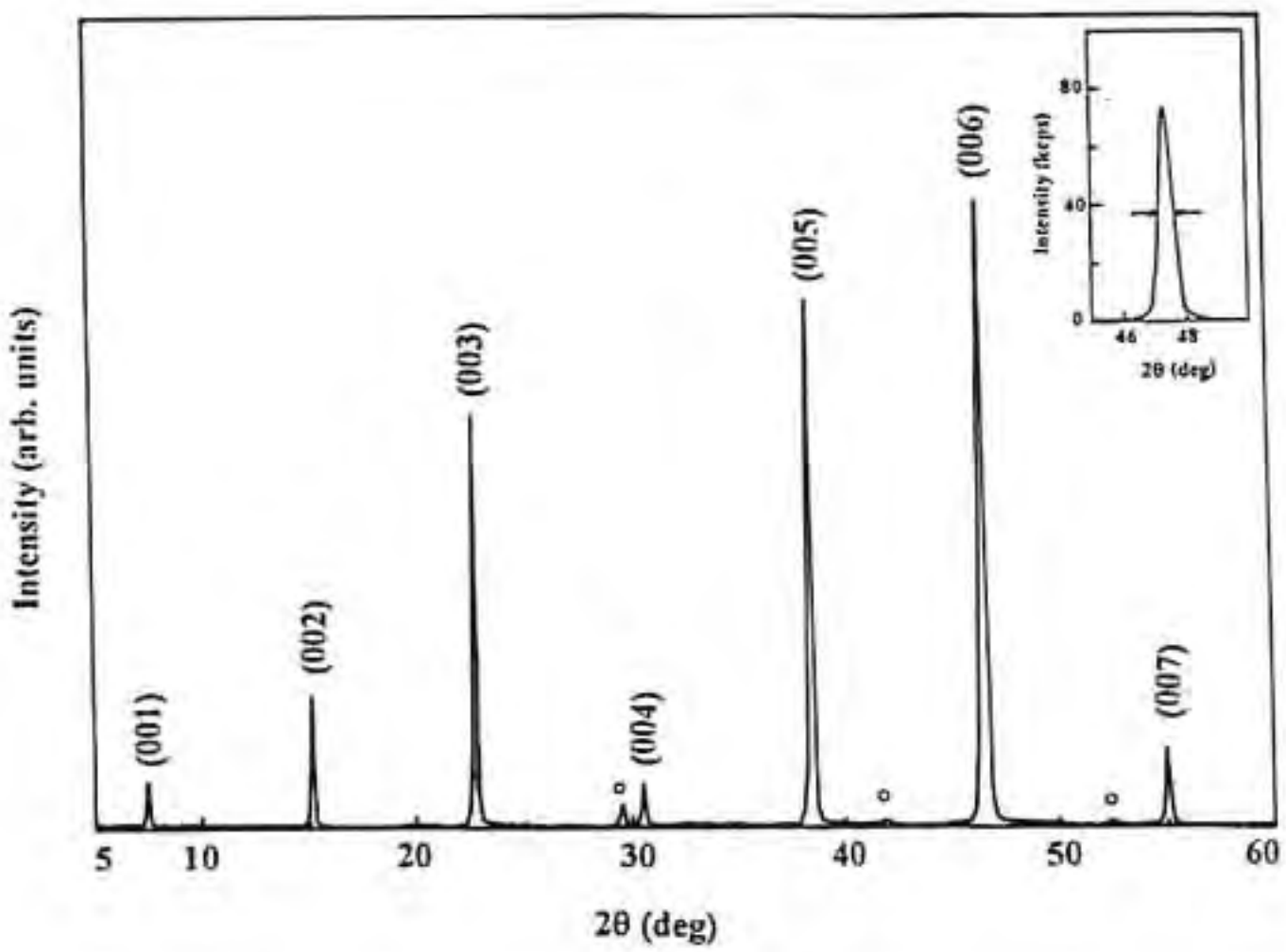

Fig. 6.4(a) The XRD pattern of laser ablated YBCO-Ag thin film on polycrystalline Ba_2NdNbO_6 substrate. The substrate peaks are marked by '∘'.The profile of (006) reflection is superposed showing the intensity in kilocounts per second.

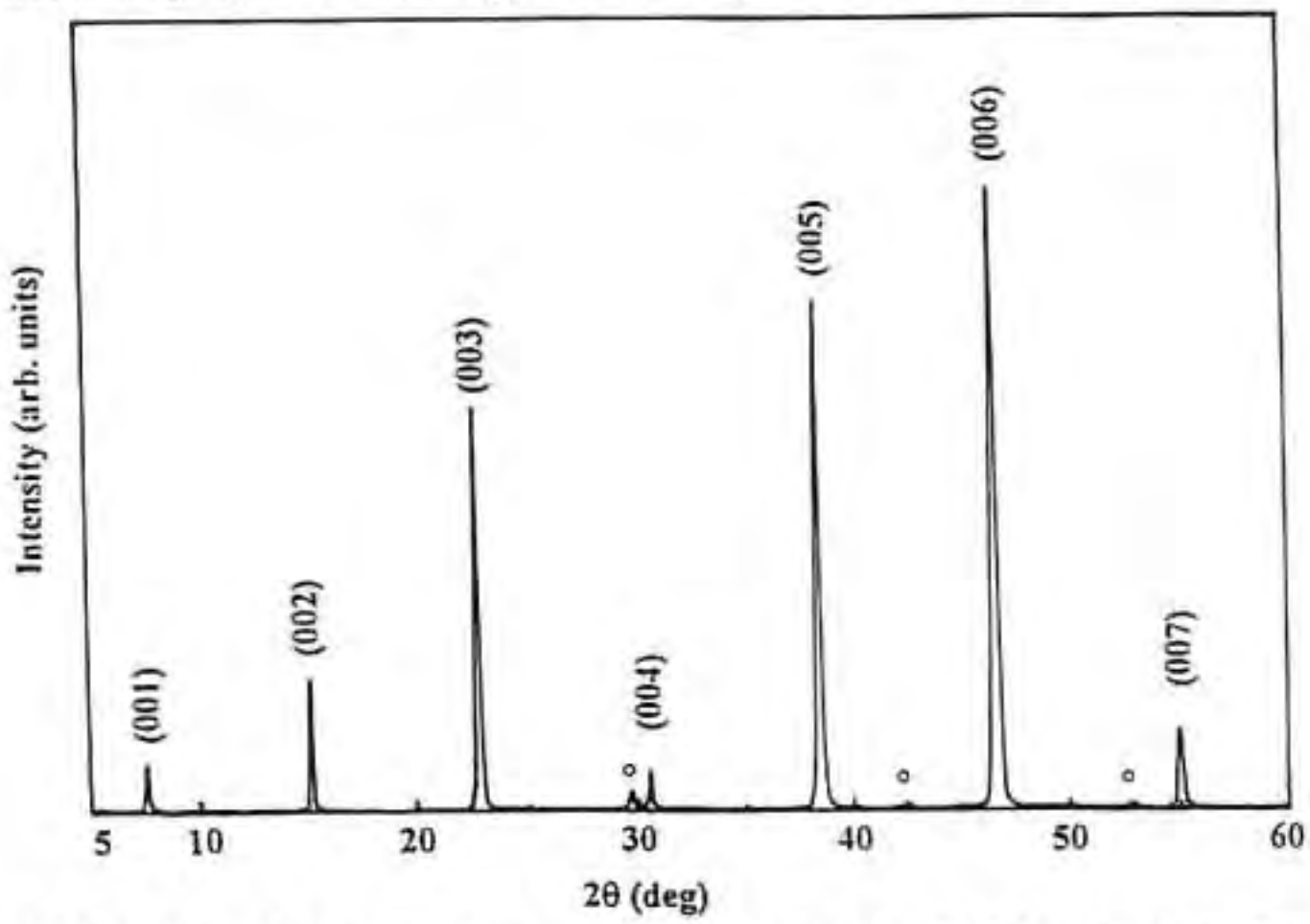

Fig. 6.4(b) The XRD pattern of laser ablated YBCO-Ag thin film on polycrystalline Ba_2SmNbO_6 substrate. The substrate peaks are marked by '∘'.

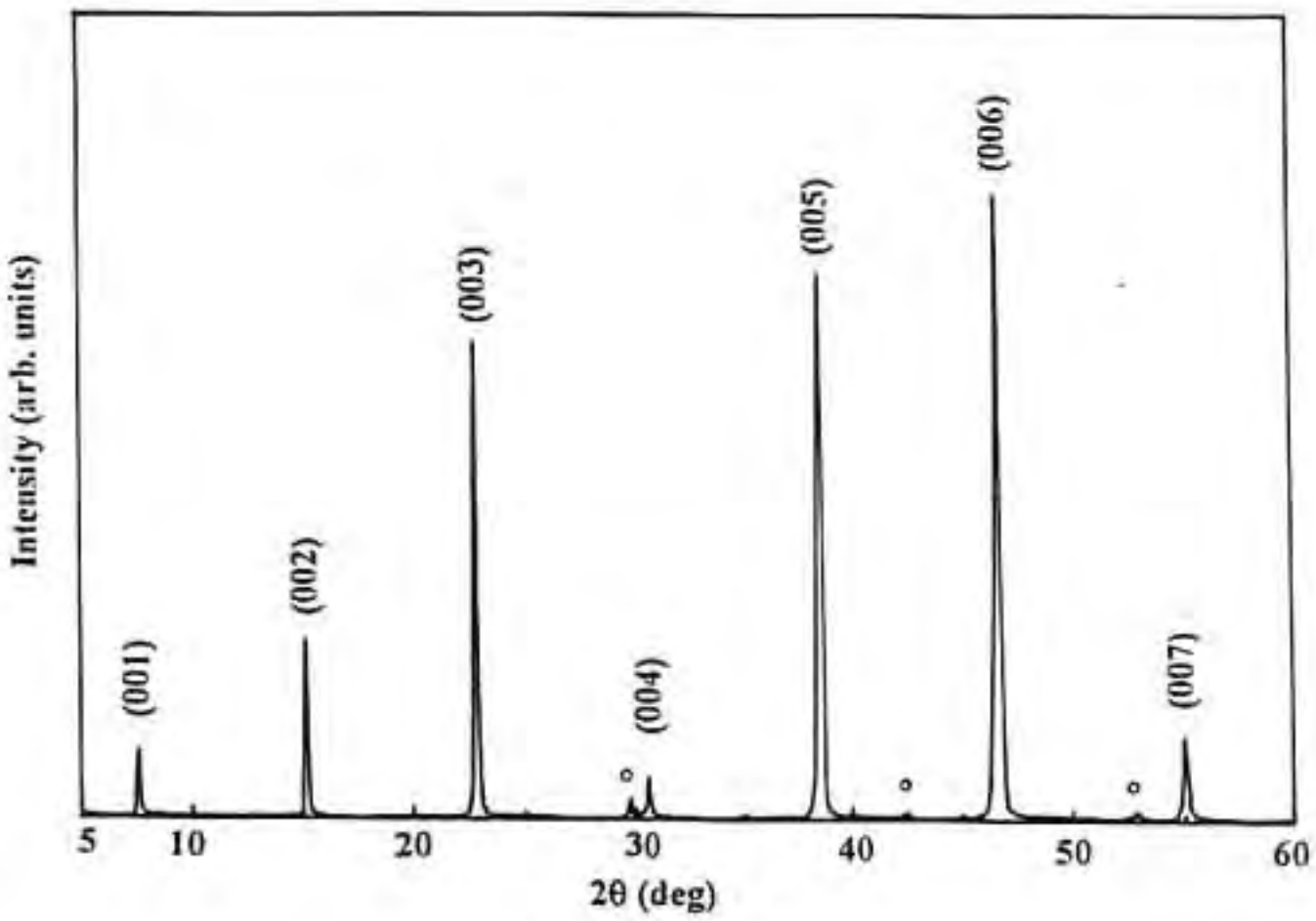

Fig. 6.4(c) The XRD pattern of laser ablated YBCO-Ag thin film on polycrystalline Ba_2EuNbO_6 substrate. The substrate peaks are marked by '∘'.

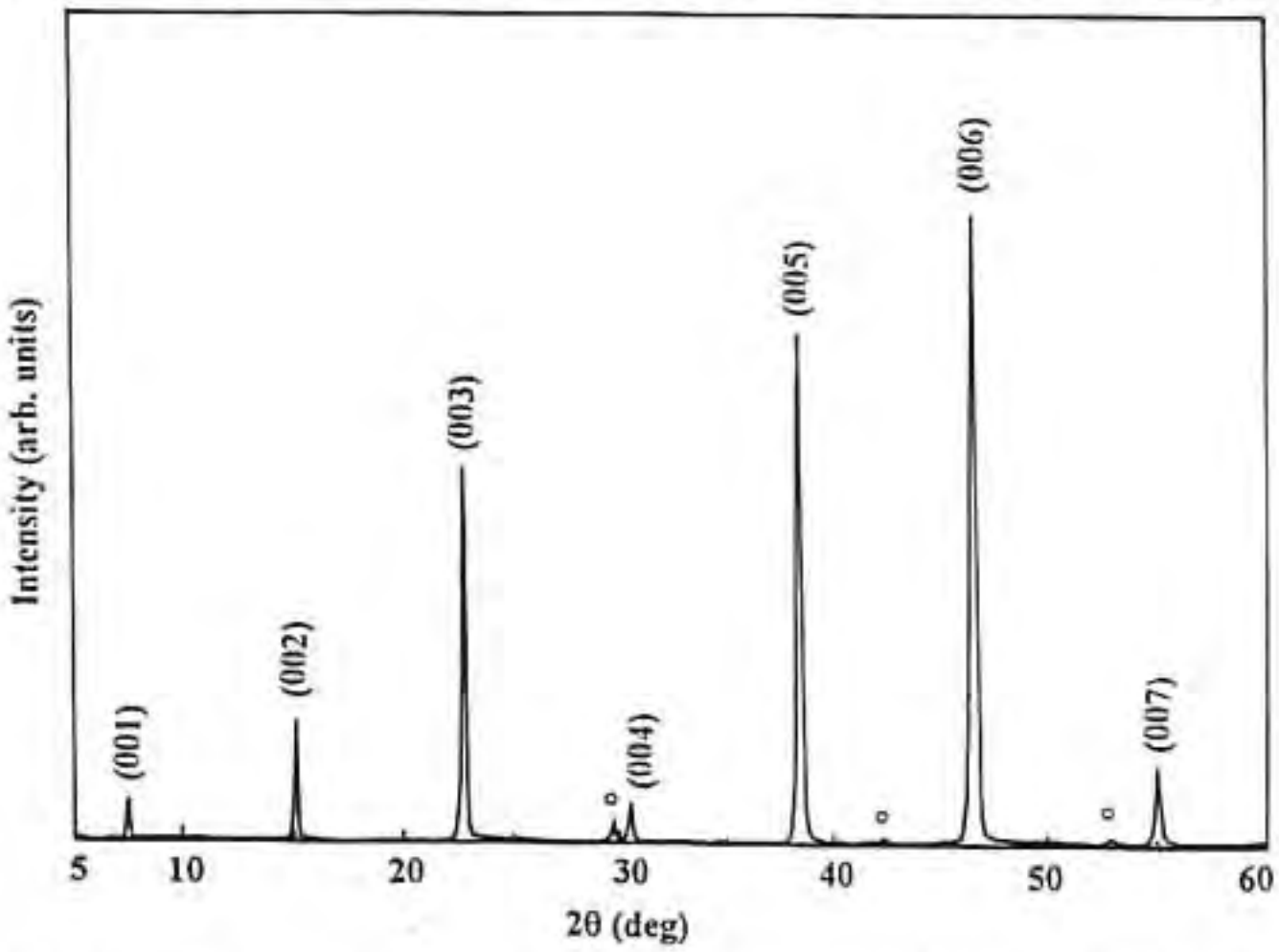

Fig. 6.4(d) The XRD pattern of laser ablated YBCO-Ag thin film on polycrystalline Ba_2GdNbO_6 substrate. The substrate peaks are marked by '∘'.

comparable to those of YBCO-Ag films grown on (100) $LaAlO_3$. This indicates that the YBCO-Ag films grown on BRENO are having good crystallinity. The full width at half maximum (FWHM) of (005) and (006) reflections (measured in 2θ scale) of YBCO in the laser ablated YBCO-Ag thin films on BRENO substrates are given in Table 6.2. It is observed that the intensity of the YBCO peaks (for example the (006) reflection of YBCO) in the YBCO-Ag films on BRENO were about 3 times intense than that of the YBCO films (without Ag) on BRENO. Figure 6.5 shows the typical surface SEM micrograph of YBCO-Ag thin films grown on polycrystalline BRENO substrates by pulsed laser ablation. The microstructure of YBCO-Ag thin films shows marked grain growth and alignment of grains resulting in the formation of smooth and continuous film. Also there was no evidence of any microcrack.

Table 6.2 Full width at half maximum (FWHM) for (005) and (006) reflections in the XRD of YBCO thin films grown on BRENO substrates by laser ablation.

Substrate	FWHM in 2θ scale for	
	(005)	(006)
Ba_2NdNbO_6	0.200	0.249
Ba_2SmNbO_6	0.207	0.251
Ba_2EuNbO_6	0.206	0.250
Ba_2GdNbO_6	0.212	0.255

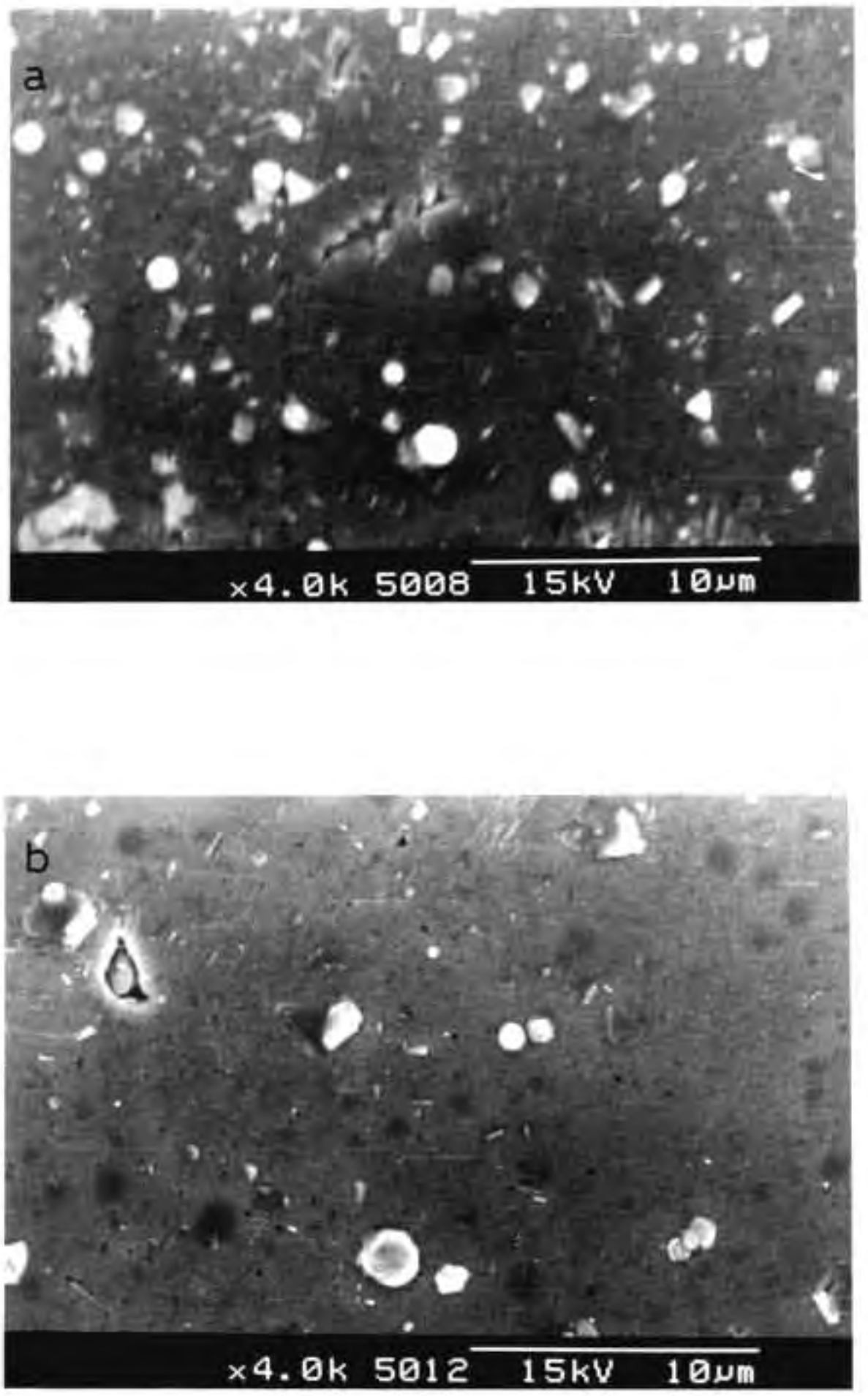

Fig. 6.5 Surface SEM micrograph of laser ablated YBCO-Ag thin films on polycrystalline (a) Ba_2EuNbO_6 and (b) Ba_2GdNbO_6 substrates.

The superconductivity of the YBCO-Ag films on polycrystalline BRENO substrates was studied by temperature-resistance measurements using the standard four probe technique. The temperature-resistivity curves of YBCO-Ag thin films on BRENO are shown in Fig. 6.6. All the films showed metallic behaviour in the normal state and gave a $T_c(0)$ of 90 K. The room temperature resistivity of the YBCO-Ag films were lower than that of YBCO films on BRENO and also the YBCO-Ag films showed better metallicity (ρ_{300K}/ρ_{100K}) when compared with YBCO films without Ag. The J_c of the films estimated at 77 K and zero field were ~ 10^5 A/cm^2. The pulsed laser ablated YBCO-Ag films on polycrystalline BRENO had excellent adhesion to the substrate.

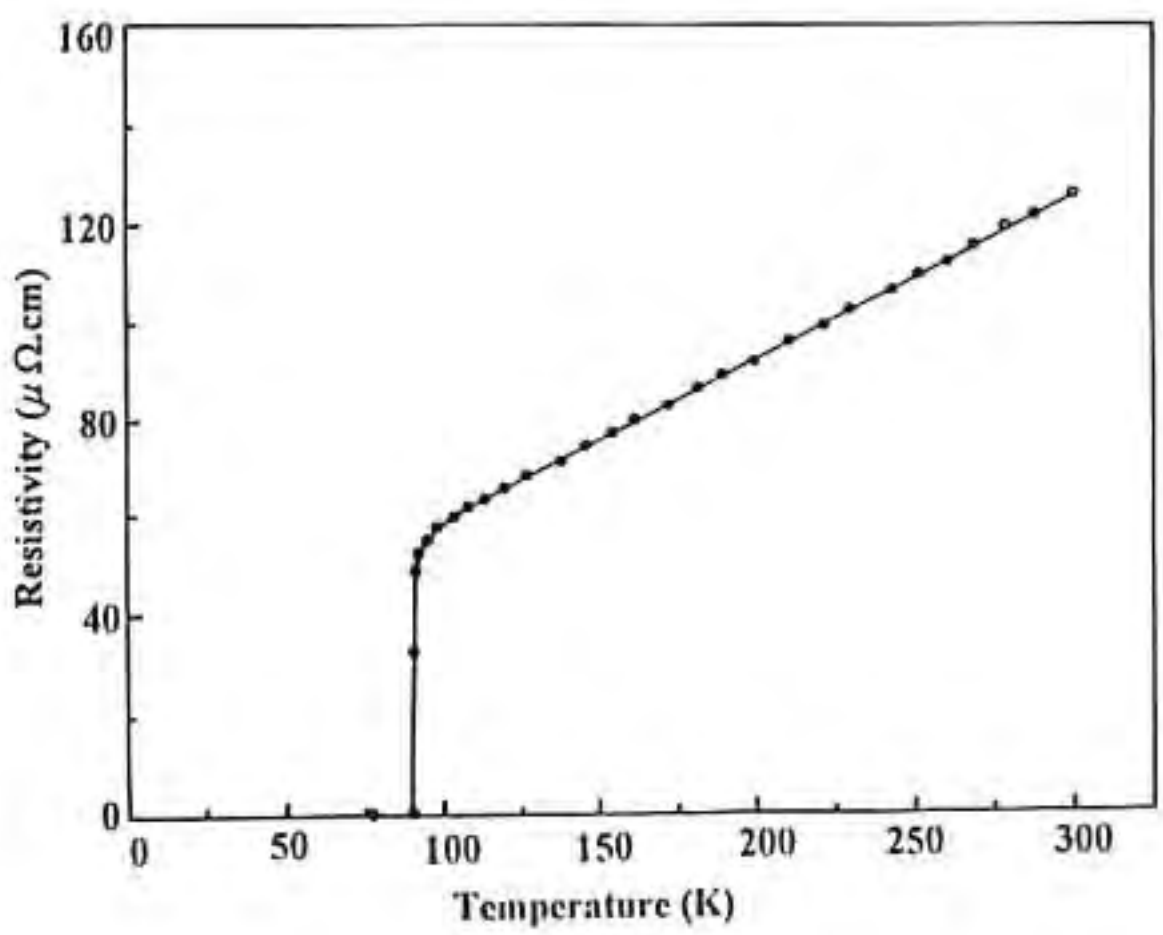

Fig. 6.6(a) Temperature-resistivity curve for laser ablated YBCO-Ag thin film on polycrystalline Ba_2NdNbO_6 substrate.

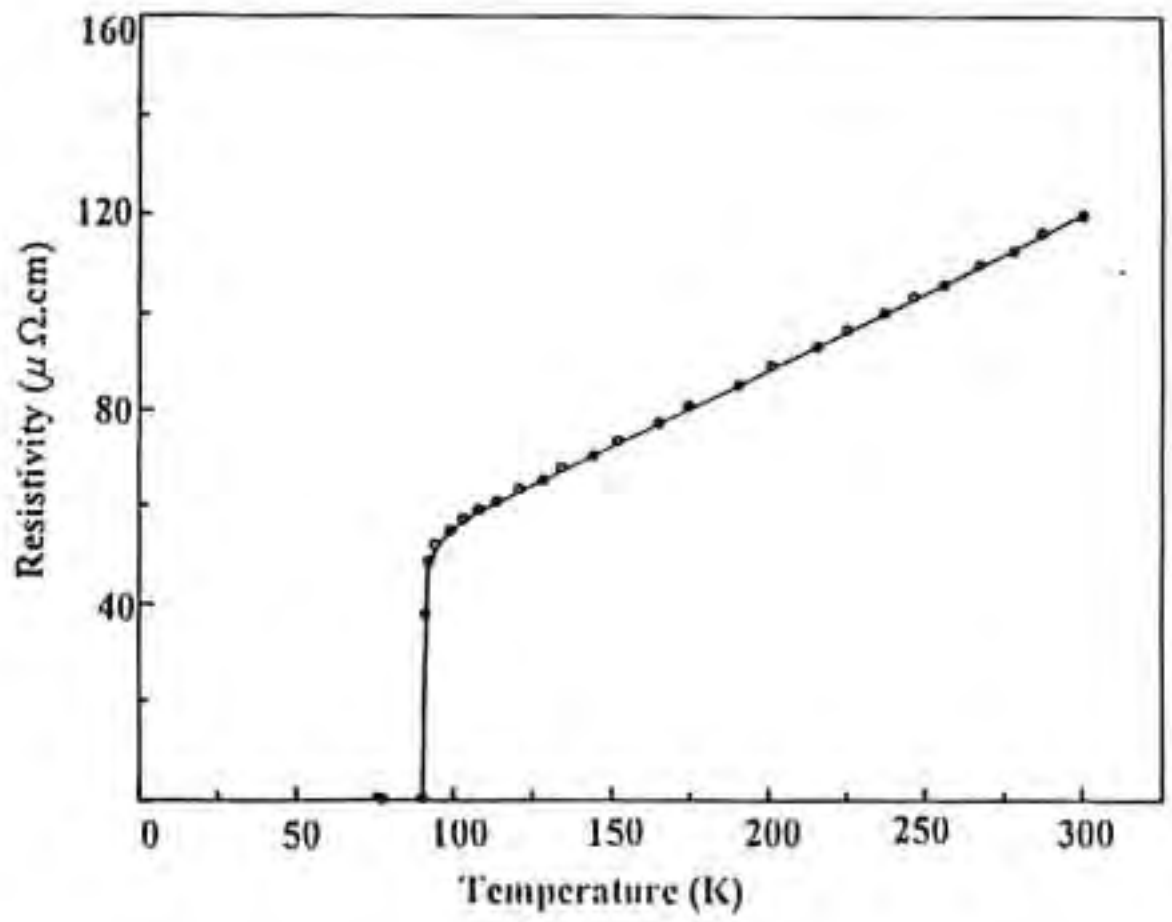

Fig. 6.6(b) Temperature-resistivity curve for laser ablated YBCO-Ag thin film on polycrystalline Ba_2SmNbO_6 substrate.

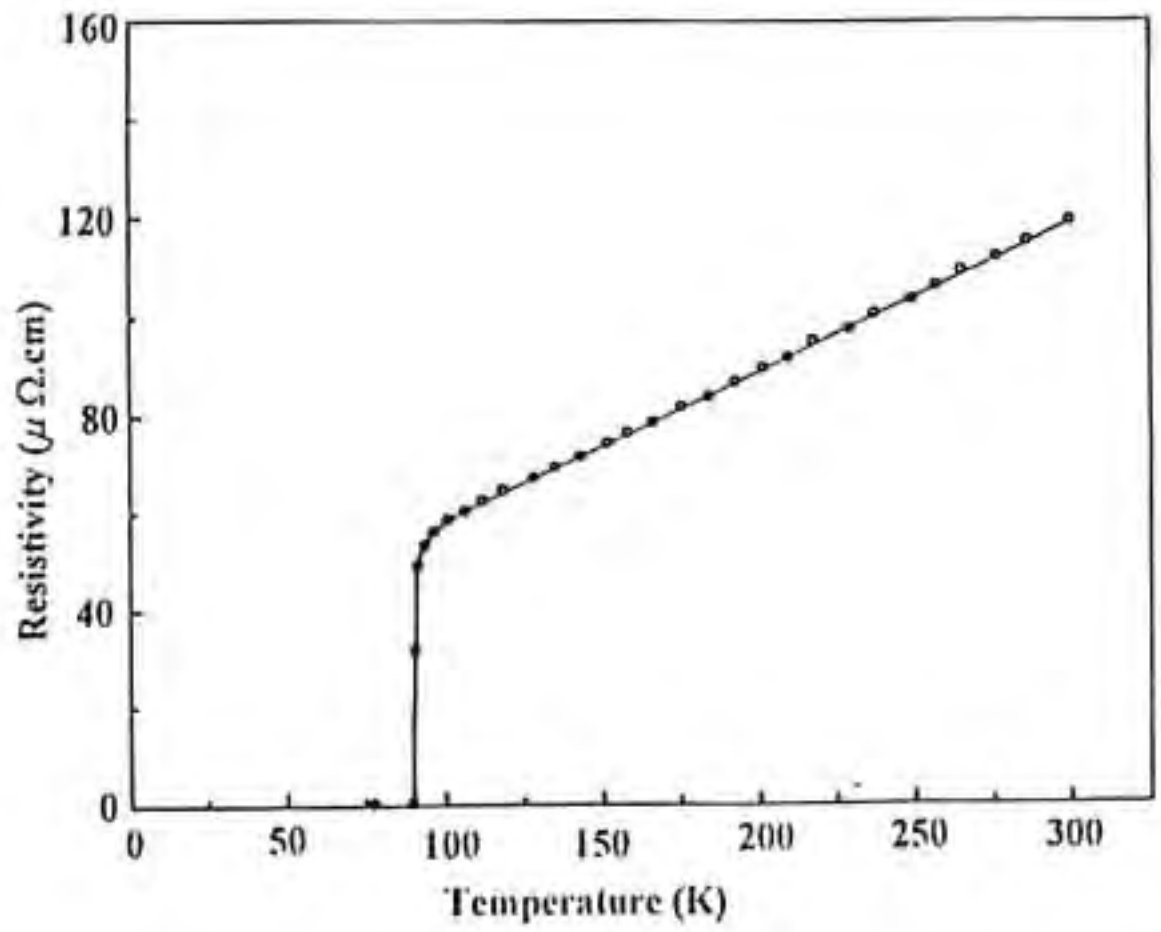

Fig. 6.6(c) Temperature-resistivity curve for laser ablated YBCO-Ag thin film on polycrystalline Ba_2EuNbO_6 substrate.

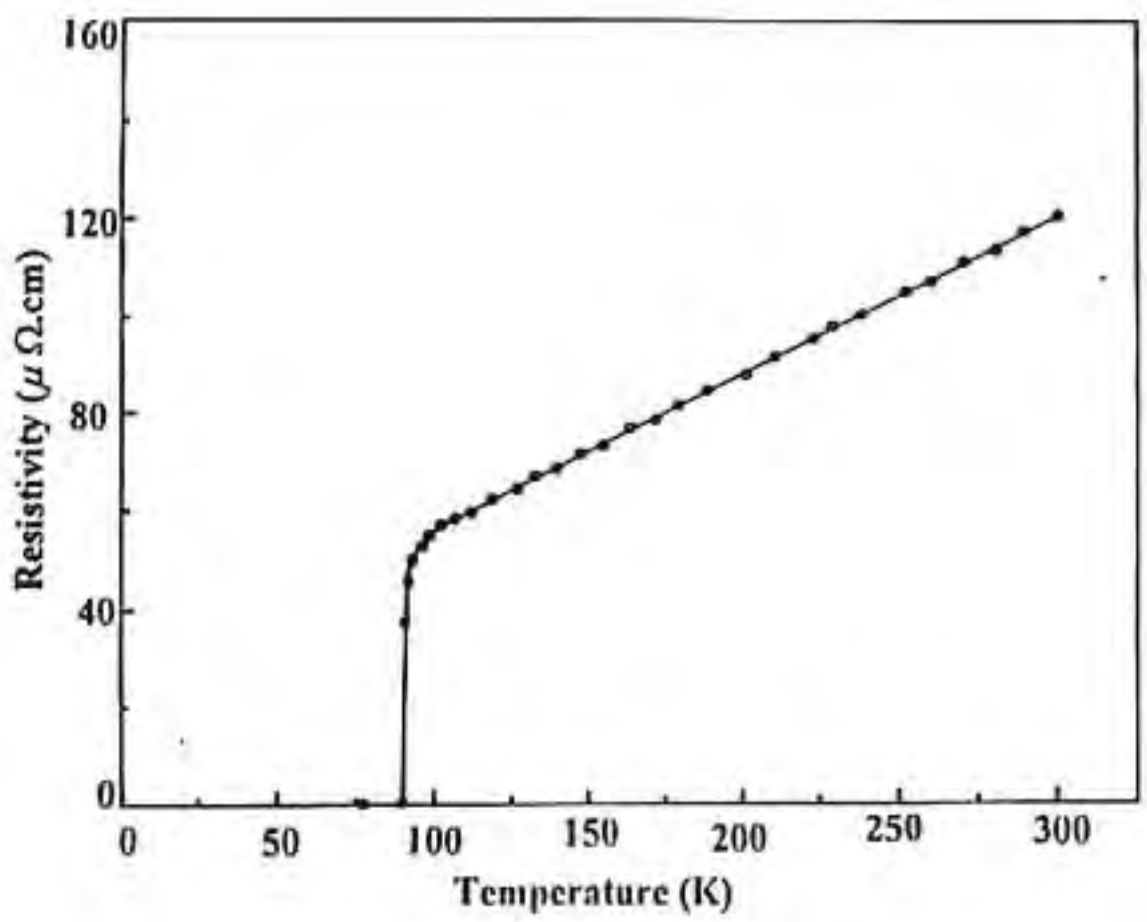

Fig. 6.6(d) Temperature-resistivity curve for laser ablated YBCO-Ag thin film on polycrystalline Ba_2SmNbO_6 substrate.

6.6. Conclusion

Superconducting YBCO and YBCO-Ag thin films were grown on polycrystalline BRENO substrates by pulsed laser ablation technique. The YBCO thin films *in situ* grown on polycrystalline BRENO substrates exhibited (00*l*) orientation of an orthorhombic YBCO phase. The YBCO films grown on BRENO substrates gave $T_C(0)$ of 90 K with a transition width of ~1.5 K and a J_C of ~$3x10^4$ A/cm^2 at 77 K and zero magnetic field. The SEM analysis of the surface of the YBCO thin films grown on BRENO shows no evidence of any microcracks. The YBCO-Ag thin films grown *in situ* on BRENO also exhibited (00*l*) orientation of an orthorhombic

YBCO phase and gave $T_c(0)$ of 90 K with a transition width of ~1.5 K. The J_c values of YBCO-Ag thin films on BRENO were ~10^5 A/cm^2 at 77 K and zero magnetic field. The intensity and width of the (00*l*) reflections of YBCO films on BRENO are comparable to those of YBCO films grown on (100) $LaAlO_3$. It is observed that the addition silver has enhanced the intensity of the peaks corresponding to the (00*l*) reflections of YBCO by about three times when compered with YBCO films grown without silver. Also the critical current density of YBCO thin films has been enhanced by about four times by the addition of silver.

References

1. F.A. Miranda, C.M. Chorey, M.A. Stan, C.E. Nordgen, R.Y. Kwor and T.S. Kalkur, Supercond. Sci. Technol., **5**, 453 (1990).
2. E.K. Hollmann, O.G. Vendik, A.G. Zaitsev and B.T. Melekh, Supercond. Sci. Technol., **7**, 609 (1994).
3. S.R. Foltyn, R.E. Muenchausen, R.C. Dye, X.D. Wu, L. Luo and D.W. Cooke, Appl. Phys. Lett., **59**, 1374 (1991).
4. R. Pinto, P.R. Apte, N. Goyal, L.C. Gupta, R. Vijayaraghavan, K. Easwar and B.K. Sarkar, Appl. Supercond., **1**, 1 (1993).
5. H.Y. To, G.J. Valco and B.K. Bhasin, Supercond. Sci. Technol., **5**, 421 (1992).
6. M. Gurvitch and A.T. Fiory, Appl. Phys. Lett., **51**, 1027 (1987).
7. I.S. Gergis, P.H. Kobrin, J.T. Cheung, E.A. Sovero, C.L. Lastufka, D.S. Deakin and L. Lopez, Physica C, **175**, 603 (1991).
8. D. Kalokitis, A. Fatty, V. Pendrick, E. Belohoubek, A. Findikoglu, A. Inam, X.X. Xi, T. Venkatesan and J.B. Barner, Appl. Phys. Lett., **58**, 537 (1991).
9. J.M. Phillips, J. Appl. Phys., **79**, 1829 (1996).
10. P. Mukhopadhyay, Supercond. Sci. Technol., **4**, 664 (1991) and references therein.
11. P.H. Ballentine, J.P. Allen, M.A. Radin and D.S. Mallory, J. Vac. Sci. Technol. A, **9**, 1118 (1991).
12. P. Berberich, B. Utz, W. Prusseit and H. Kinder, Physica C, **219**, 497 (1994).

13. R.G. Humphreys, J.S. Satchell, N.G. Chew, J.A. Edwards, S.W. Goodyear, S.E. Blenkinsop, O.D. Dosser and A.G. Cullis, Supercond. Sci. Technol., **3**, 38 (1990) and references therein.

14. R.Vaglio, Ceram. Int., **19**, 421 (1993).

15. B.C. Yang, X.P. Wang, C.Q. Wang, R.K. Wang, C.G. Cul and S.L. Li, Supercond. Sci. Technol., **4**, 143 (1991).

16. D.M. Hwang, L. Nazar, T. Venkatesan and X.D. Wu, Appl. Phys. Lett., **52**, 1834 (1988).

17. Q.Y. Ying, H.S. Kim, D.T. Shaw and H.S. Kwok, Appl. Phys. Lett., **55**, 1041 (1989).

18. R.K. Singh, O.W. Holland and J. Narayan, J. Appl. Phys., **68**, 233 (1990).

19. H.V. Krebs, C. Krauns, X. Yang and U. Geyer, Appl. Phys. Lett., **59**, 2180 (1991).

20. R. Pinto, S.P. Pai, C.P. D'Souza, L.C. Gupta, R. Vijayaraghavan, D. Kumar and M. Sharon, Physica C, **196**, 264 (1992).

21. D.H. Shin, J. Silcox, S.E. Russek, D.K. Lathrop, B. Moeckly and R.A. Buhrman, Appl. Phys. Lett., **57**, 508 (1990).

22. A.H. Carim, S.N. Basu and R.E. Muenchausen, Appl. Phys. Lett., **58**, 871 (1991).

23. T.H. Tiefel, S. Jin, R.C. Sherwood, M.E. Davis, G.W. Kammlott, P.K. Gallagher, D.W. Johnson Jr., R.A. Fastnacht and W.W. Rhodes, Mater. Lett., **7**, 363 (1989).

24. R. Pinto, P.R. Apte, S.P. Pai and D. Kumar, Physica C, **207**, 13 (1993).

25. R.K. Singh, D. Bhattacharya, J. Narayan and C.B. Lee, Appl. Phys. Lett., **60**, 255 (1992).

26. R. Pinto, N. Goyal, S.P. Pai, P.R. Apte, L.C. Gupta and R. Vijayaraghavan, J. Appl. Phys., **73**, 5105 (1993).

27. D. Kumar, M. Sharon, R. Pinto, P.R. Apte, S.P. Pai, S.C. Purandare, L.C. Gupta and R. Vijayaraghavan, Appl. Phys. Lett., **62**, 3522 (1993).

CHAPTER 7

PREPARATION AND CHARACTERISATION OF SUPERCONDUCTING Bi(2223) THICK FILMS ON Ba_2RENbO_6 (RE = Gd AND Eu)

7.1. Introduction

The superconducting compound bismuth-strontium-calcium-copper-oxide (BSCCO) has been attractive for practical applications mainly because of its high transition temperature ($T_c(0)$ = 110 K) and high environmental stability [1]. Earlier the advancement of research on industrial application of this material was sidelined by the fact that the Bi-system has two co-existing superconducting phases with T_c of 85 K {the low T_c phase or Bi(2212)} and 110 K {the high T_c phase or Bi(2223)}, and the synthesis of single phase Bi(2223) was very difficult [1-2]. Usually after firing of the Bi-system, a mixture of superconducting and non-superconducting phases are obtained [3-4]. Also, long firing times and a narrow processing temperature window are needed to obtain a high concentration of the high T_c phase [5-6]. Later it was found that the partial substitution of bismuth by lead stabilises the Bi(2223) phase and increases drastically its volume fraction [7-9]. As in the case of YBCO superconductor, the immediate applications of BSCCO superconductors are also mostly in the form of films in microelectronics, for example, superconducting quantum interference device (SQUID) instruments, interconnects for high speed analogue and digital signal processing,

sensitive infrared sensors etc. [2]. As mentioned in Chapter 3, the substrate plays a vital role in the preparation of superconducting films and the high chemical reactivity of the superconductor with most of the commonly available substrates imposes severe restrictions on the materials available as substrates for high temperature superconductors. The commonly available substrates such as Si, SiO_2, Al_2O_3, ZrO_2, etc. react with BSCCO superconductor film at the processing temperature, thereby reducing the transition temperature of the film drastically [10]. MgO is the most widely reported substrate material for BSCCO and YBCO superconductors. However, even on MgO substrate, the BSCCO films contained both the low T_c and high T_c phases [11-12]. This chapter describes in detail the studies on the chemical compatibility of $Ba_2R_ENbO_6$ (R_E = Pr, Nd, Sm, Eu and Gd) with Bi(2223) superconductor by X-ray diffraction studies and temperature-resistivity measurements. The development and characterisation of superconducting BSCCO thick films on polycrystalline BR_ENO substrates are also presented in this chapter.

7.2. Preparation of Bi(2223) Superconductor

Single phase Bi(2223) used in the present study was prepared by conventional solid state reaction method. High purity (99.9%) Bi_2O_3, PbO, $SrCO_3$, $CaCO_3$ and CuO were weighed in the precise stoichiometric ratio of $(Bi_{1.5}Pb_{0.5})Sr_2Ca_2Cu_3O_x$ and the precursor powder was thoroughly wet mixed in an agate mortar with acetone as the wetting medium. The mixture

was dried in an oven and the dried powder was calcined in air at 800°C for 36 h with three intermediate grindings, and cooled slowly at a rate of 2°C/min to room temperature. The finely ground calcined powder was pressed in the form of circular discs with dimensions of 13 mm diameter and ~1.5 mm thickness by applying a pressure of ~300 MPa. These discs were then sintered in air at 850°C for 200 h continuously and the sintered samples were then cooled slowly at a rate of 1°C/min from the sintering temperature to 800°C and finally furnace cooled to room temperature. The phase purity of the Bi(2223) samples were checked by X-ray diffraction and the XRD data was compared with the available standard data and found that they belong to phase pure Bi(2223) superconductor. The superconductivity of the samples were studied by temperature-resistivity measurements which gave a $T_C(0)$ of 109 K. These phase pure Bi(2223) samples were used for the chemical reactivity studies of Ba_2ReNbO_6 (BReNO) with Bi(2223) superconductor and for the preparation of superconducting Bi(2223) thick films.

7.3. Chemical Compatibility study between BReNO and Bi(2223)

The chemical reactivity of BReNO with Bi(2223) was studied up to a temperature of 850°C by powder X-ray diffraction technique. Also the effect of BReNO addition on the superconductivity of Bi(2223) superconductor was examined by temperature-resistivity measurements.

7.3.1. Preparation of Bi(2223)-BRENO composites

The chemical reactivity between BRENO and Bi(2223) was studied by thoroughly mixing 40 vol% of Bi(2223) with BRENO and the composite mixture was pressed in the form of circular discs with dimensions of 10 mm diameter and ~1.5 mm thickness by applying a pressure of ~300 MPa. These circular discs were then annealed in air at 850°C for 10 h and slow cooled at a rate of 1°C/min up to 800°C from the sintering temperature of 850°C and then furnace cooled to room temperature. The Bi(2223)-BRENO composites were then characterised by X-ray diffraction and temperature-resistivity measurements.

7.3.2. X-ray Diffraction Studies of Bi(2223)-BRENO Composites

The X-ray diffraction (XRD) patterns of Bi(2223)-BRENO composites containing 40 vol% of Bi(2223) annealed at 850°C for 10 h are shown in Fig. 7.1(b) to 7.1(f). Figure 7.1(a) shows the XRD pattern of pure Bi(2223) given for comparison. From the XRD patterns of annealed Bi(2223)-BRENO composites containing 40 vol% of Bi(2223), it is clear that Ba_2GdNbO_6 (BGNO) and Ba_2EuNbO_6 (BENO) does not react with Bi(2223) as no other peaks other than that of the characteristic peaks of BGNO or BENO and Bi(2223) are observed. It may be noted that even Bi(2212) phase is not formed even after annealing Bi(2223)-BGNO and Bi(2223)-BENO composites at 850°C for 10 h. On the other hand, the XRD patterns of the annealed Bi(2223)-Ba_2PrNbO_6, Bi(2223)-Ba_2NdNbO_6 and Bi(2223)-Ba_2SmNbO_6 composites shows the presence of Bi(2212) phase in addition to the characteristic peaks of Bi(2223) and BRENO. It may be noted that the

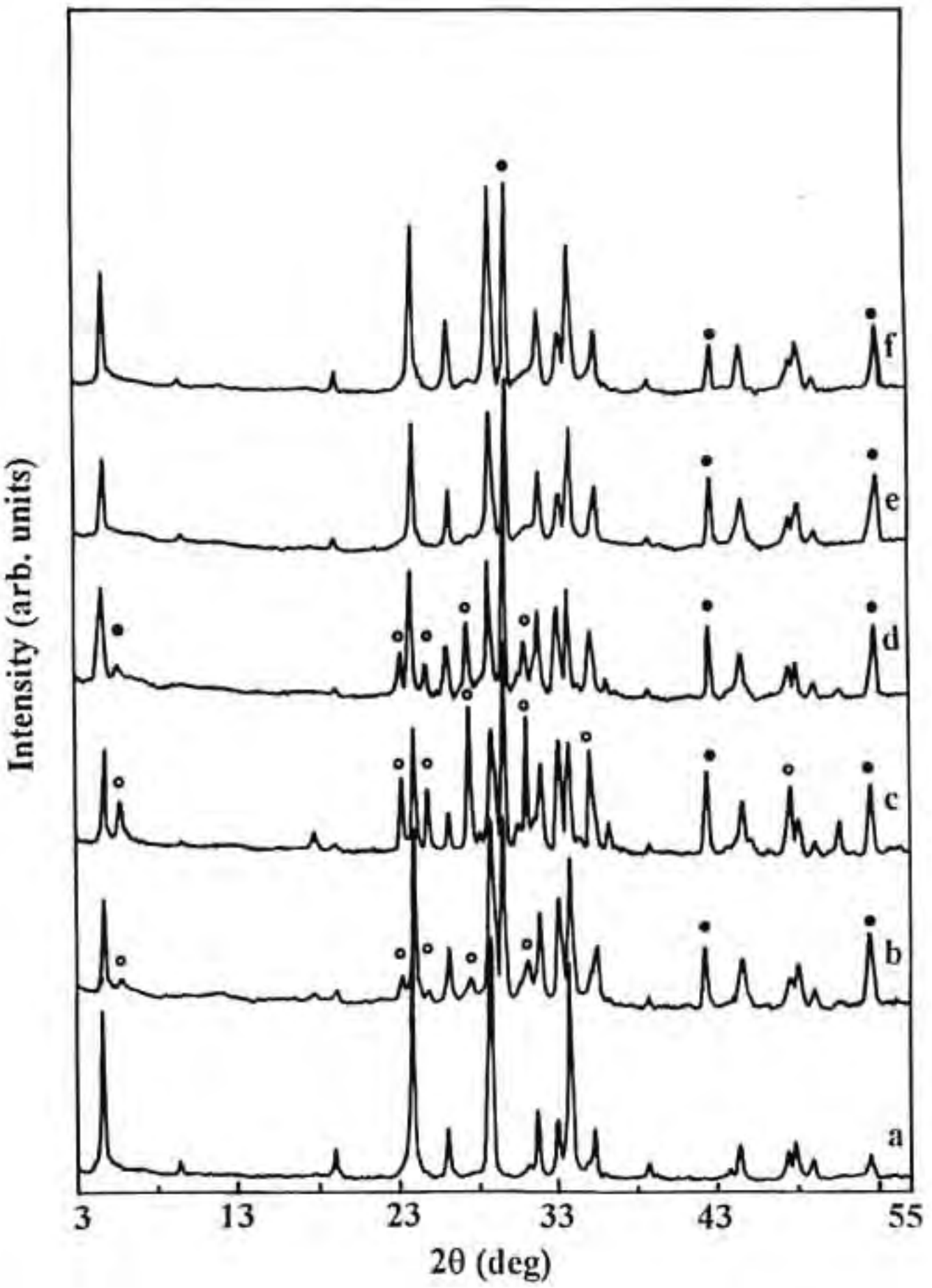

Fig. 7.1 Powder X-ray diffraction patterns of (a) pure Bi(2223), (b) 2:3 volume mixture of Bi(2223) and Ba_2PrNbO_6, (c) 2:3 volume mixture of Bi(2223) and Ba_2NdNbO_6, (d) 2:3 volume mixture of Bi(2223) and Ba_2SmNbO_6 (e) 2:3 volume mixture of Bi(2223) and Ba_2EuNbO_6 and (f) 2:3 volume mixture of Bi(2223) and Ba_2GdNbO_6; all annealed at 850°C for 10 h in air.

formation of Bi(2212) is maximum for Bi(2223)-Ba_2NdNbO_6 and next for Bi(2223)-Ba_2SmNbO_6 and least for Bi(2223)-Ba_2PrNbO_6 among these three composites. However, in all the cases, there were no additional phases formed other than those of Bi(2212), Bi(2223) and BREnO (within the precision of powder X-ray diffraction technique) in the Bi(2223)-BREnO composites. The XRD results indicate that Ba_2GdNbO_6 and Ba_2EuNbO_6 are chemically non-reacting with Bi(2223) superconductor even at the extreme annealing conditions and hence can be used as substrates for Bi(2223) superconductor films. On the other hand Ba_2SmNbO_6, Ba_2NdNbO_6 and Ba_2PrNbO_6 may be used as substrates for Bi(2212) superconductor as there were no other phases formed other than those of Bi(2223), Bi(2212) and BREnO in the annealed Bi(2223)-BREnO composites.

7.3.3. Temperature-resistivity measurements of Bi(2223)-BREnO composites

The effect of BREnO addition on the superconducting property of Bi(2223) was studied by temperature-resistivity measurements of the Bi(2223)-BREnO composites following the standard four probe technique. A Keithley current source model 220 and a Keithley nanovoltmeter model 181 were used for resistance measurements. The temperature of the composite samples were measured by a calibrated copper constantan thermocouple. Figure 7.2 shows the temperature-resistivity curves for Bi(2223)-BREnO composite samples containing 40 vol% of Bi(2223)

annealed at 950°C for 10 h. A zero-resistivity superconducting transition temperature [$T_C(0)$] of 109 K was obtained in all the composites except for Bi(2223)-Ba_2NdNbO_6 composite. In the case of Bi(2223)-Ba_2NdNbO_6 composite, no superconducting transition was observed up to 77 K. From the Fig. 7.2, it is clear that the addition of BRENO (where RE = Gd, Eu, Sm & Pr) did not have any detrimental effect on the superconducting transition temperature of Bi(2223) even after severe heat treatment.

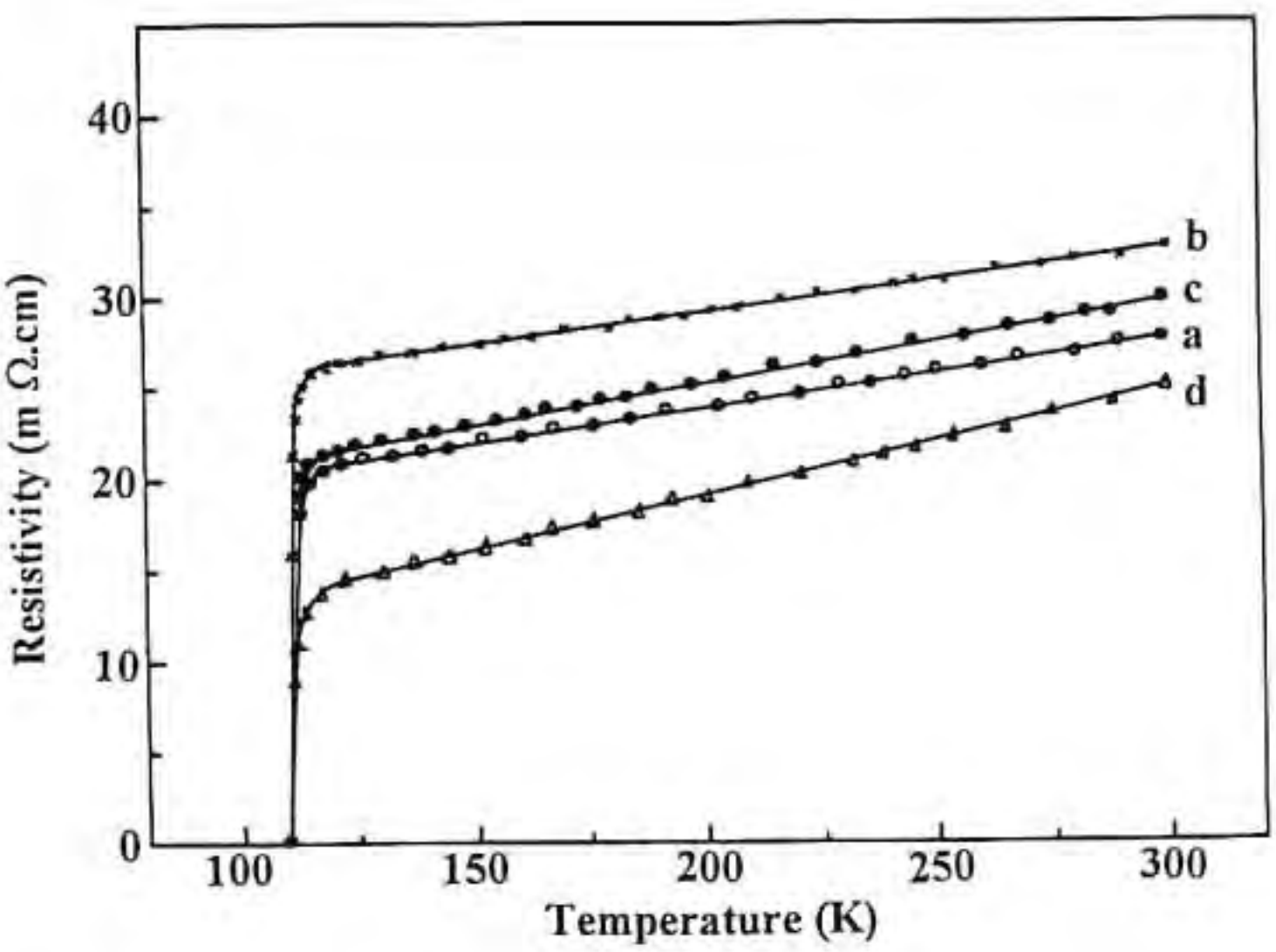

Fig. 7.2 Temperature-resistivity curves for Bi(2223)-Ba_2RENbO_6 composites containing 40 vol% of (a) Ba_2PrNbO_6, (b) Ba_2SmNbO_6, (c) Ba_2EuNbO_6 and (d) Ba_2GdNbO_6 annealed at 850°C for 10 h in air.

7.4. Preparation of Bi(2223) Thick Films on BREnO by Dip-coating

The suitability of BREnO (RE = Gd & Eu) as a substrate for Bi(2223) was confirmed by developing Bi(2223) thick films on BREnO by dip-coating method. The thick film suspension of Bi(2223) for dip-coating was prepared by mixing fine superconducting Bi(2223) powder with isopropyl alcohol or n-butanol and the viscosity of the suspension was controlled by the addition of commercially available fish oil. The polished and cleaned BREnO substrate was then dipped in the Bi(2223) suspension and dried. This procedure was repeated till the required thickness is obtained. The dip-coated films were then dried in an oven and heated in a programmable furnace at a rate of 5°C/min in air up to 880°C. The films were annealed at 880°C for ~2 min and then cooled at a rate of 1°C/min to 850°C and then annealed at this temperature for 6 h. The films were cooled at a rate of 1°C/min up to 800°C from the annealing temperature of 850°C and then furnace cooled to room temperature. A diagrammatic representation of the heating and cooling schedule adopted for the processing of Bi(2223) thick films is shown in Fig. 7.3. The films were characterised by XRD and temperature-resistance measurements.

7.5. Characterisation of Bi(2223) Thick Films

The structure of the dip-coated Bi(2223) thick films on BREnO was examined by XRD. Figure 7.4 shows that except for the characteristic peaks of BREnO, all other peaks are those of Bi(2223). The phase purity of Bi(2223) was also confirmed by calculating the volume fraction of

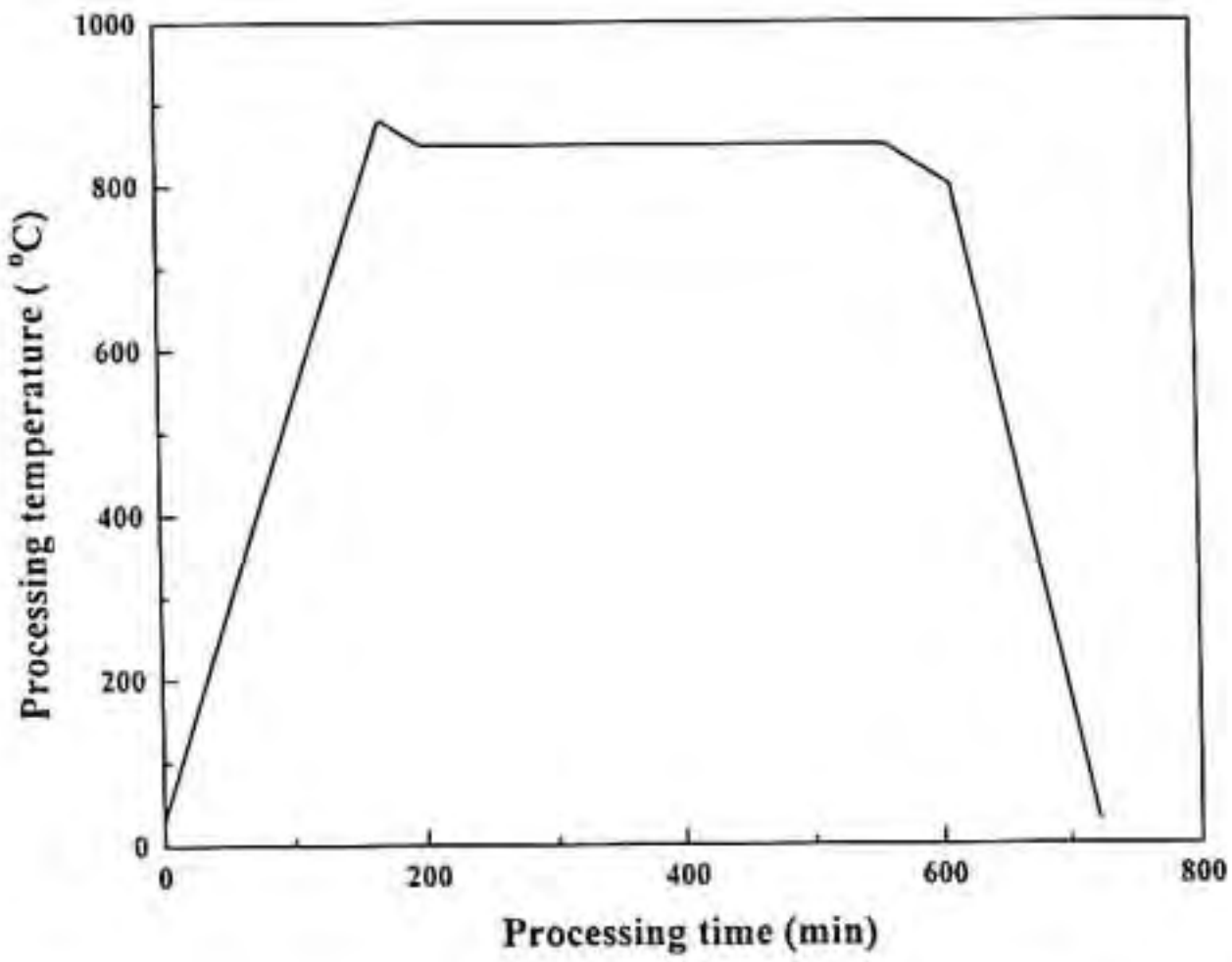

Fig. 7.3 Heating and cooling schedule adopted for the preparation of Bi(2223) thick films on BRENO substrates.

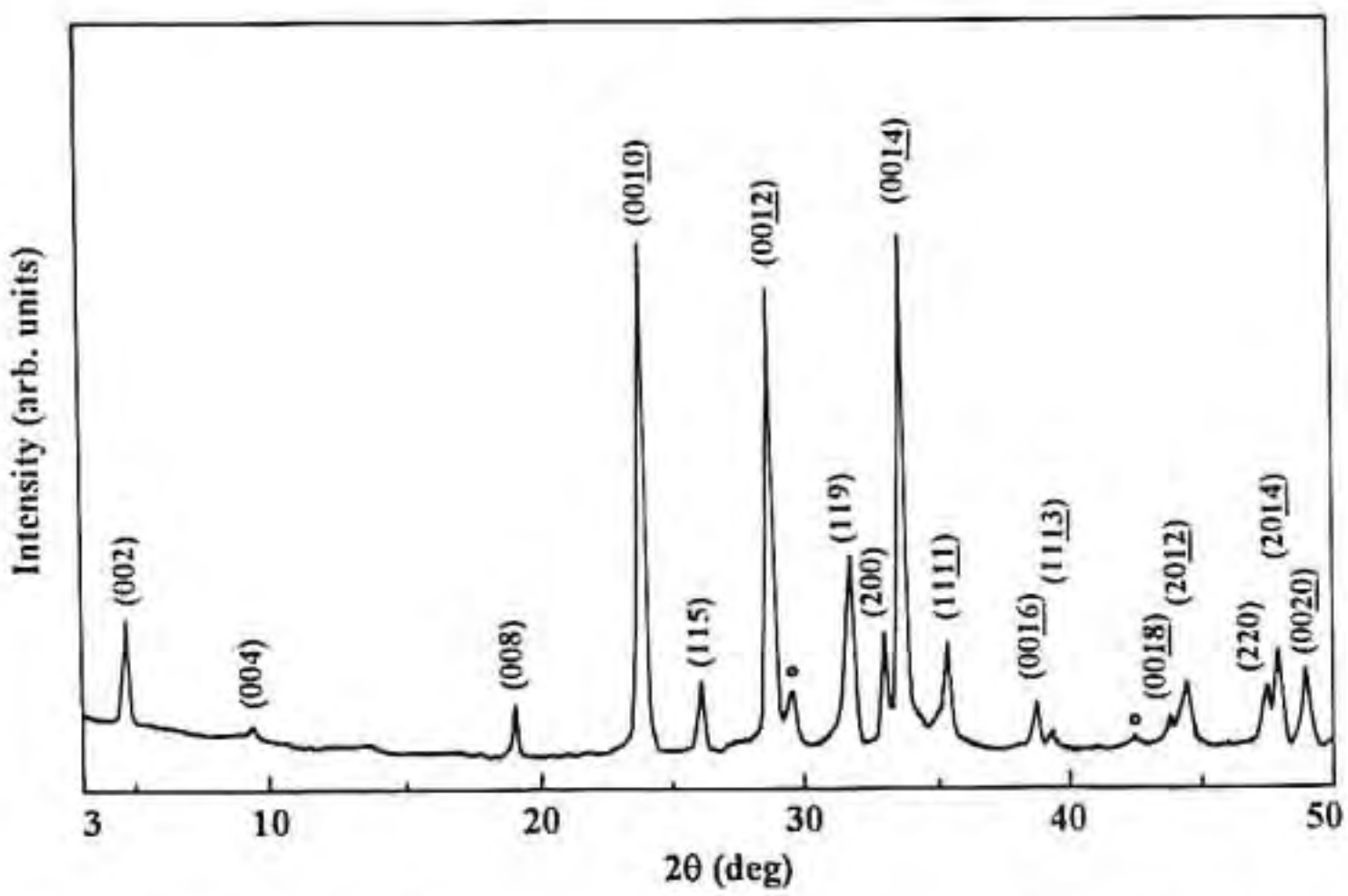

Fig. 7.4(a) The X-ray diffraction pattern of dip-coated Bi(2223) thick film on Ba_2GdNbO_6 substrate. The substrate peaks are marked by '∘'.

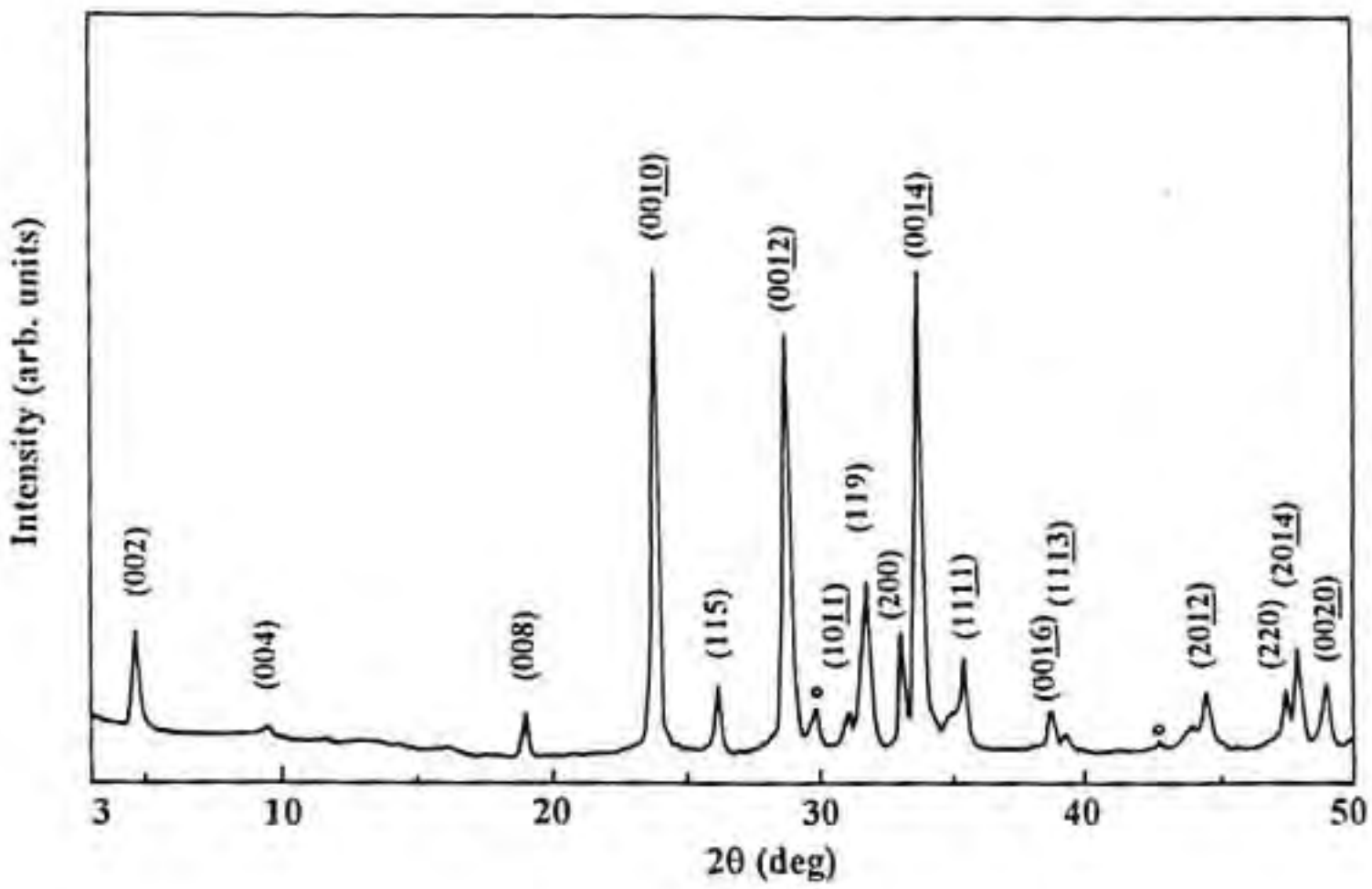

Fig. 7.4(b) The X-ray diffraction pattern of dip-coated Bi(2223) thick film on Ba_2EuNbO_6 substrate. The substrate peaks are marked by '∘'.

Bi(2223) from the computerised XRD data of the thick film (table 7.1) using the empirical relation (13)

$$V = (Y - 29.07)/(28.81 - 29.07),$$

$$28.81 < Y < 29.07$$

where Y is the volume fraction of Bi(2223) and Y = 2θ for the peak appearing between 28.81 and 29.07, caused by the interplay of the reflection of the crystal planes (0010) of Bi(2212) phase and (0012) of Bi(2223) phase. From the above calculations, a volume fraction of 100% was obtained for Bi(2223) in the dip-coated thick film.

Table 7.1(a) X-ray diffraction data of Bi(2223) thick film on Ba_2GdNbO_6 substrate.

No.	2θ	width	d (Å)	I/Io	h k l
1.	4.760	0.375	18.549	30	0 0 2
2.	9.240	0.285	9.563	11	0 0 4
3.	19.080	0.435	4.648	15	0 0 8
4.	23.910	0.409	3.719	97	0 0 10
5.	26.170	0.420	3.402	19	1 1 5
6.	28.810	0.517	3.097	90	0 0 12
7.	29.740	0.195	3.002	18	☆
8.	31.850	0.412	2.807	41	1 1 9
9.	33.100	0.404	2.704	27	2 0 0
10.	33.800	0.439	2.650	100	0 0 14
11.	35.410	0.398	2.533	26	1 1 11
12.	38.780	0.316	2.320	15	0 0 16
13.	39.320	0.412	2.290	10	1 1 13
14.	42.510	0.219	2.125	9	☆
15.	43.810	0.514	2.065	12	0 0 18
16.	44.420	0.434	2.038	18	0 2 12
17.	47.500	0.361	1.913	18	2 2 0
18.	47.960	0.375	1.895	25	2 0 14
19.	48.960	0.447	1.859	20	0 0 20

☆ Substrate peaks.

Table 7.1(b) X-ray diffraction data of Bi(2223) thick film on Ba_2EuNbO_6 substrate.

No.	2θ	width	d (Å)	I/Io	h k l
1.	4.750	0.390	18.588	29	0 0 2
2.	9.400	0.348	9.401	9	0 0 4
3.	19.020	0.418	4.662	14	0 0 8
4.	23.890	0.398	3.722	98	0 0 10
5.	26.180	0.402	3.401	19	1 1 5
6.	28.810	0.518	3.097	88	0 0 12
7.	29.820	0.209	2.994	12	☆
8.	31.400	0.401	2.847	12	1 0 11
9.	31.860	0.405	2.807	39	1 1 9
10.	33.120	0.405	2.703	30	2 0 0
11.	33.820	0.429	2.648	100	0 0 14
12.	35.400	0.400	2.534	24	1 1 11
13.	38.780	0.319	2.320	13	0 0 16
14.	39.340	0.419	2.288	8	1 1 13
15.	42.700	0.254	2.116	7	☆
16.	44.420	0.429	2.038	17	0 2 12
17.	47.480	0.369	1.913	18	2 2 0
18.	47.920	0.380	1.897	26	2 0 14
19.	48.890	0.441	1.861	19	0 0 20

☆ Substrate peaks.

Superconductivity of the dip-coated Bi(2223) thick film on polycrystalline BREnO was studied by temperature-resistance measurements using the standard four probe method. Figure 7.5 shows the temperature-resistance curves for dip-coated Bi(2223) films on BREnO substrate. The films showed a metallic behaviour in the normal state and gave a $T_c(0)$ of 109 K. The critical current density measurements of Bi(2223) films at 77 K and zero magnetic field following the 1 μV/cm criterion gave 2.1×10^3 and 3×10^3 A/cm^2 for Bi(2223) films developed on Ba_2GdNbO_6 and Ba_2EuNbO_6, respectively. The dip-coated Bi(2223) films had good adhesion to the substrate and the thickness of the films were ~4 μm.

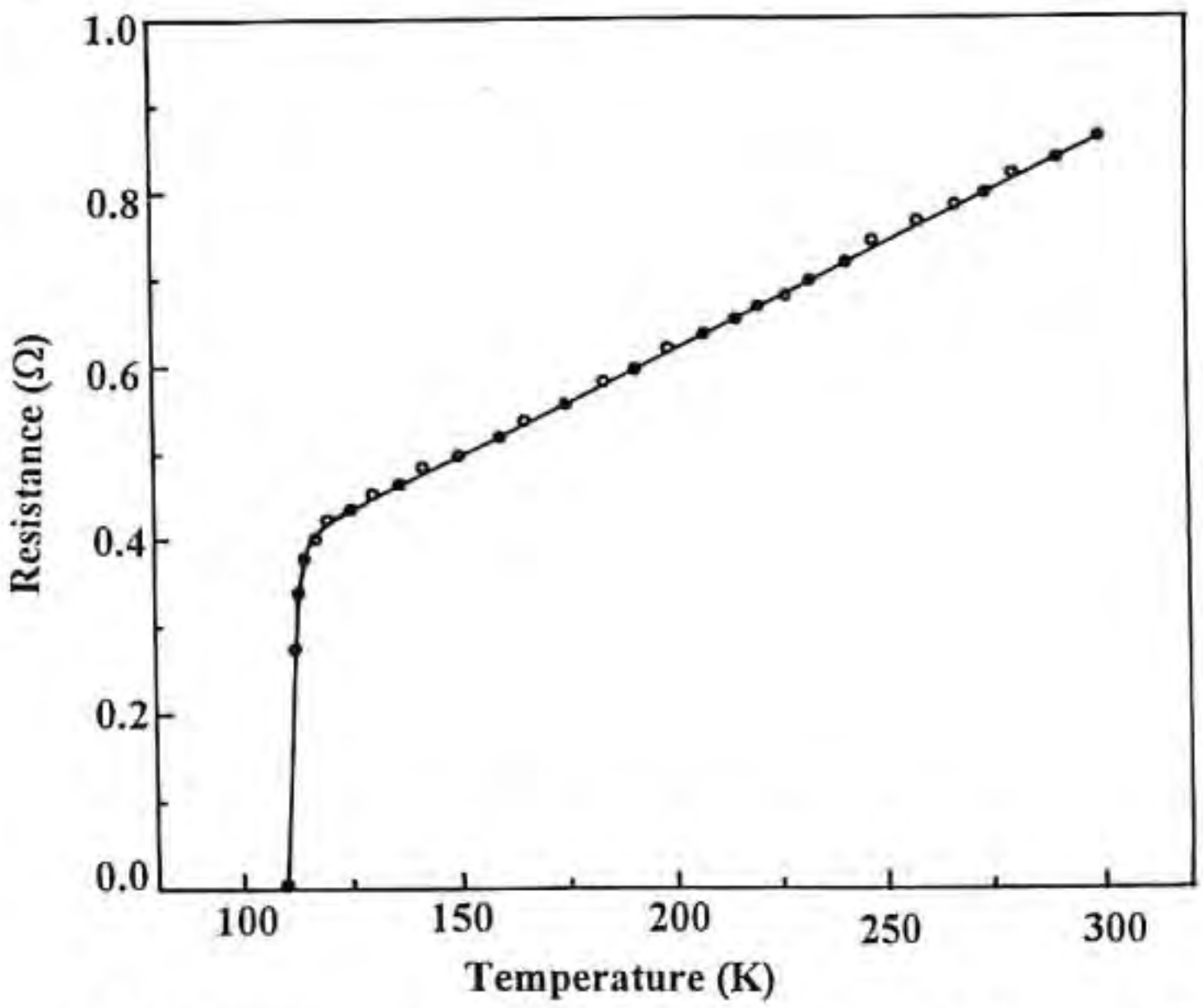

Fig. 7.5(a) Temperature-resistance curve of dip-coated Bi(2223) thick film on Ba_2GdNbO_6.

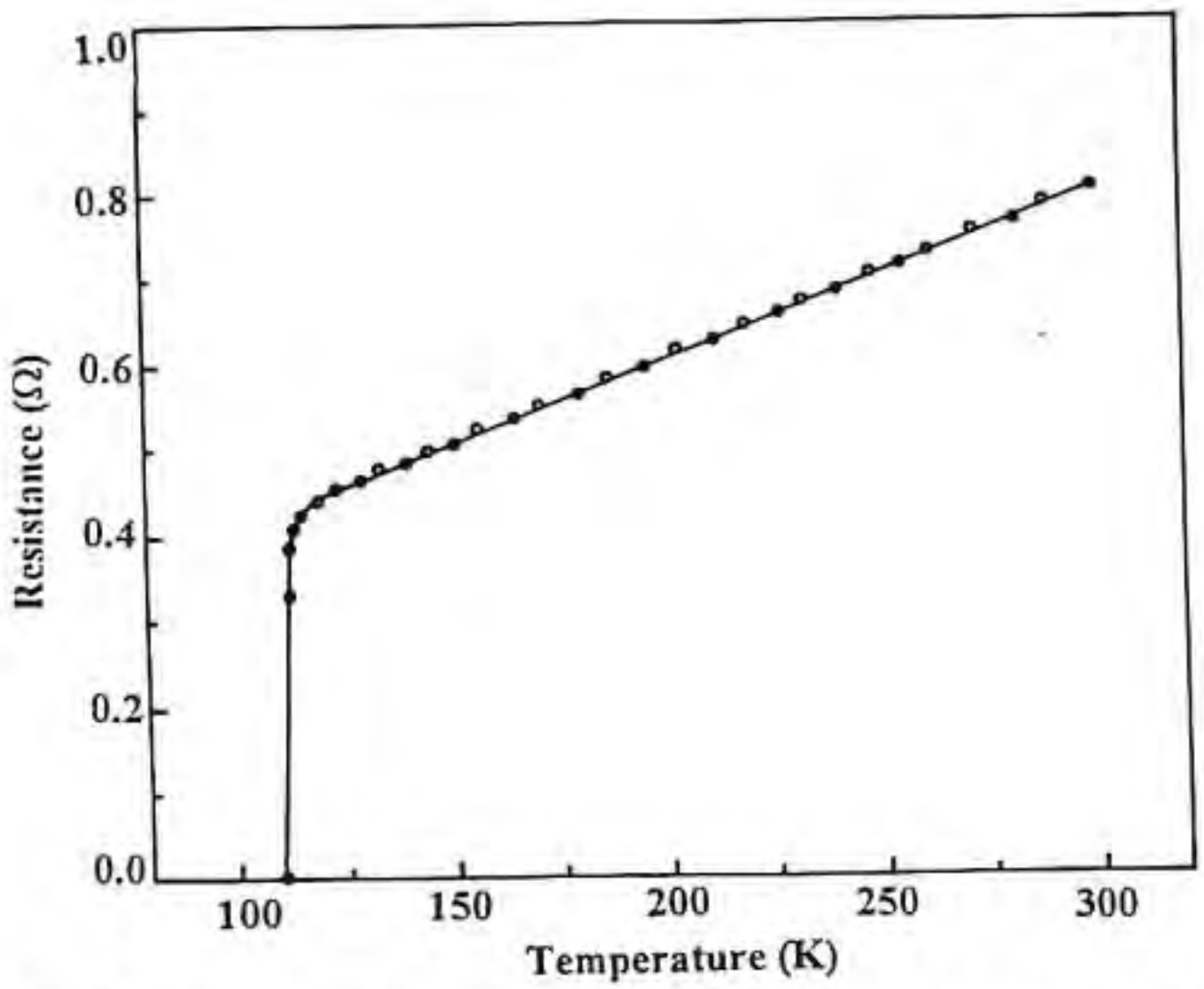

Fig. 7.5(b) Temperature-resistance curve of dip-coated Bi(2223) thick film on Ba_2EuNbO_6.

7.6. Conclusion

In the present study it was found that Ba_2GdNbO_6 and Ba_2EuNbO_6 are non-reacting with Bi(2223) superconductor even at the extreme processing conditions and an addition of 40 vol% of Ba_2GdNbO_6 or Ba_2EuNbO_6 in Bi(2223) superconductor did not show any detrimental effect on the superconducting transition temperature of Bi(2223). On the other hand, the XRD analysis of the annealed Bi(2223)-BRENO (RE = Pr, Nd and Sn) showed the presence of Bi(2212) phase along with the Bi(2223) phase and BRENO. As the annealed Bi(2223)-BRENO (RE = Pr, Nd and Sm) composites did not show the presence of any other phase other than those

of Bi(2223), Bi(2212) and the characteristic peaks of BRENO, BRENO can be used as substrates for Bi(2212) superconductor. The temperature-resistivity measurements of Bi(2223)-BRENO (RE = Pr & Sm) composites gave $T_c(0)$ of 109 K, but the Bi(2223)-Ba_2NdNbO_6 did not yield any zero reistivity superconducting transition up to 77 K. The use of Ba_2GdNbO_6 and Ba_2EuNbO_6 as substrate for Bi(2223) superconductor was confirmed by dip-coating Bi(2223) films on these polycrystalline substrates which gave a $T_c(0)$ of 109 K and a J_c of above $2x10^3$ A/cm^2 at 77 K and zero magnetic field.

References

1. K. Hoshino, H. Takahara and M. Fukutomi, Advances in Superconductivity, Proc. 1st Int. Sym. Supercond., ISS-88, Eds. Kitazawa and Ishiguro, Springer Verlag, 325 (1988).
2. M. Hrovat, S. Bernik, M. Rozman and D. Kolar, Supercond. Sci. Technol., **5**, 313 (1992) and the references therein.
3. S.A. Agnihotry, P. Ghosal, K.C. Nagpal and S. Chandra, Supercond. Sci. Technol., **4**, 7 (1991).
4. N. Knauf, J. Harnischmacher, R. Muller, R. Borowski, B. Roden and D. Wohlleben, Physica C, **173**, 414 (1991).
5. S. Bernik, M. Hrovat and D. Kolar, Proc. Int. Conf. Modern Aspects of Superconductivity, ICMAS-89, Ed. R. Suryanarayanan, 127 (1989).
6. W. Lo, Y. L. Chen, T.B. Tang and R. Stevens, Br. Ceram. Soc. J., **89**, 218 (1990)
7. S.A. Sunshine, T. Siegrist, L.F. Schneemeyer, D.W. Murphy, R.J. Cava, B. Batlogg, R.B. van Dover, R.M. Fleming, S.M. Glarum, S. Nakahara, R. Farrow, J.J. Krajewski, S.M. Zahurak, J.V. Waszczak, J.H. Marshell, P. March, L.W. Rupp and W.F. Peck, Phys. Rev. B., **38**, 893 (1988).
8. H.K. Liu, S.X. Dou, N. Savvides, J.P. Zhou, N.X. Tan, A.J. Bourdillon, M. Kuiz and C.C. Sorrell, Physica C, **157**, 93 (1989).
9. B. Zhu, L. Lei, S.L. Yuan, S.B. Tang, W. Wang, G.G. Zhang, W.Y. Guan and J.Q. Zheng, Physica C, 157, 370 (1989).

10. S.X. Dou, H.K. Liu, S.J. Guo, K.E. Esterling and J. Mikael, Supercond. Sci. Technol., **2**, 274 (1989).

11. W.C. McGinnis and J.J. Briggs, J. Mat. Res., **7**, 585 (1992).

12. A. Agrawal, R.P. Gupta, W.S. Khokale, K.D. Kundra, P.R. Deshmukh, M. Singh and P.D. Vyas, Supercond. Sci. Technol., **6**, 670 (1993).

13. F.H. Chen, H.S. Koo and T.Y. Tseng, J. Am. Ceram. Soc., **75**, 96 (1992).

CHAPTER 8

SUMMARY AND CONCLUSION

The thesis presents detailed study on (a) the development and characterisation of novel ceramic substrates for high T_C superconductors and (b) the preparation and characterisation of high T_C superconductor films with excellent superconducting characteristics on the newly developed substrates.

A group of perovskite ceramic materials $Ba_2R_ENbO_6$ (R_E = Pr, Nd, Sm, Eu and Gd) {BRENO} were prepared and sintered as single phase materials by solid state reaction method for their use as substrates for high T_C superconductors. These materials are found to be isostructural and have complex cubic perovskite structure. The lattice constant values of BRENO were found to be between 8.45 Å and 8.60 Å, and are comparable with that of MgO, a substrate used for the epitaxial growth of YBCO films. BRENO offers a reasonable number of coincidence sites with YBCO superconductor. BRENO has moderately low dielectric constants and loss factor values making them suitable as substrates for microwave applications. BRENO were found to melt congruently making single crystal growth from the melt possible. The thermal expansion coefficient values of BRENO were found to be ~8 x 10^{-6} °C^{-1} at room temperature and are comparable with that of YBCO superconductor thereby offering a reasonable thermal expansion match with YBCO. The DTA studies reveals that there is no phase transition occurring

in BREnO in the temperature range 30 to 1300°C. The thermal conductivity values of BREnO (~70 W m^{-1} K^{-1}) offers additional advantage for substrate applications. It is found that BREnO does not react with YBCO even at the extreme annealing conditions. The temperature-resistivity measurements reveals that an addition of BREnO up to 20 vol% in YBCO has no detrimental effect on the superconducting property of YBCO, indicating that BREnO are chemically compatible with YBCO even at the extreme processing conditions. The chemical compatibility, favourable dielectric and thermal properties of BREnO makes them ideal candidates as substrate for YBCO superconductor films.

The chemical non-reactivity of BREnO with YBCO was further confirmed by carrying out a detailed study on the electrical transport and percolation behaviour of superconductor-insulator composites by taking YBCO as the superconductor and BREnO as the insulator. Results obtained from the X-ray diffraction and resistivity studies of $YBa_2Cu_3O_{7-\delta}$-Ba_2GdNbO_6 (YBCO-BGNO) composites are presented in this thesis as a typical example. In the YBCO-BGNO composite system, it is found that YBCO and BGNO remains as two separate phases with their own characteristics even after the severe heat treatment conditions. The normal state percolation threshold and superconducting percolation threshold of YBCO-BGNO composite system were found to be ~17 vol.% and ~30 vol.% of YBCO in the composite system, respectively. The value of the critical exponents, t and u, describing the electrical transport properties of YBCO-BGNO, were

found to be 1.65 and 0.88 respectively. The values of the constants ρ and ρ_o' were 8.318 mΩ.cm and 5.24×10^{12} mΩ.cm respectively. The normal state percolation threshold value and the critical exponents describing the transport behaviour of the YBCO-BGNO composite system match fairly well with those expected for a perfect metal-insulator composite system.

Superconducting YBCO and YBCO-Ag composite thick films have been successfully prepared on polycrystalline BRENO substrates by both screen printing and dip-coating techniques. The successful preparation of superconducting YBCO thick films is found to be critically dependent on the processing conditions. The best results were obtained for films annealed at the partial melting temperature of YBCO (1000°C) for ~2 min. in air. The processing of the YBCO thick films at the partial melting point of YBCO enhanced the texturing of the YBCO films and also improved the adhesion of the film with the substrate. The X-ray diffraction studies of the YBCO films developed on BRENO substrates shows a high degree of c-axis orientation and there were no evidence of the formation of any second phase within the precision of X-ray diffraction technique. The microstructural analysis of the surface of the YBCO films by SEM shows that the film surface is smooth and almost free from pores and there were no evidence of any microcracks. The SEM analysis of the cross section of the YBCO thick films shows no indication of any reaction between the film and the substrate at the film-substrate interface. The YBCO thick films developed on BRENO substrates gave zero resistance superconducting

transition [$T_c(0)$] of 92 K with a transition width of ~2 K and a critical current density (J_c) value of ~10^4 A/cm^2 at 77 K and zero magnetic filed. The YBCO-Ag composite (7 wt.% of Ag) thick films developed on BRENO gave $T_c(0)$ of 92 K and a J_c of ~$3x10^4$ A/cm^2 at 77 K and zero magnetic field (The J_c of the films were measured following 1 μV/cm criterion). It was evident from the X-ray analysis that the addition of silver improves the c-axis texturing of the YBCO film. SEM analysis shows that the silver addition results in the formation of a much smoother and denser film. The silver addition also enhances the J_c of the YBCO thick films by about three times. The successful preparation of YBCO thick films free from any microcracks indicates that BRENO offers a reasonable thermal expansion match with YBCO.

Polycrystalline BRENO substrates were used for the growth of superconducting YBCO and YBCO-Ag thin films by pulsed laser ablation technique. The YBCO thin films *in situ* grown on polycrystalline BRENO substrates exhibited (00*l*) orientation of an orthorhombic YBCO phase. The YBCO films grown on BRENO substrates gave $T_c(0)$ of 90 K with a transition width of ~1.5 K and a J_c of ~$3x10^4$ A/cm^2 at 77 K and zero magnetic field. The SEM analysis of the surface of the YBCO thin films grown on BRENO shows no evidence of any microcracks. The YBCO-Ag grown *in situ* on BRENO also exhibited (00*l*) orientation of an orthorhombic YBCO phase and gave $T_c(0)$ of 90 K with a transition width of ~1.5 K. The J_c values of YBCO-Ag thin films on BRENO were ~$2x10^5$ A/cm^2 at

77 K and zero magnetic field. The intensity and width of the (00*l*) reflections of YBCO films on BRENO are comparable to those of YBCO films grown on (100) $LaAlO_3$ indicating the crystallinity of the YBCO films. It is observed that the silver addition has enhanced the intensity of the peaks corresponding to the (00*l*) reflections of YBCO by about three times when compered with YBCO films grown without silver. Also the critical current density of YBCO thin films has been enhanced by about four times by the addition of silver.

In the present study it was found that Ba_2GdNbO_6 and Ba_2EuNbO_6 are non-reacting with Bi(2223) superconductor even at the extreme processing temperature of 850°C. An addition of 40 vol% of Ba_2GdNbO_6 or Ba_2EuNbO_6 in Bi(2223) superconductor did not show any detrimental effect on the superconducting transition temperature of Bi(2223) indicating that these materials could be used as substrates for Bi(2223) superconductor. However when BRENO (RE = Pr, Nd and Sn) materials were annealed with Bi(2223) at 850°C, the presence of Bi(2212) phase was observed along with the Bi(2223) phase and BRENO. As the annealed Bi(2223)-BRENO (RE = Pr, Nd and Sm) composites did not show the presence of any other phase other than those of Bi(2223), Bi(2212) and the characteristic peaks of BRENO, these materials can be used as substrates for Bi(2212) superconductor. The use of Ba_2GdNbO_6 and Ba_2EuNbO_6 as substrate for Bi(2223) superconductor was confirmed by dip-coating Bi(2223) films on these polycrystalline substrates which gave a $T_C(0)$ of 109 K and a J_C of above $2x10^3$ A/cm^2 at 77 K and zero magnetic field.

Scope of Future Work

During the last five years there has been intense research for the development of new ideal substrates for high temperature superconductors. During our study on substrate development for high temperature superconductors, we have identified five new substrates which could be ideally suited for their use as substrates. But these materials are in polycrystalline form. For many of the electronic applications epitaxially grown superconductor films are required for better performance. These epitaxial films are usually fabricated on chemically compatible single crystal substrates which are in bulk form. Therefore single crystal growth of BRENO materials are essential. Since BRENO material melts congruently, single crystal growth by Czochralski growth technique may be possible. However another effective approach is to develop first an epitaxial layer of non-reacting substrate and then develop epitaxially superconducting films on the epitaxially grown thin layers of the non-reacting substrates. The growth of single crystal films of BRENO on technologically important substrates such as Si, SiO_2, Al_2O_3, etc. will be useful as they are commercially available and are widely used for many microelectronic applications. The successful preparation of single crystal films of BRENO epitaxially on Si and the growth of high quality superconductor films over them can have tremendous potential for application in integrating superconductivity with the existing semiconductor technology.

As the use of high temperature superconductors in high power electric applications has now taken new turns, the deposits of YBCO on textured metal tapes with suitable buffer layer may be the high temperature superconductor wire technology that enables high field electric power devices at liquid nitrogen temperatures. In this case, successful deposition of BRENO as a buffer layer on commercially available textured metal alloy tapes and the subsequent deposition of YBCO films on these BRENO layers would be a break through in superconductivity research. The YBCO-BRENO composites may have application in the construction of high frequency phase shifters and modulators as BRENO forms composites with YBCO without deuterating its superconducting properties.